Synthesis, Characterization, Photo-Physical Properties and Biological Activity of [Ru(*p*-cymene)(tmp)Cl]·CH_2Cl_2, [Ir(ppy)$_2$(tmp)]·CH_2Cl_2 and Ru(*p*-cymene)(PPh_3)Cl_2 Complexes

Vannara Soem

A Thesis Submitted in Partial Fulfillment of the Requirements for the Degree of Master of Science in Chemistry (International Program)
Prince of Songkla University
2023

Synthesis, Characterization, Photo-Physical Properties and Biological Activity of [Ru(*p*-cymene)(tmp)Cl]·CH_2Cl_2, [Ir(ppy)$_2$(tmp)]·CH_2Cl_2 and Ru(*p*-cymene)(PPh_3)Cl_2 Complexes

Vannara Soem

A Thesis Submitted in Partial Fulfillment of the Requirements for the Degree of Master of Science in Chemistry (International Program)
Prince of Songkla University
2023

Thesis Title	Synthesis, Characterization, Photo-Physical Properties and Biological Activity of [Ru(*p*-cymene)(tmp)Cl]·CH_2Cl_2, [Ir(ppy)$_2$(tmp)]·CH_2Cl_2 and Ru(*p*-cymene)(PPh_3)Cl_2 Complexes
Author	Mr. Vannara Soem
Major Program	Chemistry (International Program)

Major Advisor

....
(Asst. Prof. Dr. Nararak Leesakul)

Co-advisor

....
(Asst. Prof. Dr. Saowanit Saithong)

Examining Committee :

....Chairperson
(Asst. Prof. Dr. Luksamee Vittaya)

....Committee
(Asst. Prof. Dr. Uraiwan Sirimahachai)

....Committee
(Dr. Dhassida Sooksawat)

....Committee

....Committee
(Asst. Prof. Dr. Saowanit Saithong)

The Graduate School, Prince of Songkla University, has approved this thesis as Partial fulfillment of the requirements for the Master of Science Degree in Chemistry

....
(Asst. Prof. Dr. Thakerng Wongsirichot)
Acting Dean of Graduate School

This is to certify that the work here submitted is the result of the candidate's own investigations. Due acknowledgement has been made of any assistance received.

....Signature
(Asst. Prof. Dr. Nararak Leesakul)
Major Advisor

....Signature
(Asst. Prof. Dr. Saowanit Saithong)
Co-Advisor

....Signature
(Mr. Vannara Soem)
Candidate

I hereby certify that this work has not been accepted in substance for any degree, and is not being currently submitted in candidature for any degree.

....Signature
(Mr. Vannara Soem)
Candidate

Thesis Title Synthesis, Characterization, Photo-Physical Properties and Biological Activity of [Ru(*p*-cymene)(tmp)Cl]·CH_2Cl_2, [Ir(ppy)$_2$(tmp)]·CH_2Cl_2 and Ru(*p*-cymene)(PPh_3)Cl_2 Complexes

Author Mr. Vannara Soem

Major Program Master of Science Program in Chemistry (International Program)

Academic Year 2022

ABSTRACT

In this study, two novel ruthenium(II) and iridium(III) complexes with tris(2-methoxyphenyl)phosphine (tmp) and ruthenium(II) with triphenylphosphine (PPh_3) ligands; [Ru(*p*-cymene)(tmp)Cl]·CH_2Cl_2 (**1**), [Ir(ppy)$_2$(tmp)]·CH_2Cl_2 (**2**) were synthesized together with a known complex of Ru(*p*-cymene)(PPh_3)Cl_2 (**3**). The complexes were analyzed using single-crystal X-ray diffraction, elemental analysis, and spectroscopy techniques. The structures of complexes **1** and **3** are both distorted tetrahedral geometry. Each of them has two independent molecules with asymmetric units in one unit cell. They have the same backbone of Ru(*p*-cymene)ClL_2; L is a different kind of ancillary ligand. Complex **1** has L as a bidentate of P and O donors. Complex **3** has L as PPh_3 and Cl ligands. Complex **2** shows a distorted octahedral geometry of a bis complex with two 2-phenyl pyridine molecules and a chelating ring of P and O from the tmp ligand. All kinds of molecules were studied for the intramolecular forces in their crystal structures. Hydrogen bonds were mainly found. All complexes' photophysical properties (UV-Visible absorption and luminescence) were investigated. The maximum absorption wavelength of complex **3** is presented at 395 and 496 nm. Regarding the DFT/TDDFT calculation of complex **3**, its electronic transition is a mixed charge transfer transition (CT) type. Among studied **1-3** complexes, only complex **2** was observed in the emission band at 522 nm (excitation at 380 nm). Complex **2** showed selective sensing properties toward Fe(III) ion in dimethylformamide (DMF) solution with a 1:1 stoichiometric binding mode. The binding constant calculated from the Benesi-Hildebrand plot was 8.1×10^{2} M^{-1}. All complexes were tested for their biological activities on antibacterial, antifungal, anti-yeast, and anti-breast cancer. Complexes **1** and **2** displayed the antibacterial on Gram-positive bacteria, but not for complex **3**. The MIC/MBC values for complex **1** have been observed at 64/128 µ/mL for both *Staphylococcus aureus* ATCC25923 (SA) and methicillin-resistant *Staphylococcus aureus* (MRSA), which indicates moderate activity. Complex **2** showed MIC/MBC values for SA and MRSA inhibition of 16/32 µ/mL and 32/32 µ/mL, respectively. Only complex **3** exhibited cytotoxicity against MCF-7 by MTT assay with IC_{50} 15.99 µM which was more potent than that of cisplatin (42.2 µM), a commercial drug, for 2.6 folds.

Keywords: Anticancer, antibacterial, antimicrobial, antifungal, ruthenium(II) complex, Iridium(III) complex, P-donor ligand.

ACKNOWLEDGEMENTS

Firstly, I would like to impress my deep thanksgiving to my respectful and gorgeous advisor, Asst. Prof. Dr. Nararak Leesakul, for a crucial part of my master's degree and the main relevance of my research, responsible, generous, enthusiastic, and treasured knowledge. Under her supervision, she always straightens and guides me all the time during my research and thesis. I am proud and appreciative to have a fantastic advisor and mentor for my master's studies. Similarly, I want to express my respect to my Co-advisor Asst. Prof. Dr. Saowanit Saithong. She is the second guide for this thesis, and I am appreciative of her sacrifice to encourage the whole of my thesis.

I want to show my gratitude and dedicate this to the Royal Scholarship under Her Royal Highness Prince Maha Chakri Sirindhorn Education Project, Graduate School, and SISA PSU, Prince of Songkla University, for offering me the opportunity and financial support for my master's studies at the Department of Chemistry, Faculty of Science, Prince of Songkla University.

I want to express my profound gratitude to Prof. Dr. Adisorn Ratanaphan, Department of Pharmaceutical Chemistry, Faculty of Pharmaceutical Science, Prince of Songkla University, for the anticancer activity assay. Additionally, I would like to express my thanks to Prof. Dr. Souwalak Pongpaichit, Natural Products Research Center and Department of Microbiology, Faculty of Science, Prince of Songkla University, for the antimicrobial activity assay.

I also would like to sincerely thank the head of the examination committee, Asst. Prof. Dr. Luksamee Vittaya, for her kindness, to be a chairperson in my thesis defense. Furthermore, I would like to express my grateful thank, Asst. Prof. Dr. Uraiwan Sirimahachai and Dr. Dhassida Sooksawat for their benign as the examiner committee and good recommendation.

I am grateful to all of my lecturers in the Chemistry Department, at Prince of Songkla University, for sharing their knowledge, motivation, encouragement, and potential support.

I would love to express my gratitude to all of my seniors and all of the members of laboratory CH214, NHMR room, and especially to Dr. Ekkapong

Klamnee, and Miss. Thitirat Temrarm, and Miss. Rattanyu Kongpan, for their assistance and accompanying, motivating, and helping me.

I would like to express my thanksgiving to Dr. Kishor Kumar Maharjan, Dr. Tuan Anh Tran, Mr. Kim Chenset, and Miss. Kin Savin, Mr. Tim Somnang, and Mr. Kan Tola, for being good friends, motivating, courageous, and helpful whenever I have problems.

Last but not least, I would like to thank my lovely and respectful parents, brothers, sisters, families, and friends for always believing in me and offering me opportunities, support, motivation, and encouragement during my studies and research.

Vannara Soem

CONTENTS

Pages

LIST OF TABLES

LIST OF SCHEMES

LIST OF FIGURES

LIST OF ABBREVIATIONS AND SYMBOLES

tmp	=	Tris(2-methoxyphenyl)phosphine
PPh_3	=	Triphenylphosphine
ppy	=	2-phenylpyridine
CDM	=	Dichloromethane
$CDCl_3$	=	Deuterated chloroform or chloroform-d
DE	=	Diethyl ether
AN	=	Acetonitrile
Å	=	Angstrom unit
^{o}	=	Degree
ppm	=	Part per million
µM	=	Micromolar
µL	=	Microliter
mL	=	Milliliter
nm	=	Nanometer
HIV	=	Human immunodeficiency virus
DNA	=	Deoxyribonucleic acid
MLCT	=	Metal to ligand charge transfer
MIC	=	Minimal inhibitory concentration
MBC	=	Minimal bactericidal concentration
MFC	=	Minimal fungicidal concentration
MCF-7	=	BRCA1-competent MCF-7 breast cancer cell
MTT assay	=	(3- [4,5- dimethylthiazol-2-yl]-2,5-diphenyl tetrazolium bromide)
RAPTA	=	Ruthenium arene PTA
BT-549	=	Triple-negative breast cancer cell
MDA-MB-231	=	Triple-negative cancer cell
HCC1937	=	BRCA1-defective breast cancer cell
^{1}H-NMR	=	Proton Nuclear Resonance Spectroscopy
FTIR	=	Fourier Transform Infrared Spectroscopy
UV-Vis	=	UV-Visible absorption spectroscopy
MS	=	Mass spectroscopy

IC_{50}	=	Half maximal inhibitory concentration
A.R. grade	=	Analytical reagent grade
δ	=	Chemical shift
λ	=	Wavelength
ε	=	Molar extinction coefficient
h	=	Hour
s	=	Singlet
d	=	Doublet
t	=	Triplet
m	=	Multiplet
dt	=	Doublet of triplet
Ksv	=	Stern-Volmer constant
K_b	=	Binding constant

CHAPTER 1

INTRODUCTION

1. 1. Introduction

Ru(II)-based arene systems (Rojas *et al*., 2017) and Ir(III)-based 2-phenyl pyridine (Conesa *et al*., 2020) organometallic complexes have undergone extensive investigation in terms of biological activities like antibacterial, antitumor, and anti-cancer activities (Lapasam *et al*., 2020). In general, the Ru(II) and Ir(III) complexes demonstrate promising behavior to suppress the growth of microorganisms and significantly exhibit cytotoxicity toward cancer cells *in vitro* with low IC_{50} values (Patil *et al*., 2020). The results of research on cancer which were published in 20 different countries showed that there were 9.6 million cancer deaths and 18.1 million new cancer cases (Bray *et al*., 2018). The second biggest cause of mortality was breast cancer in women (Sung *et al*., 2021). Moreover, microorganisms such as bacteria, yeast, and filamentous fungus cause a variety of disorders (Hammadi *et al*., 2022). Likewise, *Staphylococcus aureus (S. aureus)* is a Gram-positive facultative aerobe that is commonly found in the respiratory tract and on the skin (Filkins *et al*., 2015). It is a dangerous pathogen that affects humans. Many strains exist; some can cause skin infections, lung infections, and food poisoning (Ahmad-Mansour *et al*., 2021). They can induce shock syndrome, scalded skin syndrome, or osteomyelitis in serious situations. By the way, *S. aureus* has been found to be the reason for pneumonia, and antibiotic resistance has emerged in a strain of *S. aureus* (Gurusamy *et al*., 2013).

The bacteria *Escherichia coli* (*E. coli*) is Gram-negative, and a few types of *E. coli* can cause illness in humans (Masalha *et al*., 2001). Moreover, pneumonia, urinary tract infection, and diarrhea might cause several problems. *Pseudomonas aeruginosa* is additionally a Gram-negative bacterium too. In discrete cancers that are immunocompromised, severe burn victims, and cystic fibrosis (CF), it can induce dangerous infections (Wu *et al*., 2015). Other microbial pathogens exist and *Candida albicans* is a kind of *Candida* (Mba *et al*., 2022). They are unicellular Gram-positive staining yeast-type fungi that can cause infections of the surface, mucosa, and system (Rane *et al*., 2013). *Cryptococcus neoformans* (*C. neoformans*) is another fungus that looks like yeast (Baker *et al*., 2022). It is not only the most common cause of fungal meningitis in immunocompromised adult patients but also a life-threatening illness in persons living with HIV who are poorly managed (Helbok *et al*., 2009).

Microsporum gypseum (*M. gypseum*) is a geophilic fungus that infrequently causes sickness in humans (Souza *et al*., 2016). On the contrary, dermatophytosis produced by *M. gypseum* frequently manifests as an inflammatory mycosis affecting the glabrous skin and scalp, particularly in youngsters (Souza *et al*., 2016). *Talaromyces marneffei*, or *Penicillium marneffei*, is a member of the world's most dangerous fungi (Hyde *et al*., 2018; Köhler *et al*., 2017). It was first found in 1956 and is a significant source of illness in Southeast Asians due to decreased immunity caused by HIV infection (Chastain *et al*., 2017).

Karl Klaus (1796–1864), a Russian chemist, was the first to discover Ruthenium (Ru). This element has the atomic number 44 and belongs to the platinum group (Sahu *et al*., 2018). While iridium (Ir) was first discovered by British scientist Smithson Tennant (1761–1815) in 1803, and it is an element with atomic number 77 and a member of the platinum and ruthenium group (Hunt, 1987). Iridium and ruthenium are both capable of forming a variety of organometallic compounds that are utilized in industrial catalysis, photonic devices, and pharmaceutical systems (Banerjee and Sadler, 2021). The capacity to mimic iron, the spectrum of oxidation states, and the velocity of ligand exchange are three key characteristics of ruthenium and iridium that make them suitable for use in medicine (Allardyce and Dyson, 2001). The capacity of ruthenium to mimic iron, which may attach to proteins like transferrin and albumin, accounts for the reduced toxicity of ruthenium-based drugs (Motswainyana and Ajibade, 2015).

Ruthenium and iridium were chosen as the metal-based drug materials because Ru(II), Ru(III), Ir(III), and Ir(IV) complexes had similar ligand exchange mechanisms to Pt(II) complexes (Odularu *et al*., 2019). Ruthenium and iridium ion ligand exchange is a crucial component of their biological properties (Gajera *et al*., 2016; Lapasam *et al*., 2020). The majority of interactions that ruthenium(II) and iridium(III) complexes go through when they attach to proteins, DNA base pairs, enzymes, minor donor molecules, or water are significant for their medical uses (Elsayed *et al*., 2020; Tabrizi and Chiniforoshan, 2017). In addition, cytotoxicity against normal cells is lower for Ru(II) and Ir(III) than commercial medicines like the family of platin drugs (Du *et al*. 2019; Patil *et al*., 2020). Ru(II) and Ir(III) chelating complexes often exhibit high lipophilicity and have a significant ability to enter the lipid layer of bacterial and yeast cell membranes in terms of their antibacterial properties (Lapasam and Kollipara, 2020). Consequently, it would be fascinating to develop Ru(II) and Ir(III) as antibacterial, immunosuppressive, or anticancer medicines (Gopalakrishnan *et al*., 2020; Lapasam *et al*., 2020). Recently, preclinical and clinical trials have been conducted on a few ruthenium complexes (Lee *et al*., 2020). The complexes imidazolium-*trans*-DMSO-imidazole tetrachlororuthenate (NAMI-A) (Alessio and Messori, 2019), Indazolium *trans*-[tetrachlorobis(1*H*-indazole)ruthenate(III)] (KP1019) (Hummer *et al*., 2013), and sodium *trans*-[tetrachloridobis(1*H*-indazole)ruthenate(III)] (N)(KP1339) (Zeng *et al*., 2017) have been selected for research and developed with their promising bioactivity activities (Figure 1).

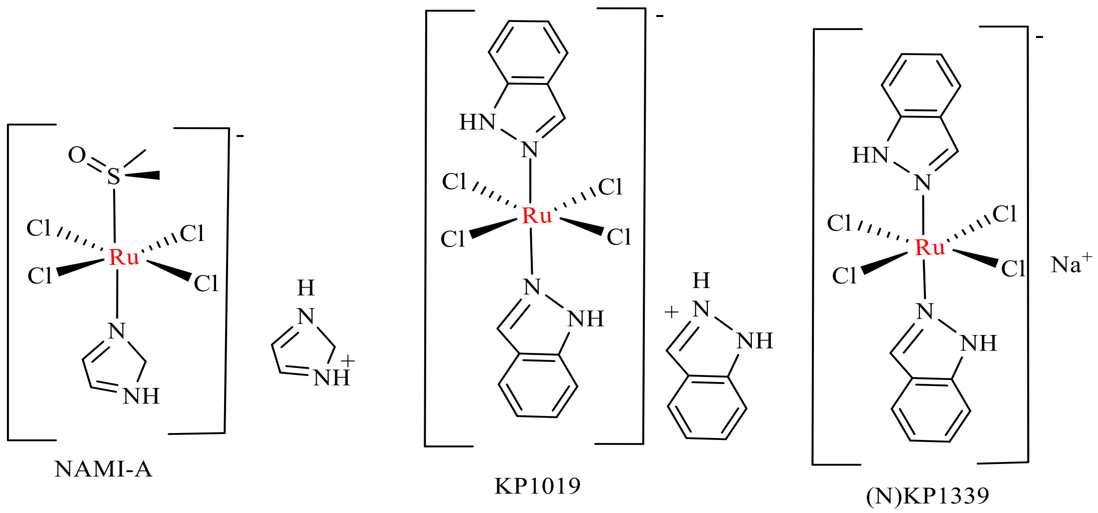

Figure 1. The structure of ruthenium clinical trial and preclinical compounds.

Organometallic Ru(II) complexes based on *p*-cymene have been developed for biological activities based on anticancer drugs with potential pharmacological properties (Gürses *et al*., 2022; Smith *et al*., 2011). In comparison to platinum medicines, the piano-stool half sandwich *p*-cymene of Ruthenium(II) complexes have already been primarily explored as antitumor drugs with less toxic to normal cells (Aird *et al*., 2002; Qin *et al*., 2019). The labile ligand chlorine atom is shown in the structural model, which is then replaced by a water molecule and further penetrated to make bonds with the cancer cell's DNA base pair (Neethu *et al.*, 2019). Organometallic ruthenium(II) complexes, such as half-sandwich ruthenium(II)-arene, have been widely researched and regarded as versatile compounds. A half-sandwich ruthenium(II)-arene design for a "piano-stool" [(η^6-arene) Ru(X)(Y)] (Figure 2) where R is the substituents on arene moiety, X and Y are ancillary ligands. (Jaouen *et al.*, 2006).

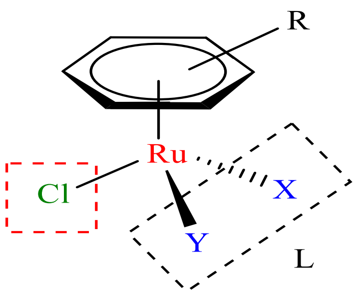

Figure 2. The structure of ruthenium(II)-*p*-cymene complex.

Due to their various chemical structures and simplicity in controlling their hydrophobic property, many d^6 metal complexes, particularly iridium(III) and ruthenium(II) complexes are now being investigated as potential chemotherapeutic agents (Hao *et al.*, 2019; Li *et al.*, 2018). For example, the [Ru(dppm)Cl_2] complex had a greater anti-breast cancer action against two cell lines, MCF-7 (IC_{50} = 1.8 µM) and MDA-MB-231 (IC_{50} = 5.8 µM) than the commercial drug like cisplatin (Das *et al.*, 2010); it also exhibited antibacterial against methicillin-resistant *Staphylococcus aureus* (ATCC 33591), *S. aureus* (ATCC 25923), and *Salmonella typhimurium* (ATCC 14028) (Odachowski *et al.*, 2020). Additionally, it has been demonstrated that iridium(III) complexes (Wang *et al.*, 2017) (Figure 3) is a new challenge in biological framework because of an enormous potential of presenting anticancer and antimicrobial activities with low toxicity to normal cells (Chen *et al.*, 2021; Tabrizi *et al.*, 2017). Bisdiphosphinoalkane bidentate P^P ligands (Figure 4) have proven to be successful ligands for ruthenium(II) and iridium(III) complexes in anticancer (Du *et al.*, 2018). They have been used in studies on cytotoxicity against specific types of cancer cells, even though their derivatives are useful ligands. Half-sandwich Ir^{III} and Ru^{II} complexes $[(Cp^x/arene)M(L\text{^}L')Z]^{0/n}$ have a significant impact on the anticancer activity (Almodares *et al.*, 2014) (Figure 5).

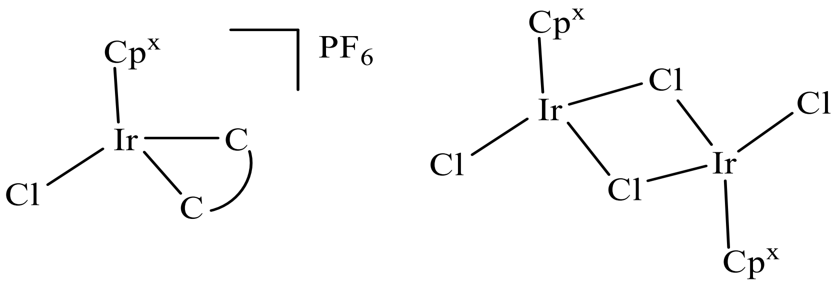

Figure 3. Iridium(III) cyclopentadienyl complexes.

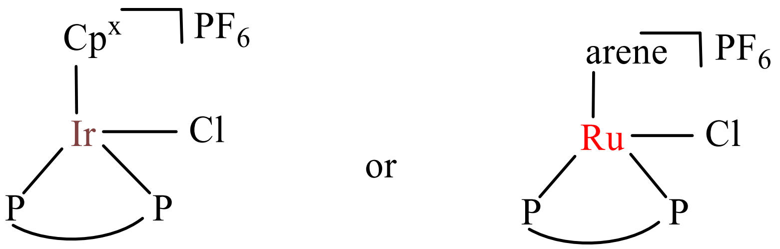

Figure 4. Iridium(III) and ruthenium(II) complexes with bidentate P^P ligands.

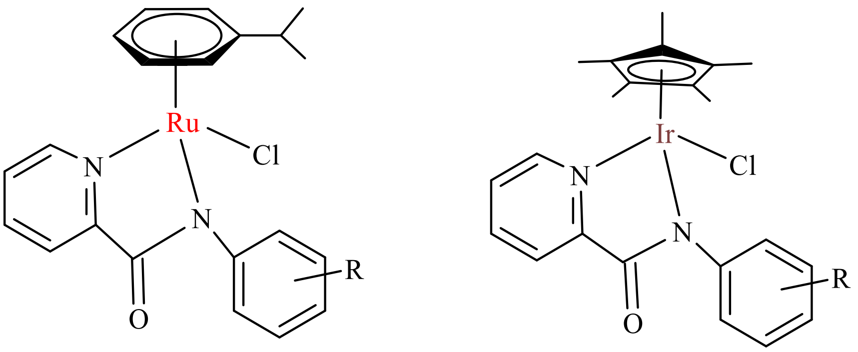

Figure 5. Iridium-Cp* and ruthenium *para*-cymene picolinamide complexes.

In the past, many researchers studied Ru(II) and Ir(III) complexes with different ligands mainly with N-donor, P-donor, O-donor, and S-donor ligands (Gichumbi *et al*., 2016; Klaimanee *et al*., 2021; Leesakul *et al*., 2019; Lapasam *et al*., 2020; Patil *et al*., 2020). Half-sandwich ruthenium(II) complexes with P donor ligands [Ru(η^6-*p*-cymene)Cl_2(1, 3, 5-triaza-7-phoshaadamantane] (RAPTA-C) (Berndsen *et al*., 2017) and [Ru(η^6-C_6H_5Me)(1, 3, 5-triaza-7-phosphaadamantane)Cl_2] (RAPTA-T) (Lee *et al*., 2017) (Figure 6) have been produced and chosen based on several types of research and their great bioactivity especially for the cytotoxicity against cancer cell over other donor atoms. Therefore, one of the structure model for this present work is Ru(*p*-cymene)Cl(L_2); L = P-donor ligand.

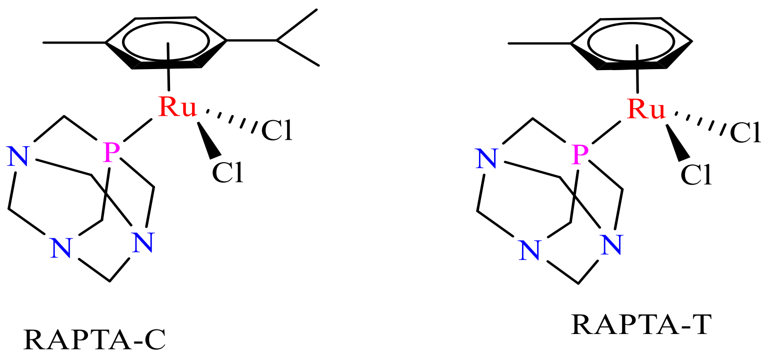

Figure 6. Example of RAPTA-C and RAPTA-T complexes.

The synthesis, structural identification, and biological activity of Ru(II) with 1, 1-bis(diphenylphosphino)methane (dppm) and *tert*-butyl pyridine (tbp) ligands were reported by our group in 2017 (Chuklin *et al*., 2017). Ru(II) with 1, 1-bis(diphenylphosphino)methane (dppm) exhibited cytotoxicity against MCF-7 and HCC1937 cell lines with IC_{50} values of 2.6 µM and 1.4 µM, respectively. The (dppm) complex exhibited great anti-breast cancer activity for a 16-fold sensitivity compared to cisplatin. The Ru(II) with *tert*-butyl pyridine (tbp), nevertheless, does not exhibit antibacterial properties. This research demonstrated that the ligand 1, 1-bis(diphenylphosphino)methane (dppm) has a significant impact on the mechanism that prevents cancer growth. In 2021, we revealed the significant cytotoxicity of [Ir(3m-ppy)$_2$(dppm)Cl] complex (Figure 7), where 3mppy is 3-methyl-2-phenyl pyridine on three breast cancer cells MCF7, HCC1937, and MDA-MB-231. The IC_{50} values of complex 1.3 µM, 0.8 µM, and 0.9 µM respectively, were significantly lower compared to cisplatin (Leesakul *et al*., 2021).

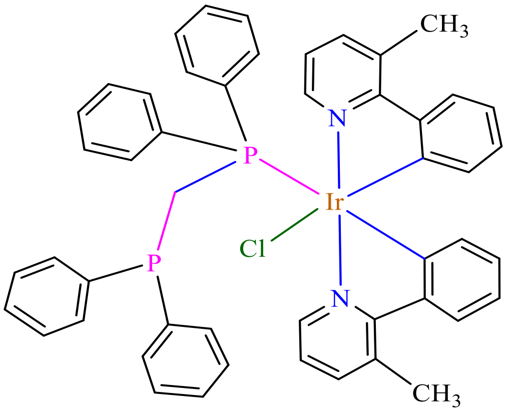

Figure 7. Structure of cyclometallated Iridium(III) complex [Ir(3m-ppy)$_2$(dppm)Cl].

Another promising and expecting to overcome the limitation and side effect of cisplatin is the investigation of using the Ir(III) complex with the same P-donor ligand. Many Ir(III) complexes exhibited promising cytotoxicity towards cancer cells *in vitro* (Liu *et al*., 2018). Our interested structure model of the Ir(III) complex is an octahedral geometry made up of the chelating ligand of 2-phenyl pyridine (ppy) and an auxiliary P-donor ligand as shown in Figure 8. The chelate ring is becoming more lipophilic due to its planarity, which makes it easier to penetrate the DNA of cancer cells and has aroused our interest in the study of P-donor ligands in cancer. Ir(III)-ppy complexes are well known structure provide the emissive luminescence which benefits in many aspects of LEDs (Leesakul *et al*., 2021), sensing, and luminescent bio-imaging (Hao *et al*., 2019), etc.

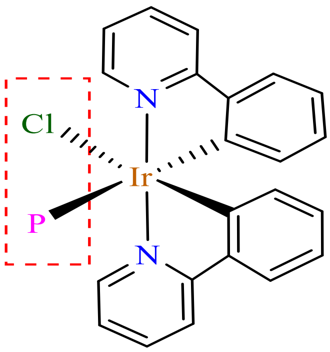

Figure 8. The Ir(III) complex octahedral geometry made up of the chelating ligand of 2-phenyl pyridine and an auxiliary P-donor ligand.

Tris(2-methoxyphenyl)phosphine (tmp) (Figure 9) is a P-donor ligand which can behave as a monodentate ligand via P atom and a bidentate ligand via P- and O- donor atoms. It is a good preference for transition metal center of the complexes. The tris(methoxyphenyl)phosphine ligand had been used as an effective ligand for Rh(II) complexes (Pruchnik *et al.*, 2001). The complexes showed good activity in vitro against tumor cell lines with higher activity than cisplatin. Besides, tmp and its derivatives were used to be ligands for Pt(II) (Crispini *et al.*, 1996), Au(I) (Bott *et al.*, 2007), Fe(II) (Liu, 2016; Niu *et al.*, 2017; Yan *et al.*, 2019), Cu(II) (Wang *et al.*, 2020), and Pd(II) (Kang *et al.*, 2009), and it is mainly used as catalyst for Suzuki coupling reaction. The complex between Ir(I) and tmp was reported the structure of [Ir(cod)(py)(tmp)](PF_6); cod is 1, 5-cycloocta-diene and py is pyridine (Bedford *et al.*, 1994). However, it has never been reported synthesis and biological activities of tris(2-methoxyphenyl)phosphine (tmp) with d^6-Ru(II) and Ir(III) structure models before. Hence, tmp ligand is our interest in generating the chelating with P- and O-donor from cracking of methoxy group possesses the novel structure with Ru(II) and Ir(III) complexes.

This study is basically to synthesize, characterize, and study their biological activities the of [Ru(*p*-cymene)(tmp)Cl]·CH_2Cl_2 (**1**), [Ir(ppy)$_2$(tmp)]·CH_2Cl_2 (**2**), and Ru(*p*-cymene)(PPh_3)Cl_2 (**3**) complexes. All the obtained complexes' structure are presented in Figure 10. Although complex 3 is not a new structure, it still lacks the reports of photo-physical properties such as the identification of electronic transition of absorption, intermolecular interaction of crystal structure and its cytotoxicity against some cancer cells. Therefore, we are interested in exploring these aspects. Various analytical techniques, such as spectroscopy (^{1}H-NMR, FTIR, UV-visible), elemental analysis, and single crystal X-ray diffraction, were used to examine the certain structure. In addition, photoactive complex [Ir(ppy)$_2$(tmp)]·CH_2Cl_2 was also studied for its photophysical properties; this complex was crucial in serving as a Fe(III) sensing property. The biological activities of all complexes were investigated. The anti-breast cancer activities were measured by using the MTT assay against MCF-7, HCC1937, BT-549, and MDA-MB-231. The measurements were measured at the Faculty of Medicine and Faculty of Pharmaceutical Science (under the supervision of Prof. Dr. Adisorn Ratanaphan), Prince of Songkla University. Additionally, the antimicrobial activities were investigated by broth microdilution method to investigate the activities of [Ru(*p*-cymene)(tmp)Cl]·CH_2Cl_2 and [Ir(ppy)$_2$(tmp)]·CH_2Cl_2 complexes on bacteria, yeast, and filamentous fungus. The samples were received and tested by the research group of Prof. Dr. Souwalak Phongpaichit, Division of Biological Science and Center of Excellent for Innovation in Chemistry, Faculty of Science, Prince of Songkla University.

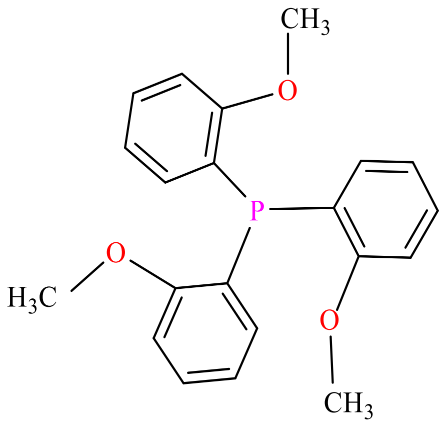

Figure 9. The structure of the tris(2-methoxyphenyl)phosphine (tmp) ligand.

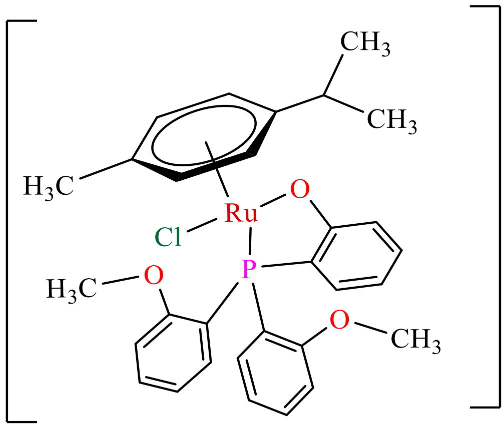

$\cdot CH_2Cl_2$ (**1**)

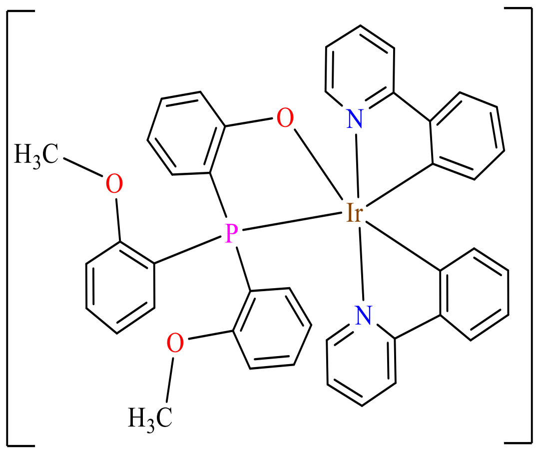

$\cdot CH_2Cl_2$ (**2**)

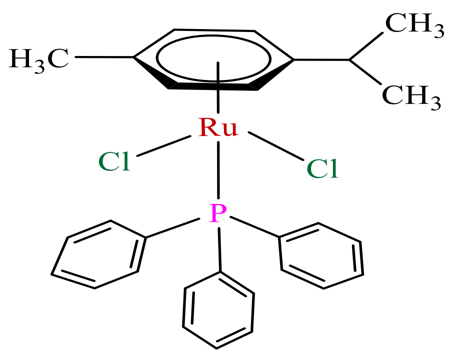

(**3**)

Figure 10. Structure of 1, 2, and 3 complexes.

1.2. Literature Review

Ruthenium and iridium complexes have gained popularity in pharmaceutical chemistry in recent years due to their fascinating biological activities and properties. Particularly, compounds containing donor atoms of N, P, O, and S show various anticancer and antibacterial properties.

Renfrew *et al.* (2010) discovered that metal complexes with phosphine ligands were attractive for medicinal chemistry, particularly ruthenium-phosphine complexes, which shown a potential antitumor activity. They also reported the synthesis of a novel bisphosphine ligand, [Ru(η^6-cymene)(PPh_2(o-C_6H_4O)-κ^2-*P, O*)(pta)]Cl (pta = 1, 3, 5-triaza-7-phosphatricyclo[3.3.1.1]decanea) complex (Scheme 1). The main purpose of this study was to design several organometallic Ru(II) molecules, RAPTA (Figure 11), including two labile chloro and pta ligands. Moreover, the complexes and ligands were characterized by many techniques such as NMR, FT-IR, MS, X-ray diffraction, and electronic techniques. The RAPTA complexes showed the growth inhabitation of A2780 ovarian cancer cell line.

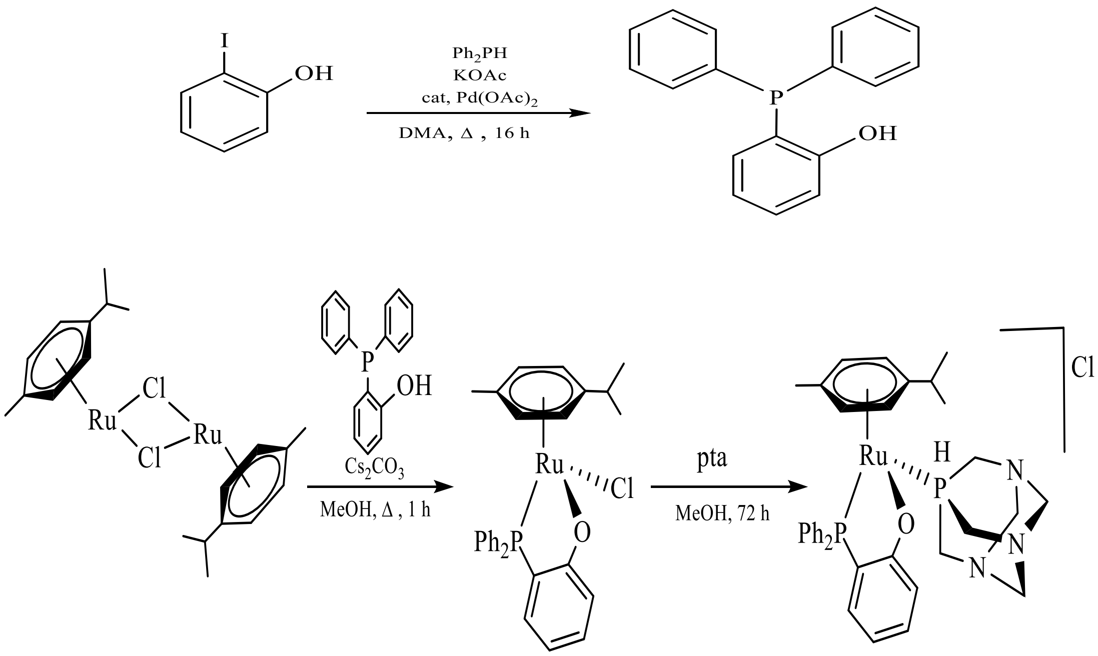

Scheme 1. Synthesis of ligand and RAPTA, -B, -C, -T.

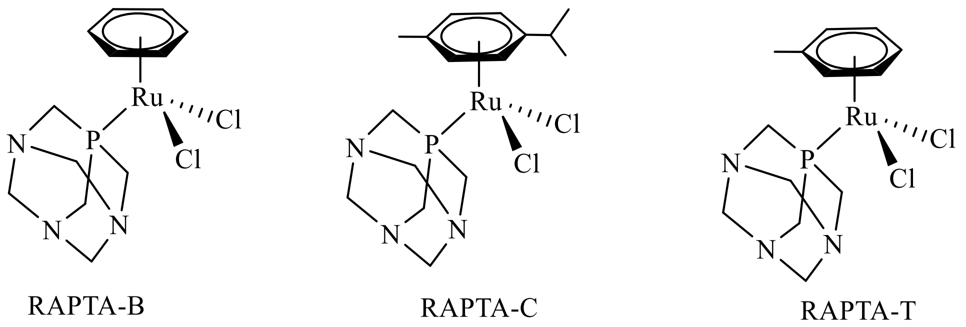

Figure 11. The initial RAPTA class of anti-metastasis drugs.

Allardyce *et al*. (2003) reported the synthesis of [Ru(η^6-*p*-cymene)X_2]$_2$ (X = Cl, Br, I, or NCS) and [Ru(η^6-*p*-cymene)X_2(pta)] (X = Cl, Br, I, or NCS; pta = 1, 3, 5-triaza-7-phosphatricyclo[3.3.1.1]decane) (Scheme 2). By the way, [H_4Ru_4(η^6-*p*-benzene)$_4$]$^{2+}$ was also synthesized. The antibacterial property of the complexes was tested by using microorganisms such as *Escherichia coli*, *Bascillus subtilis*, and *Pseudomonas aeruginosa*. Antibacterial, antifungal, and antiviral activities were all considered. The researchers examined antifungal, antiviral, and antifungal activities against *Candida albicans*, *Cladosporium resinae*, and *Trichrophyton mentagrophytes*, as well as herpes simplex and polio viruses. The findings complexes defined that the studied complexes with various ligands had variable levels of antibacterial activity.

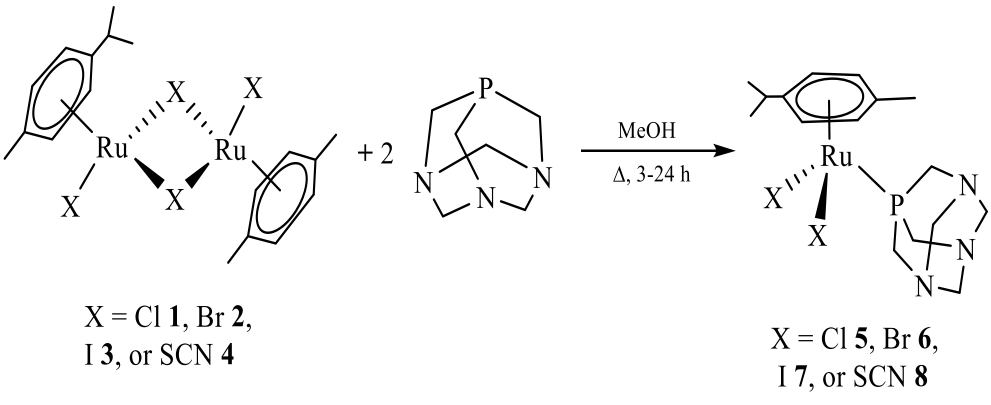

Scheme 2. The ligand and Ru(II)-arene complex are synthesized.

Honorato *et al*. (2020) synthesized and studied mononuclear, and binuclear Ru^{II}/arene/triphenylphosphine complexes with *p*-substituted benzoic acid derivatives (Scheme 3). The monocationic complexes of the [Ru(η^6-*p*-cymene)(PPh_3)L](L = benzoic acid 1, *p*-hydroxybenzoic acid 2, *p*-nitrobenzoic acid 3, and terephthalic acid 4 were characterized by NMR, matrix-assisted laser desorption/ionization-time of (MALDITOF)

MS. The geometry of complexes was confirmed by X-ray diffraction analysis. The complexes' cytotoxicity against tumorigenic [MDA-MB-231, MCF-7 (breast), A549 (lung), and DU-145 (prostate)]; non-tumorigenic [MCF-10A (breast), MRC-5 (lung), and PNT-2 (prostate)] cells were tested *in vitro*. The result defined that complex 1 prevented colony formation, generated morphological alterations in cells, and enhanced the cell cycle uptake in the Sub-G1 phase of MDA-MB-231 cells.

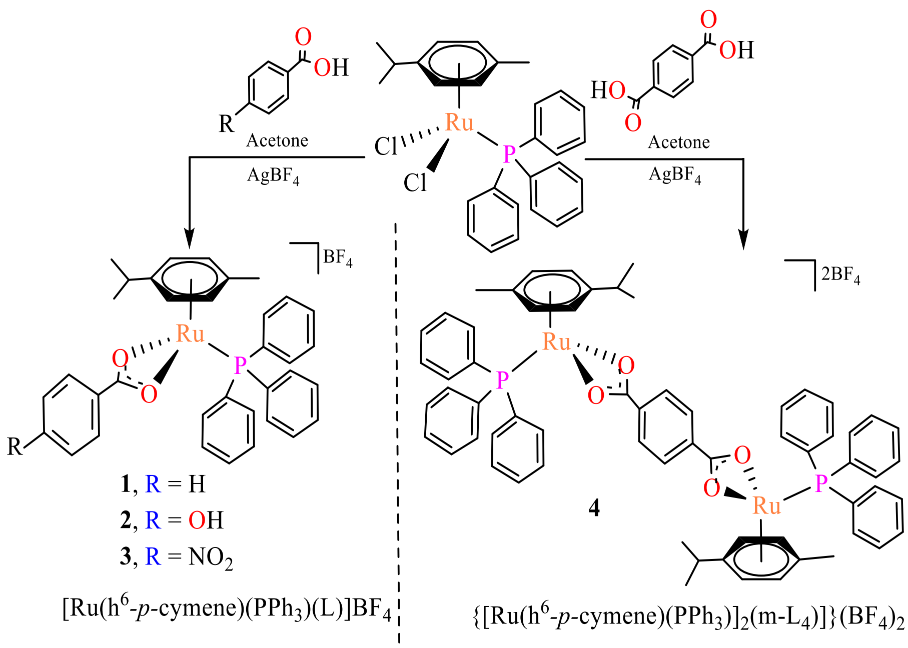

Scheme 3. Synthesis of complexes 1-3 and 4 with the following ligands: L_1, L_2, L_3, and L_4.

Engelbrecht *et al*. (2020) synthesized and investigated the anticancer activity of bis-amino-phosphine ligands with Ru(II) complexes 1. The compounds were tested by many techniques such as EA, MS, ^{1}H NMR; ^{13}C{^{1}H} NMR, and ^{31}P {^{1}H} NMR. GA113's single crystal was discovered, revealing a unique "piano-stool" structure at the Ru centers. This research emphasized a successful generalization of apoptosis in a malignant melanoma cell by two new complex 1 known as GA105 and GA113 (Scheme 4). Complexes 2 and 3 both showed good anticancer properties, with low IC_{50} values of 6.72 µM and 8.76 µM, and low toxicity against a non-malignant. Moreover, flow cytometric analyses revealed an apoptosis in the cells by complex 3.

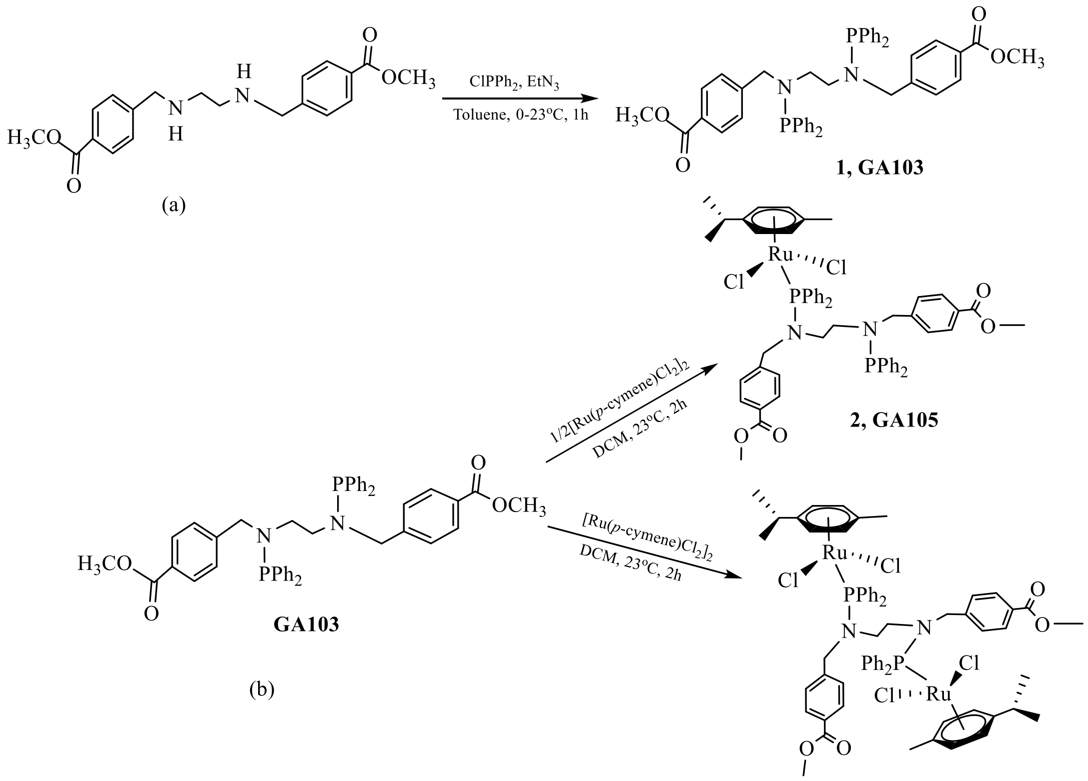

Scheme 4. Describe the synthesis of the (a) GA103, (b) GA105, and GA113 complexes.

Li *et al*. (2018) synthesized and reported on Ir^{III} pentamethylcyclopentadienyl and Ru^{II} complexes with P^P-chelating ligands that had [(Cp^x/arene)M(P^P)Cl]PF_6 (M = Ir, Cp^x was pentamethylcyclopentadienyl, or 1-biphenyl-2, 3, 4, 5-tetramethyl; M = Ru, arene was 3-phenylpropan-1-ol, 4-phenylbutan-1-ol, or (*p*-cymene), and P^P was 2, 20-bis(diphenylphosphino)-1,10-binaphthyl). Three of the compounds were characterized by X-ray crystallography, and their antitumor potential was investigated (Scheme 5). Five of these complexes had strong anticancer against HeLa and A549 but biphenyl group substitute with Cp^x in Ir complexes did not impact on antiproliferative activity. However, Ru complexes 5 had the strongest effect with 15 and 7.5 times more active than cisplatin against A549 and HeLa cells.

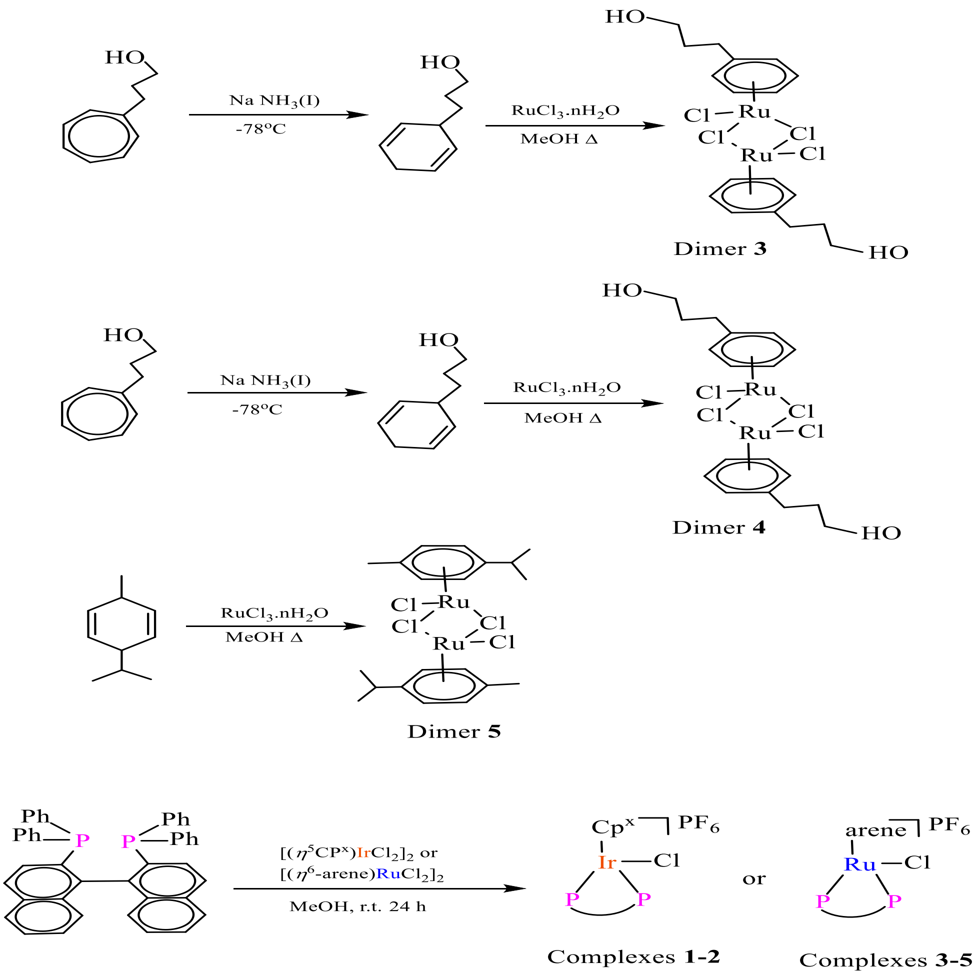

Scheme 5: Synthesis of dimers 3-5 and their respective half-sandwich Ir^{III} and Ru^{II} complexes.

Agonigi *et al*. (2015) produced and reported the antiproliferative activity of novel Ru(II) complexes and Ru(III) NAMI-A including (EA- modified-P) and (TPP) ligands (Scheme 6), (Scheme 7), and (Scheme 8). Analytical and spectroscopic approaches, as well as single-crystal X-ray diffraction, characterized all the complexes. The compounds' *in vitro* anticancer activity was investigated, and the complexes were found to have modest cytotoxicity toward human ovarian cancer cell lines. In aqueous DMSO solutions, the Ru-N bond, and N-donor-based complexes were labeled and allowed to undergo hydrolysis. The Ru-P bond was substantially steady, and separation of the EA-CO_2H was thought to occur after absorption of the related complex into the cell.

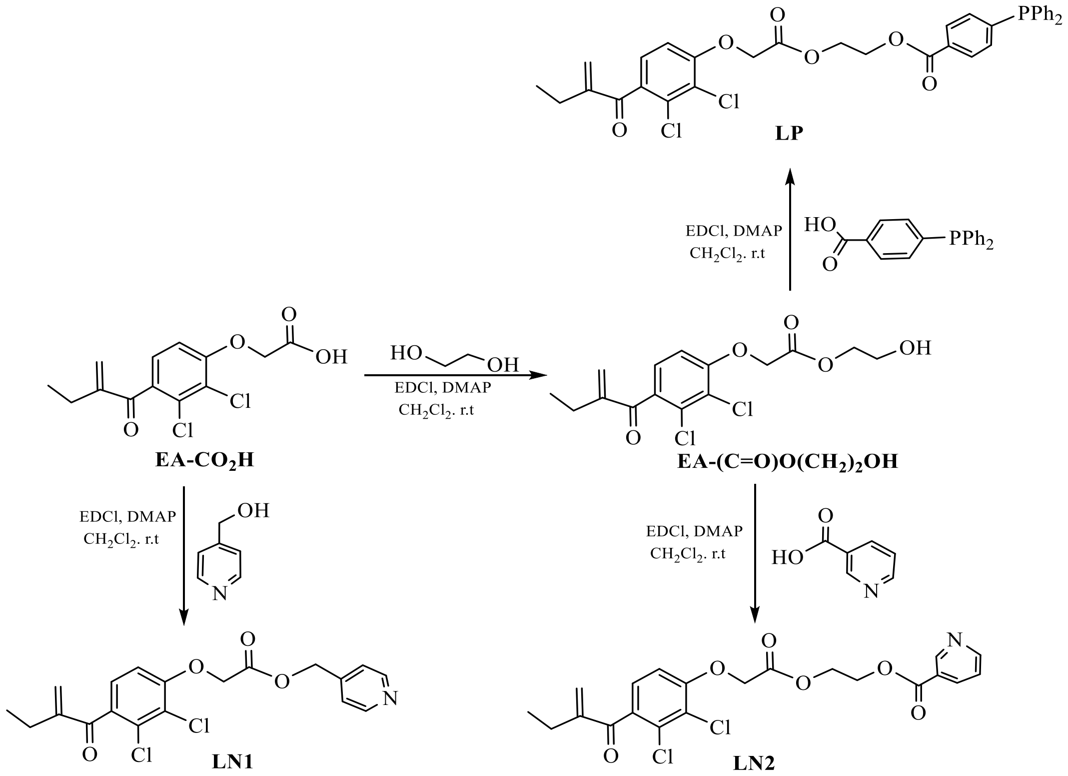

Scheme 6. Ethacrynic acid synthesis of N- and P-donor Ligands (EA-CO2H).

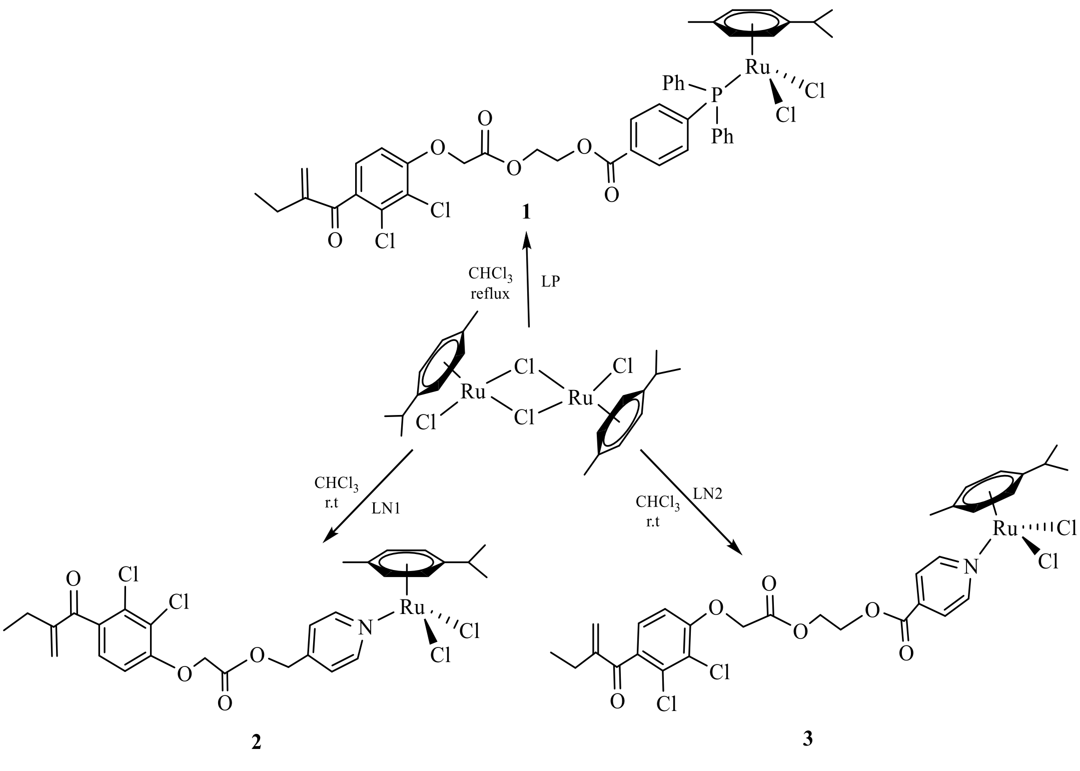

Scheme 7. Ruthenium (II)-*p*-cymene complexes containing ethacrynic-acid-sfunctionalized ligands.

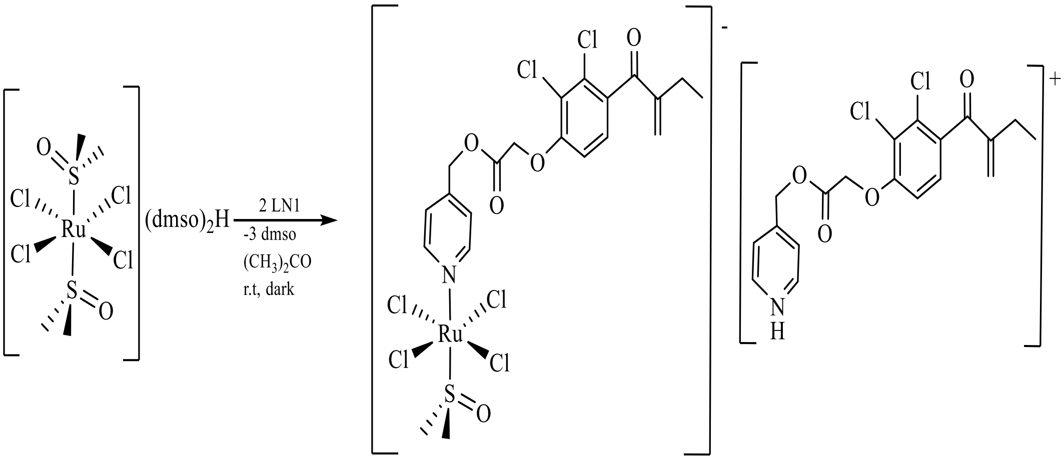

4

Scheme 8. Synthesis of 4, a NAMI-A-like complex containing the EA skeleton.

Golfeto *et al*. (2010) synthesized and studied the $[RuCl_2(NO)(dppp)(L)]PF_6$ complexes' cytotoxic activity. The complexes $[RuCl_2(NO)(dppp)(L)]PF_6$ (dppp = 1, 3 bis(diphenylphosphino)propane; L = pyridine, 4-methylpyridine, 4-phenylpyridine, and dimethyl sulfoxide) were displayed in Scheme 9. To confirm the structures of complexes with the pyridine and 4-methylpyridine ligands, elemental analysis, UV/Vis and infrared spectroscopy, cyclic voltammetry and X-ray crystallography were used to characterize the complexes. *In vitro* testing of these nitrosyl complexes exhibited cytotoxic activity against MDA-MB-231 breast carcinoma cells ranging from 7.1 to 19.0 µM, indicating that they were more active than the reference metallodrug cisplatin. At the quantities examined (highest concentration used = 200 µM), the 1, 3-bis(diphenylphosphino)propane and the N-heterocyclic ligands did not display cytotoxic sensitivity.

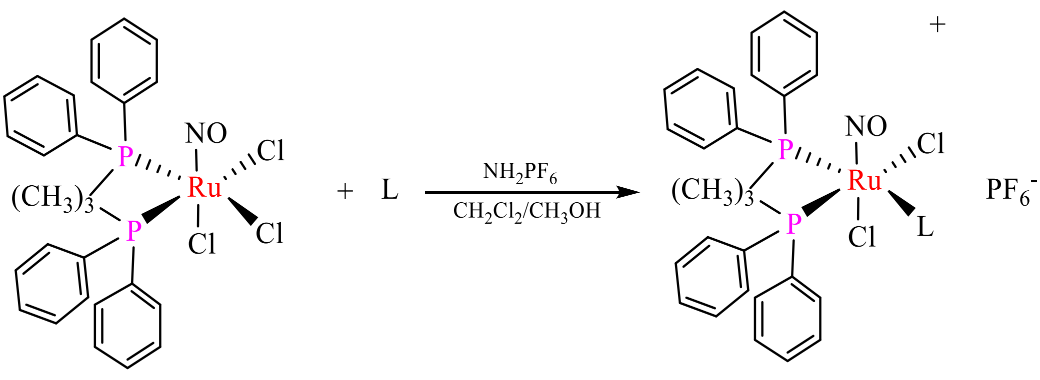

Scheme 9. L = pyridine, 4-methylpyridine, 4-phenylpyridine, and dmso.

Guerriero *et al*. (2017) developed a novel Ru(II) complexes containing the water-soluble 1, 4, 7-triaza-9-phosphatricyclo[5.3.2.1]tridecane (CAP, 1) ligand as an anticancer drug *in vitro*. Ru(II) arene complexes of CAP have been synthesized (Scheme 10 and Scheme 11). Elemental analysis, mass spectrometry, ^{1}H NMR, FT-IR, and ^{31}P{^{1}H} NMR were used to characterize. Cytotoxicity experiments against cancer cell lines showed that the compounds had more selectivity than the respective PTA counterparts in comparison to non-cancerous cells. The complexes were good cancer cell activity. The direct CAP analogue 2 was more cytotoxic to cancer cells and had a respectable level of cancer cell selectivity when compared to RAPTA-C. Other PTA-type ligands previously investigated did not exhibit the desirable cancer cell selectivity as demonstrated by the CAP.

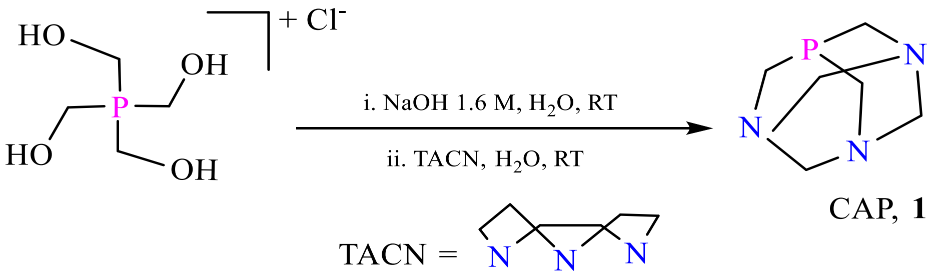

Scheme 10. Modified synthesis of ligand.

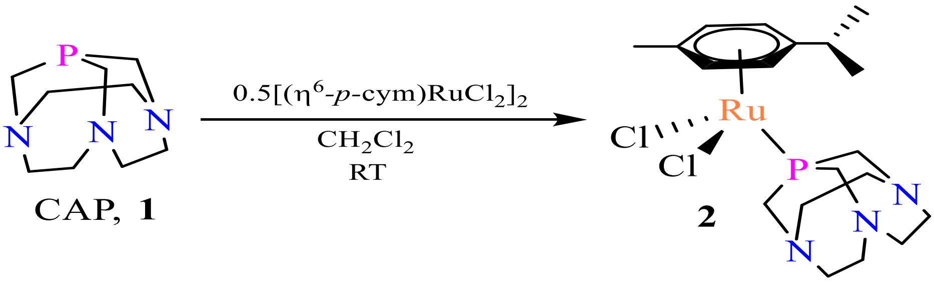

Scheme 11. Syntheses of RACAP-type complex 2.

Huber *et al*. (2012) investigated and studied Ru(II) complexes including imidazole-based P and N donor ligands. A variety of *p*-cymene Ru(II) complexes were produced with imidazol-2-yl phosphines as P and N ligands. Various complexes were synthesized: *κP, κ²N, N or κ³N, N, N*, rely on the amount of imidazolyl substitute in the ligands Ph_{3-n} $P(im)_n$ {1-3: n = 1-3, im = imidazol-2-yl (a), 1-methylimidazol-2-yl (b)} (Scheme 12). The compounds were characterized by elements analysis, MS, ^{1}H NMR, IR, UV-visible, and ^{31}P{^{1}H} NMR. The cytotoxicity of the complexes was investigated in various cancer cell lines. Most of the complexes were identified to be non-toxic; however, [(*p*-cymene)Ru(1a)Cl_2] (4a) cytotoxicity in A2780sens and Hct116 cells in the µM range, but not in H4IIE cells. The cytotoxicity was reduced when a methyl group was added, as [(*p*-cymene)Ru(1b)Cl_2] (4b) showed relatively minor toxicity in the cell lines studied. After 72 h, the *κP* complex [(*p*-cymene)Ru(2a)Cl_2] (5a) caused specific toxicity in H4IIE cells. Moreover, there was no toxicity of $\kappa^2 N, N$ [(*p*-cymene)Ru(2a)Cl]OTf (5a') complex in the tested cell lines.

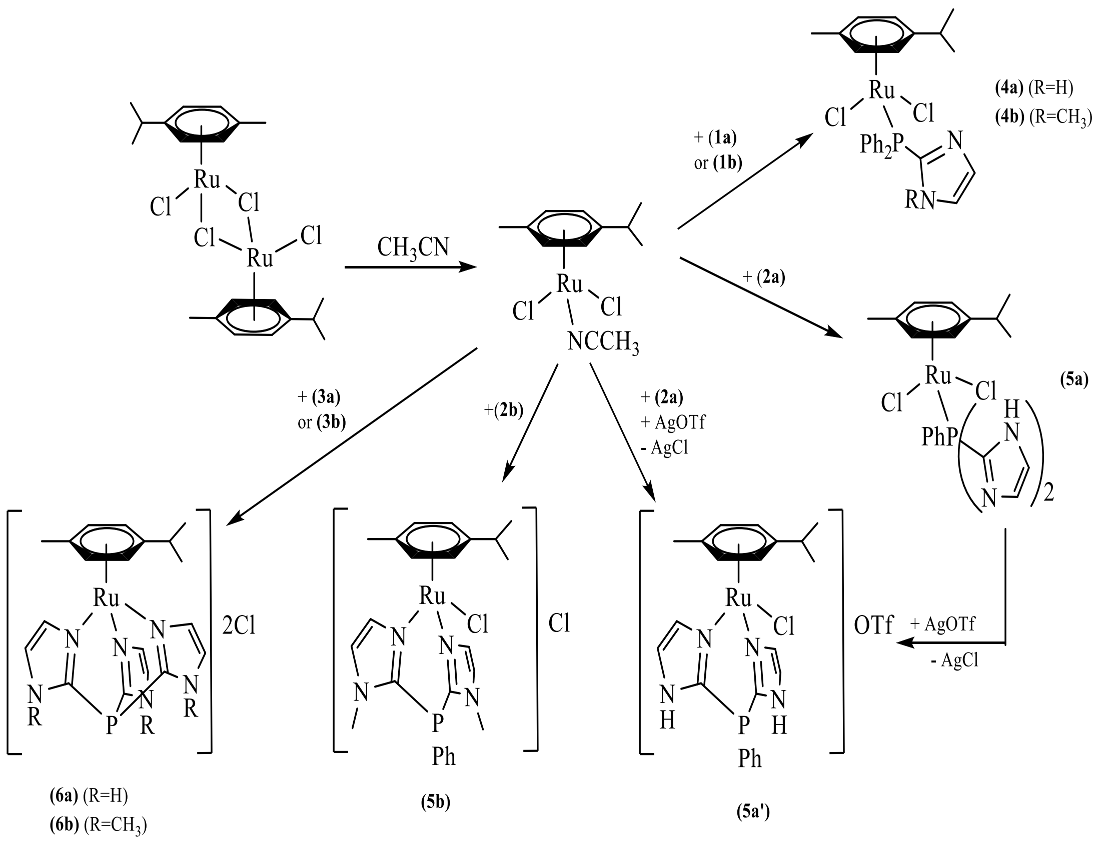

Scheme 12. Complexes were formed when [{cym)$RuCl_2$}$_2$] react with ligands in acetonitrile.

Ludwig *et al*. (2012) investigated neutral Ru(II) complexes with $Ph_2P(CH_2)_nSPh$ (n = 1, L1; 2, L2; 3, L3) reactions between ω-diphenylphosphino-functionalized alkyl phenyl sulfides, sulfoxides $Ph_2PCH_2)_nS(O)Ph$ (n = 1, L4; 2, L5; 3, L6) , and $Ph_2P(CH_2)_nS(O)_2Ph$ (n = 1, L7; 2, L8; 3, L9) and the dinuclear chloro ruthenium(II) complex [{Ru(η^6-*p*-cymen)Cl_2}$_2$] and ruthenium(II) mononuclear complexes of the [Ru(η^6-*p*-cymene)Cl_2{$Ph_2P(CH_2)_nS(O)_xPh$-κP}] coordinated

$P^nS(O)_x$ with *κP* ligands (*n/x* = 1/ 0, 1; 2/0, 2; 3/0, 3; 1/1, 4; 2/1, 5; 3/1, 6; 1/2, 7; 2/2, 8; 3/2, 9) (Scheme 13). ^1H, ^{13}C, and ^{31}P NMR techniques were used to characterize the complexes. X-ray technique was used to identify the crystal of complexes 2,7·CH_2Cl_2, and 8. Against the 518A2, 8505C, A253, MCF-7, and SW480, all complexes were tested for cytostatic activity. These complexes were sensitive against the cancer cell lines tested *in vitro*. However, Ru(II) complex of [Ru(η^6-*p*-cymene)$Cl_2Ph_2SP(CH_2)_2SPh$-*κP*] 2 had lower IC_{50} value (1.4 µM) than cisplatin (2.0 µM) in MCF-7.

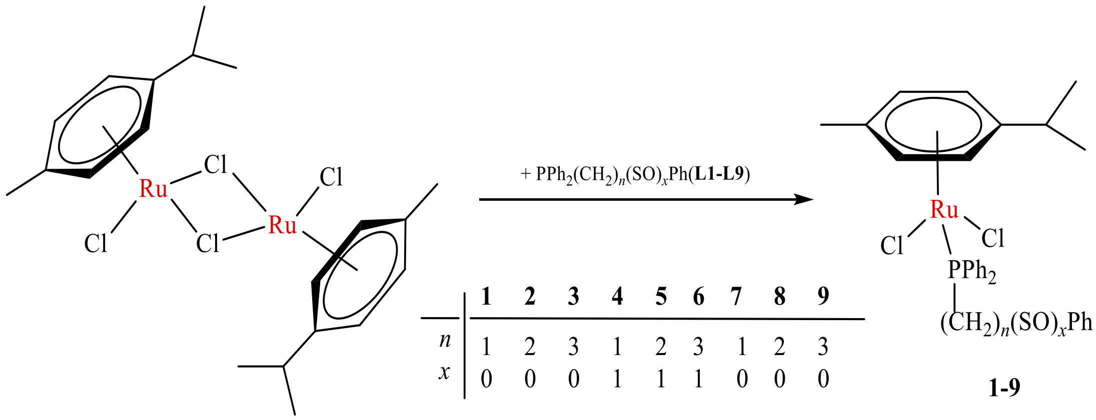

Scheme 13. Synthetic routes to Ru(II) complexes 1-9 bearing $Ph_2P(CH_2)_nS(O)_xPh$-*κP* ligands.

Sengupta *et al*. (2001) described a novel technique to synthesize Ru(II) complexes with bis(pyridine-dicarboxylato), and bis(triphenylphosphine) ligands. The X-ray diffraction analyzed the physiologically active *trans*-[$Ru(PPh_3)_2(L^1H)_2$](L^1H_2 = pyridine 2, 3-dicarboxylic acid). EA, UV-Vis, IR, NMR, and magnetic susceptibility measurements at room temperature were used to characterize the complexes. A new approach was used to make Ru(II) complexes with $Ru(LH)_2(PPh_3)_2$, (LH_2 = pyridine 2, 3-, 2, 4-, 2, 5-, and 2, 6-dicarboxylic acid) (Figure 12). All the pyridine dicarboxylic acids act as bidentate monobasic chelating donors, with one carboxyl group remaining idle. The antibacterial activity of these compounds was tested in nutritional broth against *Escherichia coli* to see they had antitumor potential. The MIC value shown that complex 1 had a very high antibacterial activity, complex 2 had a good antibacterial activity, and compounds 3 and 4 had low antibacterial selectivity.

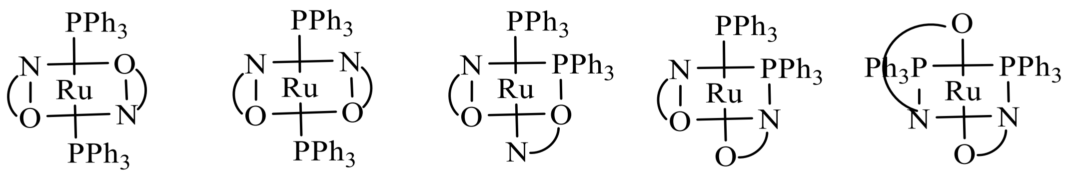

(I)	(II)	(III)	(IV)	(V)
P-P *trans*	P-P *trans*	P-P *cis*	P-P *cis*	P-P *cis*
O-O *trans*	N-O *trans*	N-O *trans*	N-N *trans*	O-O *trans*
N-N *trans*	N-O *trans*	P-O *trans*	P-O *trans*	P-N *trans*
		P-N *trans*	P-O *trans*	P-N *trans*

Figure 12. The structure of $[Ru(LH)_2(PPh_3)_2]$ (LH_2 = pyridine dicarboxylic acid) had five geometry isomers I-V complex.

Tomaz *et al*. (2012) created $[Ru^{II}(\eta^5\text{-}C_5H_5)(bipy)(PPh_3)]^+$ complex that was a prospective broad-spectrum anticancer agent, low cytotoxicity, and interaction with human serum albumin. Spectroscopic techniques (UV-Vis, NMR) were used to produce and analyze the compound. The complex was potent as an anticancer chemotherapeutic compared to cisplatin. The anticancer activity of an organometallic 'Ru^{II}Cp' compound *in vitro* was presented. $[Ru^{II}Cp(bipy)(PPh_3)][CF_3SO_3]$, also known as TM34 ($PPh_3$ = triphenylphosphine; bipy = 2, 2′-bipyridine) (Scheme 14), was tested against a panel of human tumor cell lines with different activity from cisplatin treatment, including ovarian (A2780/A2780cisR, respectively), breast (MCF7), and prostate (PC3) adenocarcinomas. TM34 was highly effective against all tumorigenic cell lines, outperforming cisplatin in terms of efficacy. The effect of TM34 on the activity of the enzyme poly (ADP-ribose) polymerase 1 (PARP-1) involved in DNA repair and apoptotic pathways was also investigated and it was discovered to be a potent PARP-1 ruthenium inhibitor in the low micromolar range (IC_{50} = 1.0 ± 0.3 μM).

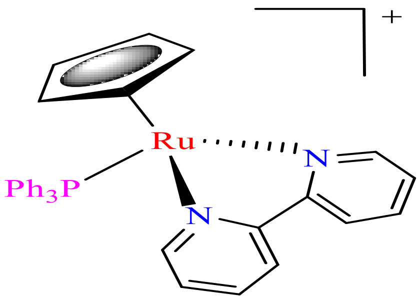

Scheme 14. Chemical structure of [RuII(η^5-C_5H_5)(bipy)(PPh_3)]$^+$ (TM34) complex.

Vijayan *et al*. (2015) synthesized the two novels Ru(II) complexes of [Ru(H-Nap-sbdtc)Cl(CO)(EPh_3)$_2$]; H-(Nap-sbdtc) = 2-hydroxy-1-napthaldehyde-S-benzyl-dithiocarbazate; E = P or As] that useful for ruthenium complexes with pharmacological properties (Scheme 15). The compounds were characterized by EA, FT-IR, UV-visible, ^{1}H, ^{13}C, and ^{31}P NMR, and ESI-MS. The complexes' interactions with DNA and BSA were further investigated by the EMB technique, which demonstrated that they had good cleavage characteristics. *In vitro* anticancer effectiveness was assessed by using MTT, (AO/EB), and (DAPI) staining against the human cervical carcinoma (HeLa).

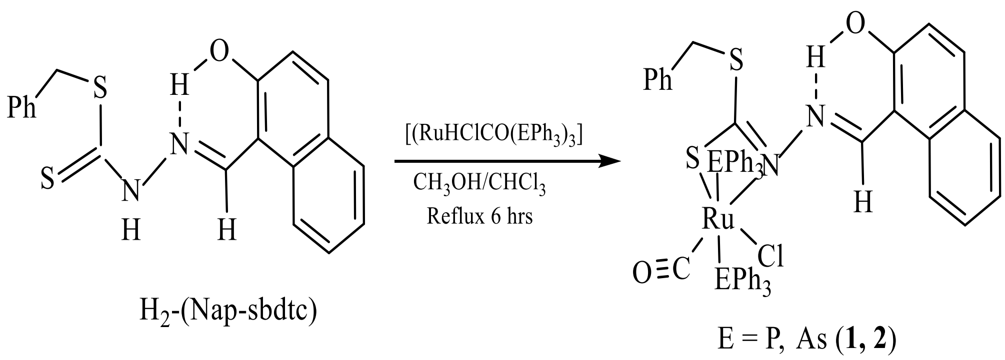

Scheme 15: The complexes disclosed in this paper's synthetic strategy. Unusual, coordinated groups were depicted in different hues.

da Silva et al. (2017) synthesized bis(diphenylphosphino) amines-containing Ru complexes as potential anti-*Mycobacterium tuberculosis* (anti-MTb) agents. This research studied the synthesis, characterization, and anti-MTb of a novel family of complexes with [RuCl(η^6-*p*-cymene)(P-N^R-P)]X (R = CH_2Py (Py = pyridine)-[1a], CH_2Ph(Ph = phenyl)-[1b], Ph-[1c], and *p*-tol (*p*-tol = *p*-tolyl)-[1d]; X = PF_6^- or BF_4^-). NMR ^{1}H, ^{31}P{^{1}H}, FT-IR, ESI-MS, MC, EA, and X-ray techniques were used to comprehensively describe the complexes (Scheme 16). The geometry of [1a]·PF_6, [1c]·BF_4, and [1d]·PF_6 had been analyzed by X-ray crystallography, spectroscopic techniques, elemental analysis, and ESI-MS. The compounds showed promise as anti-MTb drugs, with MIC_{90} values comparable to ethambutol, the study's reference medication, and compound [1a]. The additional BF_4 exhibited anti-*Mycobacterium tuberculosis* activity.

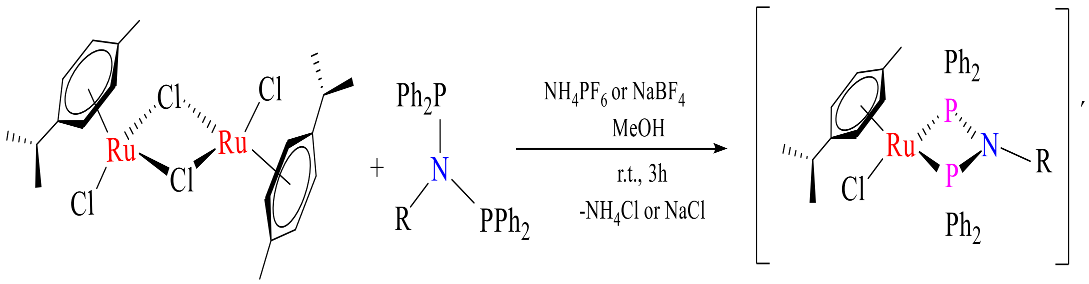

Scheme 16. The synthesis of [1a]–[1d]·X (X = BF_4^- or PF_6^-), R = CH_2Py [1a], CH_2Ph [1b], Ph [1c], and *p*-tol [1d].

Li *et al*. (2018) studied highly potent half-sandwich iridium (Ir) and ruthenium (Ru) complexes as lysosome-targeted imaging and anticancer agents. Six half-sandwiches of Ir(III) and Ru(II) complexes containing P^P-chelating ligands 1, 2-bis(diphenylphosphino)benzene (dppbz) and 1, 8-bis(diphenylphosphino)naphthalene (dppn) were synthesized (Scheme 17). The complexes were characterized by ^{1}H-NMR, ^{31}P-NMR, MS, elemental analysis, and X-ray crystallography. Complex Ir3 was measured by confocal microscopy and self-luminescence. It was discovered that Ir3 complex penetrated A549 cells through energy-dependent active transport, accumulated specifically, affected the permeabilization of the lysosomal membranes, and caused lysosomal damage, which led to caspase-dependent cell death.

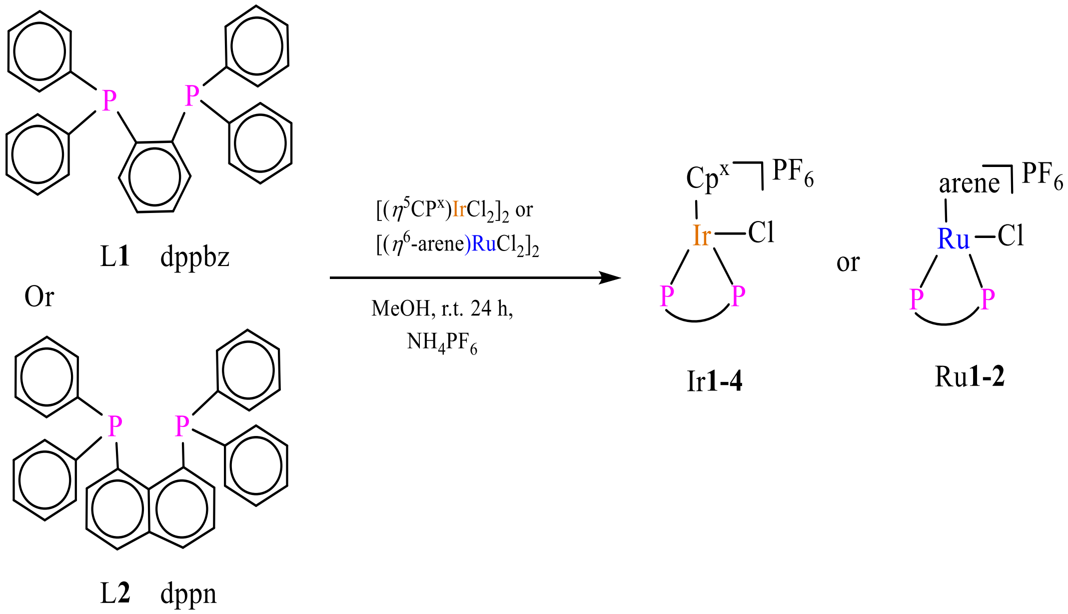

Scheme 17. Synthesis of the half-sandwich IrIII and RuII P^P complexes.

Leesakul *et al*. (2021) synthesized the reaction between the dimeric [$Ir_2(3mppy)_4Cl_2$] and (dppm) ligand in an inert atmosphere of the photoactive complex [Ir(3m-ppy)$_2$(dppm)Cl] (dppm = bis(diphenylphosphino) methane, 3-m-Hppy = 3-methyl-2-phenylpyridine). The complex exhibited a green luminescence band at 517 nm (Scheme 18). The single X-ray diffraction, ^{1}H NMR, FT-IR, ESI-MS, Luminescence, and elemental analysis were used to characterize complex. The complex exhibited against human breast cancer cell lines MDA-MB-231, MCF-7, and HCC1937. The cytotoxicity factors of the complex were 160, 32, and 25, respectively, which were significantly higher than cytotoxicity factors obtained with cisplatin.

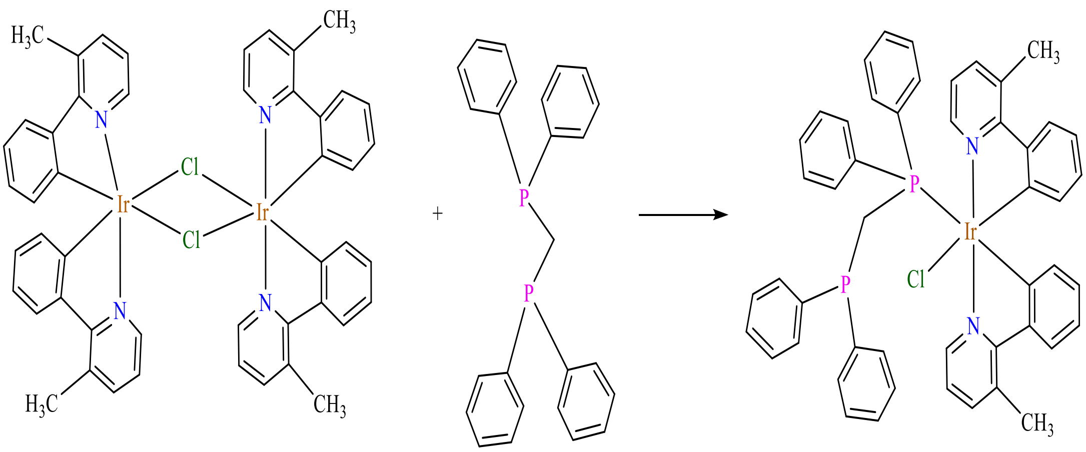

Scheme 18. Synthesis pathway of [Ir(3m-ppy)$_2$(dppm)Cl] complex.

Du *et al*. (2018) synthesized complexes anticancer activity of iridium(III) and ruthenium(II) half-sandwich of the $[(Cp^x/arene)M(P\text{^}O)Cl]PF_6$ (M = Ir, Cp^x = pentamethylcyclopentadienyl (Cp*) or its phenyl (C^{pxph} = $C_5Me_4C_6H_5$) or biphenyl (Cp^{xbiph} = $C_5Me_4C_6H_4C_6H_5$) derivatives; M = Ru, arene = *p*-cymene (*p*-cym); P^O = phosphine phosphonic amide ligand (PPOA) (Scheme 19). The complexes were characterized by single X-ray diffraction, ^1H NMR, ^{13}C NMR, MS, and elemental analysis. The complexes $[(\eta^5\text{-}C_5Me_5)Ir(P\text{^}O)Cl]PF_6$ and $[(\eta^6\text{-}p\text{-cym})Ru(P\text{^}O)Cl]PF_6$ effected and stopped the cells cycle at S phase and G_2/M phases. As the results, both complexes caused the death of HeLa carcinoma cells. Moreover, the potential platform for the synthesis of anticancer drugs was represented by this kind of this complex.

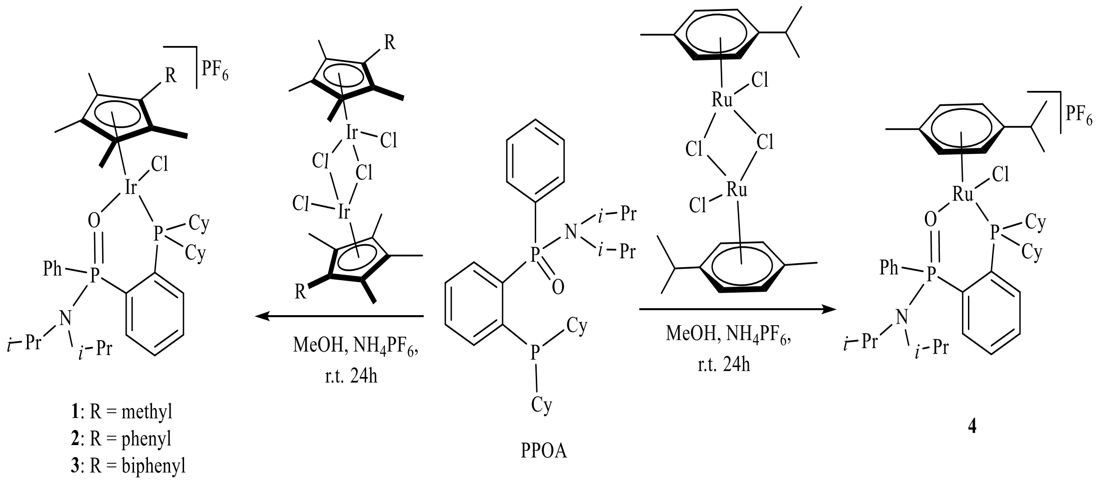

Scheme 19. Synthesis of iridium(III) and ruthenium(II) half-sandwich complexes.

Ma *et al*. (2019) studied and reported five naphthalimide-modified fluorescent biomarker half-sandwich iridium and ruthenium complexes ($[(\eta^5\text{-}Cp^x)Ir(N\text{^}N)Cl]PF_6$, $[(\eta^6\text{-}p\text{-cym})Ru(N\text{^}N)Cl]PF_6$) (Scheme 20). These complexes were characterized by ^1H-NMR, MS, UV-Visible, Fluorescence, elemental analysis, and hydrolysis. Complexes 2 and 4 showed anticancer activity higher than the activity of cisplatin as well as that exhibited by complex 5 without a fluorophore when the anticancer activities of the complexes were tested against several cancer cell lines. Flow cytometry was also used to conduct several biological experiments on complex 2, and the results showed that the complex had a range of potential antimetastatic ability to cancer cells.

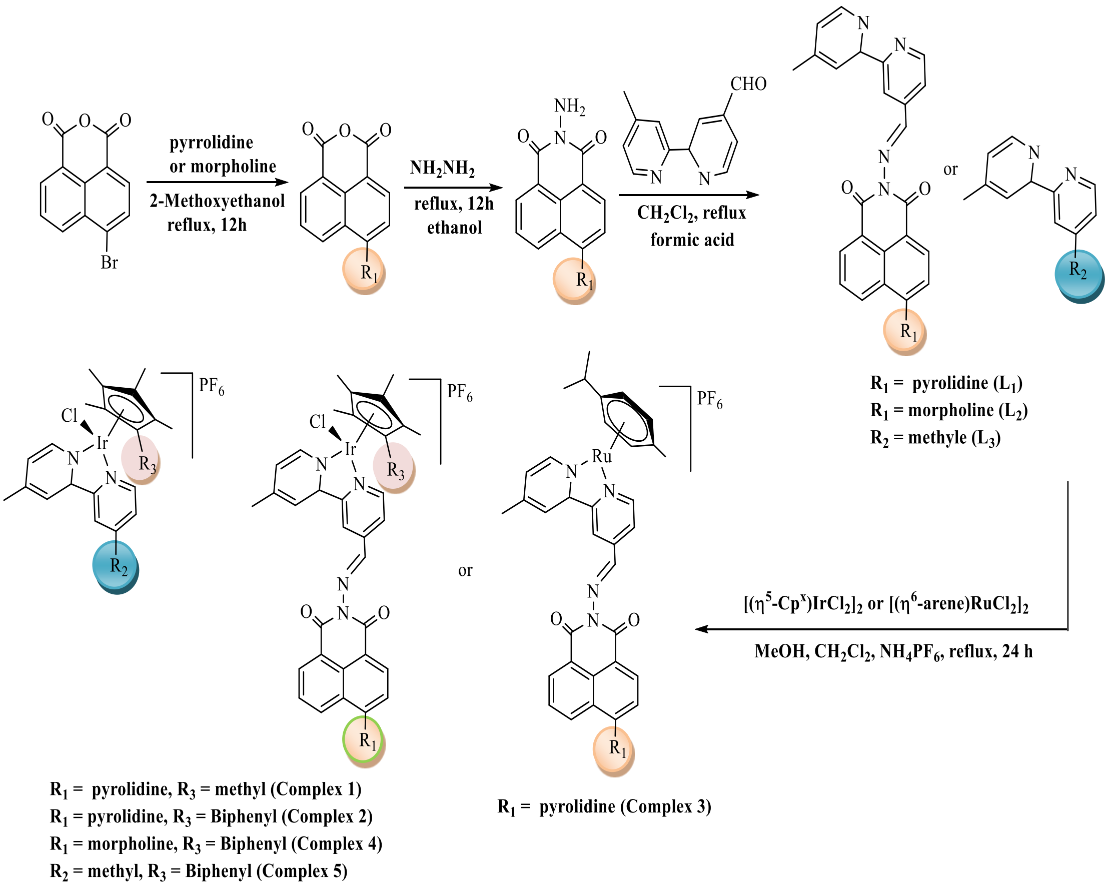

Scheme 20. Synthesis of $L_1 \sim L_3$ and complexes 1-5.

Sarwar *et al*. (2021) synthesized and created schiff-bases three new dinuclear Ir(III) azomethine complexes from *N*, *N*-bis-(3, 4-dihydroxybenzaldehyde)-4, 4-diaminodiphenylsulphide (HL^1), *N*, *N*-bis-(2-hydroxy-5-nitrobenzaldehyde)-4, 4-diaminodiphenylsulphide (HL^2), and *N*, *N*-bis-(2-hydroxy-5-chlorobenzaldehyde)-4, 4-diaminodiphenylsulfide (HL^3) (Scheme 21). The complexes were characterized by elemental analysis, FT-IR, NMR, EDX, PXRD, UV-Visible, and Photoluminescence spectroscopy. Thermogravimetric measurement of all the complexes $IrHL^3$ and $IrHL^2$ revealed thermal stability greater than 230°C before going through a breakdown and displayed the stoke's shift (Δλ) values at 285 and 289 nm. Otherwise, The $IrHL^2$ complex with a *p*-nitro substituent had the greatest activity on *Streptococcus mutant*, *Staphylococcus aureus*, and *Pseudomonas aeruginosa*, similarly with the $IrHL^3$ complex with a *p*-chloro derivative for *Streptococcus mutant*.

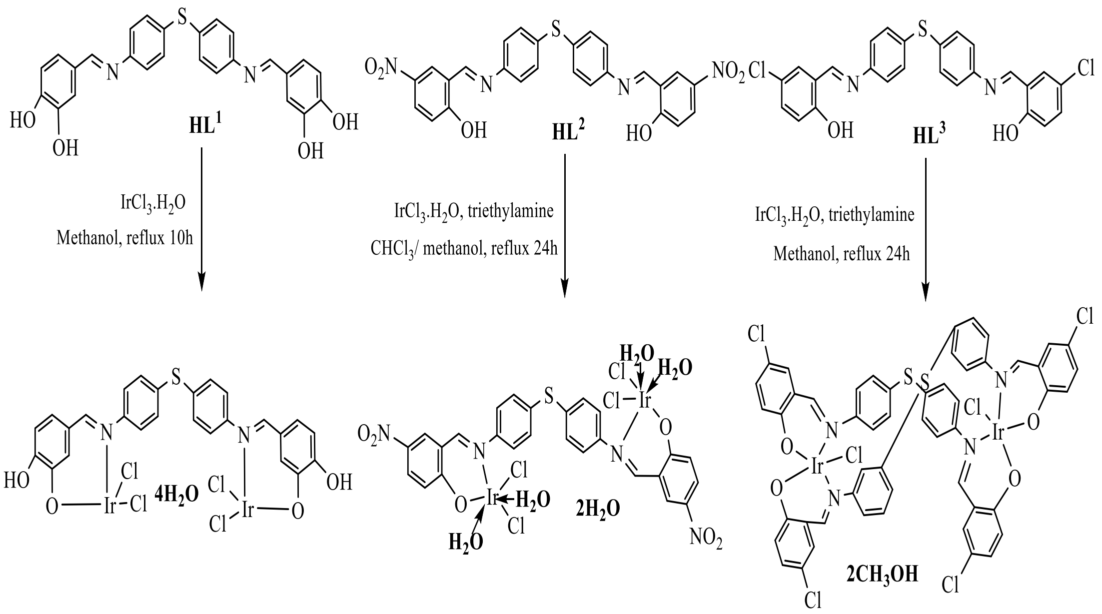

Scheme 21. Synthesis of dinuclear Ir(III) azomethine complexes (IrHL[1]-IrHL[3]).

Liu *et al.* (2019) synthesized a type of phosphorescent Ir(III) complexes containing four diverse P^P-chelating ligands of the type $[Ir(ppy)_2(L)][PF_6]$, (ppy = 2-phenylpyridine); where were L = 1, 2-bis(diphenylphosphino)benzene (L1), 1, 2-bis(diphenylphosphino)ethane (L2), 1, 2-bis(diphenylphosphino)propane (L3) and 1, 8-bis(diphenylphosphino)naphthalene (L4) (Figure 13). The complexes were characterized by single crystal X-ray diffraction, ^{1}H-NMR, UV-Visible, Fluorescence, MS, and elemental analysis. Iridium complexes, in particular complex Ir1, showed excellent antiproliferative properties against A549 cancer cells with IC_{50} = 2.4 µM lower than cisplatin (21.3 µM). It was also able to determine the subcellular localization using the self-luminescence of complex Ir1.

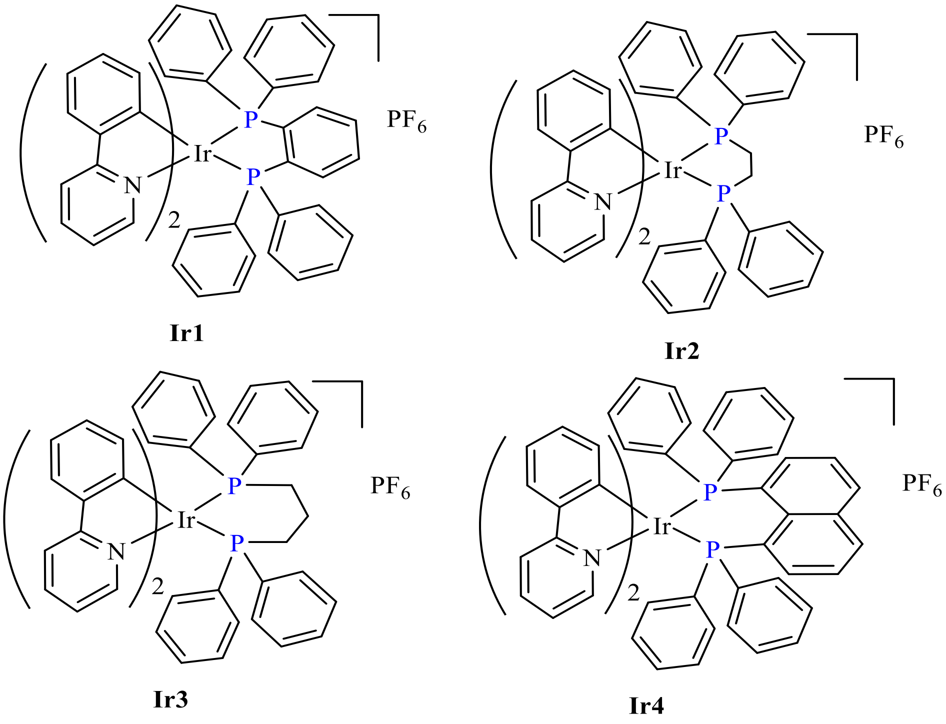

Figure 13. The structure of Ir1-Ir4 complexes.

Hao e*t al*. (2019) reported and synthesized the monitoring viscosity of mitochondria and anticancer of phosphorescence of six Ir(III) complexes (Ir1-Ir6) in the model of [Ir(ppy)$_2$L] (PF$_6$) and [Ir(ppy-CHO)$_2$)L]; L = dppm, dppe, and 1, 2-bis(diphenylphosphino)ethene (dppeth) (Figure 14). The complexes were characterized by single crystal X-ray diffraction, ^{1}H-NMR, UV-Visible, MS, and elemental analysis. Among of Ir(III) complexes, Ir6 was environment-sensitive long lifetime emission and high two-photon absorption (TPA) properties. Moreover, Ir6 was potent cytotoxicity to assemble in mitochondria leading to apoptosis and cell death.

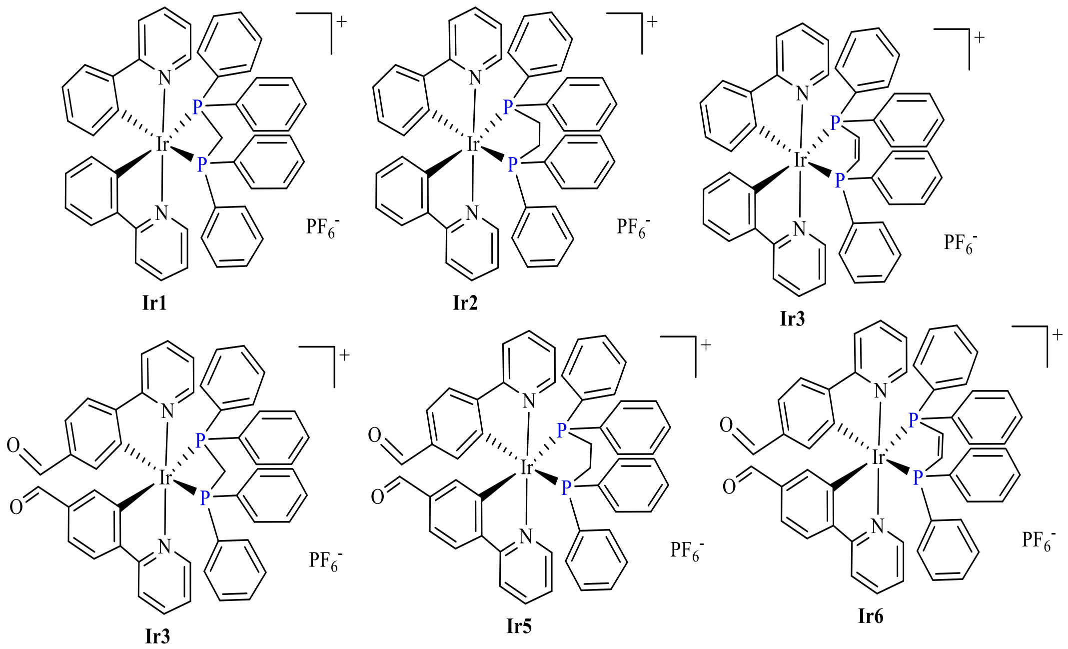

Figure 14. The structure of Ir1-Ir6 complexes.

Conesa *et al*. (2020) studied and synthesized the iridium half-sandwich complex [Ir(η^5: κ^1-$C_5Me_4CH_2$py)(2-phenylpyridine)]PF_6 (Figure 15). The complex was characterized by 3D correlative cryo-epifluorescence, cryo soft X-ray tomography (cryo-SXT), and cryo X-ray fluorescence (cryo-XRF) imaging. The complex was tested with many cancer cell lines MCF7, MDA-MB-231, MDA-MB-157, HCT 116, and A2780. Moreover, the complex was extremely low cytotoxicity against all cancer cell lines than the cisplatin used in clinical trials.

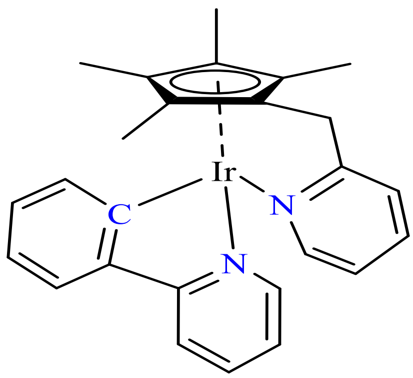

Figure 15. The structure of Iridium(III) cyclopentadienyl complex.

Bouamaied *et al*. (2012) synthesized and reported the structure of complexes [Ir(ppy)$_2$L](PF$_6$); L = 4-methylthio-6-phenyl-2, 2′-bipyridine, corresponding sulfoxide , and sulfone (Scheme 22). The complexes were characterized by single crystal X-ray diffraction, NMR, MS, UV-visible, Fluorescence, and elemental analysis. The effect of these hard and soft donor sets on the light-emitting of Ir(III) complexes were investigated. It was found that the complexes were emissive at 600, 647, and 672 nm, respectively and preliminary investigations of the electroluminescent characteristics of the Ir(III) complex with 2′-bipyridine exhibited that the complexes was not good LEC candidates.

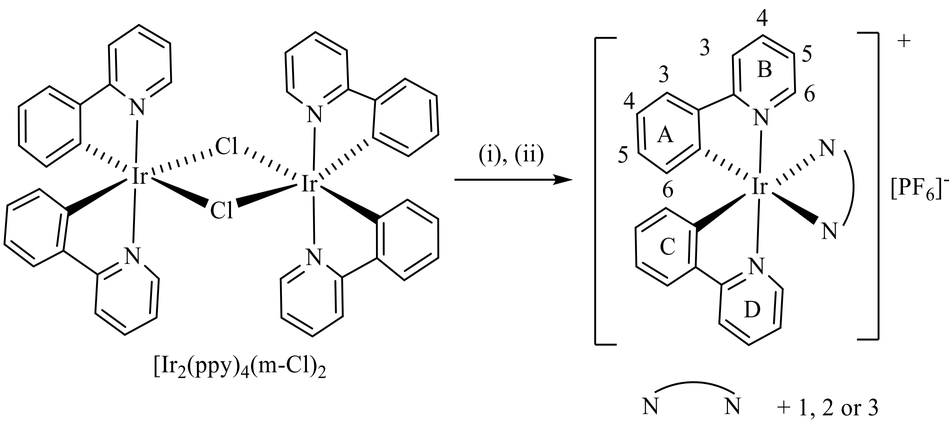

Scheme 22. Syntheses of [Ir(ppy)$_2$(L)][PF$_6$] (L = 1, 2 or 3): (i) L, (ii) NH_4PF_6.

1.3. Objectives of research

1. To synthesize [Ru(*p*-cymene)(tmp)Cl]·CH_2Cl_2, [Ir(ppy)$_2$(tmp)]·CH_2Cl_2, and Ru(*p*-cymene)(PPh_3)Cl_2 complexes and characterize by using spectroscopic methods, elemental analysis, and single crystal X-ray diffraction.
2. To assess the biological activities of the synthesized complexes against antibacterial, antifungal, and anti-breast cancer.
3. To study photo-physical properties and application on luminescent sensor of [Ir(ppy)$_2$(tmp)]·CH_2Cl_2 complex toward metal ions.

CHAPTER 2

EXPERIMENT

2.1. Synthesis of complexes

2.1.1. Materials

2.1.1.1. Chemical substances

- Products from SIGMA-ALDRICH CHEMIE GmbH
  1. 2-Ethoxylethanol, $C_2H_5OCH_2CH_2OH$, A.R. grade
- Products from TCI
  1. Dichloro(*p*-cymene) ruthenium(II) dimer, $C_{20}H_{28}Cl_4Ru_2$. A.R. grade
  2. Tris(2-methoxylphenyl)phosphine, $C_{21}H_{21}O_3P$. A.R. grade
  3. Triphenylphosphine, $C_{18}H_{15}P$. A.R. grade
  4. Iridium(III) Chloride Hydrate, $IrCl_3.xH_2O$. A.R. grade
  5. 2-Phenylpyridine, C11H9N. A.R. grade

2.1.1.2. Solvents

- Products from LOBA Chemie
  1. Benzene, C_6H_6, A.R. grade
  2. Methanol, CH_3OH, A.R. grade
  3. Diethyl ether, $(C_2H_5)_2O$, A.R. grade
- Products from RCL labScan
  1. Acetone, CH_3COCH_3, A.R. grade
  2. Acetonitrile, CH_3CN, A.R. grade
  3. Dichloromethane, CH_2Cl_2, A.R. grade
  4. Dimethylformamide (DMF), $HCON(CH_3)_2$, A.R. grade
  5. Dimethyl sulfoxide (DMSO), $(CH_3)_2SO$, A.R. grade
  6. Ethanol, C_2H_2OH, A.R. grade
  7. Hexane, C_6H_{14}, A.R. grade
  8. Tetrahydrofuran (THF), C_4H_8O, A.R. grade
- Products from BHD
  1. Chloroform, $CHCl_3$, A.R. grade

- <u>Product from Fisher Chemical</u>
    1. Ethyl acetate, $CH_3COOC_2H_5$, A.R. grade

2.2. Synthesis

2.2.1. Synthesis of [Ru(p-cymene)(tmp)Cl]·CH_2Cl_2, complex 1

The [Ru(*p*-cymene)(tmp)Cl]·CH_2Cl_2 complex was prepared by the reaction between dichloro(*p*-cymene)ruthenium(II) dimer (0.183g, 0.3 mmol) with tris(2-methoxyphenyl)phosphine (0.211g, 0.6 mmol) ligand in dichloromethane (DCM 15 mL) at room temperature under Ar gas. The mixing solution of these substances was stirred for 1.5 h. After that, the compounds were crystallized by adding dichloromethane and acetonitrile ratio (2:1 mL) and left it a few days to get the single crystal. The obtained brown crystal was washed with diethyl ether twice. The percent yield was 28.50% and melting point was 197-198^{o}C.

2.2.2. Synthesis of [Ir(ppy)$_2$(tmp)]·CH_2Cl_2, complex 2

The [Ir(ppy)$_2$(tmp)]·CH_2Cl_2 complex was prepared by the reaction between the [Ir_2(2-ppy)$_4$$Cl_2$] dimer (0.134g, 0.125 mmol) and tris(2-methoxyphenyl)phosphine (0.250 mmol, 0.088g) ligand in dichloromethane (DCM 20 mL) then refluxed for 8 h at 40^{o}C under Ar gas. After that, the synthesized compounds were filtrated and evaporated to half of volume then crystallized by dichloromethane and left it for few days to obtain the single crystal. The obtained yellow crystal gave percent yield 41.81% and melting point at 350^{o}C.

2.2.3. Synthesis of Ru(*p*-cymene)(PPh_3)Cl_2, complex 3

The Ru(*p*-cymene)(PPh_3)Cl_2 complex was prepared by the reaction between dichloro(*p*-cymene)ruthenium(II) dimer (0.183g, 0.3 mmol) consequence with triphenylphosphine (0.157g, 0.6 mmol) ligand in tetrahydrofuran (THF 20 mL) at 40^{o}C. The mixing solution of these substances was stirred for 1.5 h. After that, the compounds were filtrated and crystallized by adding dichloromethane and acetonitrile 1:2 ratio and diffused vapor with diethyl ether 10 mL and left it a few days to receive the single crystal. The obtained brown single crystals of complexes were recovered and washed again with diethyl ether. The obtained brown single crystals gave percent yield of 61.86% and melting point of 194-195^{o}C. In dichloromethane and $CDCl_3$, the complex crystals were entirely soluble. The complex was recrystallized again in the same solvent mixture. The complex crystals were entirely soluble in dichloromethane and $CDCl_3$.

2.3. Characterization

2.3.1. Elemental analysis

Elemental analyzers operate by rapidly increasing an element's temperature to the temperature where it combusts. Subsequently, it was introduced into the analyzer while remaining in a gaseous condition. The researcher used a computer to read the information that a detector reads about the elements present. The elemental analysis data was obtained by using Dynamic Flash Combustion, CHNS/O analyzer, Flash 2000, and Thermo-Scientific, Italy. The complexes were weighed 30 mg and sent to the office of Science Instrument and Testing (OSIT), Prince of Songkla University.

2.3.2. Nuclear magnetic resonance spectroscopy

In order to obtain an NMR spectrum, the magnetic field needs to be varied or swept over a narrow range while the sample's RF signal is being monitored. Adjusting the frequency of the RF radiation while keeping the external field constant is an equally efficient technique. With a Varian Bruker Avance 300 MHz NMR spectrometer, proton nuclear magnetic resonance (^{1}H-NMR) spectra were obtained by using $CDCl_3$ solvent and tetramethyl silane as an internal standard (TMS).

2.3.3. Fourier transformation infrared spectroscopy

The sample was set in a holder in the IR source's path. The analog signal was read by a detector, which then transforms it into a spectrum. The signals were analyzed to find the peaks using a computer. A partially silver mirror splits an IR beam into two equal-intensity beams. A BX Perkin Elmer FT-IR spectrophotometer was used to record Fourier transform infrared (FTIR) spectra (KBr disk, 3500-500 cm^{-1}).

2.3.4. Single crystal X-ray diffraction

The Bruker SMART APEX CCD diffractometer was used to analyze the crystal structures of [Ru(*p*-cymene)(tmp)Cl]·CH_2Cl_2, [Ir(ppy)$_2$(tmp)]·CH_2Cl_2, and

Ru(p-cymene)(PPh_3)Cl_2 using graphite-mono-chromated Mo Kα radiation (λ = 0.71073Å). The SMART program was used to get the raw diffraction data of 33,925 reflections. Using SAINT v8.34A and SADABS software, raw data were merged, and absorption was adjusted. The structures of [Ru(p-cymene)(tmp)Cl]·CH_2Cl_2, [Ir(ppy)$_2$(tmp)]·CH_2Cl_2, and Ru(p-cymene)(PPh_3)Cl_2 complexes were solved by SHELXT software and refined by SHELXL. Anisotropic thermal parameters were refined for all non-hydrogen atoms. The WinGX and Mercury programs were used to organize all the materials and molecular for publication.

2.4. Photo-physical properties determination

2.4.1. Computational study

The calculations were performed using the Gaussian 09 program. The computation was carried out using the PBE0 (Tabares *et al*., 2019) and B3LYP basis sets (Klaimanee *et al*., 2021) of density functional theory (DFT) in the gas phase. The ground state of the Ru(II) complex 3 was perfectly optimized in terms of shape. The basis sets of 6-31G(d) and LANL2DZ were chosen for non-metal atoms and the ruthenium atom, respectively (Roy *et al*., 2008). Then, using the (TDDFT) program and the polarizable continuum model (PCM) in dichloromethane, the electronic absorption spectrum was simulated (Mennucci *et al*., 1997).

2.4.2. UV-Visible absorption spectroscopy

A standard 1 cm cuvette was used in a UV-Visible spectrophotometer, model TU-1950, to record electronic spectra (200-800 nm). The visible and ultraviolet light sources were provided tungsten and deuterium lamps, respectively. The [Ru(p-cymene)(tmp)Cl]·CH_2Cl_2, [Ir(ppy)$_2$(tmp)]·CH_2Cl_2, and Ru(p-cymene)(PPh_3)Cl_2 complexes were prepared by different concentrations with dichloromethane for complexes **1** and **3**, and complex **2** with dimethylformamide (DMF) at room temperature. Beer-Lambert's law was used for calculating the molar coefficient as shown in equation 1.

$$A = \varepsilon bc \qquad (\mathbf{1})$$

Definition:

- A is the absorbance value of the sample.

- ε is molar extinction coefficient (M^{-1} cm^{-1}).
- b is the path length of light throughout the sample (cm).
- c is the concentration of the sample (M).

2.4.3. Photoluminescence and quantum yield

The relative quantum yield was measured by comparing the luminescent intensities and absorbances (as optical density) of complex **2** and reference standard of coumarin 6. The following equation 2 of Kotelevskiy (Kotelevskiy, 1998) was used to compute the internal emission quantum yields (Φ):

$$\Phi_S = \Phi_R \times \frac{I_S(1-1^{-OD_R})}{I_R(1-1^{-OD_S})} \times \left(\frac{n_S}{n_R}\right)^2 \quad \textbf{(2)}$$

<u>Definition</u>:

- $\Phi_{\boldsymbol{S}}$ represents quantum yield (%) of the sample [Ir(ppy)$_2$(tmp)]·CH_2Cl_2.
- $\Phi_{\boldsymbol{R}}$ represents quantum yield (%) of reference standard (coumarin 6).
- I_S represents integrated areas of the sample.
- I_R represents integrated areas of reference.
- OD_S is the optical density of the sample wavelength (nm).
- OD_R is the optical density of the reference wavelength (nm).
- n_S is the refractive index of solvent use with sample.
- n_R is the refractive index of solvent use with reference.

Using the Kotelevskiy equation, the relative quantum yield of [Ir(ppy)$_2$(tmp)]·CH_2Cl_2 in dimethylformamide (DMF) was estimated at 25^{o}C. The concentration 5.0 μM of courmarin-6 was diluted in ethanol at 25^{o}C as a reference standard, and the corresponding concentration of [Ir(ppy)$_2$(tmp)Cl]·CH_2Cl_2 sample was diluted in DMF. The absorbances of these two solutions were below 0.05 of absorbance, which prevented a self-quenching reaction. The emission spectra were excited at 380 nm. The quantum yield of the reference standard, coumarin-6 in ethanol at 25°C, is 0.78 (Jiménez Riobóo *et al*., 2009; Yoopensuk *et al*., 2012).

2.4.4. Quenching reaction

The luminescence of [Ir(ppy)$_2$(tmp)]·CH_2Cl_2 complex was performed the quenching reaction with various types of metal ions (Ba^{2+}, Co^{2+}, Cu^{2+}, Fe^{3+}, Ni^{2+},

Mg^{2+}, Pb^{2+}, and Zn^{2+}). Solutions containing a fix concentration at 3×10^{-5} M of $[Ir(ppy)_2(tmp)]\cdot CH_2Cl_2$ complex and varied concentrations of 1×10^{-6}-9×10^{-5} M of metal ions were created. Moreover, the Stern-Volmer plot was used to determine the Stern-Volmer constant in order to give the result of how good electron can be transferred.

The job plot was used to determine whether the complex formed in a 1:1 ratio of stoichiometric binding mode. By maintaining the molar concentration of the Ir(III) complex and changing the mole fraction (χ) of Fe(III) solution, the approach could be investigated. The mole fraction of selective metal ion is shown on the x-axis of this plot, while the monitoring physical characteristic (fluorescence intensity times the mole fraction of the selective metal ion) is shown on the Y-axis. The greatest point at χ = 0.5 gives the 1:1 stoichiometry of Ir(III) and Fe(III). For the binding constant (K_b) between the complex 2 and the selective metal ion using the Benesi-Hildebrand equation 3.

$$\frac{1}{I_O - I} = \frac{1}{I_0 - I_C} + \frac{1}{K_b(I_0 - I_C)\times[Q]} \quad \textbf{(3)}$$

Definition:

- I_0 is the initial fluorescence intensity of a complex without quencher.
- I_c is fluorescent intensity of quencher bounded with complex.
- I is fluorescence intensity of complex in each concentration of quencher.
- $[Q]$ is the concentration of metal ions.

2.5. Biological activity

2.5.1. Antimicrobial activity

2.5.1.1. Test microbial activity

Bacteria

- *Staphylococus aureus* ATCC25923
- *Eschericchia coli* ATCC25922
- *Pseudomonas aeruginosa* ATCC27853
- Methiciline-resistant *Staphylococus aureus* SK1 (MRSA-SK1) isolated from the patient by the pathology Department, Faculty of Medicine, Prince of

Songkla University.

<u>Yeast</u>

- *Candida albricans* ATCC90028
- *Cryptococcus neoformans* ATCC90113 (*C. neoformans*)

<u>Filamentous fungus</u>

- *Microsporum gypseum* SK-MU4
- *Talaromyces marneffei* PSU-SK

2.5.1.2. Chemical

- 5% of Sodium hypochlorite (Clorox)
- Ethanol (Commercial grade)
- Lacto phenol cotton blue
- 0.85% of NaCl and Normal Saline solution (NSS)
- Teepol
- McFarland Standard
- 15% of glycerol (MERCK)

2.5.1.2.1. Media

▪ Potato dextrose agar (PDA)	(Difco)
▪ Potato dextrose broth (PDB)	(Difco)
▪ Mueller-Hinton agar (MHA)	(Difco)
▪ Sabouraud dextrose agar (SDA)	(Difco)
▪ Sabouraud dextrose broth (SDB)	(Difco)
▪ Nutrient agar (NA)	(Difco)
▪ Nutrient broth (NB)	(Difco)
▪ RPMI-1640 without phenol-red (pH = 7)	(Sigma Chemical)

2.5.1.2.2. Antibiotics

▪ Vancomycin	(Fujisawa)
▪ Amphotericin B	(Bristol-Myer Squibb)
▪ Clotrimazole	(Public Pharmaceutical Lab)
▪ Gentamicin	(Oxoid)

2.5.2. Method

2.5.2.1. Screening for antimicrobial activities

2.5.2.1.1. Inoculum preparation

On Sabouraud dextrose agar (SDA), *Candida albicans* ATCC90028 and *Candida neoformans* ATCC90112 were streaked. After that *C. albricans* ATCC90028 was incubated for 18-24 h at 35^{o}C. Otherwise, *C. neoformans* ATCC90112 was incubated at room temperature for 48 h.

Moreover, all the bacteria (*S. aurea* ATCC25923, MRSA-SK1, *P, aeruginosa* ATCC27853, and *E. coli* ATCC25922) were streaked on nutrient agar (NA) then incubated at 35^{o}C for 18-24 h. The *C. albicans* ATCC9008 and *C. neoformans* ATCC90112 were collected in RPMI-1640. In nutritional broth (NB), three to five isolated bacterial colonies were gathered. Both bacteria were shaken at 150 rpm/min for 3 to 5 h at 35 °C. However, using sterile normal saline (NSS), yeast and bacteria reduced the turbidity to the equivalent of 2.0 MF and 0.5 McFarland standard (MF), respectively. *M. gypseum* and *P. maeneffei* agar plugs were placed on SDA and cultured for a period of two to three weeks at 25°C, or until they produced spores. The spores were carped using sterile glass plate beads and stored in a suspension with 2 mL of 0.85% NSS. A hemacytometer was used to adjust the spore suspension to 8×10^{3} spores/mL.

2.5.2.1.2. Testing for antibacterial activity (Modification of CLSI MA7-A4, 2002a)

The complexes were dissolved in dimethyl sulfoxide (DMSO) to create the stock solution, which was subsequently diluted with MHB 1 mg/mL. MHB diluted the inoculation of 0.5 MF bacteria to a concentration of 1:200 (~10^{6} CFU/mL). Then, sterile 96-well microtiter plates were filled with 20 µL of samples (1 mg/mL), 30 µL MHB, and 50 µL of bacteria inoculation (10^{6} CFU/mL). In the end, 200 µg/ml was the concentration. Moreover, the plates were incubated at 35^{o}C for 15-18 h. The plates were then incubated at 35°C for a further 3 h after 10 µL of 0.18% resazurin indicator was added to each well. To compare with our study samples, the standard antibacterial agent Gentamycin and Vancomycin were used at a final dosage of 4 µg/mL.

2.5.2.1.3. Testing for antifungal activity (yeast) (Modification of CLSI MA27-A2, 2002c)

Yeasts were tested similarly as bacteria using RPMI-1640 media. *C. albicans* microtiter plates were incubated at 35°C for 24 h, while *C. neoformans* microtiter plates were incubated at room temperature for 48 h. Then, each well received 10 µL of resazurin indicator, 0.18%, and was incubated once more at 35°C for 5 h. (Drummond and Waigh, 2000). Amphotericin (4 µL/mL) was used as the positive inhibitory control to compare with the tested samples.

2.5.2.1.4. Testing for antifungal activity (filamentous fungus) (Modification of CLSI MA38-8, 2002b)

Like the previous approach of evaluating bacteria, filamentous fungus (*M. gypmseum* and *P. marneffei*) was studied using RPMI-1640 media. Microtiter plates were first incubated for 4-7 days at room temperature. Then, 10 µL of resazurin indicator 0.18% was added to each well, and the plates underwent a second incubation for one day at 25 °C.

To compare with the examined sample, *M. gypseum* and *P. marneffei* controls were quantified using standard doses of Clotrimazole and Amphotericin B (4µL/mL), respectively. The results were presented with the positive (growth inhibition) in blue or purple and the negative (growth uninhibited) in pink. The substance's minimal fungicidal concentration (MFC), minimal bactericidal concentration (MBC), and minimal inhibitory concentration (MIC) were all assessed.

2.5.21.5. Determination of minimal inhibitory (MIC), minimal bactericidal concentration (MBC), and minimal fungicidal concentration (MFC)

The LCSI MA7-A4 (CLSI, 2002a), CLSI MA27-A2 (CLSI, 2002c), and CLSI MA38-A (CLSI, 2002b) against bacteria, yeast, and *M. gypseum*, respectively, were modified for use with the broth microdilution method for MICs testing. The testing samples were prepared using the serial dilution technique. The starting concentration of 128 µL/mL was diluted to 64, 32, 16, 8, 4, 2, 1, 0.5, and 0.25 µL/mL. Moreover, the samples were tested in triplicate.

To determine the lowest concentration that prevents microbial growth, the samples were incubated under specific conditions and the MIC method was applied (presented in purple or blue color).

The MFCs and MBCs of the compound were determined using the streaking method. Bacterial MICs were streaked on the NA plate, whereas yeasts and filamentous fungi were streaked on the SDA plate. The test samples were diluted to a level below MIC concentration.

2.6. Anticancer activity

By using the reduction of tetrazolium salt MTT [3-(4, 5 dimethylthiazolyl-2)-2, 5-diphenyltetrazolium bromide] assay (Hongthong *et al.*, 2021), it was possible to compare the cytotoxicity of [Ru(*p*-cymene)(tmp)Cl]·CH_2Cl_2, [Ir(ppy)$_2$(tmp)]·CH_2Cl_2, and Ru(*p*-cymene)(PPh_3)Cl_2 complexes to that of cisplatin and doxorubicin as the positive control in the case of MCF-7, HCC1937, BT-549, and triple-negative MDA-MB-231. At a density of 1×10^4 cells/100µL well in 96-well plates, cells were grown and left to grow for 24 h at 37°C in a 5% CO_2 incubator. The cell culture media was extracted after 24 h of incubation, and the cells were subsequently treated with various concentrations of ruthenium and iridium complexes. The [Ru(*p*-cymene)(tmp)Cl]·CH_2Cl_2, [Ir(ppy)$_2$(tmp)]·CH_2Cl_2, complexes were dissolved in 0.1% of dimethyl sulfoxide (DMSO), with final concentrations of (0, 0.625, 1.25, 2.5, 5, and 10 µg/mL) and Ru(*p*-cymene)(PPh_3)Cl_2 (0.01, 0.1, 1.5, 10, 25, 50, and 100 mM), and then incubated for 48 h at 37°C with 5% CO_2. Cells were washed twice with 100 mL of phosphate-buffered saline (PBS) after being exposed to the complexes for 48 h. Then, 100 µL of a 0.5 mg/mL MTT solution was added, and the cells were incubated for a further 4 h at 37^{o}C with 5% CO_2. After that, each well received 200 mL of 100% DMSO solvent to dissolve the purple (E, Z)-5-(-4, 5-dimethylthiazolyl-2)1, 3-diphenylformazan (formazan) crystal compound. An automated microplate reader was used to measure absorbance at 570 nm and the cell viability percentage was calculated from equation 4.

$$\text{The \% cell viability} = \frac{(\text{absorbance of Ru cpx, or Ir cpx treated cells})}{(\text{absorbance of vehicle treated cells})}\times 100 \qquad \textbf{(4)}$$

The log of the cell viability percentage versus concentration was plotted to determine the IC_{50} values. Four separate experiments were conducted, at least in triplicate, to acquire the results. The standard error of the mean S.E.M. was used to express the data as mean $\pm$ S.E.M. The variations between the mean values were compared using one-way ANOVA.

Statistical significance was defined as a probability of 0.01 or less. In this study, a $p < 0.01$ in relation to the control is denoted by the asterisk notation, *. A modified version of the Clinical and Laboratory Standards Institute (CLSI) microdilution method M07-A9 was used to evaluate the antibacterial effects of each complex in dmso solvent.

CHAPTER 3

RESULTS AND DISCUSSION

3.1. Synthesis and characterization of [Ru(*p*-cymene)(tmp)Cl]·CH_2Cl_2, complex 1

The complex **1** was prepared by the reaction between dichloro(*p*-cymene)ruthenium(II) dimer and tris(2-methoxyphenyl)phosphine ligand in dichloromethane (Scheme 23). Complex **1** is a neutral compound. The solubility of this complex is shown in Table 1. Complex **1** can completely be dissolved in organic solvents like dichloromethane, chloroform, acetonitrile, acetone, DMF, DMSO, ethanol and methanol. However, it cannot be dissolved in water.

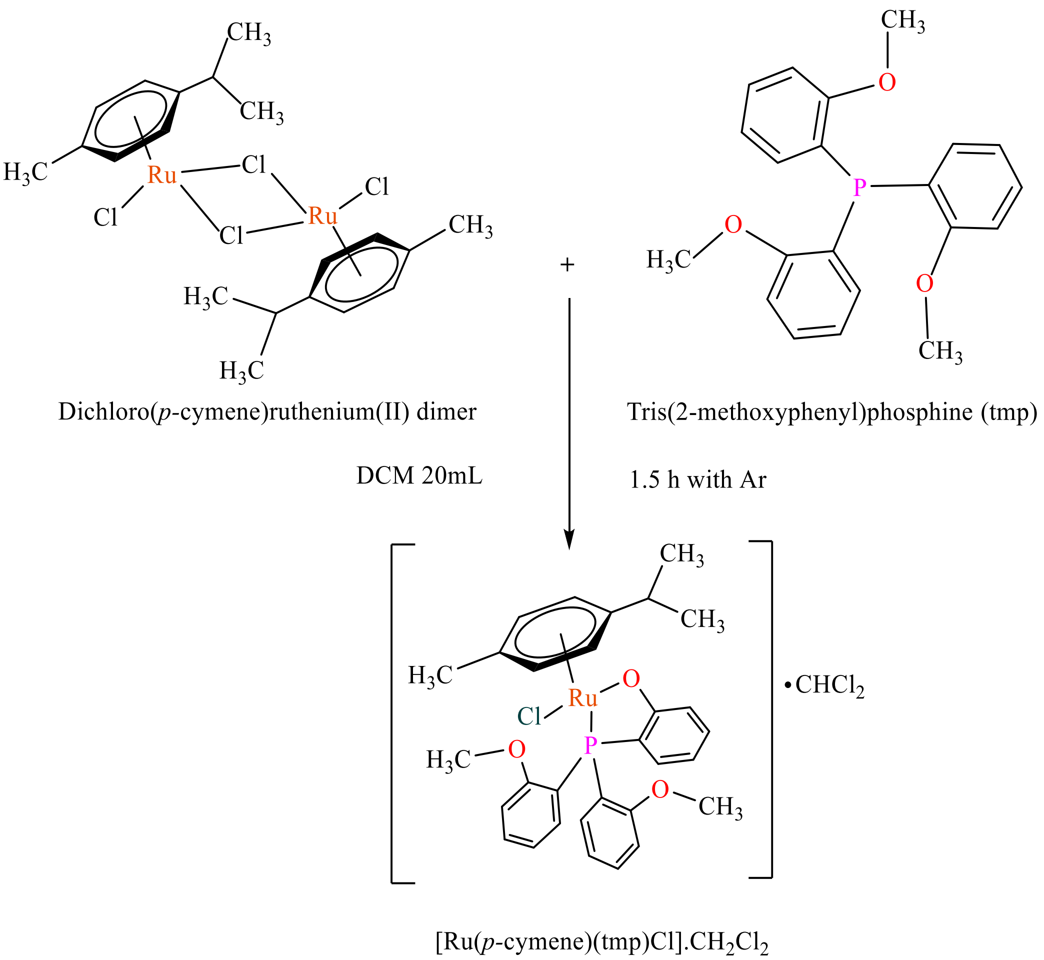

Scheme 23. Synthetic pathway of [Ru(*p*-cymene)(tmp)Cl]·CH_2Cl_2 complex.

Table 1. The solubility of [Ru(*p*-cymene)(tmp)Cl]·CH_2Cl_2 complex.

Solvent	Solubility
Dimethyl sulfoxide (DMSO)	+ + +
Dimethylformamide (DMF)	+ + +
Diethyl ether	-
Tetrahydrofuran	-
Dichloromethane	+ + +
Ethyl acetate	+
Chloroform	+ + +
Acetonitrile	+ + +
Acetone	+ + +
Methanol	+ + +
Ethanol	+
Water	-

Note:

+++ (Completely dissolved), ++ (Dissolved), + (Slightly dissolved), - (Insoluble).

Our complex m = 0.0010 g dissolved with 1 mL of each solvent.

The [Ru(*p*-cymene)(tmp)Cl]·CH_2Cl_2 structure was characterized by the following techniques:

- ^{1}H-Nuclear Magnetic Resonance Spectroscopy (NMR)
- Fourier Transform Infrared Spectroscopy (FTIR)
- Single crystal x-ray diffraction
- UV-Visible absorption spectroscopy (UV-Vis)
- Elemental Analysis (EA)

Biological activities of complex **1** such as antimicrobial and antifungal were tested.

3.1.1. ¹H-Nuclear magnetic resonance spectroscopy

The structure of complex **1** was analyzed by 1D and 2D NMR spectroscopy techniques like ^{1}H-NMR, ^{1}H-^{1}H COSY NMR, ^{13}C NMR, DEPT 90, and DEPT 135 NMR, ^{1}H-^{13}C HMQC NMR, and ^{13}C-^{13}C HMBC NMR. The spectra of complex **1** was recorded in chloroform ($CDCl_3$). The tetramethyl silane (TMS) was used as the internal standard. The ^{1}H-signals yielded from phenyl rings of *p*-cymene and tmp ligand which were identified as the primary distinctive peaks from 4.75-8.21 ppm. The coordination of the Ru(II) complex and (tmp) ligand created the downfield shift around 6.45-8.21 ppm. The coordination with *p*-cymene ring was found 4.75-5.90 ppm. The proton labeling structure of complex **1** was assigned in Figure 16.

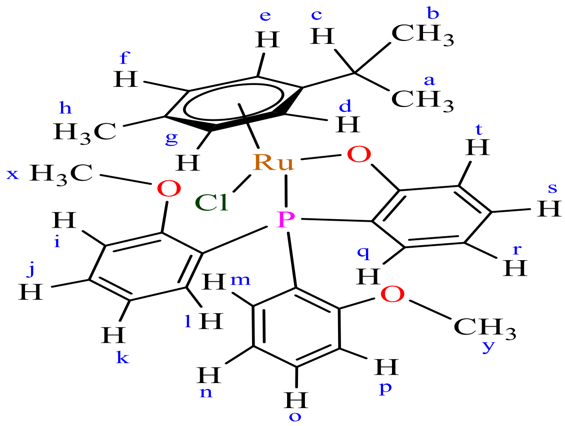

Figure 16. The proton labeling structure of [Ru(*p*-cymene)(tmp)Cl]·CH_2Cl_2 complex.

There were indications in the ^{1}H-NMR and ^{1}H-^{1}H-NMR COSY signals of the [Ru(*p*-cymene)(tmp)Cl]·CH_2Cl_2 complex (Figure 17 and Figure 18). Table 2 provided an overview of each associated chemical shift and coupling constant.

The protons at *a* and *b* were six protons from methyl group (-CH_3) that substitute on the *p*-cymene ring. Its couplings with a proton at the *c* position generated doublet peaks and show the chemical shift average at δ = 1.09 ppm with coupling constant J = 14.4, 6.9 (*Hz*).

The proton *c* was a single proton of -CH located next to proton *a* and *b*. It created a coupling with six protons of a and b positions that cumulated the multiplet peaks with chemical shift δ = 2.54 ppm and couple constant J = 13.8, 6.9 (*Hz*).

The proton *e* and *d* were two equivalent protons on the phenyl ring of the *p*-cymene. They made a coupling with proton *f* and *g*, for each *e* and *d*, respectively yielded the doublet peaks with chemical sift average *δ* = 5.05 ppm and couple constant *J* = 5.58 (*Hz*).

The proton *f* and *g* were the protons next to each *d* and *e* position on the *p*-cymene ring that interacted with the protons *e* and *d*, respectively. It produced doublet peaks at the chemical shift average *δ* = 5.69 ppm and couple constant *J* = 5.4, 5.8 (*Hz*).

The proton *h* were photos from the (-CH3) group located at the para position of the phenyl ring of *p*-cymene and it made up a singlet peak at chemical sift *δ* = 1.97 ppm and couple constant *J* = 15.2 *(Hz)* from three protons.

The protons *x* and *y* were the inequivalent protons from the methyl ($-CH_3$) group that substitute in the methoxy group of tmp ligand. Each proton offered a singlet peak separately with the chemical shift *δ* = 3.35, and 3.57 ppm and couple constant *J* =25.5 *(Hz)*, respectively from three protons.

The protons *k* and *n* were the most downfield protons located on the phenyl ring of tmp at para positions to the free methoxy groups of tmp. They were inequivalent protons. Therefore, these protons were produced by separating triplet and doublet of doublet peaks, respectively from a coupling with two neighboring protons giving the chemical shift *δ* = 6.38 and 8.21 ppm with the couple constant *J* = 6.6, 14.9, 7.5 (*Hz*).

The protons *(r, s, t)* were the protons from the protons from the methoxy group of tmp ligand provided the multiplet peaks with the chemical shift *δ = 7.36* ppm and the couple constant *J* = 28.1, 19.4, 19.2, and 14.18 (*Hz*) from three proton. The last group of protons *(i, j, l, m, o, p, q)* were the protons from the methoxy group of tmp ligand provided the multiplet peaks with the chemical shift *δ* = 6.94 ppm from seven protons.

Table 2. (δ-) Chemical shifts, (J-) couple constants, signal characters of protons of [Ru(*p*-cymene)(tmp)Cl]·CH_2Cl_2 complex.

H-Position	δ_H (ppm)	Coupling constant J (*Hz*)	Signal character	Amount of H
a, b	0.97, 1.21	14.4, 6.9	d	3, 3
c	2.54	13.8, 6.9	m	1
d, e	5.01, 5.10	5.8	d	2
f, g	5.60, 5.79	5.4, 5.8	d	2
h	1.97	15.2	s	3
x	3.35	-	s	3
y	3.57	25.5	s	3
k	6.38	6.6	t	1
n	8.21	14.9, 7.5	dd	1
i, j, l, m, o, p, q	6.94	-	m	7
r, s, t	7.36	28.1, 19.4, 19.2, 14.18	m	3

Note:

d = doublet, dd =doublet of doublet, m = multiplet, s = singlet, t = triplet.

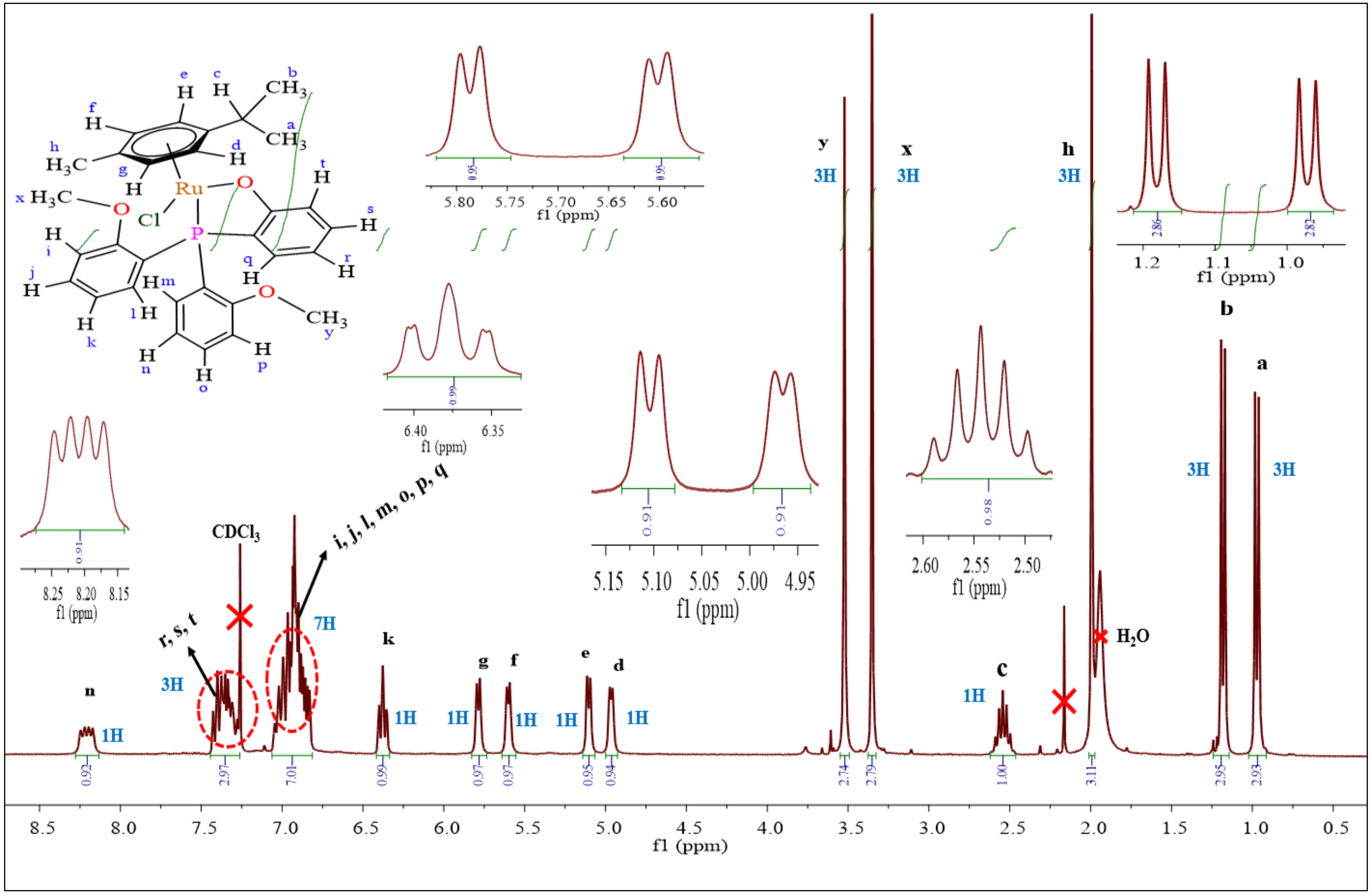

Figure 17. [1]H-NMR spectrum of [Ru(p-cymene)(tmp)Cl]·CH_2Cl_2 complex in $CDCl_3$.

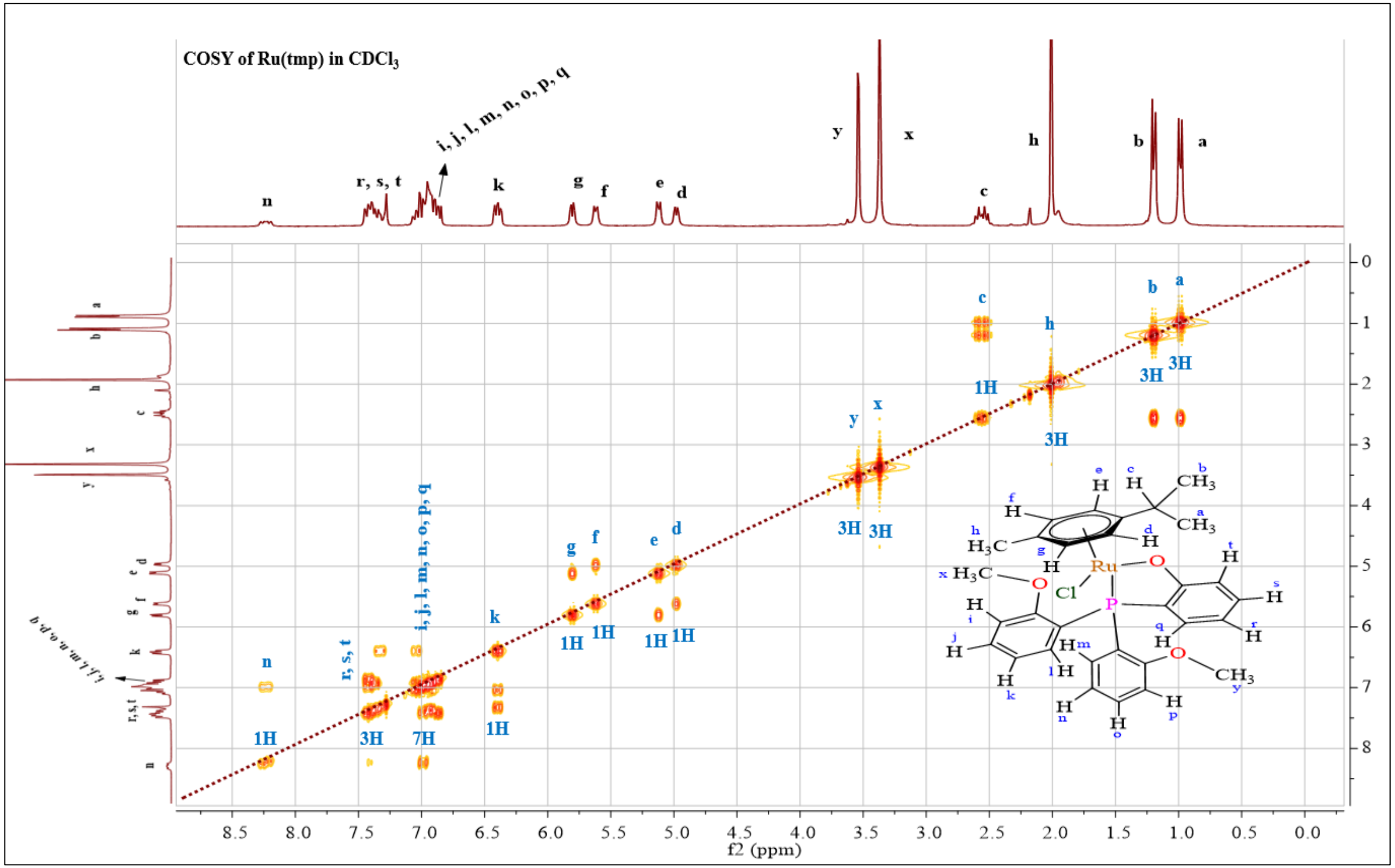

Figure 18. ^{1}H-1H-NMR COSY spectrum of [Ru(p-cymene)(tmp)]·CH_2Cl_2 complex in $CDCl_3$.

3.1.2. ^{13}C-NMR Spectroscopy

The ^{13}C-NMR of complex **1** showed signals 30 of carbon analogous with the structure. The 1D and 2D data of complex **1** was displayed in table 3. The structure with carbon numbering is exhibited in Figure 19. The complex was made up of methyl carbon (CH_3), signals of methine carbon (CH), and signals of quaternary carbon (C) shown in Figure 20. The (') symbol was denoted as the equivalent carbon. Methine carbons were analyzed by DEPT 90 (Figure 21). Methyl and methylene carbons were analyzed by DEPT 135 (Figure 22). The association of carbon-proton and carbon-carbon were analyzed by ^{1}H-^{13}C HMQC NMR and ^{13}C-^{13}C HMBC, respectively. The HMBC and HMQC spectra were displayed in Figure 23 and 24.

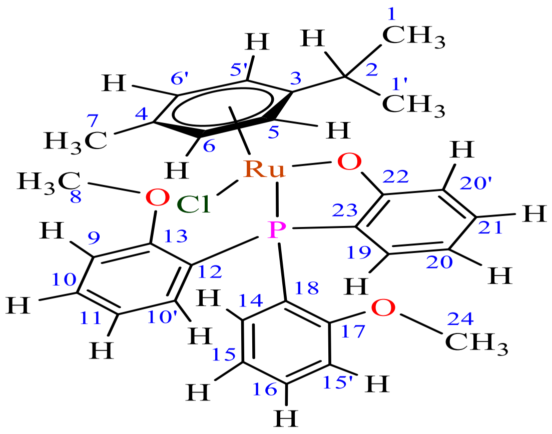

Figure 19. The structure of complex **1** with carbon numbering.

Table 3. 1D and 2D NMR data of [Ru(*p*-cymene)(tmp)]·CH_2Cl_2 complex.

[Ru(*p*-cymene)(tmp)]·CH_2Cl_2						
C-No.	δ_C (ppm)	Dept 90/135	^{1}H	HMQC δ_C (mult., *J (Hz)*, No. H)	HMBC	COSY
1	91.81	C	-	-	-	-
2	94.97	C	-	-	-	-
3	115.11	C	-	-	-	-
4	116.24	C	-	-	-	-
5	131.13	C	-	-	-	-
6	132.15	C	-	-	-	-
7	161.11	C	-	-	-	-
8	176.75	C	-	-	-	-
9	87.10, 93.22	CH	*e, d*	5.01, 5.10, d, 5.8 *Hz*, 2H	5, 3	*e, d*
10	85.28	CH	*g, f*	5.60, 5.79, d, 5.4, 5.8 *Hz*, 2H	6, 6’	*g, f*
11	30.36	CH	*c*	2.54, m, 13.8, 6.9 *Hz*	2	*c*
12	115.42	CH	*k*	6.38, t, 6.6 *Hz*, H	12	*k*
13	125.13, 132.69, 135.5	CH	*i, j, l, m, o, p, q*	6.94, m, 10H	16’, 15’, 18, 19	*i, j, l, m, o, p, q*
14	139.75	CH	*n*	8.21, dd, 14.9, 7.5 *Hz*, H	22	*n*
15	136.43, 137.4	CH	*r, s, t*	7.36, m, 3H	17, 19	*r, s, t*
16	21.84, 22.49	CH_3	*a, b*	0.97, 1.21, d, 14.4, 6.9, 6H	1, 1’	*a, b*
17	54.95	CH_3	*x*	3.35, s, 3H	8	*x*
18	55.67	CH_3	*y*	3.57, s, 3H	24	*y*
19	17.81	CH_3	*h*	1.97, s, 3H	7	*h*

Methine carbon (CH) of C5 with the chemical shift δ_H = 87.10 ppm corresponding to proton *e* (δ_H = 5.01 ppm) located next to the carbon C6 (δ_H = 85.28 ppm).

Methine carbon (CH) of carbon C6 with the chemical shift δ_H = 85.28 ppm correlated with proton *f* (δ_H = 5.79 ppm) located next to carbon C5 (δ_H = 87.10 ppm).

Methine carbon (CH) of C2 (δ_H = 30.36 ppm) correlated with proton *c* next to carbon C3 (δ_H = 93.22 ppm) and C1 (δ_H = 21.81 ppm).

Methyl carbon (CH_3) C24 with chemical shift δ_H = 54.95 ppm correlated with proton *y* (δ_H = 3.57 ppm).

Methyl carbon (CH_3) C1 with chemical shift δ_H = 21.84 ppm correlated with proton *a* (δ_H = 0.97 ppm) next to carbon C2 (δ_H = 30.36 ppm).

Methyl carbon C7 with chemical shift δ_H = 17.81 ppm correlated with proton h (1.97 ppm).

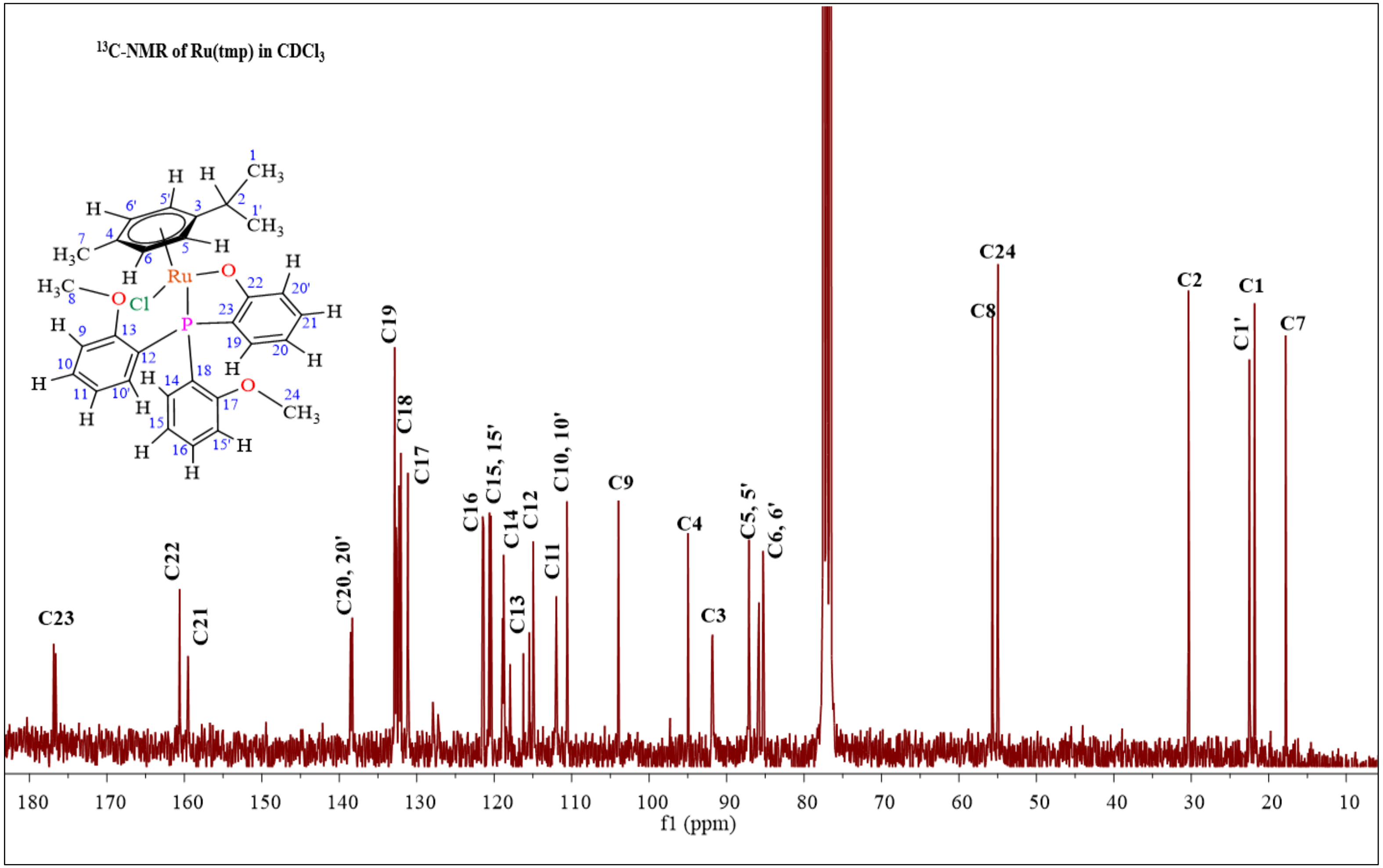

Figure 20. ^{13}C-NMR spectrum of [Ru(*p*-cymene)(tmp)]·CH_2Cl_2 complex in $CDCl_3$.

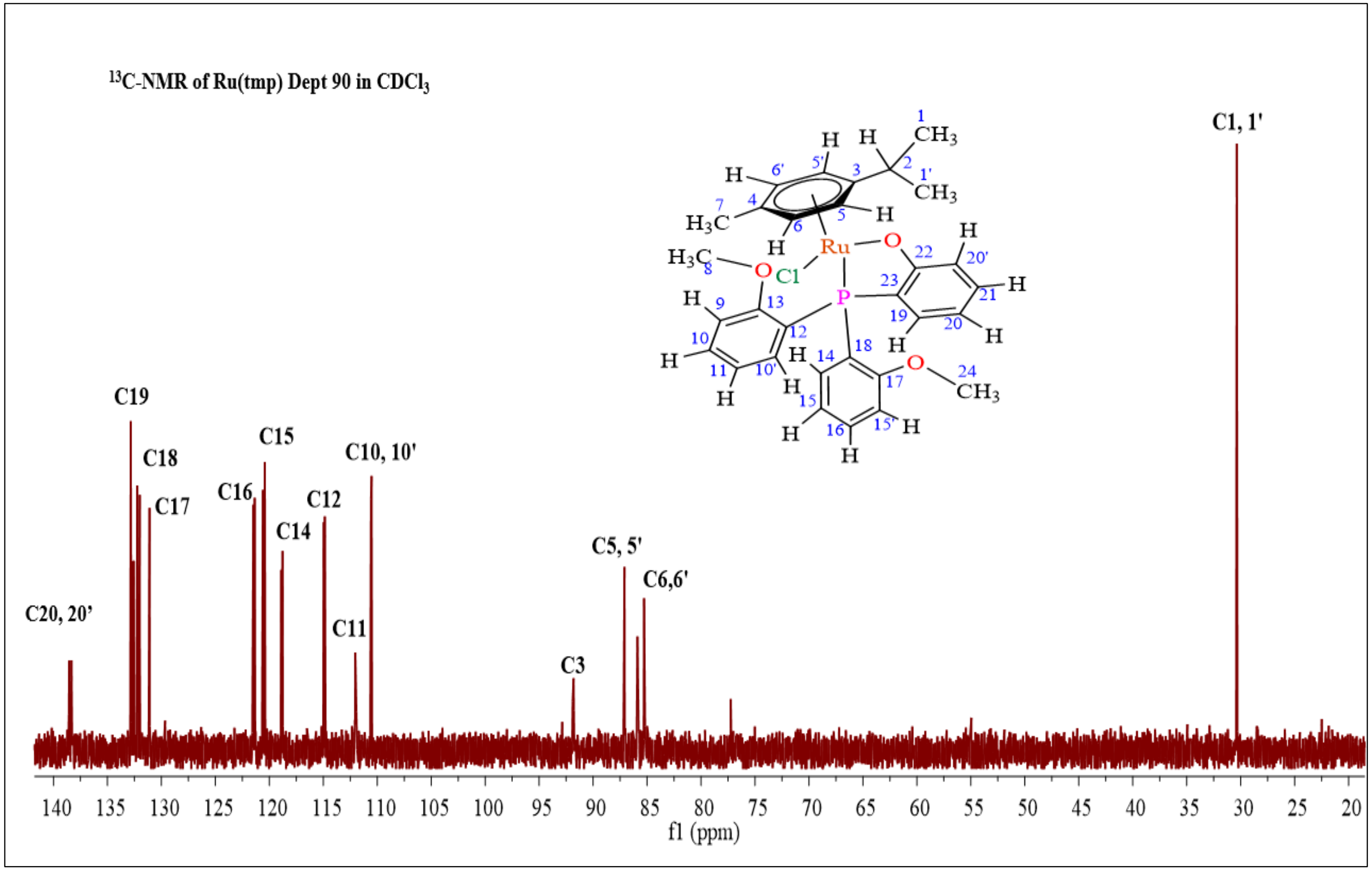

Figure 21. DEPT 90 NMR spectrum of [Ru(p-cymene)(tmp)]·CH_2Cl_2 complex in $CDCl_3$.

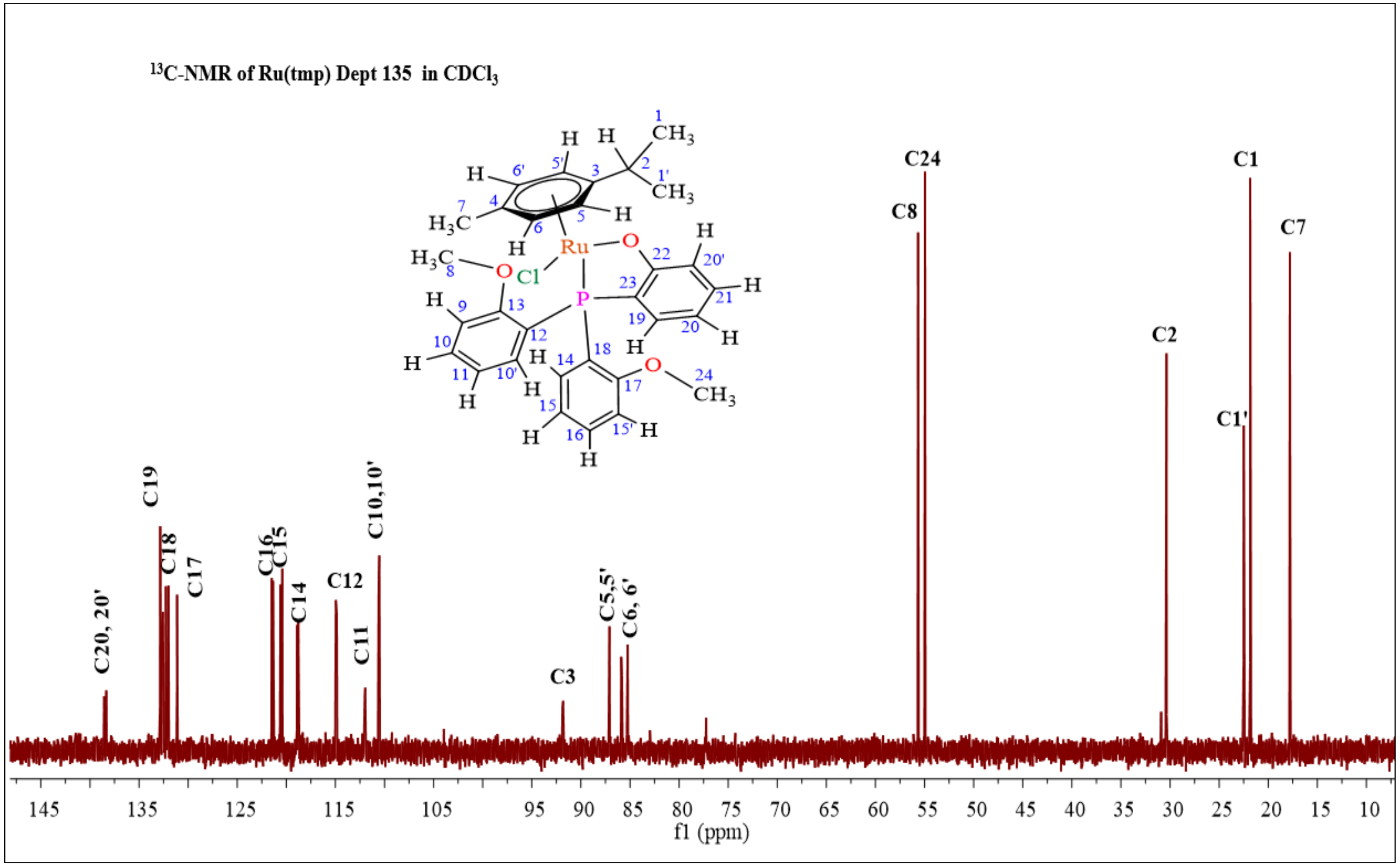

Figure 22. DEPT 135 NMR spectrum of [Ru(*p*-cymene)(tmp)]·CH_2Cl_2 complex in $CDCl_3$.

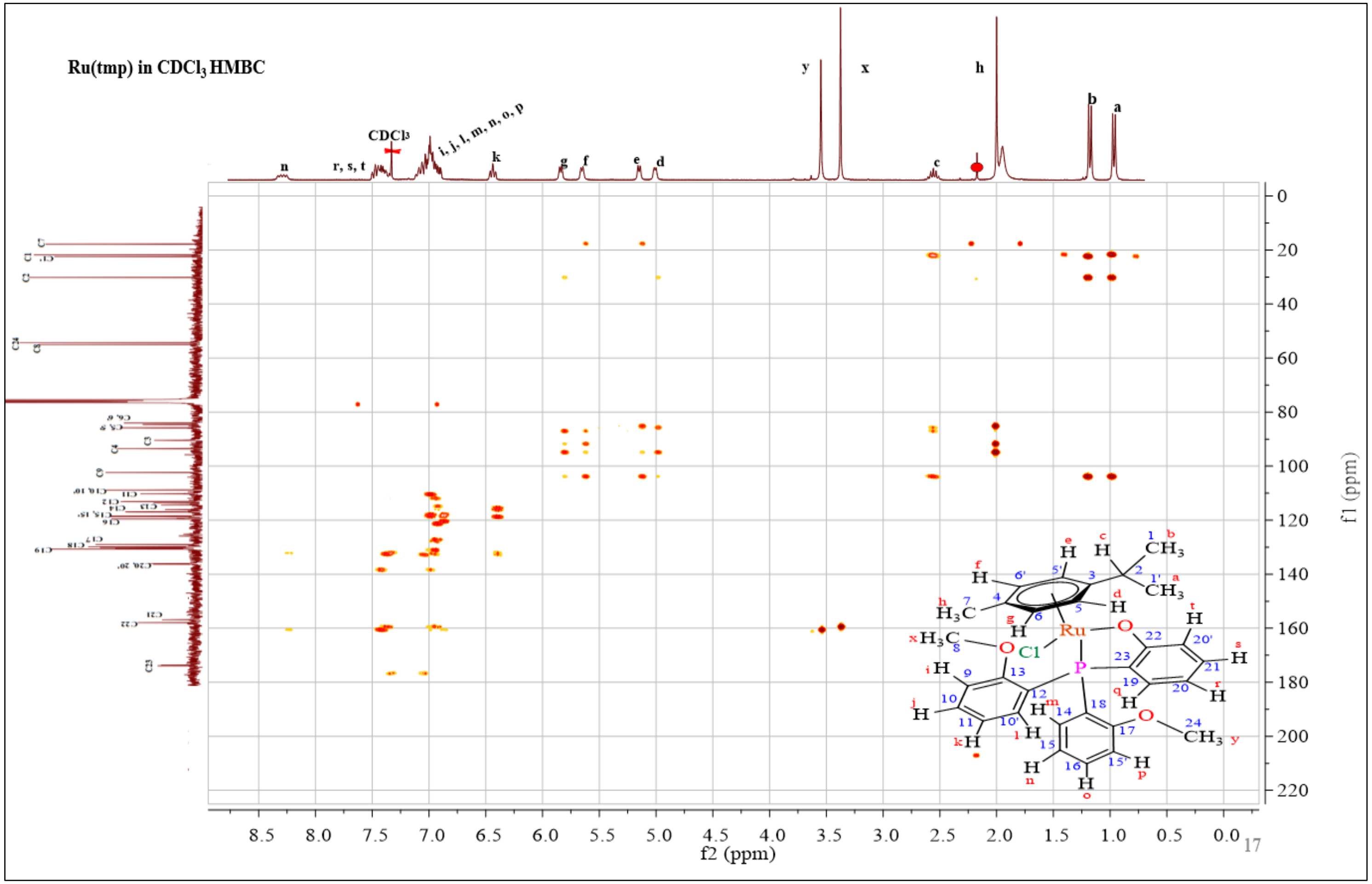

Figure 23. ^{13}C-^{13}C NMR spectrum of [Ru(*p*-cymene)(tmp)]·CH_2Cl_2 complex in $CDCl_3$.

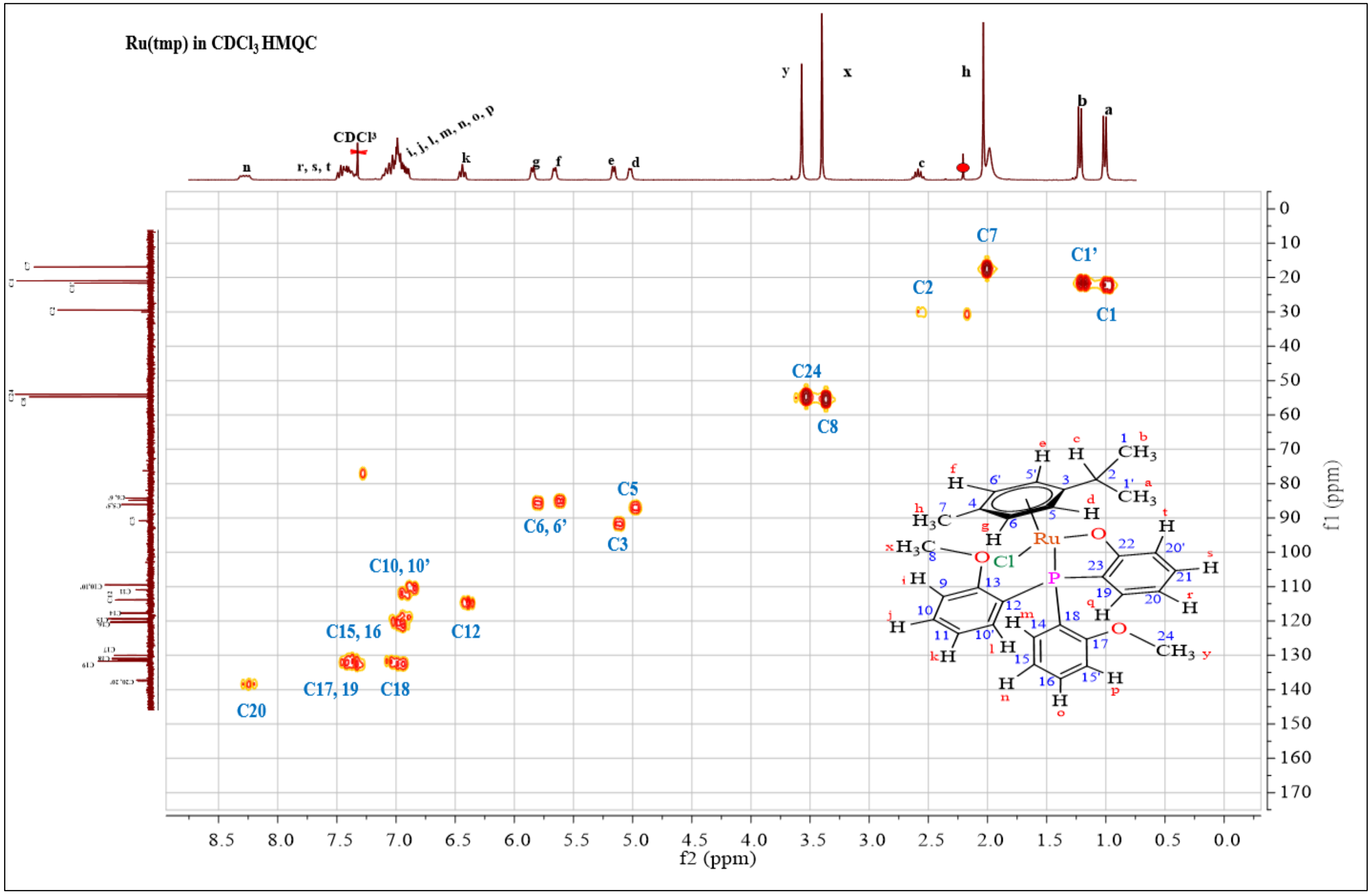

Figure 24. ${}^{1}H$-${}^{13}C$ NMR spectrum of [Ru(*p*-cymene)(tmp)]·CH_2Cl_2 complex in $CDCl_3$.

3.1.3. Fourier transformation infrared spectroscopy

The complex's functional group was investigated using Fourier transform infrared spectroscopy. A KBr pellet was used to create the compound [Ru(*p*-cymene)(tmp)Cl]·CH_2Cl_2, which was then detected by a BX Perk Elmer FTIR Spectrophotometer in the 3500-500 cm^{-1} range. The infrared spectroscopic data of some characteristic peaks of [Ru(*p*-cymene)(tmp)Cl]·CH_2Cl_2 were reported in Table 4 and IR characteristic peaks were shown in Figure 25.

Table 4. The vibrational modes and frequencies of [Ru(p-cymene)(tmp)Cl]·CH_2Cl_2 complex.

Vibrational modes	Frequencies (cm^{-1})
Ru-Cl stretching	500
Ru-O stretching	545
Ru-P stretching	576
P-C stretching	753
C-C stretching	1249
C = C stretching	1454
CH_3 bending	1579
C-H stretching	2963

The coordination of tris(2-methoxyphenyl)phosphine (tmp) ligand with the Ru-*p*-cymene metal center was observed in the FTIR characteristic spectrum of the [Ru(*p*-cymene)(tmp)Cl]·CH_2Cl_2 complex. The [Ru(*p*-cymene)(tmp)Cl]·CH_2Cl_2 complex's υ(P-C) vibrational frequency occurred at 753 cm^{-1} because of the transition metal Ru^{2+} made bond with tmp ligand by accepting one pair of electrons from tmp ligand so called sigma (σ) bonding or σ donor, but Ru^{2+} had their own electron d^6 (rich electron). Therefore, Ru^{2+} sent electron back to tmp ligand and the orbital that accepted electron back from Ru^{2+} was π* orbital. When π* orbital was increased the electron, the bond order was decreased. Moreover, the stretching frequency of tmp free ligand located at 753 cm^{-1} which was extremely similar to stretching frequency 768, 756 cm^{-1}, respectively as reported by (He *et al*., 2019; Wang *et al*., 2020) due to the electron π-back bonding from d^6 orbital of $Ru^{2+} \rightarrow \pi^*$ orbital of tmp ligand.

Additionally, the coordination between the metal center and tmp ligand can be determined by the Ru-O and Ru-P stretching vibrational frequencies. For Ru-O and Ru-P, the stretching frequencies appeared at 545, 576 cm^{-1}, respectively, which were different from stretching frequency of others research (Honorato *et al.*, 2020; Sengupta *et al.*, 2001).

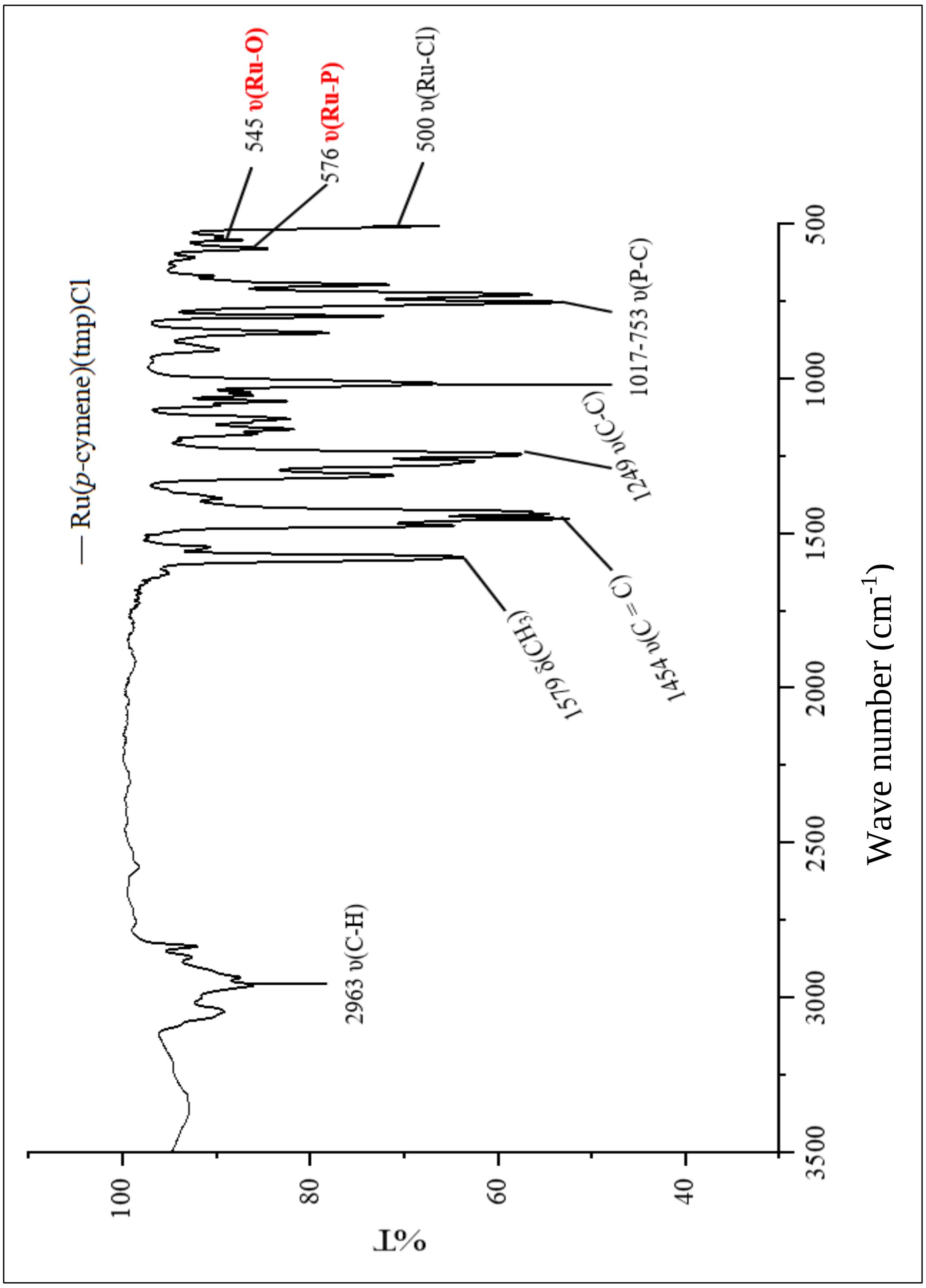

Figure 25. The IR spectrum of [Ru(*p*-cymene)(tmp)Cl]·CH_2Cl_2 complex in KBr pellet.

3.1.4. Single crystal X-ray diffraction

By using X-ray crystallography, the molecular structure of the brown crystal of [Ru(*p*-cymene)(tmp)Cl)]·CH_2Cl_2 complex **1** was investigated. Table 5 showed the crystallographic information for complex **1**. The crystal system was triclinic with the $P\bar{1}$ space group. The coordination occurred through the η^6 π-bonding of the *p*-cymene ring, one Cl atom, and chelating with tmp ligand via atoms O and P atom. The geometry of the Ru(II) complex was distorted into a tetrahedral shape. There were two independent molecules, Ru1 and Ru2 molecules, of complex **1** including two independent dichloromethane molecules in the unit cell which had different bond lengths and bond angles in one unit cell, as shown in Figure 26. The selected bond distances and bond angles were shown in Table 6. The Ru-Cl average distance for was 2.41945 Å closely with the distance of other similar complexes: [(η^6-*p*-cymene)]$RuCl_2(PPh_2Py)$] 2.4195 Å (Govindaswamy *et al*., 2004) and [Ru_2(*p*-cymene)$_2$(dppp)Cl_4] 2.4415 Å (Klaimanee *et al*., 2021). The average distances between Ru-P and Ru-O were 2.3323 and 2.079 Å, respectively which were similar to the distances search from other relevant structures of 2.3756, 2.13 Å (Honorato *et al*., 2020) and 2.3085, 2.0933 Å for (Renfrew *et al*., 2010). Moreover, the average distances of Ru-C atoms in *p*-cymene are 2.20875 Å which were closely to the distances previously studied ruthenium complexes with ethacrynic-acid-modified pyridine and triphenylphosphine ligands 2.2247 Å (Agonigi *et al*., 2015). The angles of O(1)-Ru(1)-Cl(1) and P(1)-Ru(1)-Cl(1) were 84.79(10)^o and 87.32(5)^o, respectively which were deviated from 90^o of ideal octahedral responding to other works of Ru(II)| complexes of [Ru(η^6-*p*-cymene)(NSAID-H)]$^+$ 84.93(5)^o (Mandal *et al*., 2018) and [Ru(η^6-*p*-cymene)Cl_2{$Ph_2PCH_2CH_2SPh$-κP}] 87.6(1)^o (Ludwig *et al*., 2012). Both independent molecules of the complex 1 presented two types of C-H···O and C-H···Cl intra-molecular H-bonding interactions. The C-H···O interaction was observed between C-phenyl ring donor atom and O-methoxy acceptor of tmp, C(2)-H(2)···O(2) for Ru1 molecule and C(32)-H(32)···O(6) for Ru2 molecule with the H···O accepter distances at 2.41 and 2.42 Å, respectively. For the C-H···Cl interaction, C(8)-H(8)···Cl(1) for Ru1 molecule and C(45)-H(45)···Cl(2) for Ru2 molecule were found with the H···Cl lengths at 2.74 and 2.71 Å as mentions in the Figure 27. On the other hand, dichloromethane molecules in packing were also linked with both Ru1 and Ru2 molecules via C-H···Cl H-bonding interaction, C(61)-H(61B)···Cl(1) for Ru1 molecule and C(62)-H(62B)···Cl(2) and C(62)-H(62B)···O(4) for Ru2 molecule as depicted in Figure 28. All the distances data of the H-bonds were given in Table 7.

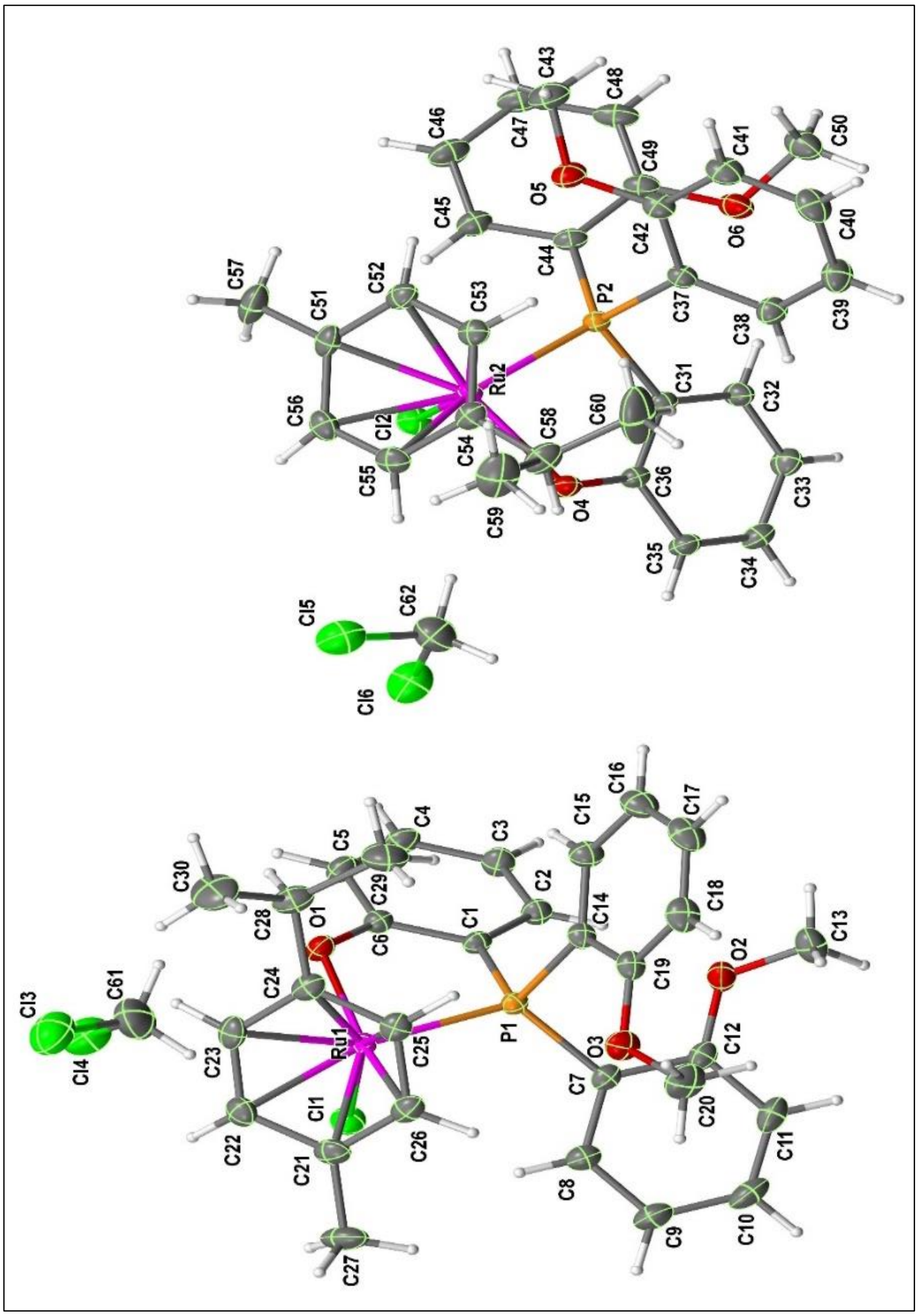

Figure 26. Molecular structure of [Ru(*p*-cymene)(tmp)Cl)]·CH_2Cl_2 complex.

Table 5. Crystal data and structure refinement for [Ru(*p*-cymene)(tmp)Cl]·CH_2Cl_2 complex.

Identification code	[Ru(*p*-cymene)(tmp)Cl]·CH_2Cl_2
Empirical formula	$C_{30}H_{32}ClO_3PRu$, CH_2Cl_2
Formula weight	692.97
Temperature	296(2) K
Wavelength	1.54178 Å
Crystal system	Triclinic
Space group	$P\bar{1}$
Unit cell dimensions	a = 10.0522(2) Å α = 83.5800(10)° b = 10.8482(2) Å β = 75.5990(10)° c = 16.1698(3) Å γ = 65.0900(10)°
Volume	1548.95(5) $Å^3$
Z	2
Density (calculated)	1.486 Mg/m^3
Absorption coefficient	7.208 mm^{-1}
F(000)	708
Crystal size	0.238 × 0.146 × 0.061 mm^3
Theta range for data collection	2.821 to 68.486°
Index ranges	-12<=h<=12, -13<=k<=13, -18<=l<=19
Reflections collected	47929
Independent reflections	10521 [*R*(int) = 0.0404]
Completeness to theta = 67.679°	99.2 %
Absorption correction	Semi-empirical from equivalents
Max. and min. transmission	0.7531 and 0.4158
Refinement method	Full-matrix least-squares on F^2
Data / restraints / parameters	10521/3/714
Goodness-of-fit on F^2	1.026
Final *R* indices [$I>2\sigma(I)$]	*R1* = 0.0267, *wR2* = 0.0695
R indices (all data)	*R1* = 0.0269, *wR2* = 0.0698
Absolute structure parameter	0.104(8)
Extinction coefficient	n/a
Largest diff. peak and hole	0.442 and -0.413 e.$Å^{-3}$

Table 6. Selected bond lengths (Å) and angles (°) for [Ru(p-cymene)(tmp)Cl]·CH_2Cl_2 complex.

Bond lengths			
Ru(1)-O(1)	2.079(3)	Ru(1)-C(23)	2.213(5)
Ru(2)-O(4)	2.079(3)	Ru(1)-C(22)	2.237(6)
Ru(1)-C(26)	2.189(5)	Ru(2)-P(2)	2.3301(12)
Ru(1)-C(21)	2.204(5)	Ru(1)-P(1)	2.3345(13)
Ru(1)-C(25)	2.206(5)	Ru(1)-Cl(1)	2.4207(13)
Ru(1)-C(24)	2.212(4)	Ru(2)-Cl(2)	2.4182(13)
Ru(2)-C(52)	2.181(5)	Ru(2)-C(53)	2.198(5)
Ru(2)-C(51)	2.207(4)	Ru(2)-C(55)	2.215(5)
Ru(2)-C(54)	2.216(5)	Ru(2)-C(56)	2.227(6)
Angles			
O(1)-Ru(1)-C(26)	158.18(17)	C(25)-Ru(1)-C(22)	78.9(2)
O(1)-Ru(1)-C(21)	152.35(18)	C(24)-Ru(1)-C(22)	66.9(2)
C(26)-Ru(1)-C(21)	37.1(2)	C(23)-Ru(1)-C(22)	35.9(2)
O(1)-Ru(1)-C(25)	120.27(18)	O(1)-Ru(1)-P(1)	80.65(9)
C(26)-Ru(1)-C(25)	37.9(2)	C(26)-Ru(1)-P(1)	99.59(14)
C(21)-Ru(1)-C(25)	67.7(2)	C(26)-Ru(1)-P(1)	99.59(14)
O(1)-Ru(1)-C(24)	92.24(15)	C(21)-Ru(1)-P(1)	126.42(16)
C(26)-Ru(1)-C(24)	68.03(18)	C(25)-Ru(1)-P(1)	95.61(15)
C(21)-Ru(1)-C(24)	80.57(19)	C(24)-Ru(1)-P(1)	116.97(14)
C(25)-Ru(1)-C(24)	37.2(2)	C(23)-Ru(1)-P(1)	153.37(16)
O(1)-Ru(1)-C(23)	91.25(17)	C(22)-Ru(1)-P(1)	164.34(18)
C(26)-Ru(1)-C(23)	78.8(2)	O(1)-Ru(1)-Cl(1)	84.79(10)
C(21)-Ru(1)-C(23)	66.8(2)	C(26)-Ru(1)-Cl(1)	117.03(15)
C(25)-Ru(1)-C(23)	66.6(2)	C(21)-Ru(1)-Cl(1)	90.50(16)
C(24)-Ru(1)-C(23)	37.5(2)	C(25)-Ru(1)-Cl(1)	154.93(15)
O(1)-Ru(1)-C(22)	114.8(2)	C(24)-Ru(1)-Cl(1)	154.78(15)
O(1)-Ru(1)-C(22)	114.8(2)	C(23)-Ru(1)-Cl(1)	117.36(16)
C(26)-Ru(1)-C(22)	67.1(2)	C(22)-Ru(1)-Cl(1)	91.60(18)
C(21)-Ru(1)-C(22)	37.9(2)	P(1)-Ru(1)-Cl(1)	87.32(5)
O(4)-Ru(2)-C(52)	156.70(17)	O(4)-Ru(2)-C(53)	118.67(18)

C(52)-Ru(2)-C(51)	37.1(2)	C(53)-Ru(2)-C(51)	68.0(2)
O(4)-Ru(2)-C(55)	92.58(16)	C(52)-Ru(2)-C(55)	78.78(19)
C(53)-Ru(2)-C(55)	67.0(2)	C(51)-Ru(2)-C(55)	67.0(2)
C(52)-Ru(2)-C(54)	68.17(18)	C(53)-Ru(2)-C(54)	37.5(2)
C(51)-Ru(2)-C(54)	80.89(19)	C(55)-Ru(2)-C(54)	37.7(2)
O(4)-Ru(2)-C(56)	117.0(2)	C(52)-Ru(2)-C(56)	67.1(2)
C(53)-Ru(2)-C(56)	79.2(2)	C(51)-Ru(2)-C(56)	38.2(2)
C(55)-Ru(2)-C(56)	35.7(2)	C(54)-Ru(2)-C(56)	66.9(2)
O(4)-Ru(2)-P(2)	80.67(9)	C(52)-Ru(2)-P(2)	98.18(14)
C(53)-Ru(2)-P(2)	95.50(14)	C(51)-Ru(2)-P(2)	123.97(16)
C(55)-Ru(2)-P(2)	155.43(15)	C(54)-Ru(2)-P(2)	118.40(14)
C(56)-Ru(2)-P(2)	162.07(18)	O(4)-Ru(2)-Cl(2)	84.37(10)
C(52)-Ru(2)-Cl(2)	118.92(15)	C(53)-Ru(2)-Cl(2)	156.96(15)
C(51)-Ru(2)-Cl(2)	91.23(15)	C(55)-Ru(2)-Cl(2)	115.23(15)
C(54)-Ru(2)-Cl(2)	152.61(14)	C(56)-Ru(2)-Cl(2)	90.73(17)
P(2)-Ru(2)-Cl(2)	87.77(5)		

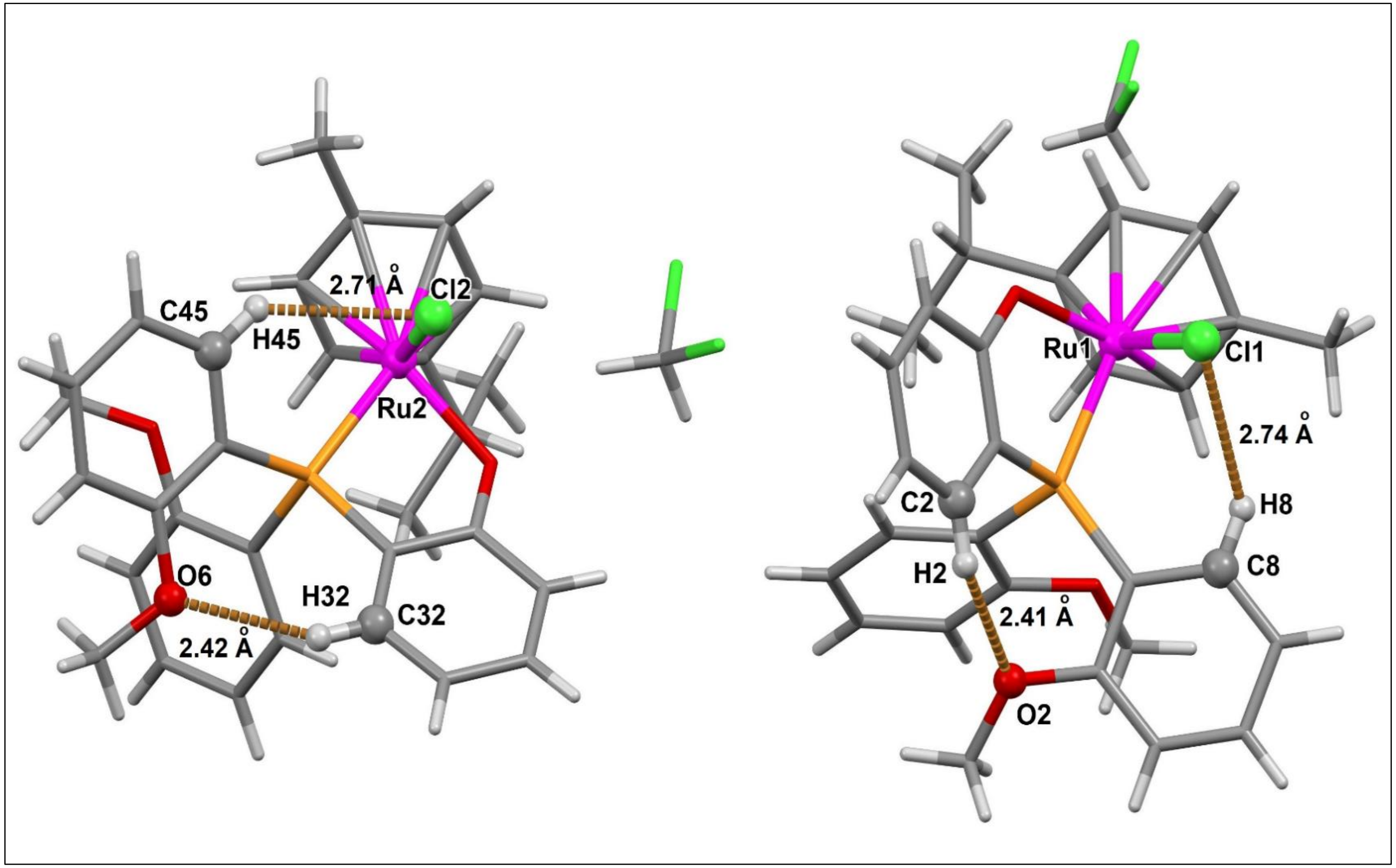

Figure 27. Intra-molecular H-bond interactions of [Ru(*p*-cymene)(tmp)Cl]·CH_2Cl_2 complex.

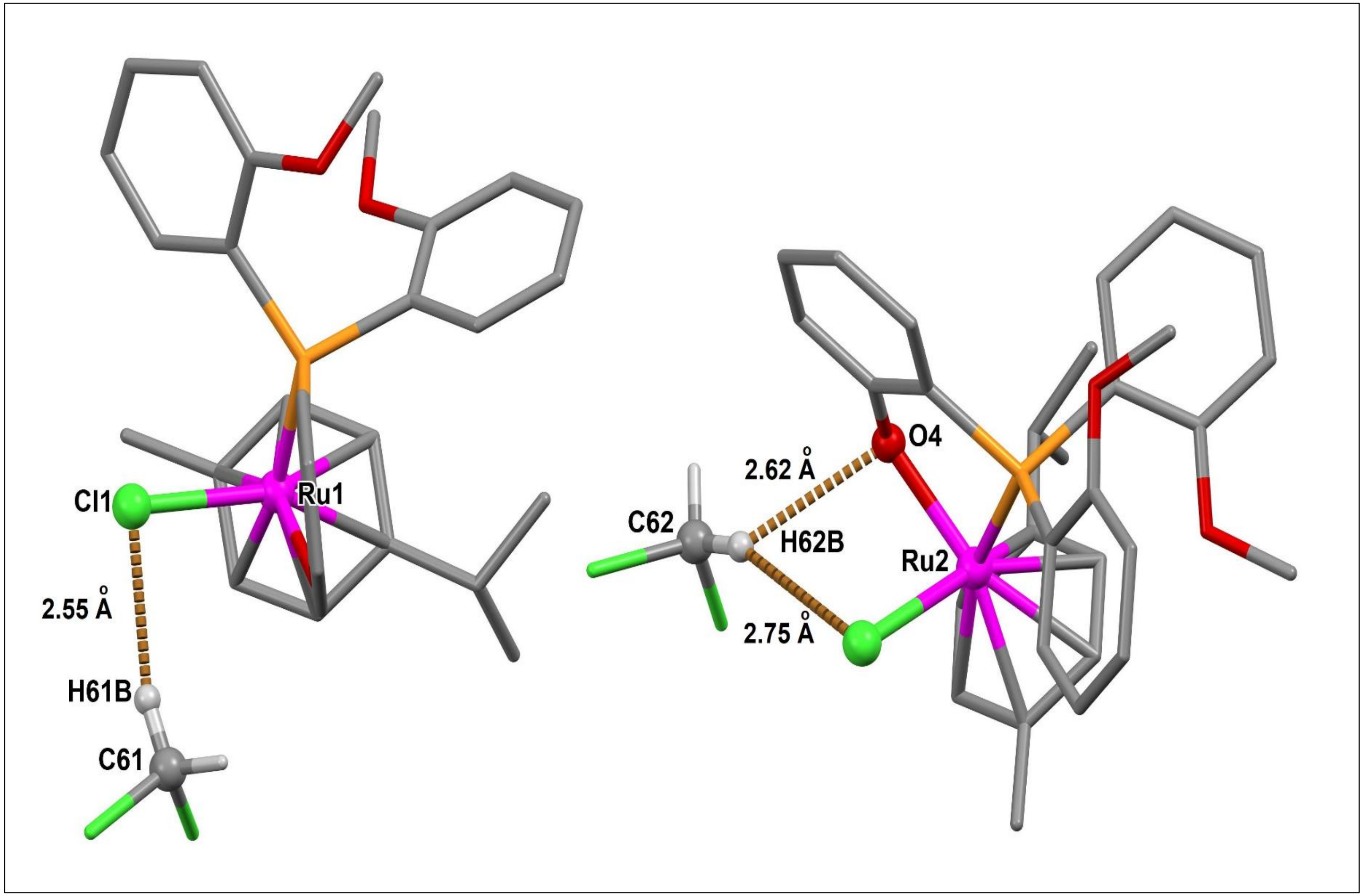

Figure 28. Intra-molecular interactions of [Ru(*p*-cymene)(tmp)Cl]·CH_2Cl_2 complex.

Table 7. Hydrogen bonds [Å and º] of [Ru(*p*-cymene)(tmp)Cl]·CH_2Cl_2 complex.

D-H···A	Distance of d(D-H) (Å)	Distance of d(H···A) (Å)	Distance of d(D···A) (Å)	Angles of <(DHA) (º)
C(2)-H(2)···O(2)	0.93	2.41	3.159(6)	137.5
C(8)-H(8)···Cl(1)#1	0.93	2.74	3.425(6)	131.3
C(32)-H(32)···O(6)	0.93	2.42	3.180(6)	138.4
C(45)-H(45)···Cl(2)	0.93	2.71	3.418(6)	133.3
C(61)-H(61B)···Cl(1)	0.97	2.55	3.503(11)	166.2
C(62)-H(62B)···O(4)	0.97	2.62	3.295(10)	126.9
C(62)-H(62B)···Cl(2)	0.97	2.75	3.657(10)	156.6

Note:

D = C atom (donor), A = O or Cl atom (acceptor).

Symmetry transformations were used to generate equivalent atoms: #1 x-1,y+1,z.

3.1.5. Elemental analysis

In order to confirm the structure, elemental analysis was an important technique for comparison the percentage of C, H and O available in the expected structure. Between the theoretical calculation and experiment. It was discovered that the compound's elemental analysis results matched each other within a reasonable deviation range. According to Table 8, the synthesized molecule had the formular $RuC_{31}H_{34}Cl_2O_3P$ corresponding to the crystal structure.

Table 8. Elemental analysis data of [Ru(*p*-cymene)(tmp)Cl]·CH_2Cl_2 complex.

Elemental analysis			
Elements (%)	C	H	O
Calculated	59.25	5.26	7.90
Found	59.17	5.32	7.94
Deviation (Δ)	± 0.08	± 0.06	± 0.04

<u>Note</u>:

The acceptance deviation of each element in the compound was Δ = 0.04.

3.1.6. UV-Visible absorption spectroscopy

Dichloromethane (CH_2Cl_2) was used as a solvent to evaluate the UV-Visible absorption spectrum of complex **1** between 400-800 nm at a concentration of 1×10^{-3} M. One broad band was observed at $\lambda_{(max)}$ = 480 nm as shown in Figure 29, which assigned to a charge transfer (MLCT) transition by the molar excitation coefficient ($\varepsilon_{(480)} = 3.7\times10^2\ M^{-1}\ cm^{-1}$) related to the DFT/TD-DFT of complex **3**.

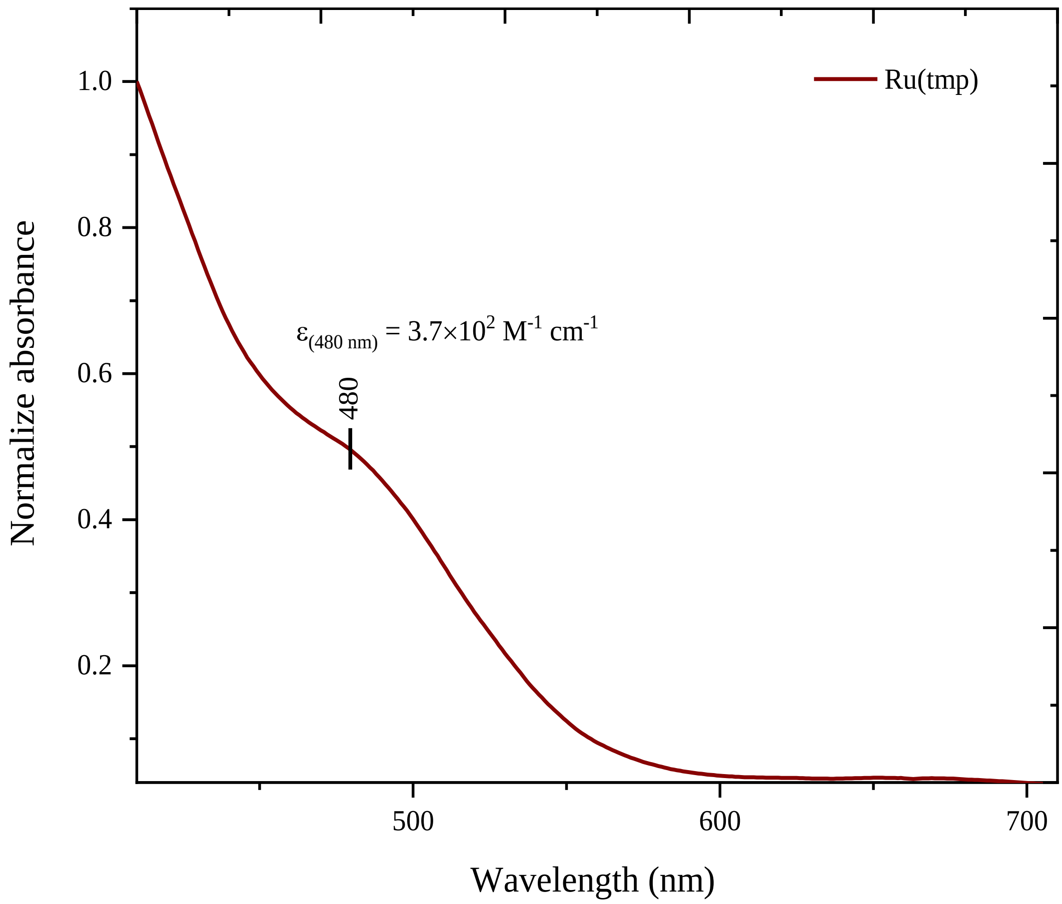

Figure 29. UV-Visible absorption spectrum of 1×10^{-3} M of [Ru(*p*-cymene)(tmp)Cl]·CH_2Cl_2 complex in dichloromethane (CH_2Cl_2).

3.1.7. Antimicrobial and antifungal activity

By using colorimetric broth microdilution technique, the antibacterial activity of complex **1** was examined against bacteria, yeast, and filamentous fungi. Table 9 shows the MIC/MBC and MIC/MFC values. The complex **1** exhibited a moderate antibacterial activity against two types of Gram-positive bacteria, including *Staphylococcus aureus* (SA) and methicillin-resistant *Staphylococcus aureus* (MRSA), with MIC/MBC values of 64/128 µg/mL and 64/128 µg/mL, respectively. Additionally, complex **1** had weak activity against yeast, with *Cryptococcus neoformans* (CN90112) MIC/MFC values 200/200 and (CN90113) MIC/MFC values of 200/>200 µg/mL. However, Vancomycin and Amphotericin B, two commercial antibacterial and antifungal drugs showed lower MIC/MBC and MIC/MFC values than the complex **1**. Gram-positive bacteria have no outer cell membrane like gram-negative bacteria, but they are surrounded by thick layers of peptidoglycan which consisting of repeating units of β-1, 4-linked N-acetylglucosamine and N-acetylmuramic acid disaccharide, cross-linking by short peptides. Therefore, it has both polar and non-polar lipids. It is complicated to identify the exact mechanism from our work. However, it probably arises from the ability of our studied complex to penetrate the gram-positive bacteria cell by having an appropriate polarity with the cell.

Table 9. The results of MIC and MFC of [Ru(*p*-cymene)(tmp)Cl]·CH_2Cl_2 complex.

Complex	Bacteria (µg/mL)				Yeast (µg/mL)												Filamentous fungus (µg/mL)			
	SA		MRSA		PA		EC		CA90028		CA3153		CN90112		CN90113		MG		TM	
	MIC	MBC	MIC	MBC	MIC	MBC	MIC	MBC	MIC	MFC	MIC	MFC	MIC	MFC	MIC	MFC	MIC	MFC	MIC	MFC
1	64	128	64	128	NA	NA	NA	NA	NA	NA	NA	NA	200	200	200	>200	NA	NA	NA	NA
Vancomycin	0.25	0.5	1	1	-	-	-	-	-	-	-	-	-	-	-	-	-	-	-	-
Amphotericin **B**	-	-	-	-	-	-	-	-	-	-	-	-	0.25	0.5	0.25	0.5	-	-	-	-

SA = *Staphylococcus aureus* ATCC25923, MRSA = methicillin-resistant *Staphylococcus aureus* SK1, PA = *Pseudomonas aeruginosa* ATCC27853, EC = *Escherichia coli* ATCC25922, AB005 = *Acinetobacter baumannii* NPRC005,AB007 = *Acinetobacter baumannii* NPRC007. CA3153 = *Candida albicans* NCPF3153, CN90113 = *Cryptococcus neoformans* ATCC90113 flucytosine-resistant, MG = *Microsporum gypseum* SK-MU4, TM = *Talaromyces marneffei* PSU-SKH1. MIC = minimum inhibitory concentration (µg/ml), MBC = minimum bactericidal concentration (µg/ml), MFC = minimum fungicidal concentration

3.1.8. Anti-breast cancer activity

Regarding the negative results in the testing the cytotoxicity against 3 cell lines in the range of concentrations between 0.1-10 µM, the complex **1** needs more study in the higher range of concentration to identify the real IC_{50} value (Table 10).

Table 10. The IC_{50} value of complex **1** with concentration range 0.1-10 µM.

Cell type	IC_{50} (µg/ml)
MCF-7	Not inhibited
BT-549	Not inhibited
MDA-MB-231	Not inhibited

Positive control: Doxorubicin had IC_{50} = 1.15 $\pm$ µM, 0.71 $\pm$ 0.11 µM, and 0.79 $\pm$ 0.04 µM of MCF-7, BT-549, and MDA-MB-231, respectively.

3.2. Synthesis and characterization of [Ir(ppy)$_2$(tmp)]·CH_2Cl_2, complex 2

The complex **2** was prepared by the reaction between the [Ir$_2$(2-ppy)$_4$Cl$_2$] dimer and tris(2-methoxyphenyl)phosphine ligand in dichloromethane as shown (Scheme 24).

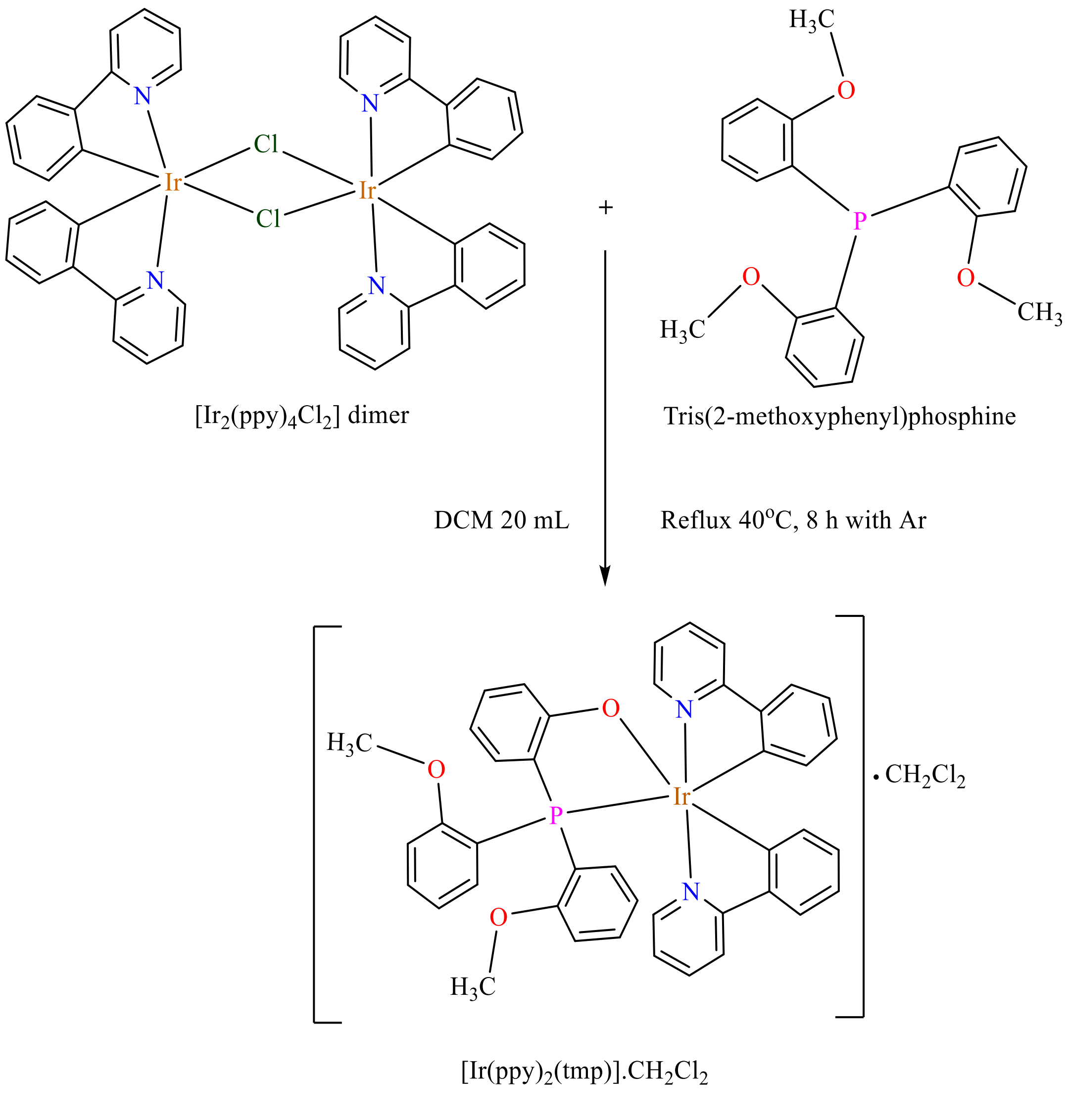

Scheme 24. Synthesis pathway of [Ir(ppy)$_2$(tmp)]·CH_2Cl_2 complex.

The solubility of neutral complex **2** was similar with complex **1**. It can be dissolved in a broad range of polarity. However, it showed less solubility in ethanol which means that it has a bit less polar than complex **1**. The solubility data was displayed in Table 11.

Table 11. Solubility of $[Ir(ppy)_2(tmp)]·CH_2Cl_2$ complex.

Solvent	Solubility
Dimethyl sulfoxide (DMSO)	+ + +
Dimethylformamide (DMF)	+ + +
Diethyl ether	-
Tetrahydrofuran	-
Dichloromethane	+ + +
Ethyl acetate	+
Chloroform	+ + +
Acetonitrile	+ + +
Acetone	+ + +
Methanol	+ + +
Ethanol	+
Water	-

Note:

+++ (Completely dissolved), ++ (Dissolve), + (Slightly dissolve), - (Insoluble).

Our complex m = 0.0010 g dissolved with 1mL of each solvent.

The structure of complex **2** was characterized by the following techniques:

- ^{1}H-Nuclear Magnetic Resonance Spectroscopy (NMR)
- Fourier Transform Infrared Spectroscopy (FTIR)
- Single crystal x-ray diffraction
- UV-Visible absorption spectroscopy (UV-Vis)
- Fluorescence spectroscopy
- Elemental Analysis (CHNO)

Biological activities of complex **2** were studied.

3.2.1. [1]H-Nuclear magnetic resonance spectroscopy

The structure of complex **2** was analyzed by 1D and 2D NMR spectroscopy techniques like ^{1}H-NMR, ^{1}H-^{1}H COSY NMR, ^{13}C NMR, DEPT 90, and DEPT 135 NMR, ^{1}H-^{13}C HMQC NMR, and ^{13}C-^{13}C HMBC NMR. The spectra of complex **2** was recorded in chloroform ($CDCl_3$). The tetramethyl silane (TMS) was used as the internal standard. $CDCl_3$ solvent was used to study the ^{1}H-NMR spectra of [Ir(ppy)$_2$(tmp)]·CH_2Cl_2 complex with protons numbering in Figure 30. The main distinguishing peaks were found from the 2-phenylpyridine rings and tmp ligand. The downfield shifting in the range of 6.04-6.75 ppm was produced by the coordination of the Ir(III) complex with (tmp) ligand. The ^{1}H-NMR signals were observed in the range of 2-9 ppm. There were 9 signals which were assigned as follows.

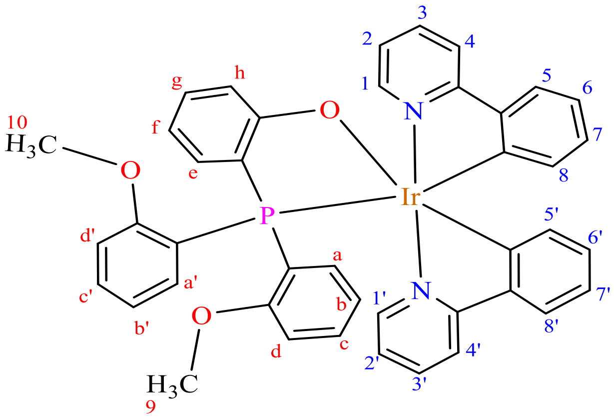

Figure 30. The proton labeling structure of [Ir(ppy)$_2$(tmp)]·CH_2Cl_2 complex.

The indications of the ^{1}H-NMR and ^{1}H-^{1}H-NMR COSY signals of the [Ir(ppy)$_2$(tmp)]·CH_2Cl_2 complex was exhibited in Figure 31 and 32. Each signal's description was indicated in Table 12 below.

Proton *1* came from pyridine rings. It interacted with proton *2*. The signal character of proton *1* was a doublet peak with the chemical shift δ = 8.27 ppm, and coupling constant, J = 5.8 *(Hz)* which was downfield because of locating next to the N hetero atom.

The pyridine ring was another source of proton *2*. It made up a coupling with neighboring protons *1* and *3*. A triplet peak with the chemical shift δ = 7.63 ppm was the signal characteristic of proton *2*.

Proton *4* was located next to proton *3*. The interaction between these protons gave doublet peaks with the chemical shift δ = 7.84 ppm and coupling constant, *J* = 7.7 *(Hz)*.

Proton 3, *5*, *6*, *7*, *8* were the proton from phenyl rings. The signal of [1]H-NMR was multiplet peaks with chemical shift δ = 7.40 ppm from 5 protons.

For the methoxy group of the tmp ligand, protons *9* and *10* were from the methyl (-CH_3) groups. These groups provided two singlet peaks with 3 protons that had a chemical shift δ = 3.15 and 2.62 ppm.

The *a* and *b* on the phenyl ring of tmp ligand. These protons also generated doublet and triplet peaks with chemical shifts δ = 8.27 and 6.39 ppm with *J* coupling constant *J* = 5.8, 0 *(Hz)*.

The produced the group protons *(c, d, a', b', c', d', e, f, g, h)*, which were used to construct the multiplet peaks with a chemical shift δ = 6.93-657 ppm from 10H protons.

Table 12. The (δ-) Chemical shifts, (*J*-) Couple constants, Signal characters of protons of [Ir(ppy)$_2$(tmp)]·CH_2Cl_2 complex.

H-Position	δ_H (ppm)	Coupling constant *J* (*Hz*)	Signal character	Amount of H
1	8.27	5.8	1	s
2	7.63	-	1	t
4	7.84	7.7	1	d
3, 5, 6, 7, 8	7.40	-	5	m
9	3.15	-	3	s
10	2.62	-	3	s
a	8.27	5.80	1	d
b	6.39	-	1	t
c, d, a', b', c', d', e, f, g, h	6.93-657	-	10	m

<u>**Note**</u>:

d = doublet, m = multiplet, s = singlet, t = triplet.

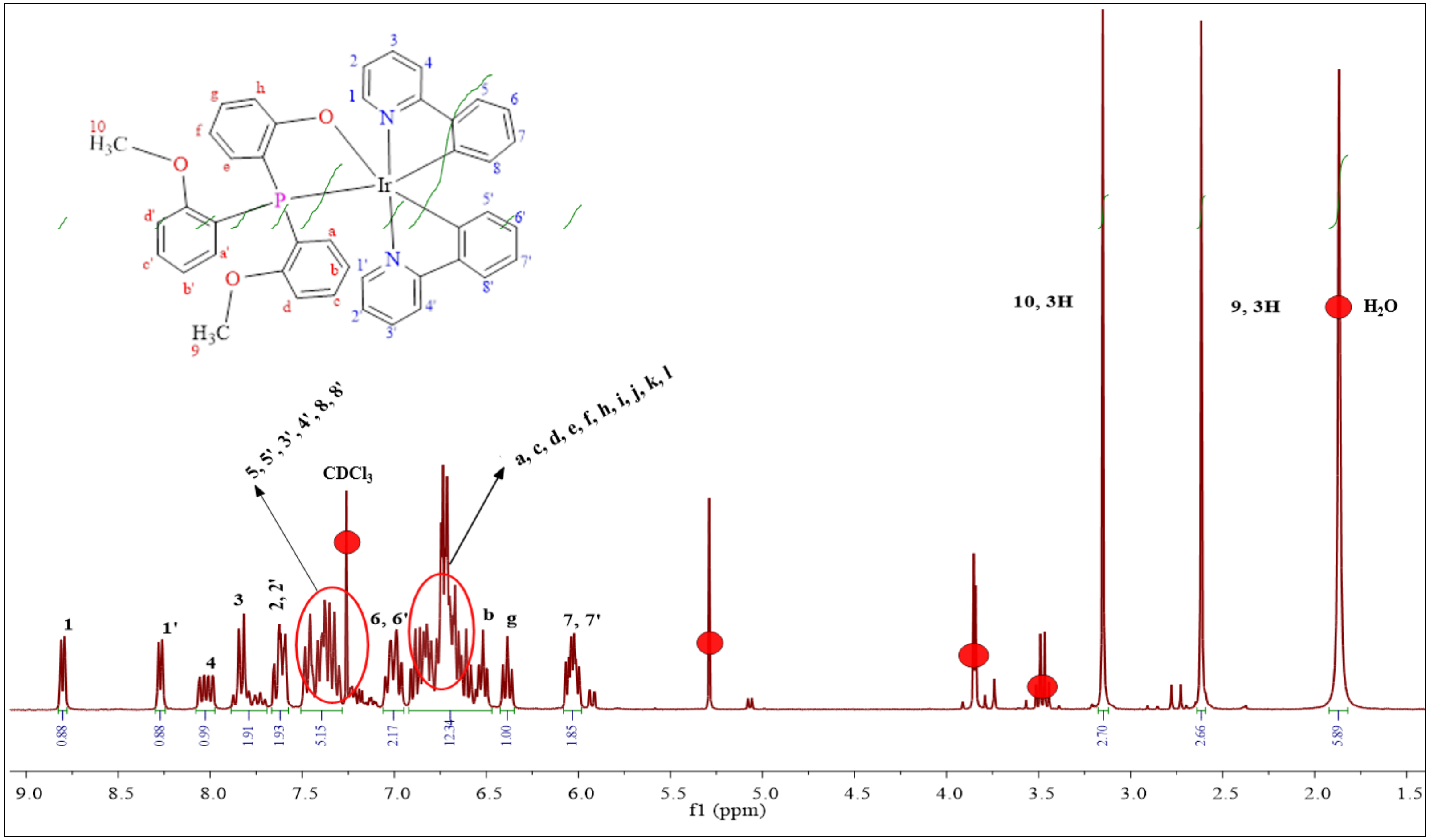

Figure 31. ^{1}H-NMR spectrum of [Ir(ppy$_2$(tmp)]·CH_2Cl_2 complex in $CDCl_3$.

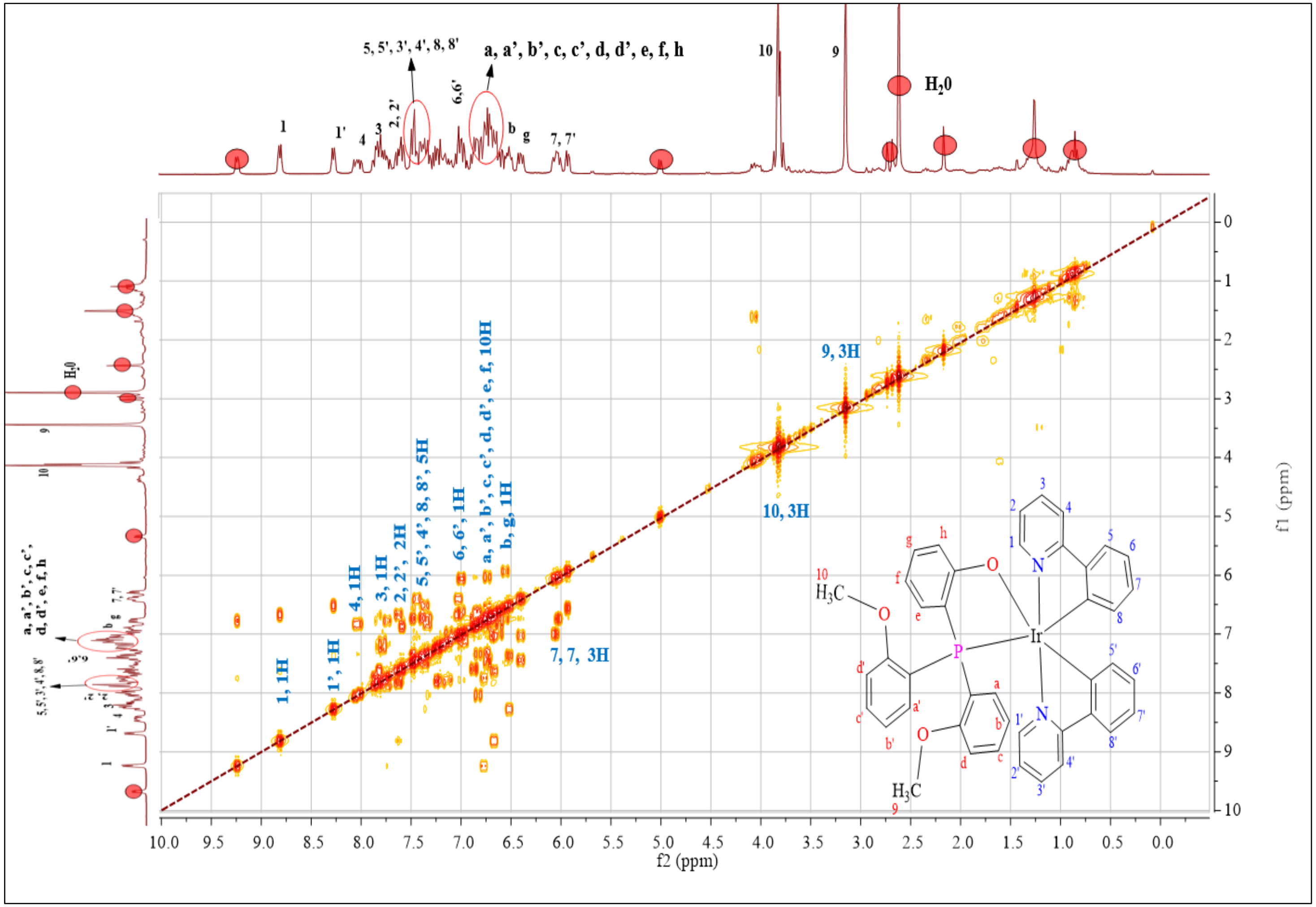

Figure 32. ^{1}H-^{1}H-NMR COSY spectrum of $[Ir(ppy)_2(tmp)]\cdot CH_2Cl_2$ complex in $CDCl_3$.

3.2.2. [13]C-NMR Spectroscopy

The ^{13}C-NMR of complex **2** showed 42 signals of carbon analogous to the structure. 1D and 2D data of complex **2** displayed in Table 13. The structure with carbon numbering exhibited in Figure 33. The complex was made up of methyl carbon (CH_3), signals of methine carbon (CH), and signals of quaternary carbon were displayed in Figure 34. Methine carbon was analyzed by DEPT 90 (Figure 35). Methyl and methylene carbons were analyzed by DEPT 135 as shown in Figure 36. The association of carbon-proton and carbon-carbon were characterized by ^{1}H-^{13}C HMQC NMR and ^{13}C-^{13}C HMBC. The HMBC and HMQC spectra were presented in Figure 37 and Figure 38.

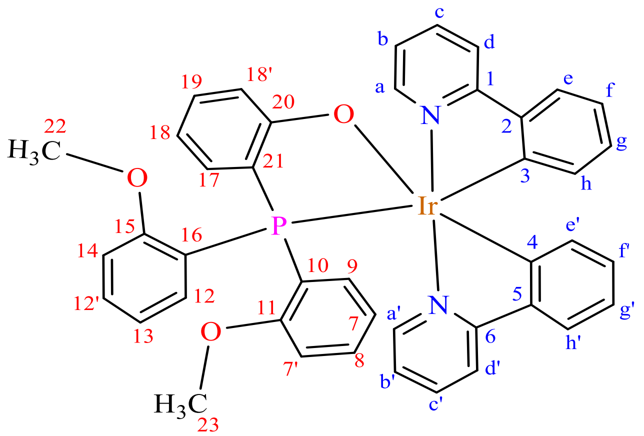

Figure 33. The structure of complex **2** with carbon numbering.

Table 13. 1D and 2D NMR data of [Ir(ppy)$_2$(tmp)]·CH_2Cl_2 complex.

[Ir(ppy)$_2$(tmp)]·CH_2Cl_2						
C-N$_0$.	δ_C (ppm)	Dept 90/135	^{1}H	HMQC δ_C (mult., *J (Hz),* No. H)	HMBC	COSY
1	155.55	C	-	-	-	-
2	143.83	C	-	-	-	-
3	151.74	C	-	-	-	-
4	134.53	C	-	-	-	-
5	132.43	C	-	-	-	-
6	112.84	C	-	-	-	-
7	118.74	C	-	-	-	-
8	121.48	C	-	-	-	-
9	129.16	C	-	-	-	-
10	124.12	C	-	-	-	-
11	132.02	C	-	-	-	-
12	132.43	C	-	-	-	-
13	135.14	CH	*1*	8.27, s, 5.8 *Hz*, H	5,7, 17	*1*
14	135.14	CH	*2*	7.63, t, H	6, g, g'	*2*
15	130.65	CH	*4*	7.84, d, 7.7 *Hz*, H	14, 15	*4*
16	116.78, 121.48, 123.18	CH	*3, 5, 6, 7, 8*	7.40, m, 5H	7', 8, 9, 10	*3, 5, 6, 7, 8*
17	122.26	CH	*a*	8.27, d, 5.80 *Hz*, H	7, 7', 8, 9, 10, 11	*a*
18	114.51	CH	*b*	6.39, t, H	7'8	*b*
19	124.12, 122.26, 119.60	CH	*c, d, a', b', c', d', e, f, h*	6.93, 657, m, 10H	10, 11, 11', 12, 13	*c, d, a', b', c', d', e, f, g, h*
20	53.33	CH_3	*9*	3.15, s, 3H	22	*9*
21	54.90	CH_3	*10*	2.62, s, 3H	23	*10*

Methyl carbon (CH_3) C22 with chemical shift of δ_H = 53.33 ppm correlated with proton *9* (δ_H = 3.15 ppm).

Methyl carbon (CH_3) C23 with chemical shift of δ_H = 54.90 ppm correlated with proton *10* (δ_H = 2.62 ppm).

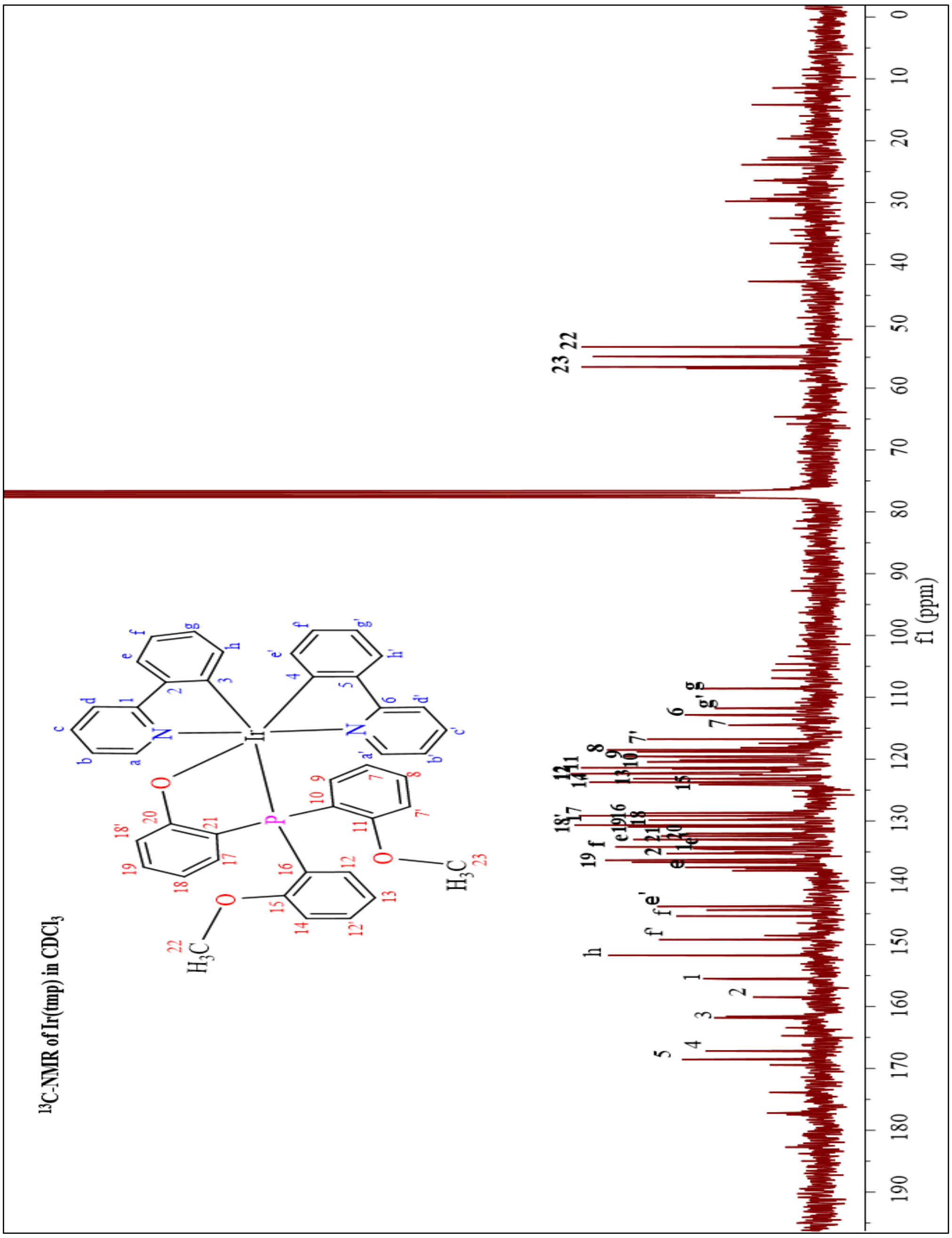

Figure 34. ^{13}C-NMR spectrum of [Ir(ppy)$_2$(tmp)]·CH_2Cl_2 complex in $CDCl_3$.

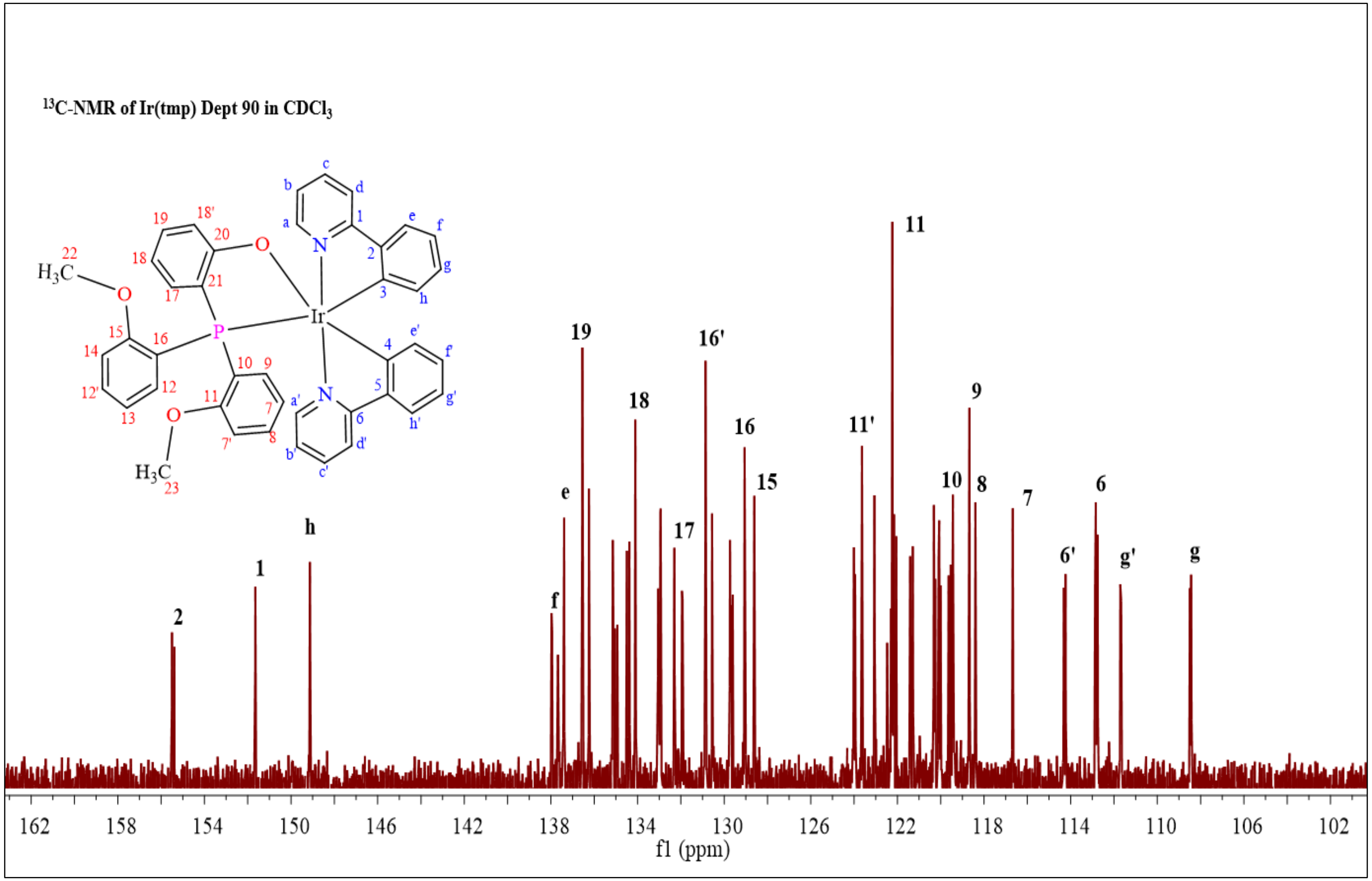

Figure 35. DEPT 90 NMR spectrum of $[Ir(ppy)_2(tmp)]\cdot CH_2Cl_2$ complex in $CDCl_3$.

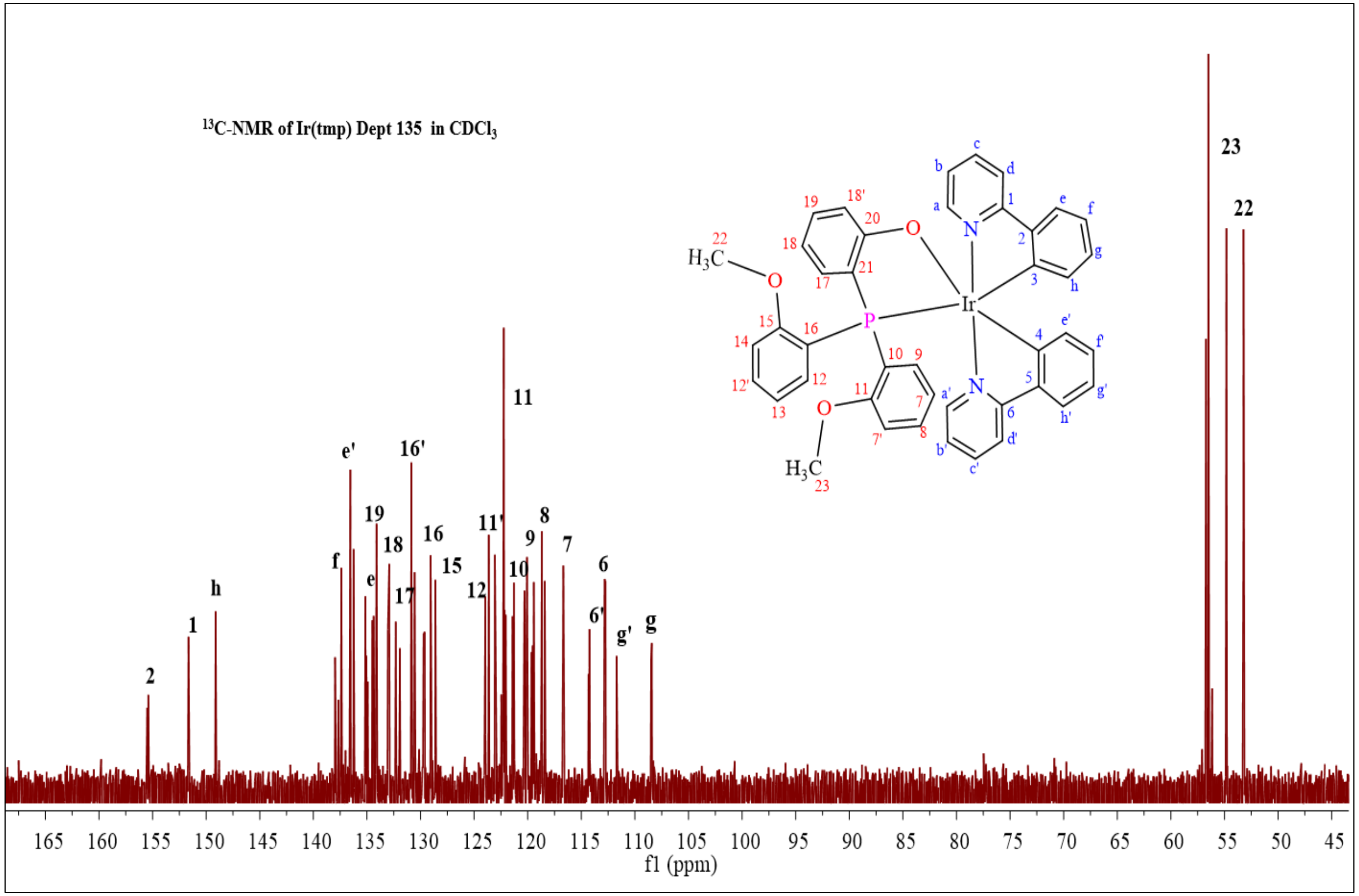

Figure 36. DEPT 135 NMR spectrum of $[Ir(ppy)_2(tmp)]\cdot CH_2Cl_2$ complex in $CDCl_3$.

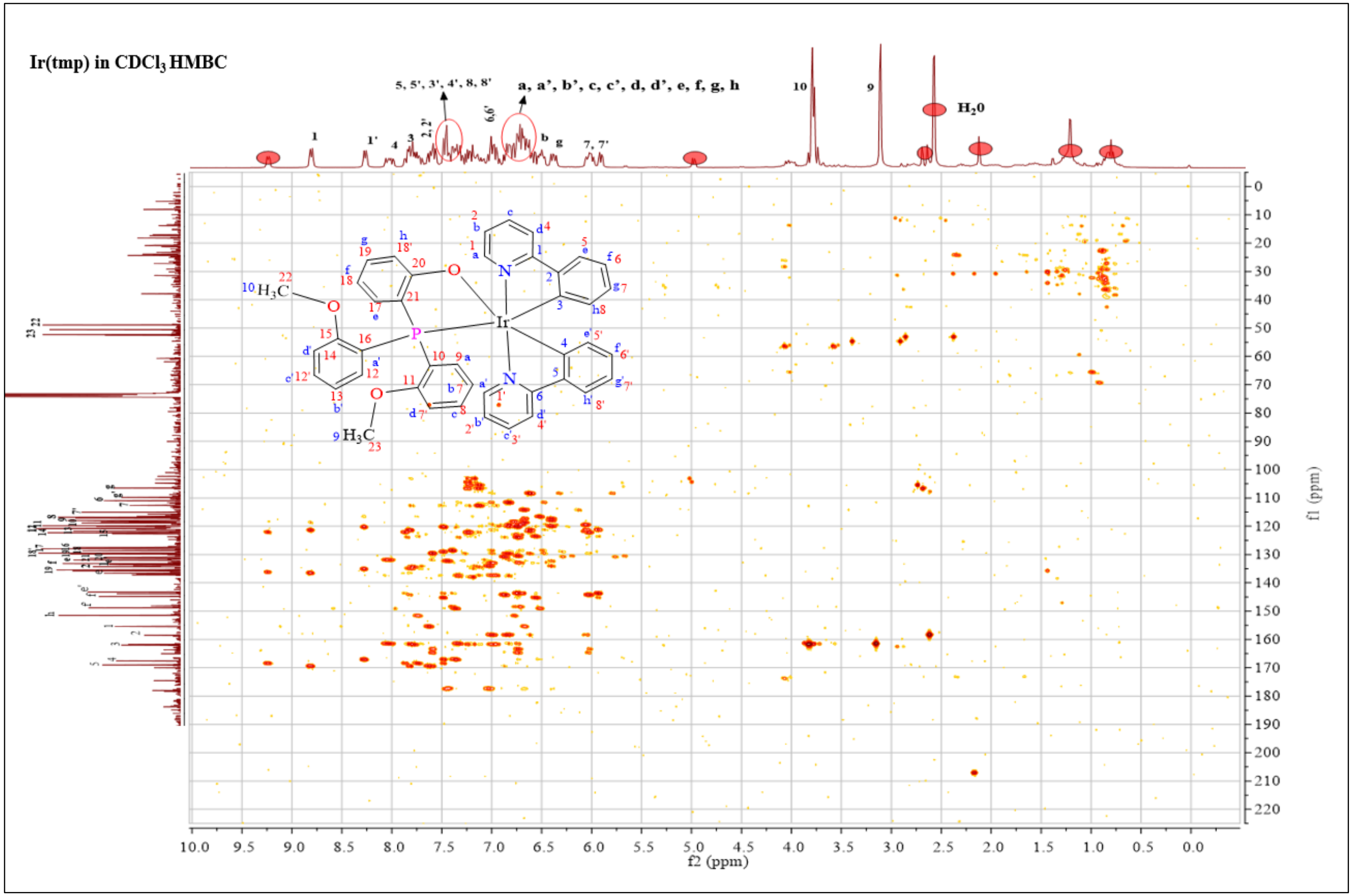

Figure 37. ^{13}C-^{13}C-NMR spectrum of $[Ir(ppy)_2(tmp)]\cdot CH_2Cl_2$ complex in $CDCl_3$.

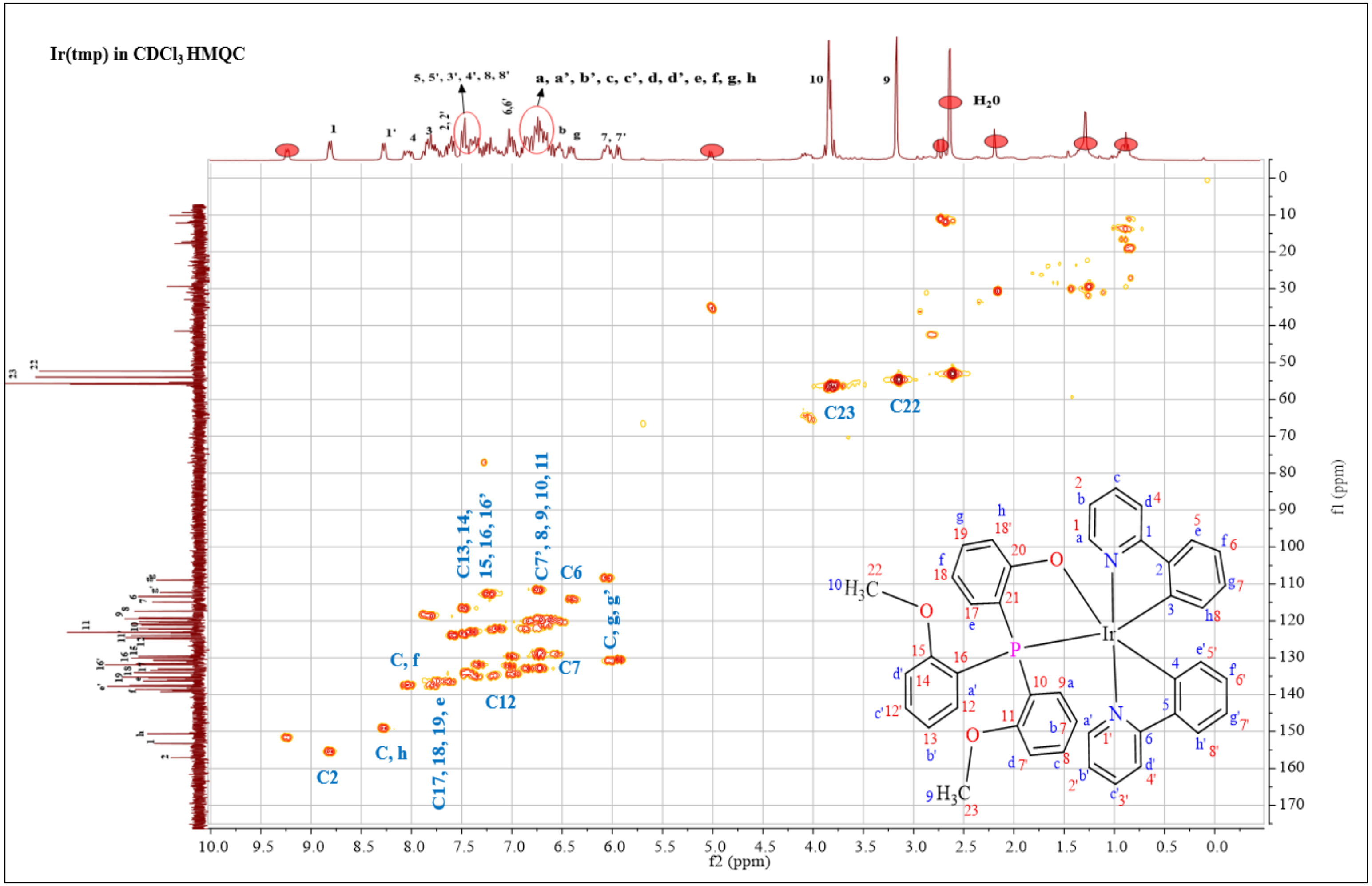

Figure 38. ^{1}H-^{13}C NMR spectrum of $[Ir(ppy)_2(tmp)]\cdot CH_2Cl_2$ complex in $CDCl_3$.

3.2.3. Fourier transforms infrared spectroscopy

The FTIR data of $[Ir(ppy)_2(tmp)]\cdot CH_2Cl_2$ complex are presented in Table 14 and IR characteristic peaks are illustrated in Figure 39.

Table 14. The vibrational modes and frequencies of $[Ir(ppy)_2(tmp)]\cdot CH_2Cl_2$ complex.

Vibrational mode	Frequencies (cm^{-1})
Ir-O Stretching	410
Ir-P Stretching	500
Ir-N Stretching	569
P-C Stretching	753
N-C Stretching	1007
C-C Stretching	1145-1261
C = C Stretching	1426
C = N Stretching	1467
CH_3 bending	1579
C-H Stretching	3041

The FTIR spectrum of complex 2 pointed out that the coordination with the Ir^{3+} metal center was observed. Due to the electron back bonding from the d orbital of $Ir^{3+} \rightarrow \pi^*$ orbital of tmp ligand. The stretching vibrational frequencies of Ir-O, Ir-P, and Ir-N can also be used to determine the coordination between the metal center and tmp ligand. Stretching frequencies of 410, 500, 569 cm^{-1}, respectively, which were similar with others reported (Leesakul *et al*., 2021; Du *et al*., 2018). However, it cannot be explained from the stretching vibrational frequency of P-C bond like as observed for the complex 1 because the peak occurred at 753 cm^{-1}, which is exactly the same with the stretching frequency of tris(2-methoxyphenyl)phosphine (tmp) free ligand, which was reported by (Niu *et al*., 2017; Liu, 2016).

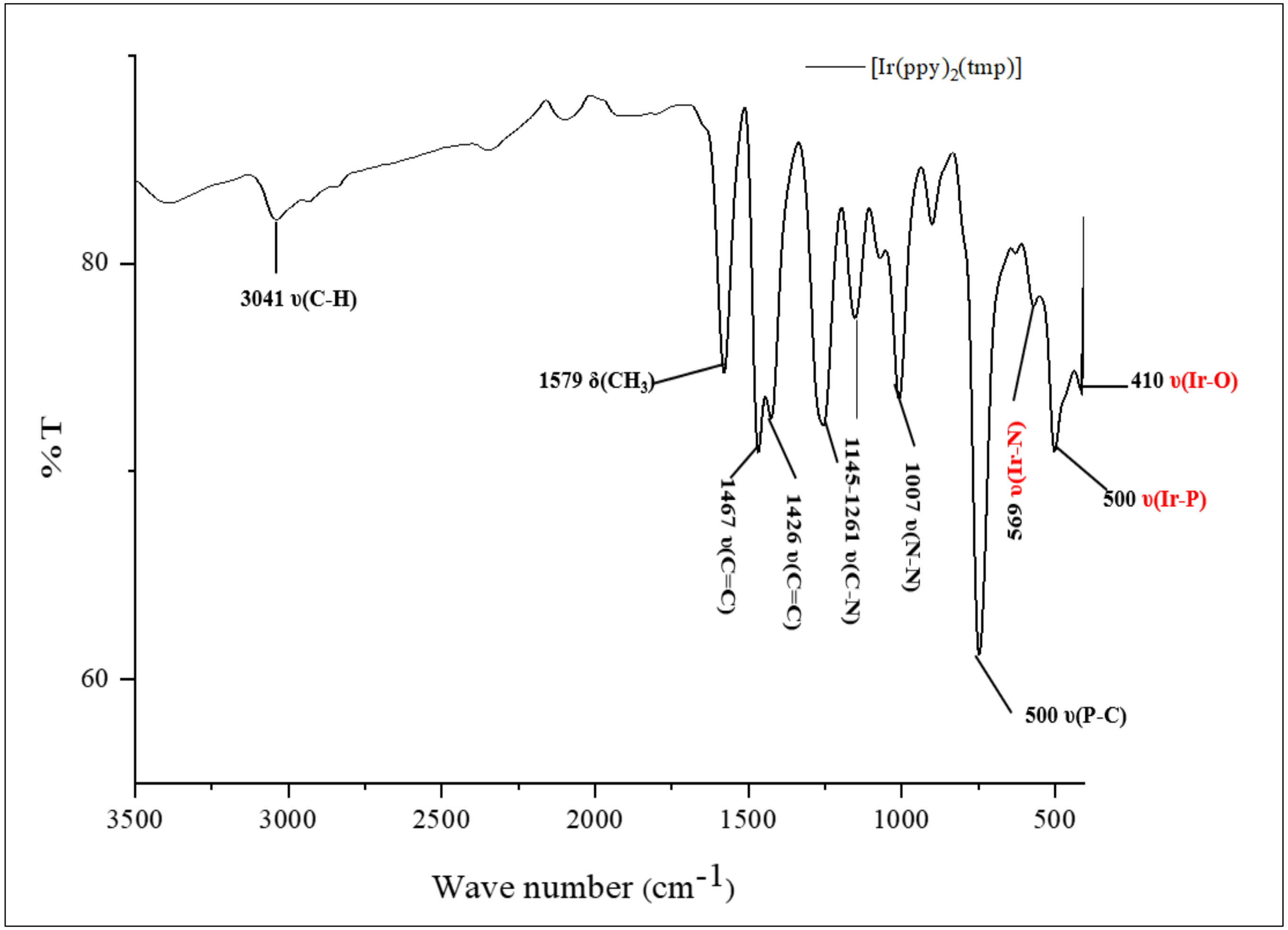

Figure 39. The IR spectrum of $[Ir(ppy)_2(tmp)Cl]\cdot CH_2Cl_2$ complex in KBr pellet.

3.2.4. Single crystal X-ray diffraction

The structure of yellow crystal [Ir(ppy)$_2$(tmp)]·CH$_2$Cl$_2$ complex **2** was monoclinic system with *P*2$_1$/*c* space group as shown in Figure 40 and the crystallographic information data were given in Table 15. Ir(III) ion was coordinated by two 2-phenylpyridine molecules in bis-complexes and one of tris(2-methoxyphenyl)phosphine (tmp) by bidentate mode generating a chelating ring via phosphorous and oxygen atoms. Thus, the geometry of the Ir(III) complex was distorted by an octahedral shape. Table 16 displays the chosen bond lengths and angles for the [Ir(ppy)$_2$(tmp)]·CH$_2$Cl$_2$ complex. The bond distance of Ir-C-phenyl rings, 2.014(3) and 2.039(3) Å, and Ir-N pyridine rings, at 2.034(3) and 2.065(3) Å, which were possibility confirming to the distances reported for other related complexes [Ir(3m-ppy)$_2$(dppm)Cl] (dppm = bis(diphenylphosphino)methane, 3m-Hppy = 3-methyl-2-phenylpyridine) 2.007(5)-2.035(6) Å, and 2.061(5) Å (Leesakul *et al*., 2021) and chloro-bis-[2-(2-pyridyl)-phenyl-$\kappa^2 N,C^1$] (tri-phenyl-phosphine-κP) iridium(III) complexes dichloromethane sesquisolvate 2.024(7)-2.03(8) Å, and 2.043(6)-2.044(6) Å (Wang *et al*., 2005). The distances between Ir-O(1) and Ir-P(1) were 2.154(2) and 2.3766(8) Å, respectively, which were similar to the distances for other relevant researched Ir(III) and Ru(II) half-sandwich organometallic complexes containing phosphine-sulfonate ligands 2.166(9)-2.345(3) Å (Du *et al*., 2019; Liu *et al*., 2019). The angles of C(22)-Ir(1)-N(1), C(11)-Ir(1)-N(1), N(2)-Ir(1)-P(1), and N(1)-Ir(1)-P(1) were 97.06(12)^o, 79.77(13)^o, 90.87(7)^o, and 98.22(8)^o, respectively, which were close to other study of Ir(III) complexes [(dfppy)$_2$Ir(ttz) 97.36(13)^o, 79.52(13)^o (Li *et al*., 2018) and tris-cyclometalated complex [Ir(ppy)$_2$(nppy)] (ppy = 2-phenylpyridyl, nppy = 2-(4-nitrophenyl)pyridyl) from [{Ir(μ-Cl)(ppy)$_2$}$_2$] complex, the ligand 2-(4-nitrophenyl)pyridine 84.39(13)^o, 101.69(15)^o, which were deviated from 90^o of ideal octahedral responding to other works of (Böttcher *et al*., 2005; Leesakul *et al*., 2021). Moreover, the angles of N(2)-Ir(1)-O(1) and C(11)-Ir(1)-O(1) were 95.12(10)^o and 89.31(11)^o, which were comparable to other related research of Ir(III) complexes and [Ir(ppy)$_2$(L)]$^{0/+}$ (ppy = 2-phenyl pyridine, L = Schiff base) 95.12(10)^o and 89.71(8)^o (Pradhan *et al*., 2020). The intra-molecular H bonding of C-

H···O type is formed between pyridine group and methoxy group, C(12)-H(12)···O(1), with the H(12)···O(1) accepter distance at 2.56 Å. In addition, this interaction was also found between phenyl ring of tmp and methoxy group which the H(24)···O(3) accepter length of C(24)-H(24)···O(3) at 2.43 Å. Both of these intra-molecular interactions and the data were shown in Figure 41 and Table 17. Additionally, the dihedral angle between the mean planes (plane **A** and **B**) of the ppy molecules of the complex **2** was 86.73^{o}, indicating the *cis* form of the chelate rings (Figure 42).

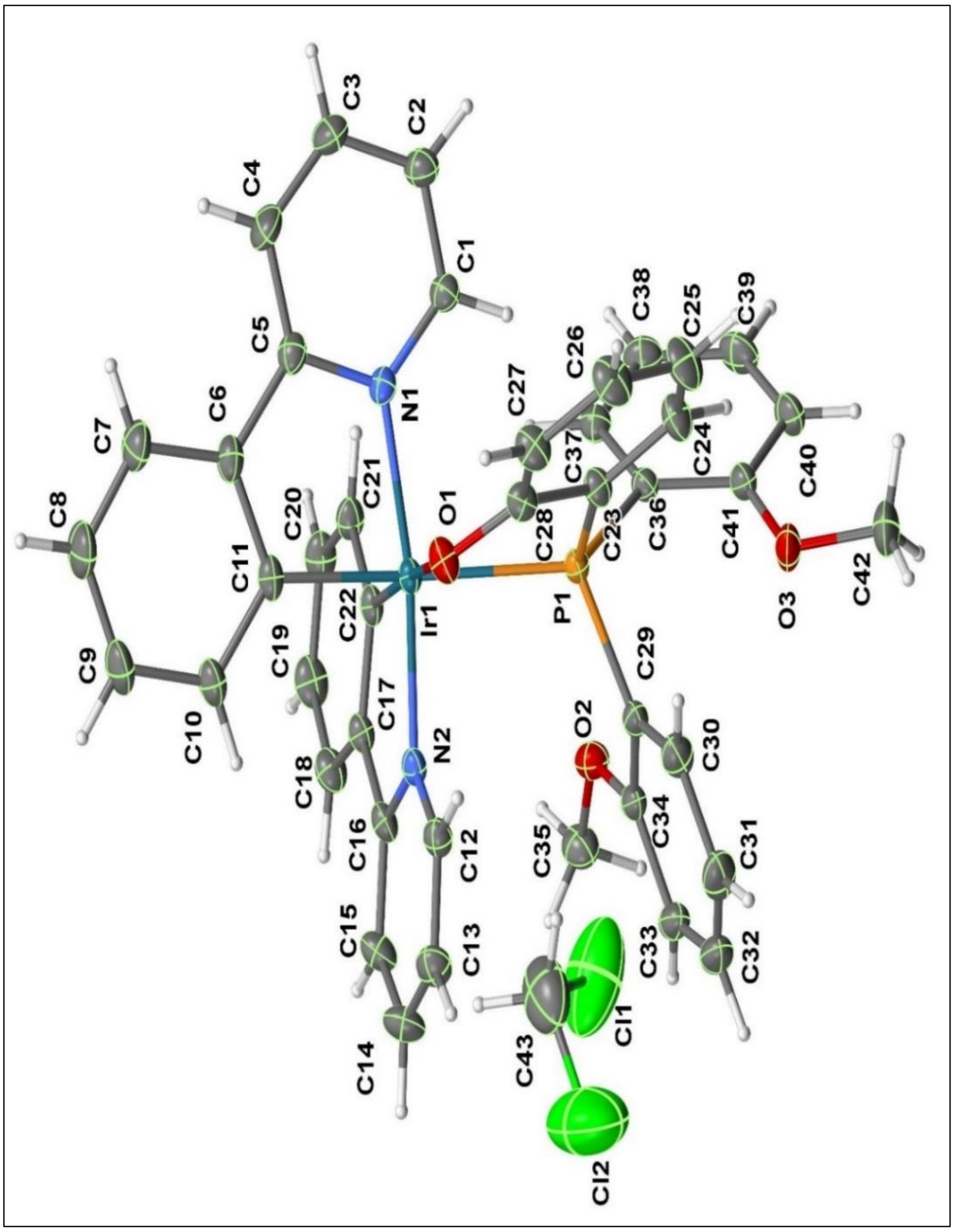

Figure 40. Molecular structure of [Ir(ppy)$_2$(tmp)]·CH_2Cl_2 complex.

Table 15. Crystal data and structure refinement for [Ir(ppy)$_2$(tmp)]·CH_2Cl_2 complex.

Identification code	[Ir(ppy)$_2$(tmp)]·CH_2Cl_2
Empirical formula	$C_{42}H_{34}IrN_2O_3CH_2Cl_2$
Formula weight	922.83
Temperature	296(2) K
Wavelength	1.54178 Å
Crystal system	Monoclinic
Space group	$P2_1/c$
Unit cell dimensions	a = 12.6715(4) Å α = 90° b = 12.5690(4) Å β = 94.8360(10)° c = 24.3914(8) Å γ = 90°.
Volume	3870.9(2) Å^3
Z	4
Density (calculated)	1.583 Mg/m^3
Absorption coefficient	8.670 mm^{-1}
F(000)	1832
Crystal size	0.393 × 0.110 × 0.066 mm^3
Theta range for data collection	5.062 to 70.063°
Index ranges	-14<=h<=15, -15<=k<=15, -29<=l<=29
Reflections collected	79532
Independent reflections	7312 [R(int) = 0.0456]
Completeness to theta = 67.679°	99.1 %
Absorption correction	Semi-empirical from equivalents
Max. and min. transmission	0.7536 and 0.3235
Refinement method	Full-matrix least-squares on F^2
Data / restraints / parameters	7312/0/471
Goodness-of-fit on F^2	1.053
Final R indices [I>2σ(I)]	$R1$ = 0.0292, $wR2$ = 0.0778
R indices (all data)	$R1$ = 0.0296, $wR2$ = 0.0783
Extinction coefficient	n/a
Largest diff. peak and hole	1.377 and -1.003 e.Å^{-3}

Table 16. Selected bond lengths (Å) and angles (º) for $[Ir(ppy)_2(tmp)]\cdot CH_2Cl_2$ complex.

Bond lengths			
Ir(1)-C(22)	2.014(3)	Ir(1)-N(1)	2.065(3)
Ir(1)-N(2)	2.034(3)	Ir(1)-O(1)	2.154(2)
Ir(1)-C(11)	2.039(3)	Ir(1)-P(1)	2.3766(8)
Angles			
C(22)-Ir(1)-N(2)	80.52(12)	C(11)-Ir(1)-O(1)	89.31(11)
C(22)-Ir(1)-C(11)	87.92(12)	N(1)-Ir(1)-O(1)	86.81(10)
N(2)-Ir(1)-C(11)	91.35(13)	C(22)-Ir(1)-P(1)	103.74(9)
C(22)-Ir(1)-N(1)	97.06(12)	N(2)-Ir(1)-P(1)	90.87(7)
N(2)-Ir(1)-N(1)	170.91(10)	C(11)-Ir(1)-P(1)	168.33(9)
C(11)-Ir(1)-N(1)	79.77(13)	N(1)-Ir(1)-P(1)	98.22(8)
C(22)-Ir(1)-O(1)	174.76(11)	O(1)-Ir(1)-P(1)	79.09(7)
N(2)-Ir(1)-O(1)	95.12(10)		

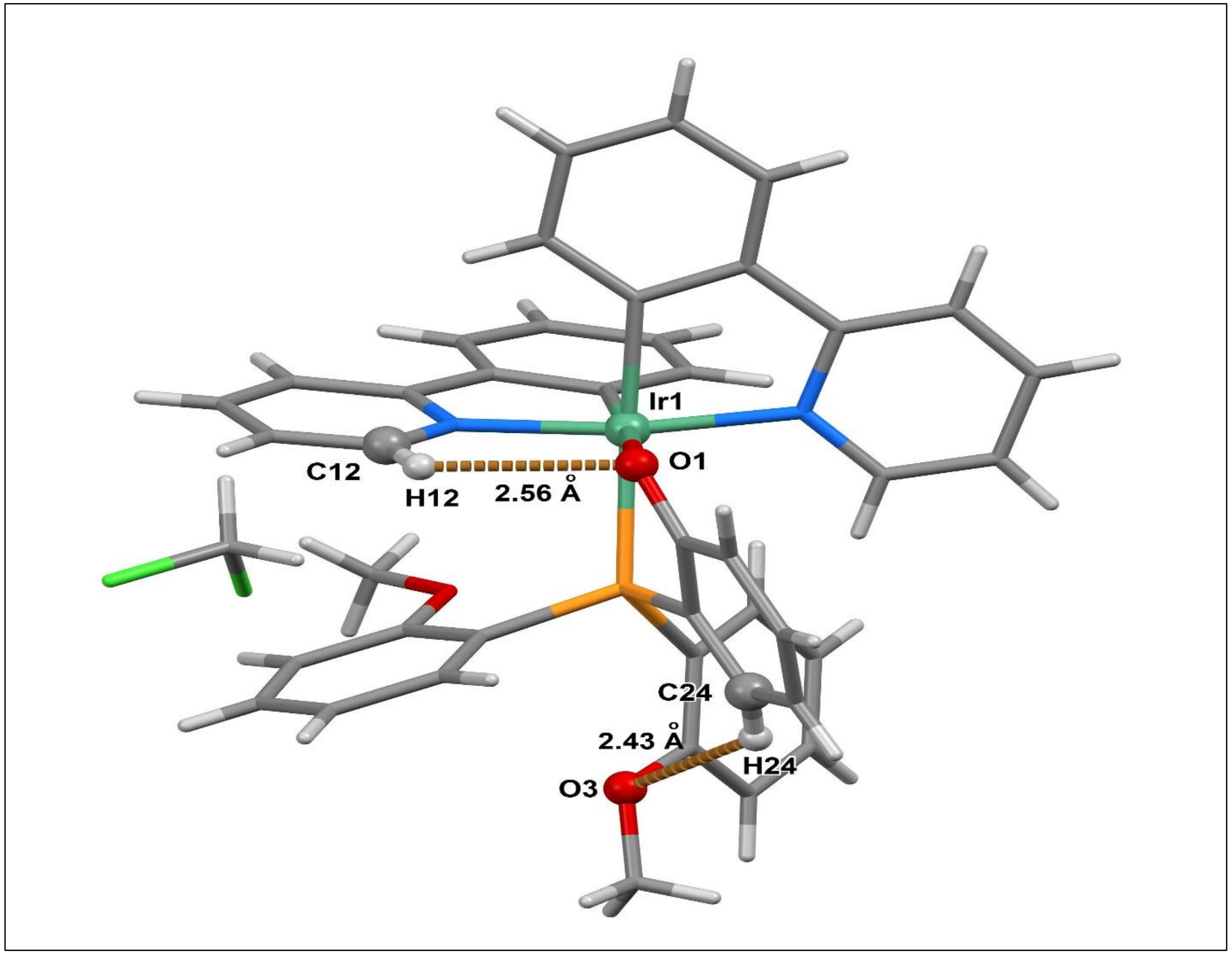

Figure 41. Intra-molecular H-bond interactions of $[Ir(ppy)_2(tmp)]\cdot CH_2Cl_2$ complex.

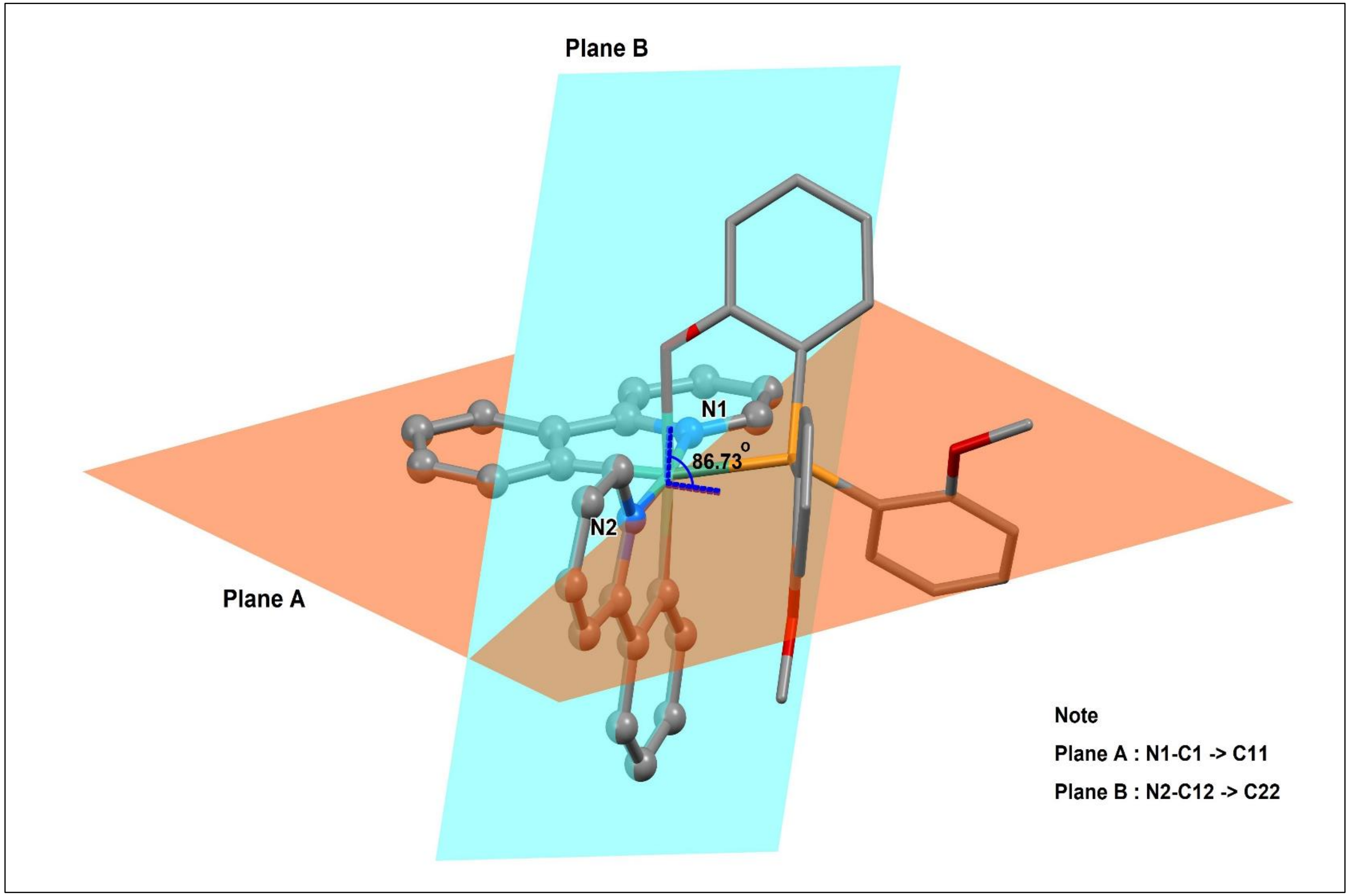

Figure 42. The mean plane between ppy molecules of $[Ir(ppy)_2(tmp)]\cdot CH_2Cl_2$ complex.

Table 17. Hydrogen bonds [Å and º] of $[Ir(ppy)_2(tmp)]\cdot CH_2Cl_2$ complex.

D-H···A	Distance of d(D-H) (Å)	Distance of d(H···A) (Å)	Distance of d(D···A) (Å)	Angles of <(DHA) (º)
C(12)-H(12)···O(1)	0.93	2.56	3.143(4)	121.0
C(24)-H(24)···O(3)	0.93	2.43	3.118(5)	131.2

Note:

D = donor (C atom), A = acceptor (O atom).

3.2.5. Elemental analysis

It should be noted that the results of determination of the C, H, N, and O percentages between the calculation and experiment of $[Ir(ppy)_2(tmp)]\cdot CH_2Cl_2$ complex aligned to each other with a small deviation as shown in Table 18.

Table 18. Elemental analysis data of $[Ir(ppy)_2(tmp)]\cdot CH_2Cl_2$ complex.

Elemental analysis				
Elements (%)	C	H	N	O
Calculated	57.215	3.901	3.034	5.201
Found	57.225	3.898	3.400	5.378
Deviation (Δ)	± 0.01	± 0.003	± 0.3	± 0.17

Note:

The acceptance deviation of each element in the compound was Δ = 0.3.

3.2.6. Photo-physical properties of absorption and emission of complex 2

The complex **2** is measured for its UV-Visible absorbance spectrum between 200-800 nm at a concentration of 5×10^{-5} M using dimethylformamide (DMF) as a solvent. The absorption spectrum showed a single broad band at λ_{max} = 400 nm, which was attributed to the charge transfer transition with the molar excitation coefficient ($\varepsilon_{(400)}$ = 15×10^{3} M^{-1} cm^{-1}). A luminescent broad band at 522 nm was observed at 522 nm in the DMF when excited at 380 nm at room temperature (Figure 43).

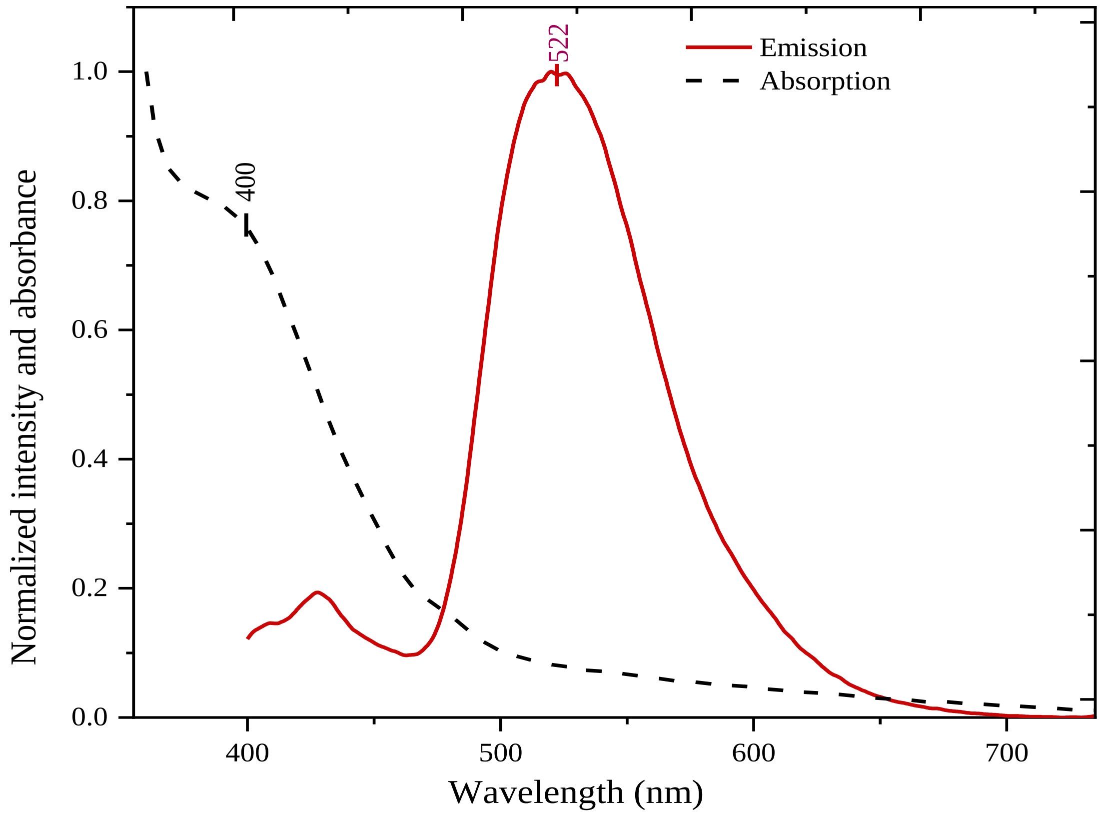

Figure 43. Normalized absorption and emission spectra of 5×10^{-5} M of $[Ir(ppy)_2(tmp)]\cdot CH_2Cl_2$ complex in dimethylformamide (DMF).

3.2.7. Photoluminescence and quantum yield

The emission λ_{em} = 522 nm and absorption λ_{abs} = 400 nm of $[Ir(ppy)_2(tmp)]\cdot CH_2Cl_2$ complex in dimethylformamide (DMF) 25°C at the concentration 1×10^{-6} M were observed as shown in Figure 44 (**a** and **b**). The complex and coumarin-6 were used at low concentration and lower absorbance than 0.05 in order to prevent self-quenching reaction. The $[Ir(ppy)_2(tmp)]\cdot CH_2Cl_2$ complex and coumarin-6 as reference standard were excited at 380 nm. At 298 K, the complex's emission quantum yield was 0.38. According to the Kotelevskiy equation (Jiménez Riobóo *et al*., 2009; Yoopensuk *et al*., 2012), the quantum yield at room temperature related quantum yield 0.18 of coumarin 6 used as a reference standard at the same concentration in ethanol 25°C.

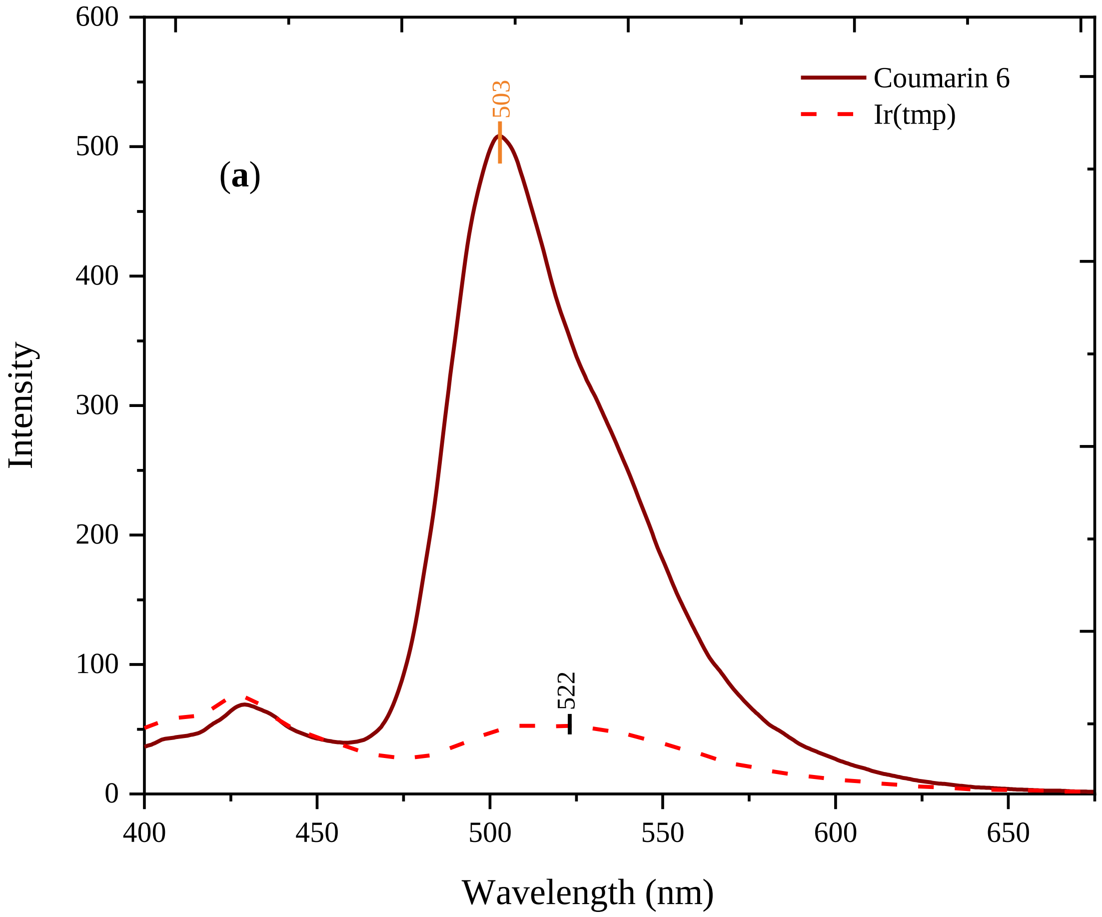

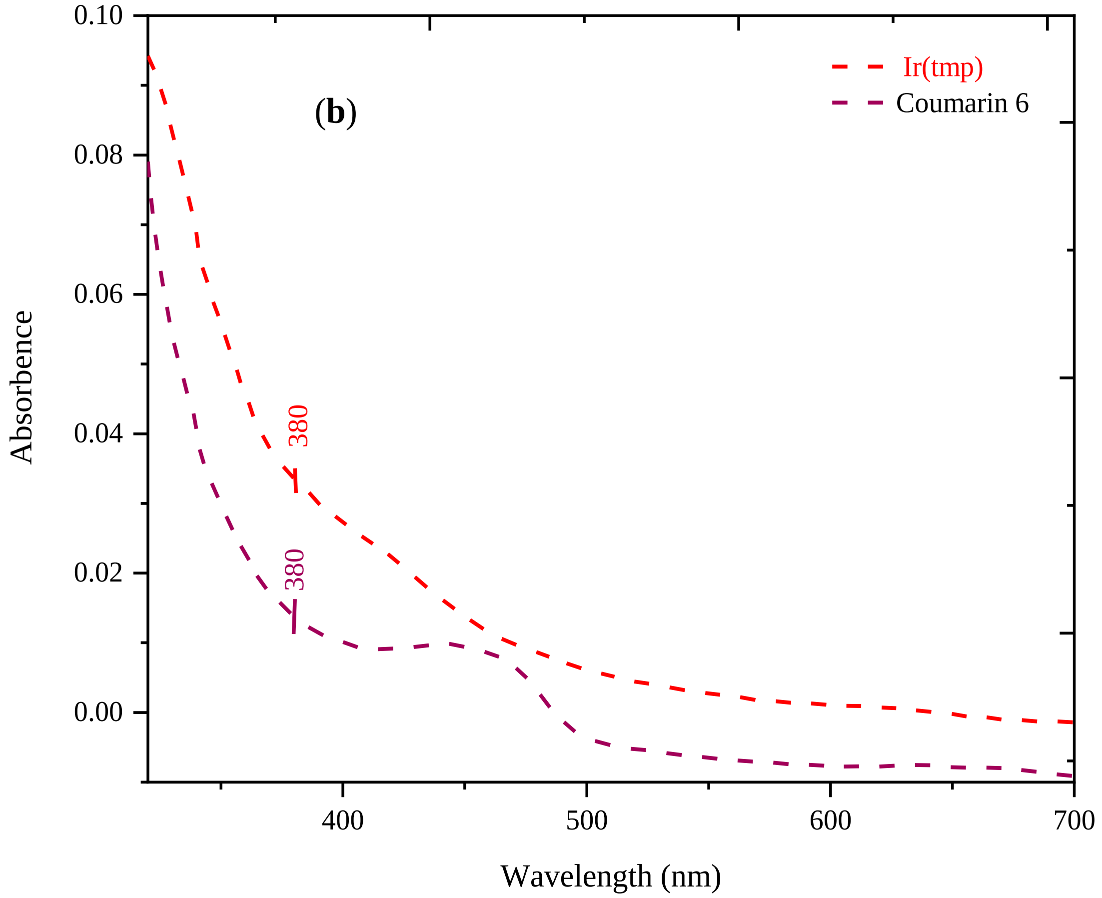

Figure 44. The emission (**a**) and absorption (**b**) spectra of [Ir(ppy)$_2$(tmp)]·CH_2Cl_2 and coumarin 6 at the same concentration.

3.2.8. Quenching reaction

Quenching of complex **2** with different metal ions, including Ba^{2+}, Co^{2+}, Cu^{2+}, Fe^{3+}, Ni^{2+}, Mg^{2+}, Pb^{2+}, and Zn^{2+} were examined in dimethylformamide (DMF) solvent. According to the bar graph in Figure 45 it was discovered that none of the other metal ions interfered with the detection of Fe(III). The luminescence of our complex in the study was greatly quenched by the presence of Fe(III). The concentration range between 1×10^{-5} to 2.3×10^{-4} M was used to study the complex in this study, which was selective to Fe^{3+} ion. While the Fe^{3+} concentrations increased as shown in Figure 46, the luminescent intensities of complex **2** gradually decreased. The detection limit (DL) was 1.17×10^{-3} M, and quenching effectiveness was above 90% using 0.03 mM of Ir(III) complex.

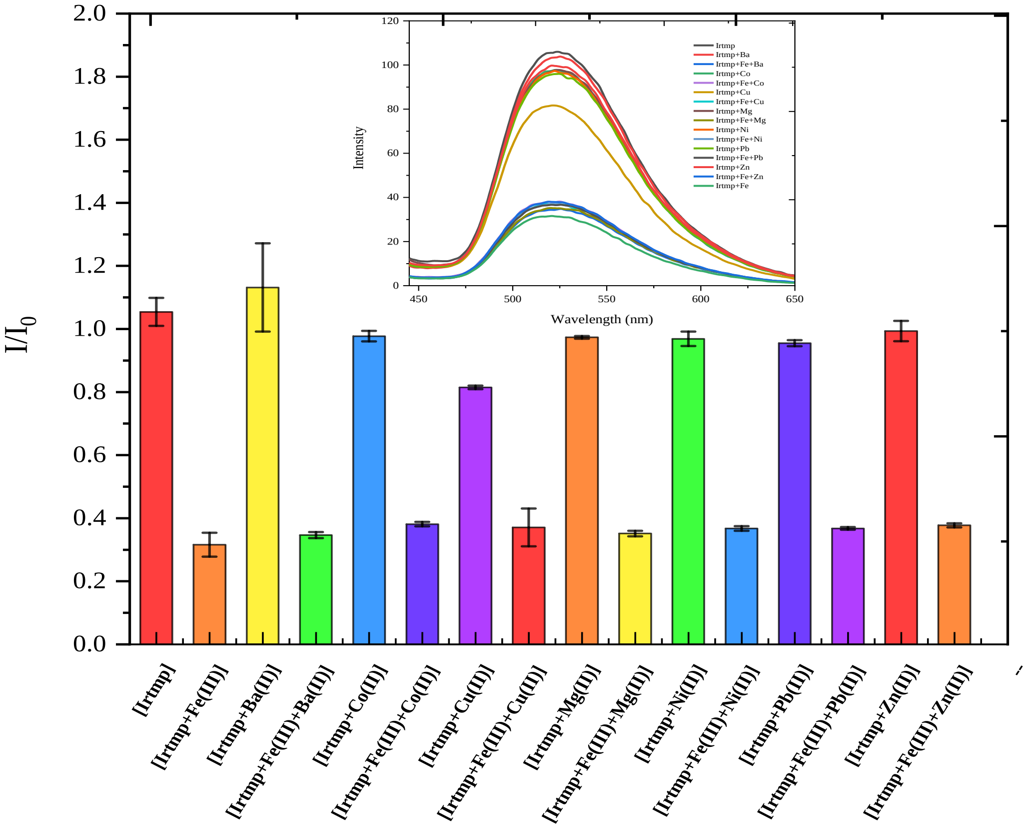

Figure 45. A bar graph showing the luminescence spectrum of the $[Ir(ppy)_2(tmp)]\cdot CH_2Cl_2$ complex solution after the addition of several metal cations.

The photo-induced electron transfer was supposed to be occurring between Ir(III) complex and Fe^{3+} ion in the mechanism below:

$$\text{Ir(III)} + \text{Fe(III)} \rightleftharpoons [Ir^{3+}\,(\text{donor})\cdots Fe^{3+}\,(\text{acceptor})]$$

$$Ir^{3+} + Fe^{3+} \longrightarrow Ir^{4+} + Fe^{2+}$$

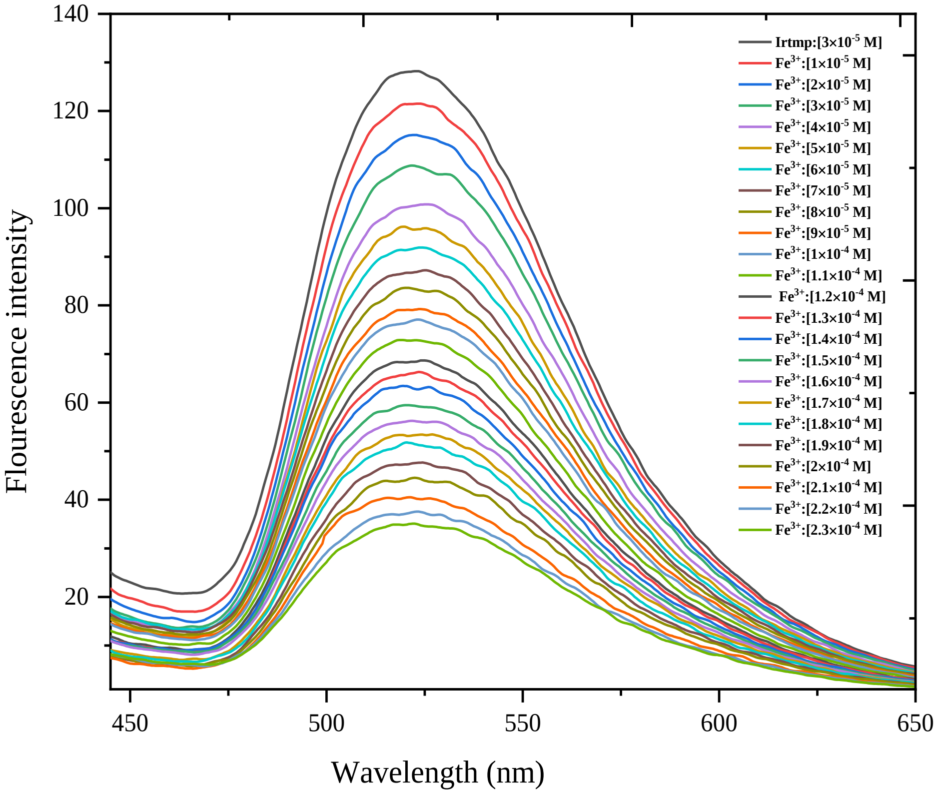

Figure 46. Quenching reaction of $[Ir(ppy)_2(tmp)]\cdot CH_2Cl_2$ complex in dimethylformamide (DMF).

From the SV plot, the Stern-Volmer constant (K_{SV}), which characterizes the electron transfer between Fe^{3+} and Ir(III), has been computed (Figure 47). From the quenching study in the range of studied concentration, the upward bending to the y-axis was observed which did not obey the linear regression of SV plot. It meant that in higher concentrations of Fe^{3+}, there might be the ground state complex formation. The linearity was available up to 1×10^{-5} M concentration of Ir(III), the K_{SV} was 6830 $M^{-1.}$

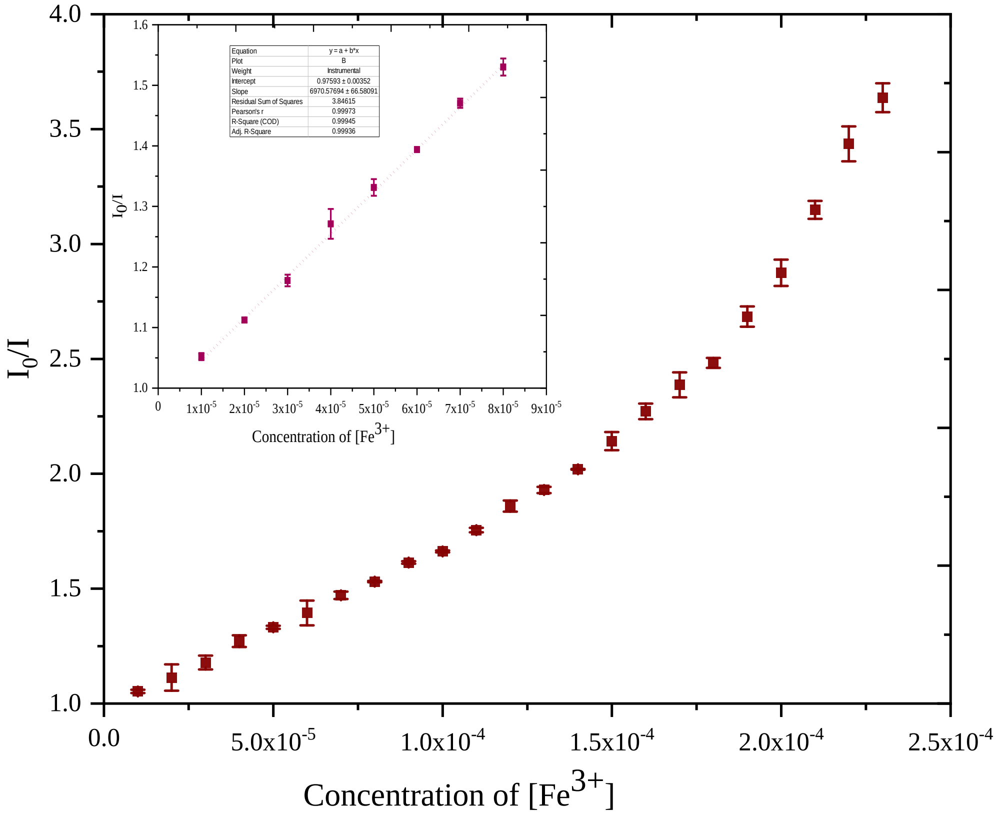

Figure 47. Stern-Volmer and linearity plots from quenching reaction between complex **2** with different concentrations of Fe(III).

Continuous variation Job's method was a method used for identification of the stoichiometric ratio of the complex **2** Fe(III). The binding of complex **2** to the Fe(III) was represented by the Job plot. For a 1:1 ratio. The mole fraction of Fe(III) provided the crossing point for this study at $\chi = 0.5$ (Figure 48). A binding constant (K_b) for the quenching reaction was determined after investigating the Benesi-Hildebrand equation. This constant, (K_b), indicated the strength binding between complex **2** and Fe(III), and it was 1850 M^{-1}. Figure 49 shows the 1:1 complex creation using a Benesi-Hildebrand plot (linear plot). It demonstrated high binding interaction between Fe^{3+} and Ir(III).

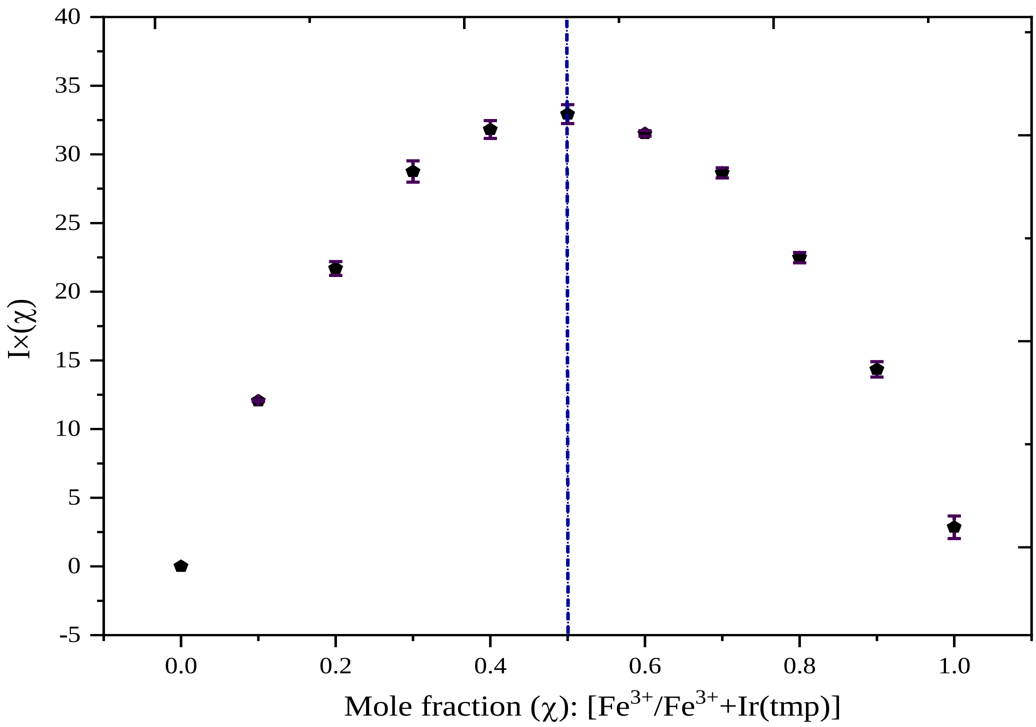

Figure 48. Job's plot for analyzing the stoichiometry of [Ir(ppy)$_2$(tmp)Cl]·CH_2Cl_2 complex to Fe(III).

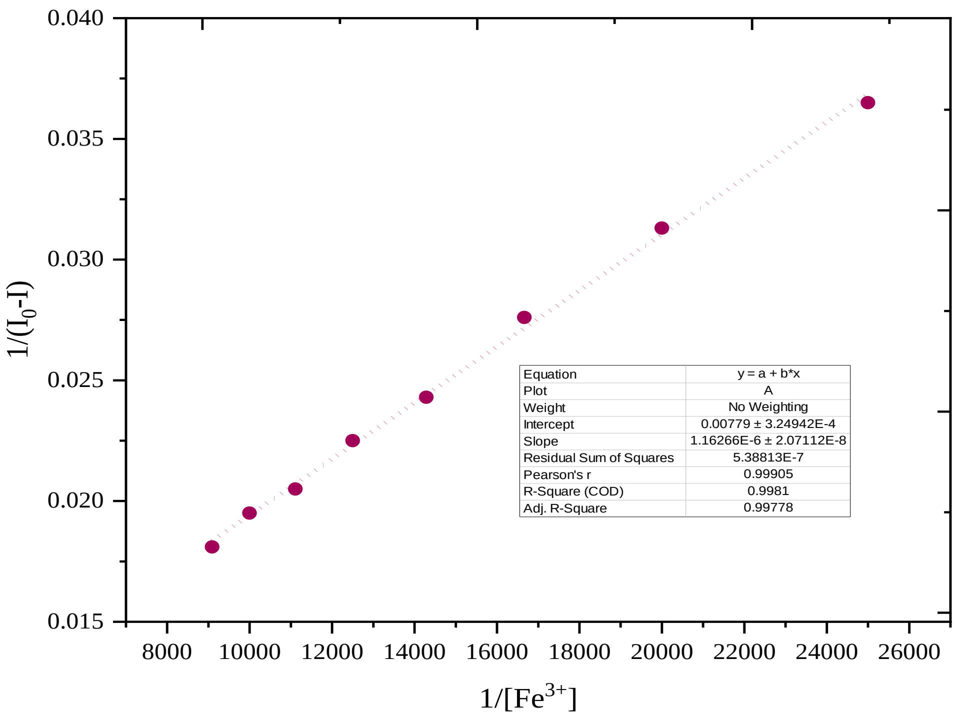

Figure 49. Fe(III) luminescence titration between [Ir(ppy)$_2$(tmp)]·CH_2Cl_2 complex and different Fe(III) concentrations, represented by a Benesi-Hildebrand plot.

3.2.9. Antimicrobial and antifungal activity

By using colorimetric broth microdilution technique, the antibacterial activity of complex **2** was examined against bacteria, yeast, and filamentous fungi**.** Table 19 shows the MIC/MBC and MIC/MFC values. The complex **2** exhibited a good to moderate antibacterial activity against two types of gram-positive bacteria, including *Staphylococcus aureus* (SA) and methicillin-resistant *Staphylococcus aureus* (MRSA), with MIC/MBC values of 16/32 µg/mL and 32/32 µg/mL, respectively. Additionally, complex **2** had weak activity against yeast, with *Cryptococcus neoformans* (CN90112) MIC/MFC values 128/200 and (CN90113) MIC/MFC values of 128/200 µg/mL. However, Vancomycin and Amphotericin B, two commercial antibacterial and antifungal drugs showed lower MIC/MBC and MIC/MFC values than the complex **2**. Gram-positive bacteria had no outer cell membrane as like as gram-negative bacteria, but they were surrounded by thick layers of peptidoglycan which consisting of repeating units of β-1, 4-linked N-acetylglucosamine and N-acetylmuramic acid disaccharide, cross-linking by short peptides. Therefore, it had both polar and non-polar lipids. It was complicated to identify the exact mechanism from our work. However, it probably arises from the availability of our studied complex to penetrate to the gram-positive bacteria cell by having an appropriate polarity like the cell.

Table 19. The results of MIC and MFC of $[Ir(ppy)_2(tmp)]\cdot CH_2Cl_2$ complex.

Complex	Bacteria (µg/mL)				Yeast (µg/mL)												Filamentous fungus (µg/mL)			
	SA		MRSA		PA		EC		CA90028		CA3153		CN90112		CN90113		MG		TM	
	MIC	MBC	MIC	MBC	MIC	MBC	MIC	MBC	MIC	MFC	MIC	MFC	MIC	MFC	MIC	MFC	MIC	MFC	MIC	MFC
2	16	32	32	32	NA	NA	NA	NA	NA	NA	NA	NA	128	200	128	200	NA	NA	NA	NA
Vancomycin	0.25	0.5	1	1	-	-	-	-	-	-	-	-	-	-	-	-	-	-	-	-
Amphotericin **B**	-	-	-	-	-	-	-	-	-	-	-	-	0.25	0.5	0.25	0.5	-	-	-	-

SA = *Staphylococcus aureus* ATCC25923, MRSA = methicillin-resistant *Staphylococcus aureus* SK1, PA = *Pseudomonas aeruginosa* ATCC27853, EC = *Escherichia coli* ATCC25922, AB005 = *Acinetobacter baumannii* NPRC005,AB007 = *Acinetobacter baumannii* NPRC007. CA3153 = *Candida albicans* NCPF3153, CN90113 = *Cryptococcus neoformans* ATCC90113 flucytosine-resistant, MG = *Microsporum gypseum* SK-MU4, TM = *Talaromyces marneffei* PSU-SKH1. MIC = minimum inhibitory

3.2.10. Anti-breast cancer activity

Regarding the negative results in the testing the cytotoxicity against 3 cell lines in the range of concentrations between 0.1-10 µM, the complex **2** needs more study in the higher range of concentration to identify the real IC_{50} value (Table 20).

Table 20. The IC_{50} value of complex **2** with concentration range 1-10 µM.

Cell type	IC_{50} (µg/ml)
MCF-7	Not inhibited
BT-549	Not inhibited
MDA-MB-231	Not inhibited

Positive control: Doxorubicin had IC_{50} = 1.15 ± µM, 0.71 ± 0.11 µM, and 0.79 ± 0.04 µM of MCF-7, BT-549, and MDA-MB-231, respectively.

3.3. Synthesis and characterization of Ru(p-cymene)(PPh_3)Cl_2, complex 3

The Ru(*p*-cymene)(PPh_3)Cl_2 complex was prepared by the reaction between dichloro(*p*-cymene)ruthenium(II) dime and with triphenylphosphine (PPh_3) ligand in tetrahydrofuran (THF) 20 mL at 40°C (Scheme 25).

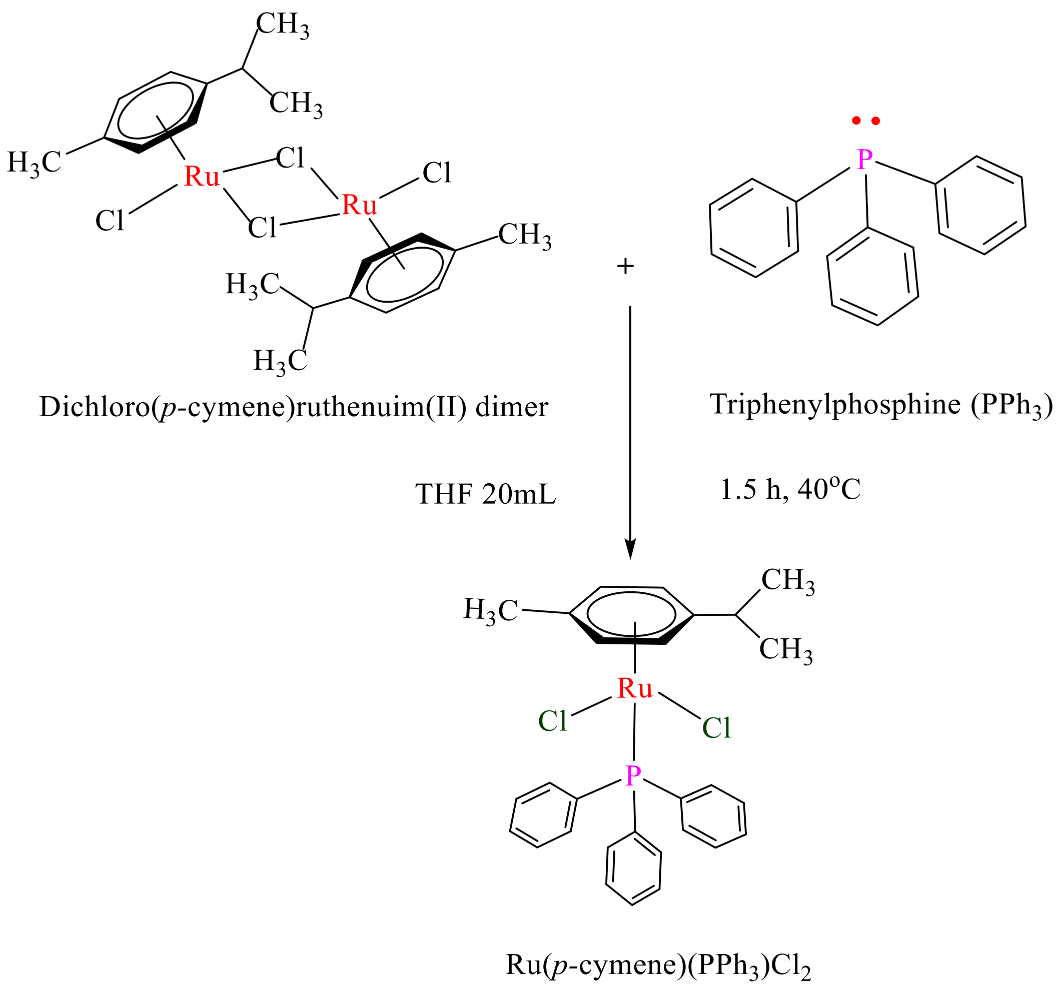

Scheme 25. The synthetic pathway of Ru(*p*-cymene)(PPh_3)Cl_2 complex.

Complex **3** was a moderate polar molecule because of the dipole moment of each solvent. The solubility of complex **3** was displayed in Table 21.

Table 21. The Solubility result of Ru(*p*-cymene)(PPh_3)Cl_2 complex.

Solvent	Solubility
Dimethyl sulfoxide (DMSO)	+ + +
Dimethylformamide (DMF)	+ + +
Diethyl ether	-
Tetrahydrofuran	-
Dichloromethane	+ + +
Ethyl acetate	+
Chloroform	+ + +
Acetonitrile	+ + +
Acetone	+ + +
Methanol	+
Ethanol	+
Water	-
Hexane	-

Note:

+++ (Completely dissolved), ++ (Dissolve), + (Slightly dissolve), - (Insoluble).

Our complex m = 0.0010 g dissolved with 1 mL of each solvent.

The Ru(*p*-cymene)(PPh_3)Cl_2 structure was characterized by the following techniques:

- ^{1}H-Nuclear Magnetic Resonance Spectroscopy (NMR)
- Fourier Transform Infrared Spectroscopy (FTIR)
- Single crystal x-ray diffraction
- UV-Visible absorption spectroscopy (UV-Vis)
- Elemental Analysis (CHO)

Biological activity of complex **3** such as anticancer was tested.

3.3.1. ¹H-Nuclear magnetic resonance spectroscopy

$CDCl_3$ solvent was used to measure the ¹H-NMR spectra of complex **3**. The phenyl ring and triphenylphosphine (PPh_3) ligand were identified as the primary distinctive peaks. The coordination of the Ru(II) complex with the PPh_3 ligand contributed to the downfield shifting in the range of 7.25-8.00 ppm. The proton labeling structure of complex **3** was exhibited in Figure 50.

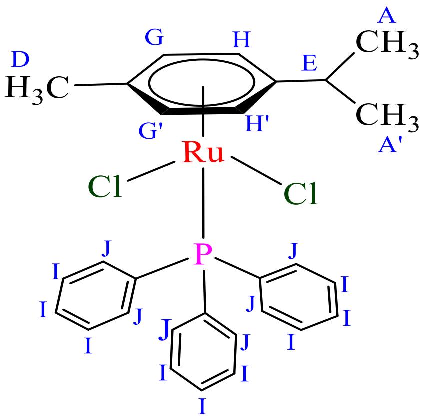

Figure 50. The proton labeling structure of Ru(*p*-cymene)(PPh_3)Cl_2 complex.

The ¹H-NMR signals of complex **3** contained 7 groups of signals (Figure 51). The description of each signal will be provided as shown in Table 22 below.

The proton at *A* and the proton at *A′* are groups of signals substituted in the *p*-cymene ring. Its couplings with a proton at the *E* location produced doublet peaks and exhibited the chemical shift at δ = 1.10 ppm with a coupling constant of J = 6.8 (*Hz*).

Proton *E* is located next to proton *A*, and *A′* together for six protons to generating multiplet peaks with chemical shifts at δ = 2.85 ppm and J = 6.8 (*Hz*).

On the phenyl of the *p*-cymene ring, protons *H* and *H′* are two equivalent protons which made a coupling with G and G' protons, respectively. The doublet peaks were generated by these protons at the chemical sift δ = 5.19 ppm with a couple constant of J = 7.5 (*Hz*).

The G and G’ proton is equivalent. Each of them interacted with protons *H* and *H′*, respectively, generating doublet peaks at the chemical shift δ = 4.99 ppm and coupling constant J = 7.5 (*Hz*).

The proton *D* is a methyl ($-CH_3$) group, which presents on the *p*-cymene ring. It gave a singlet peak at chemical shift at δ = 1.87 ppm from 3H protons.

The protons *I* are protons of the phenyl ring of the triphenylphosphine ligand. The signal character shows triplet peaks with chemical shift δ = 7.37 ppm and coupling constant J = 7.5 (*Hz*).

The protons *J* are the protons from the phenyl ring of the triphenylphosphine ligand and the signal character exhibited doublet of doublet peaks with chemical shift δ = 7.82 ppm and couple constant J = 7.5 (*Hz*).

Table 22. (δ-) Chemical shifts, (J-) Coupling constant, Signal character or related protons of Ru(*p*-cymene)(PPh_3)Cl_2 complex.

H-Position	δ_H (ppm)	Coupling constant J (*Hz*)	Signal character	Amount of H
A, A'	1.10	6.8	6	d
D	1.87	-	3	s
E	2.85	6.8	1	m
G, G'	4.99	7.5	2	d
H, H'	5.19	7.5	2	d
I	7.37	7.5	9	t
J	7.82	7.5	6	dd

Note:

d = doublet, dd = doublet of doublet, m = multiplet, s = singlet, t = triplet.

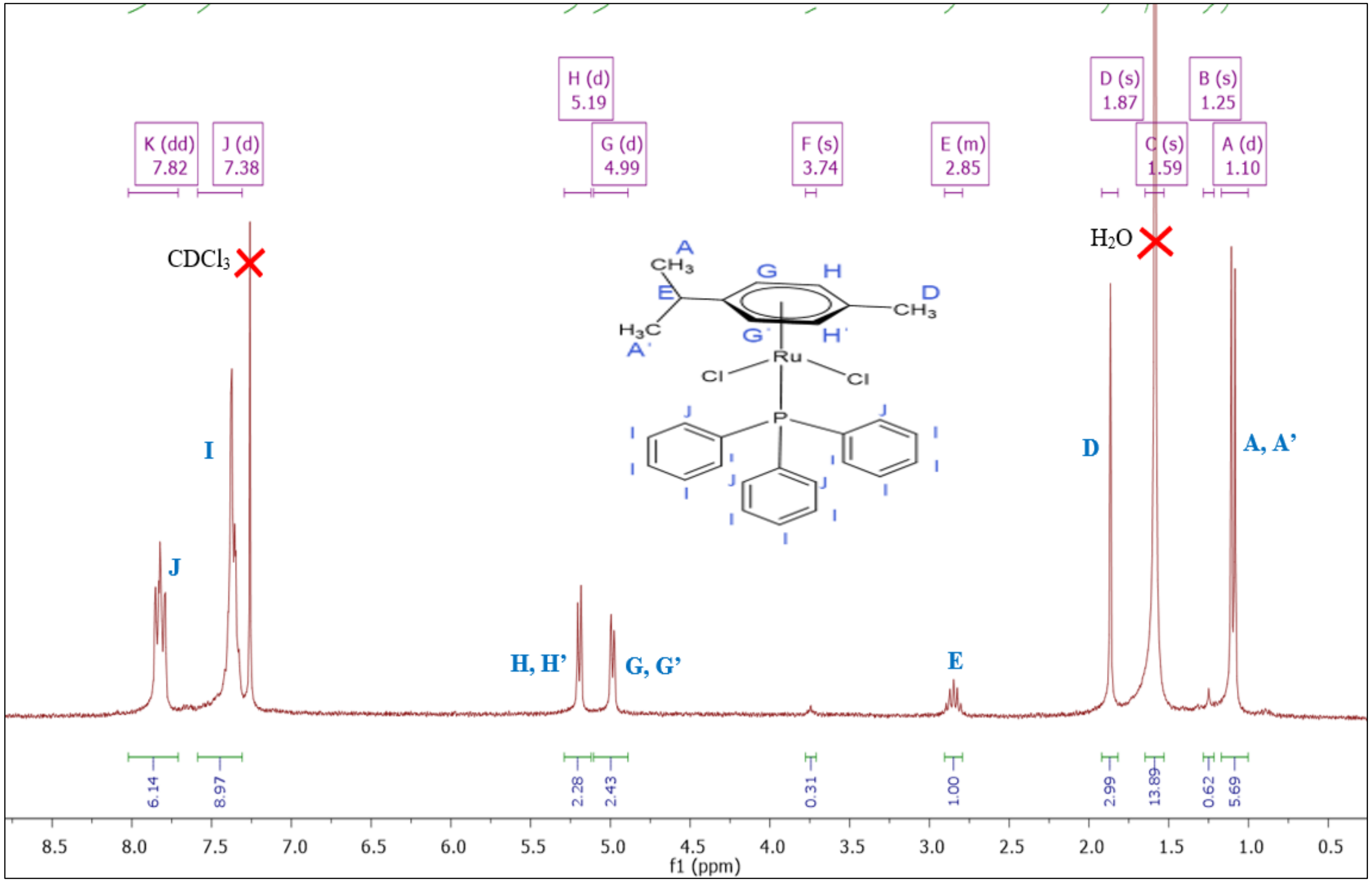

Figure 51. [1]H-NMR spectrum of Ru(*p*-cymene)(PPh_3)Cl_2 complex in $CDCl_3$.

3.3.2. Fourier transforms infrared spectroscopy

The coordination between the PPh_3 ligand and the Ru^{2+} metal center was seen in the FTIR signal spectrum and vibrational modes of the Ru(*p*-cymene)(PPh_3)Cl_2 complex (Figure 52 and Table 23). Due to the electron π-back bonding from the d^6 orbital of Ru^{2+}→π* orbital of the PPh_3 ligand, the Ru(*p*-cymene)(PPh_3)Cl_2 complex's υ(P-C) vibrational frequency occurred at 696 cm^{-1}, which stretching is weaker comparison with free ligand because of π-back bonding (He *et al*., 2019; Wang *et al*., 2020). Moreover, υ(Ru-Cl) is 508 cm^{-1} extremely similar to the stretching frequency of the triphenylphosphine ligand as reported by (Ajibade and Andrew, 2021). Additionally, the coordination between the metal center and PPh_3 ligand can be determined by the Ru-P stretching vibrational frequencies. For Ru-P, the stretching frequencies appeared 525 cm^{-1} , which was similar with others research 522 cm^{-1} υ(Ru-P) (Klaimanee *et al* ., 2021).

Table 23. The vibrational modes and frequencies of Ru(*p*-cymene)(PPh_3)Cl_2 complex.

Vibrational mode	Frequencies (cm^{-1})
Ru-Cl	508
Ru-P stretching	525
P-C stretching	696
P-Ph stretching	1092
C = C stretching	1436
C-H stretching	3049

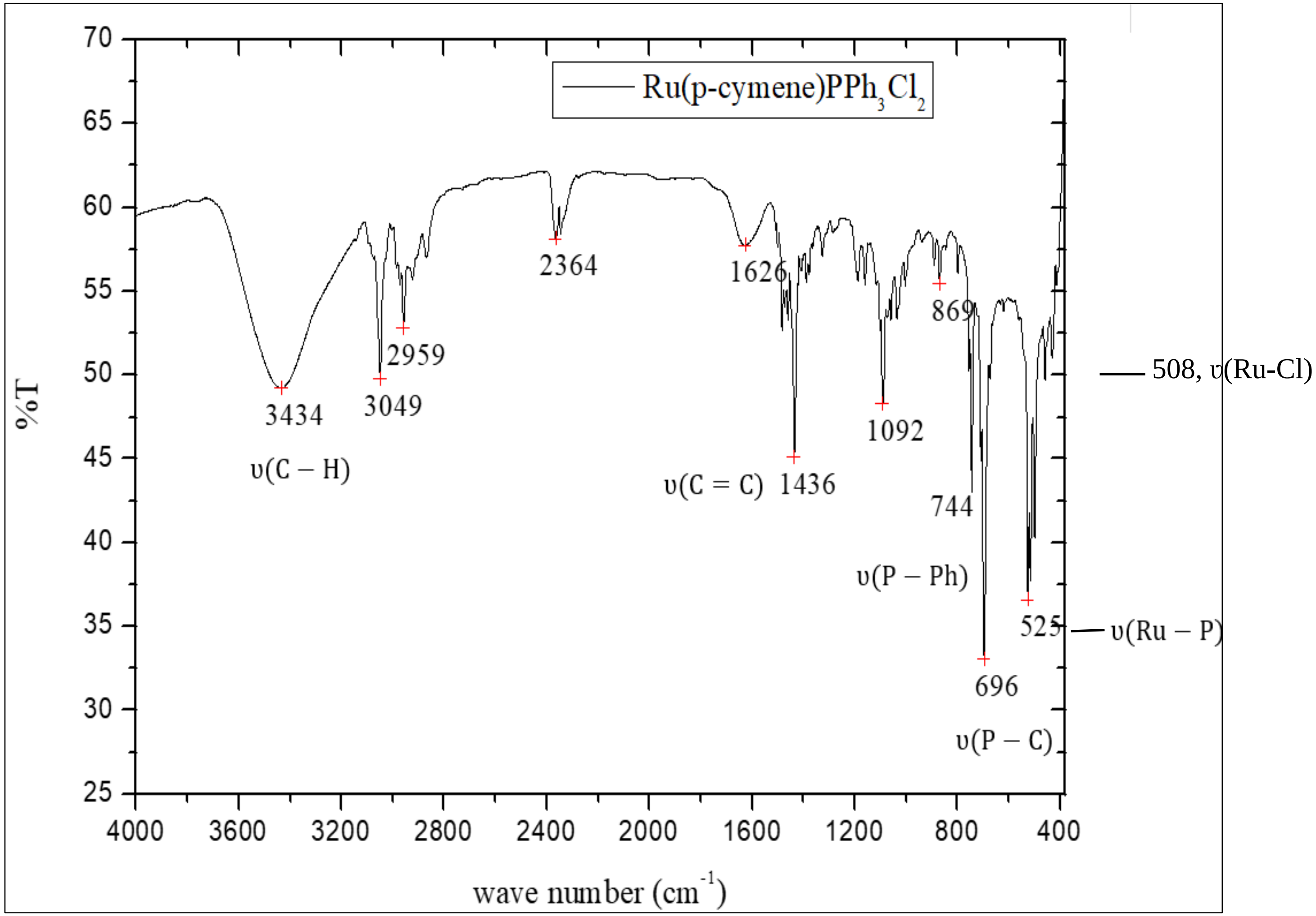

Figure 52. The IR spectrum of Ru(*p*-cymene)(PPh_3)Cl_2 complex in KBr pellet.

3.3.3. Single crystal X-ray diffraction

The structure of the Ru(*p*-cymene)(PPh_3)Cl_2 complex **3** (Figure 53) adopted the distorted octahedral geometry with η^6-bonding of *p*-cymene, a single molecule of triphenylphosphine, and two Cl^- ligands. Table 24 shows the crystallographic data for complex **3**. The monoclinic crystal system with $P2_1/n$ space group of the complex **3** obeyed the prior study (Elsegood *et al*., 2006). Table 25 shows the selected bond angles and bond distances of complex **3**. There were two molecules in the asymmetric unit (the label Ru(1) and Ru(2) refer to molecules 1 and 2, respectively). The average bond lengths of Ru-Cl, Ru-C, and Ru-P are 2.2191, 2.4133 and 2.3488 Å, respectively which distances are close to the previously studied distances (Elsegood *et al*., 2006). The results were comparable to other related structures of [(η^6-*p*-cymene)]RuCl_2(PPh_2Py) complex (Govindaswamy *et al*., 2004) and [Ru_2(*p*-cymene)$_2$(dppp)Cl_4] complex (Klaimanee *et al*., 2021). The bond angles of P-Ru-Cl(1), P-Ru-Cl(2), and Cl(1)-Ru-Cl(2) were 90.21(2)^o, 87.112(19)^o, and 88.46(2)^o, respectively for molecule 1 and P(2)-Ru(2)-Cl(4), P(2)-Ru(2)-Cl(3), and Cl(1)-Ru(1)-Cl(2) were 87.62(2)^o, 89.81(2)^o, and 88.81(2)^o for the molecule 2 pointing out that the complex 3 distorted tetrahedral as like as earlier studies (Elsegood *et al*., 2006; Ludwig *et al*., 2012). The C-H···Cl intra-molecular H-boning is detected in both molecules (Ru1 and Ru2 molecules). There are two interactions of this type found in Ru1 molecule, C(12)-H(12)···Cl(1) and C(18)-H(18)···Cl(1), while the others three interactions are observed in Ru2 molecule, C(40)-H(40)···Cl(3), C(50)-H(50)···Cl(3) and C(40)-H(40)···Cl(4), respectively. All interactions and the contact distances are shown in Figure 54 and Table 26. Moreover, the inter-molecular C-H···π contact, C(47)−H(47)···*Cg8*, was also formed between two adjacent Ru2 molecules generating a pair of interactions with the H47···centriod of *Cg8* distance at 2.81 Å (Figure 55).

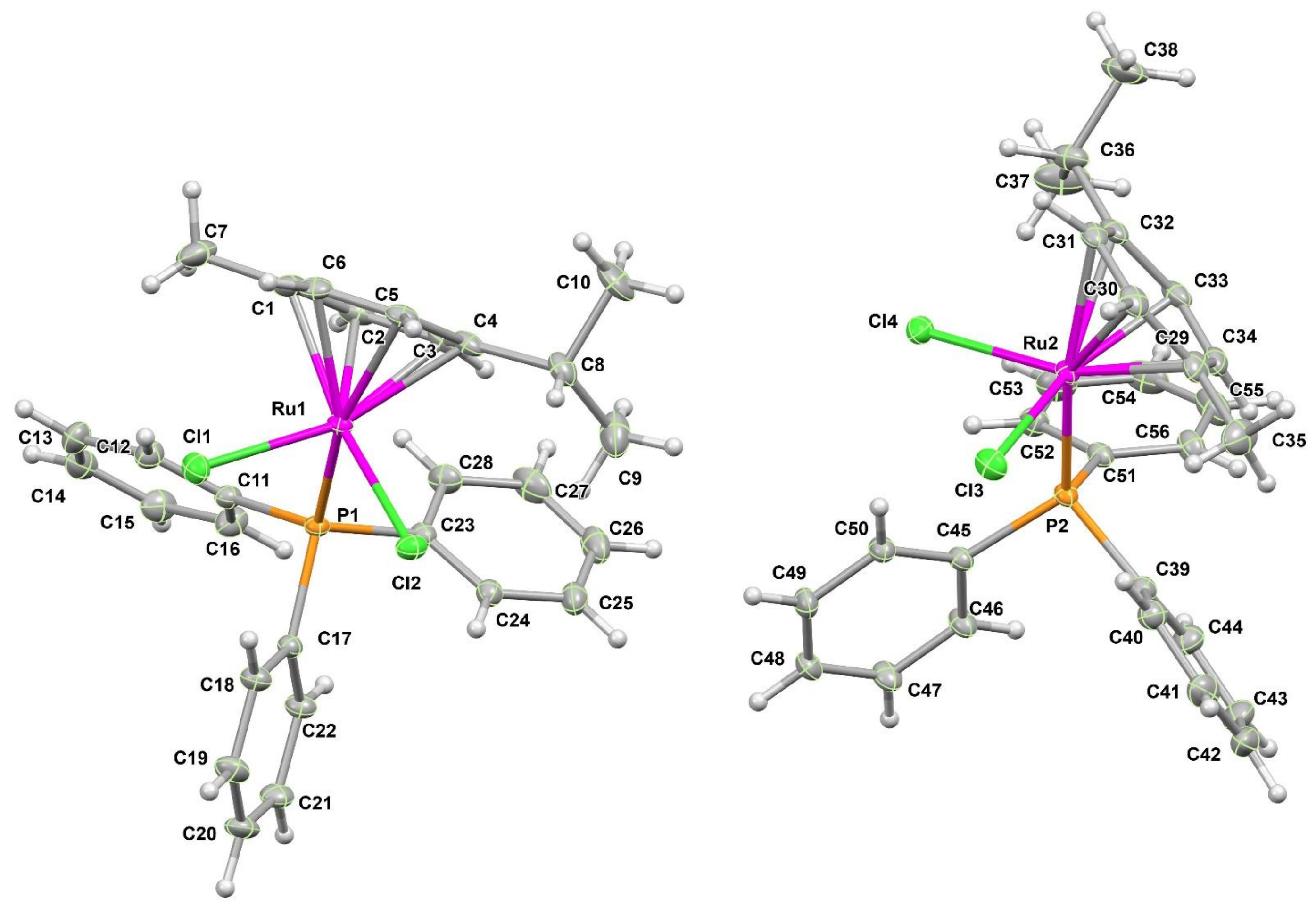

Figure 53. The ORTEP structures of Ru(p-cymene)(PPh_3)Cl_2 complex with atom numbering.

Table 24. Crystal data and structure refinement for Ru(*p*-cymene)(PPh_3)Cl_2 complex.

Empirical formula	$C_{28}H_{29}Cl_2PRu$
Formula weight	568.45
Wavelength	1.54178 Å
Crystal system	Monoclinic
Space group	$P2_1/n$
Unit cell dimensions	a = 15.5596(3) Å α = 90°
	b = 9.2708(2) Å β = 96.2930(10)°
	c = 35.2545(6) Å γ = 90°
Temperature	296(2) K
Z	8
Density (calculated)	1.494 Mg/m^3
Absorption coefficient	7.659 mm^{-1}
F(000)	2320
Crystal size	0.429 x 0.080 x 0.055 mm^3
Theta range for data collection	2.994 to 68.539°
Index ranges	-18<=h<=18, -9<=k<=11, -42<=l<=42
Reflections collected	142578
Independent reflections	9273 [*R*(int) = 0.0542]
Completeness to theta = 67.679°	99.8 %
Absorption correction	Semi-empirical from equivalents
Max. and min. transmission	0.7531 and 0.4727
Refinement method	Full-matrix least-squares on F^2
Data/restraints/parameters	9273/0/583
Goodness-of-fit on F^2	1.092
Final *R* indices [$I>2\sigma(I)$]	$R1$ = 0.0267, $wR2$ = 0.0680
R indices (all data)	$R1$ = 0.0267, $wR2$ = 0.0680
Extinction coefficient	n/a
Largest diff. peak and hole	0.467 and -0.438 e.$Å^{-3}$

Table 25. Selected bond lengths (Å) and angles (º) for complex **3**.

Bond lengths			
Ru(1)-C(2)	2.176(2)8	Ru(1)-C(3)	2.211(2)
Ru(1)-C(6)	2.221(2)	Ru(1)-C(1)	2.221(3)
Ru(1)-C(5)	2.245(2)	Ru(1)-C(4)	2.248(2)
Ru(1)-P(1)	2.3489(5)	Ru(1)-Cl(1)	2.4134(6)
Ru(1)-Cl(2)	2.4145(6)	Ru(2)-C(34)	2.175(2)
Ru(2)-C(33)	2.210(2)	Ru(2)-C(29)	2.215(3)
Ru(2)-C(30)	2.218(2)	Ru(2)-C(32)	2.244(2)
Ru(2)-C(31)	2.245(2)	Ru(2)-P(2)	2.3486(5)
Ru(2)-Cl(4)	2.4119(6)	Ru(2)-Cl(3)	2.4135(6)
Angles			
C(2)-Ru(1)-C(3)	37.42(11)	C(2)-Ru(1)-C(6)	66.61(10)
C(3)-Ru(1)-C(6)	78.27(10)	C(2)-Ru(1)-C(1)	37.35(11)
C(3)-Ru(1)-C(1)	67.61(12)	C(6)-Ru(1)-C(1)	37.65(10)
C(2)-Ru(1)-C(5)	78.32(9)	C(3)-Ru(1)-C(5)	66.02(9)
C(6)-Ru(1)-C(5)	36.11(10)	C(1)-Ru(1)-C(5)	66.96(10)
C(2)-Ru(1)-C(4)	67.04(10)	C(3)-Ru(1)-C(4)	36.73(9)
C(6)-Ru(1)-C(4)	66.35(10)	C(1)-Ru(1)-C(4)	80.08(11)
C(5)-Ru(1)-C(4)	37.05(9)	C(2)-Ru(1)-P(1)	90.39(7)
C(3)-Ru(1)-P(1)	96.15(6)	C(6)-Ru(1)-P(1)	149.14(8)
C(1)-Ru(1)-P(1)	112.05(7)	C(5)-Ru(1)-P(1)	161.51(7)
C(4)-Ru(1)-P(1)	124.84(6)	C(2)-Ru(1)-Cl(1)	124.19(9)
C(3)-Ru(1)-Cl(1)	160.23(8)	C(6)-Ru(1)-Cl(1)	86.68(8)
C(1)-Ru(1)-Cl(1)	92.65(8)	C(5)-Ru(1)-Cl(1)	108.23(7)
C(4)-Ru(1)-Cl(1)	144.48(6)	P(1)-Ru(1)-Cl(1)	90.21(2)
C(2)-Ru(1)-Cl(2)	147.28(9)	C(3)-Ru(1)-Cl(2)	110.49(8)
C(6)-Ru(1)-Cl(2)	123.43(8)	C(1)-Ru(1)-Cl(2)	160.79(7)
C(5)-Ru(1)-Cl(2)	94.48(7)	C(4)-Ru(1)-Cl(2)	87.91(7)
P(1)-Ru(1)-Cl(2)	87.112(19)	Cl(1)-Ru(1)-Cl(2)	88.46(2)
C(34)-Ru(2)-C(33)	37.42(11)	C(34)-Ru(2)-C(29)	37.34(11)
C(33)-Ru(2)-C(29)	67.58(12)	C(34)-Ru(2)-C(30)	66.55(10)
C(33)-Ru(2)-C(30)	78.27(10)	C(29)-Ru(2)-C(30)	37.54(10)
C(34)-Ru(2)-P(2)	90.47(7)	C(34)-Ru(2)-P(2)	90.47(7)
C(33)-Ru(2)-P(2)	96.40(7)	C(29)-Ru(2)-P(2)	111.97(7)
C(30)-Ru(2)-P(2)	148.89(8)	C(32)-Ru(2)-P(2)	125.25(7)
P(2)-Ru(2)-Cl(4)	87.62(2)	Cl(4)-Ru(2)-Cl(3)	88.81(2)
P(2)-Ru(2)-Cl(3)	89.81(2)	Cl(1)-Ru(1)-Cl(2)	88.46(2)

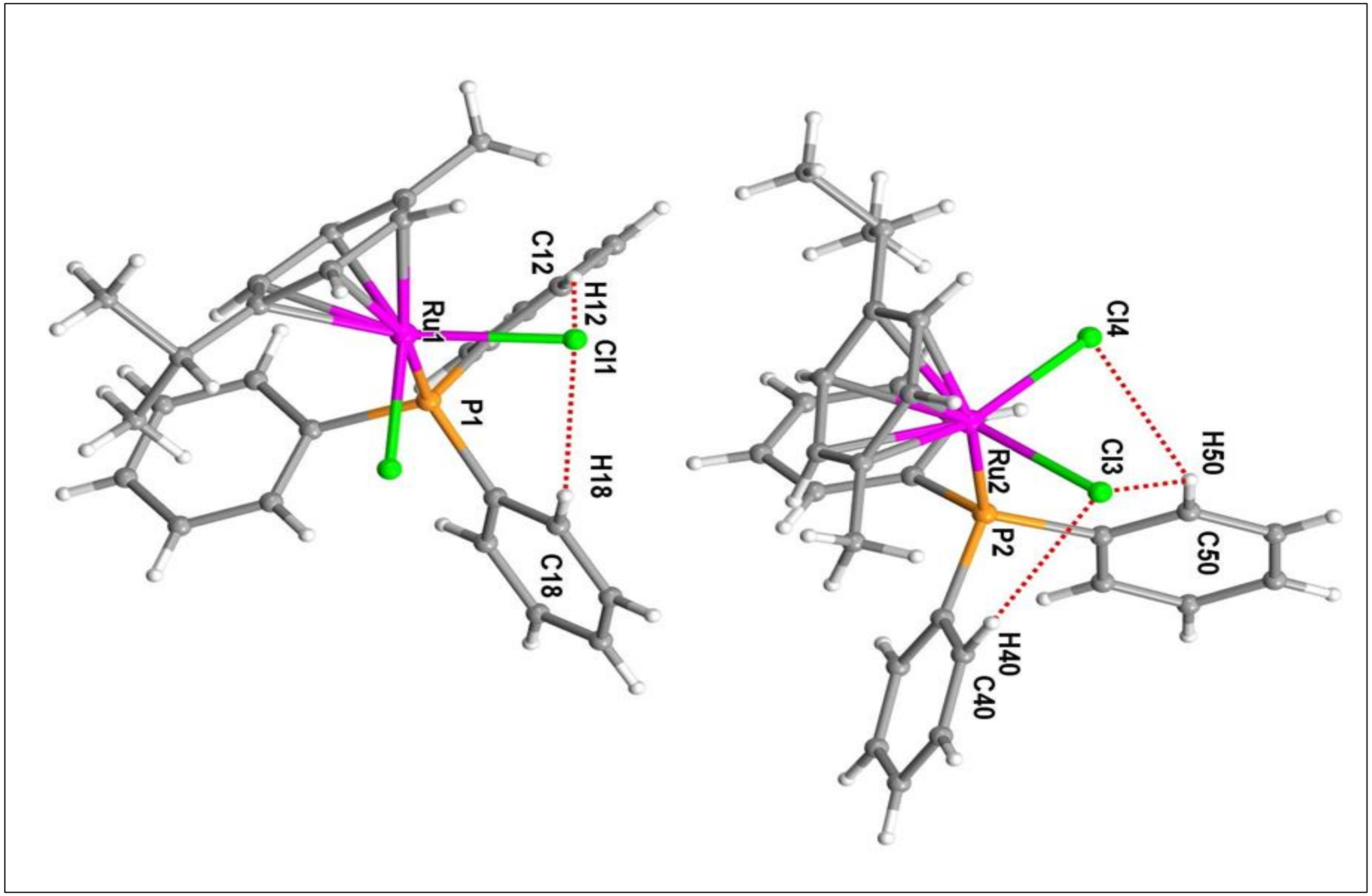

Figure 54. The intra-molecular hydrogen bond interactions of Ru(p-cymene)(PPh_3)Cl_2 complex.

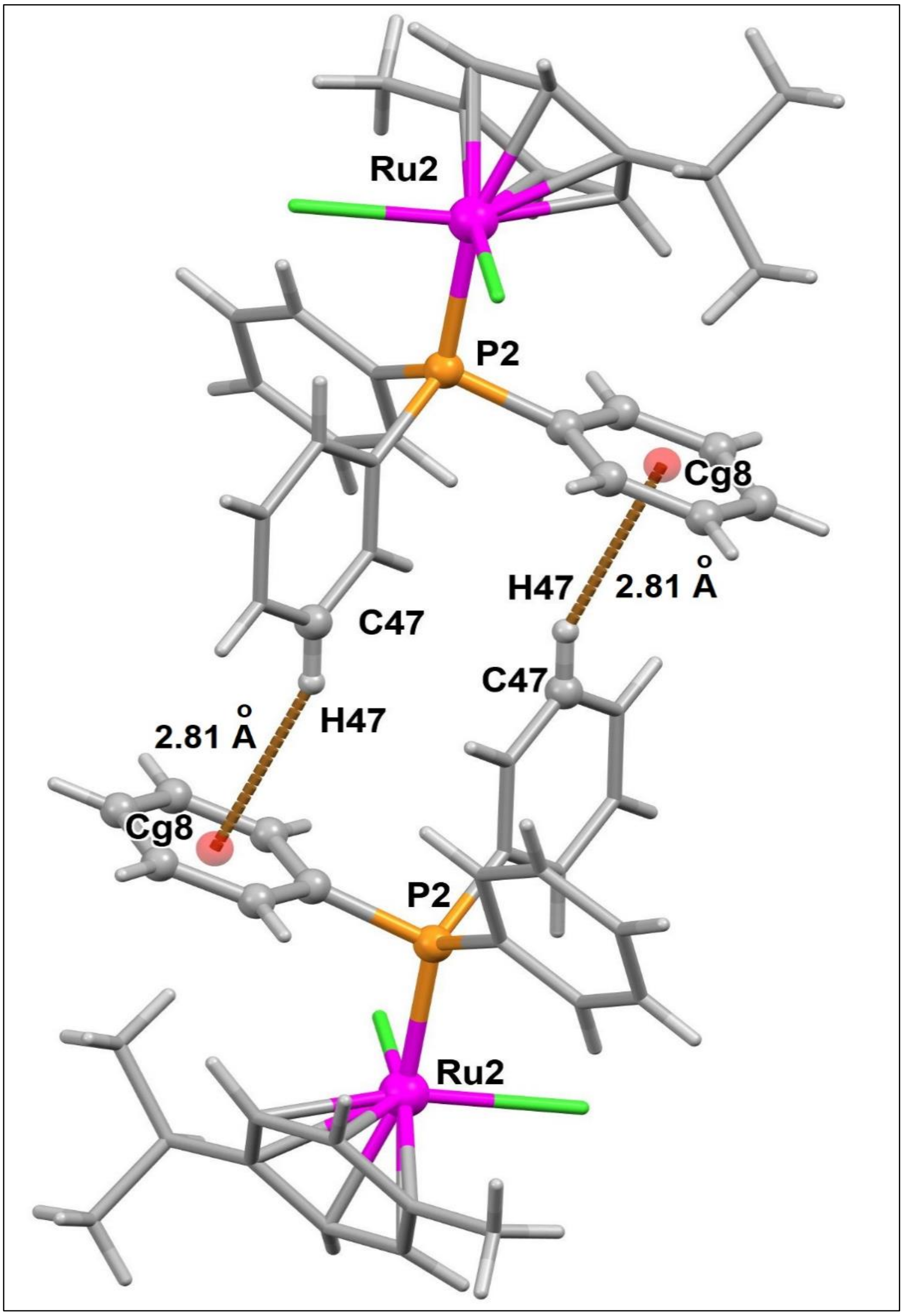

Figure 55. Inter-molecular interactions of Ru(p-cymene)(PPh_3)Cl_2 complex.

Table 26. Hydrogen bonds for Ru(*p*-cymene)(PPh_3)Cl_2 complex [Å, º].

D-H···A	Distance of d(D-H) (Å)	Distance of d(H···A) (Å)	Distance of d(D···A) (Å)	Angles of <(DHA) (º)
C(12)-H(12)···Cl(1)	0.93	2.74	3.564(3)	147.9
C(18)-H(18)···Cl(1)	0.93	2.71	3.476(3)	140.1
C(18)-H(18)···Cl(2)	0.93	2.85	3.345(2)	114.6
C(40)-H(40)···Cl(3)	0.93	2.71	3.548(3)	149.7
C(50)-H(50)···Cl(3)	0.93	2.72	3.435(2)	134.2
C(50)-H(50)···Cl(4)	0.93	2.72	3.295(2)	121.1

Note:

D = donor (C atom), A = acceptor (O and Cl atoms).

3.3.4. Elemental analysis

The C and H percentages between the theoretical values were in good agreement with the experimental found for the complex 3 as shown in Table 27. It fits Ru(*p*-cymene)(PPh_3)Cl_2 structure.

Table 27. Elemental analysis data of Ru(*p*-cymene)(PPh_3)Cl_2 complex.

Elemental analysis		
Elements (%)	C	H
Calculated	59.10	5.10
Found	58.99 ± 0.09	5.07 ± 0.09
Deviation (Δ)	± 0.11	± 0.03

<u>Note</u>:

The acceptance deviation of each element in the compound was Δ = 0.03

3.3.5. UV-Visible absorption spectroscopy

The UV-visible absorption spectrum of Ru(*p*-cymene)(PPh_3)Cl_2 was measured in dichloromethane (CH_2Cl_2) with the concentration of 8×10^{-6} M between 200 and 800 nm (Figure 56 and Figure 57). The absorption spectrum of the Ru(*p*-cymene)(PPh_3)Cl_2 complex appeared for three maximum absorption bands at the wavelengths (with molar extinction coefficient) of 228 nm (8.0×10^4 M^{-1} cm^{-1}), 373 nm (4.3×10^3 M^{-1} cm^{-1}) and 496 nm (1.2×10^3 M^{-1} cm^{-1}), respectively.

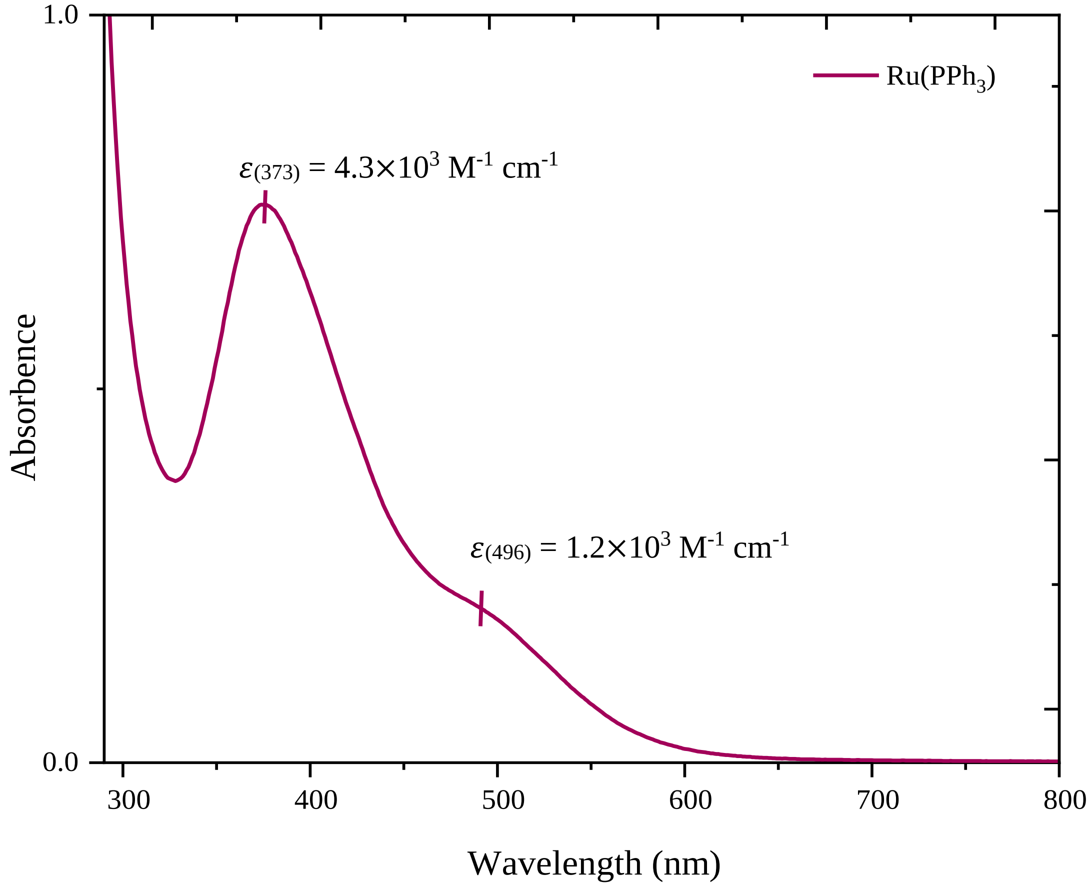

Figure 56. UV-Visible absorption spectrum of 8 $\times10^{-6}$ M of complex **3** in dichloromethane (CH_2Cl_2).

Table 28 displayed the results of the photophysical experiment and the predicted vertical electronic transitions. The electronic absorption spectrum of dichloromethane was simulated using time-dependent on-density functional theory (TDDFT) in order to interpret the electronic transitions leading to the absorption bands. The calculation was performed using the PCM-TD-PBE0/6-31+G*+LANL2DZ basis sets. The vertical lines in Figure 57 represent the electronic transitions of the Ru(*p*-cymene)(PPh_3)Cl_2 complex as they correspond to the measured absorption spectrum. The mixed types of charge transfer transition were the predominant transitions for those three absorption bands. The ligand-to-ligand charge transfer transition (LLCT) from the PPh_3 to the *p*-cymene moiety resulted in a HOMO→LUMO (79%) transition ($\lambda_{calc.}$ = 516 nm, Osc. Strength (f) = 0.0084), which was responsible for the band at 496 nm. The band at 373 nm ($\lambda_{calc.}$ = 395 nm, Osc. Strength (f) = 0.0213), exhibited combination of MLCT (d-Ru(1)→ ***π****-P(PPh_3) and XLCT (Cl→ ***π****-P(PPh_3) halogen to ligand charge transfer from HOMO→L+1 (65%) transition, as illustrated in Figure 58. Table 28 summarizes the calculation data.

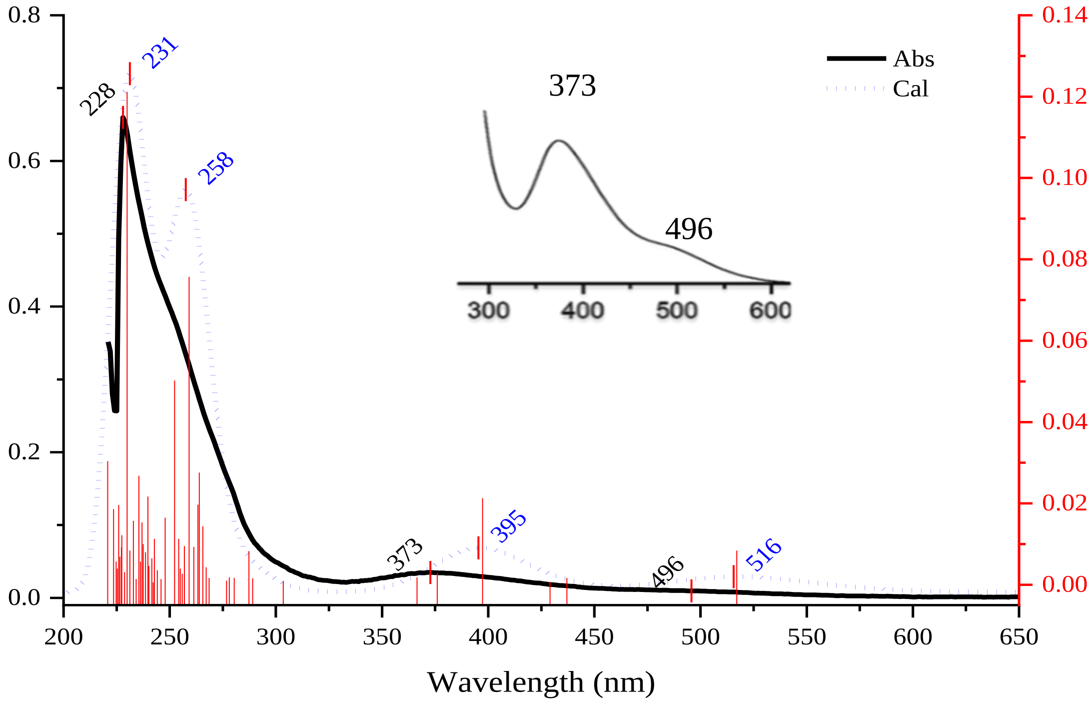

Figure 57. The UV-vis absorption spectra of complex **3** overlaid with the PCM-TD-PBE0/6-31 + G* +LANL2DZ simulated spectra (dotted line). Corresponding oscillator strengths are shown as sets of vertical lines.

Table 28. Photophysical data and vertical electronic transitions were calculated for Ru(*p*-cymene)(PPh_3)Cl_2 complex**.**

No.	Wavelength (nm)		Osc. Strength (f)	Major contribution	Assignment
	Cal	Exp			
1	516	496 (sh)	0.0084	HOMO→LUMO (79%)	LLCT (PPh_3→*p*-cymene)
4	395	373	0.0213	HOMO→L+1 (65%)	MLCT, XLCT (Cl→PPh_3)
19	258	-	0.0757	H-5→L+1 (39%)	LLCT (PPh_3→*p*-cymene) LMCT (PPh_3→Ru)
41	231	228	0.1212	H-4→L+2 (18%) H-3→L+2 (42%)	XLCT (Cl→PPh_3)

sh = shoulder

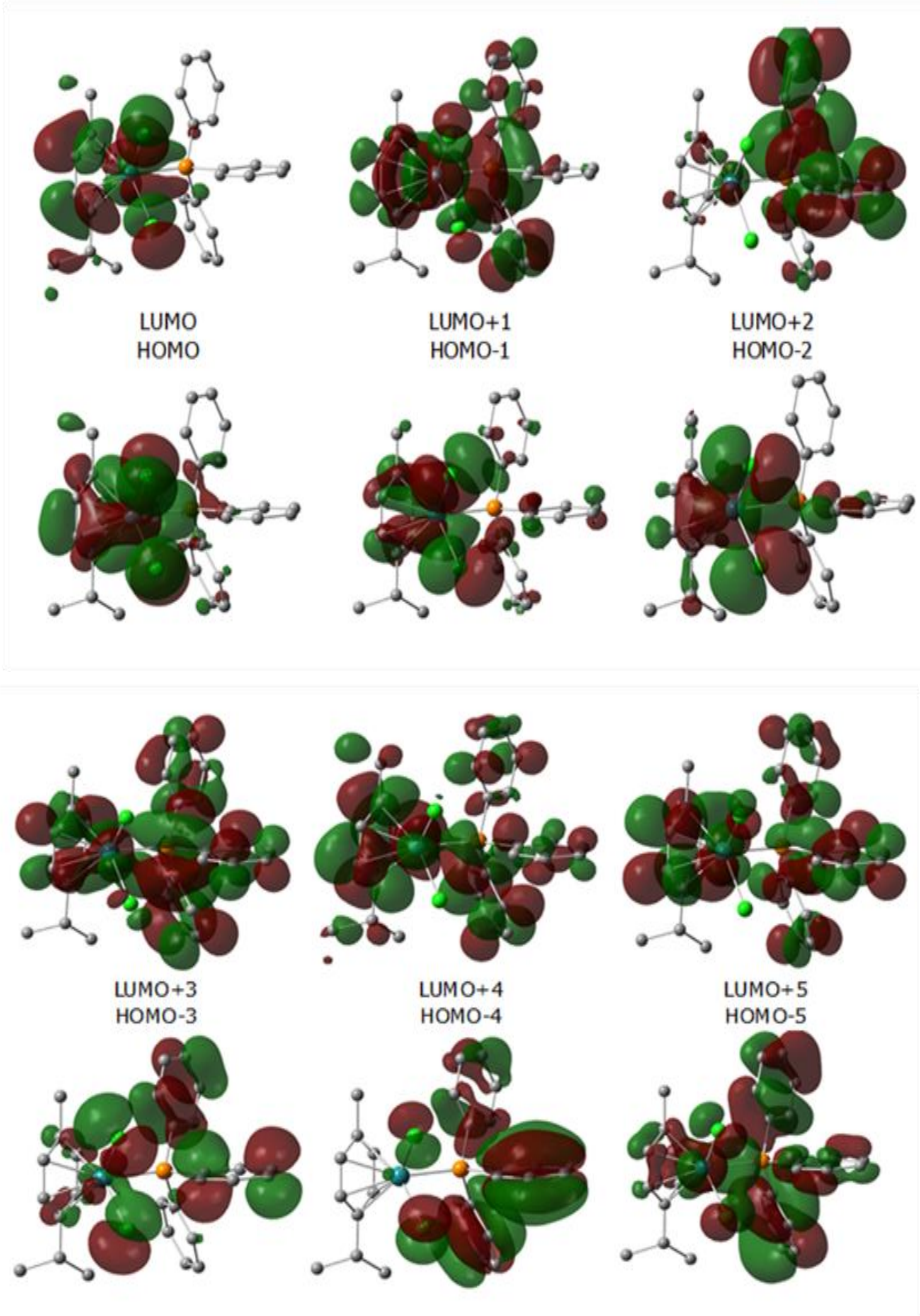

Figure 58. The contour plots of HOMO and LUMO molecular orbitals of the Ru(*p*-cymene)(PPh_3)Cl_2 complex.

3.3.6. *In vitro* antiproliferative activity

Figure 59 shows the plot between cell viability percentage against the tested concentration of Ru(*p*-cymene)(PPh_3)Cl_2 complex in the range from 0.01 to 100 µM regarding MCF-7, HCC1937, and MDA-MB-231 cell lines. The Ru(*p*-cymene)(PPh_3)Cl_2 complex showed the best activity *in vitro* for cytotoxicity selectively against MCF-7 cell line presenting the IC_{50} value of 15.99 µM which was better sensitivity than that of cisplatin and triphenylphosphine (PPh_3) free ligand as summarized in Table 29. For other examined breast cancer cells, the IC_{50} values were all less sensitive than cisplatin with higher concentration than 100 µM against those two cell lines. The result for MCF-7 is corresponding to the report from Honorato *et al*., 2020. The presence of PPh_3, which is a lipophilic group, can increase the cellular uptake of the complex influencing the cytotoxicity towards the cancer cell. Nevertheless, in order to explain the selectivity to MCF-7 needs to be further investigated for the possible mechanism of cancer cell growth inhibition.

Table 29. IC_{50} mean values (µM) for [Ru(*p*-cymene)(PPh_3)Cl_2] and cisplatin against HCC1937, MCF-7, and MDA-MB-231 cells after 48 h of treatment. (All data are the mean and standard errors obtained from four independent experiments, each performed in at least triplicate).

Metal complex	IC_{50} (µM)		
	MCF-7	HCC1937	MDA-MB-231
Cisplatin	42.2 ± 8*,**	23.4 ± 7*,**	128.2 ± 7*,**
$RuPPh_3$	15.99 ± 5 *,**	>100 *,**	>100 *,**
PPh_3	>100 *,**	54.3 ± 0.2 *,**	>100 *,**

Statistical significance differences are indicated by *p < 0.01, compared to the IC_{50} values of the same complex on cell lines, and **p < 0.001, compared to the IC_{50} values of the complexes on each cancer cell line (HCC1937, MCF-7, and MDA-MB-231).

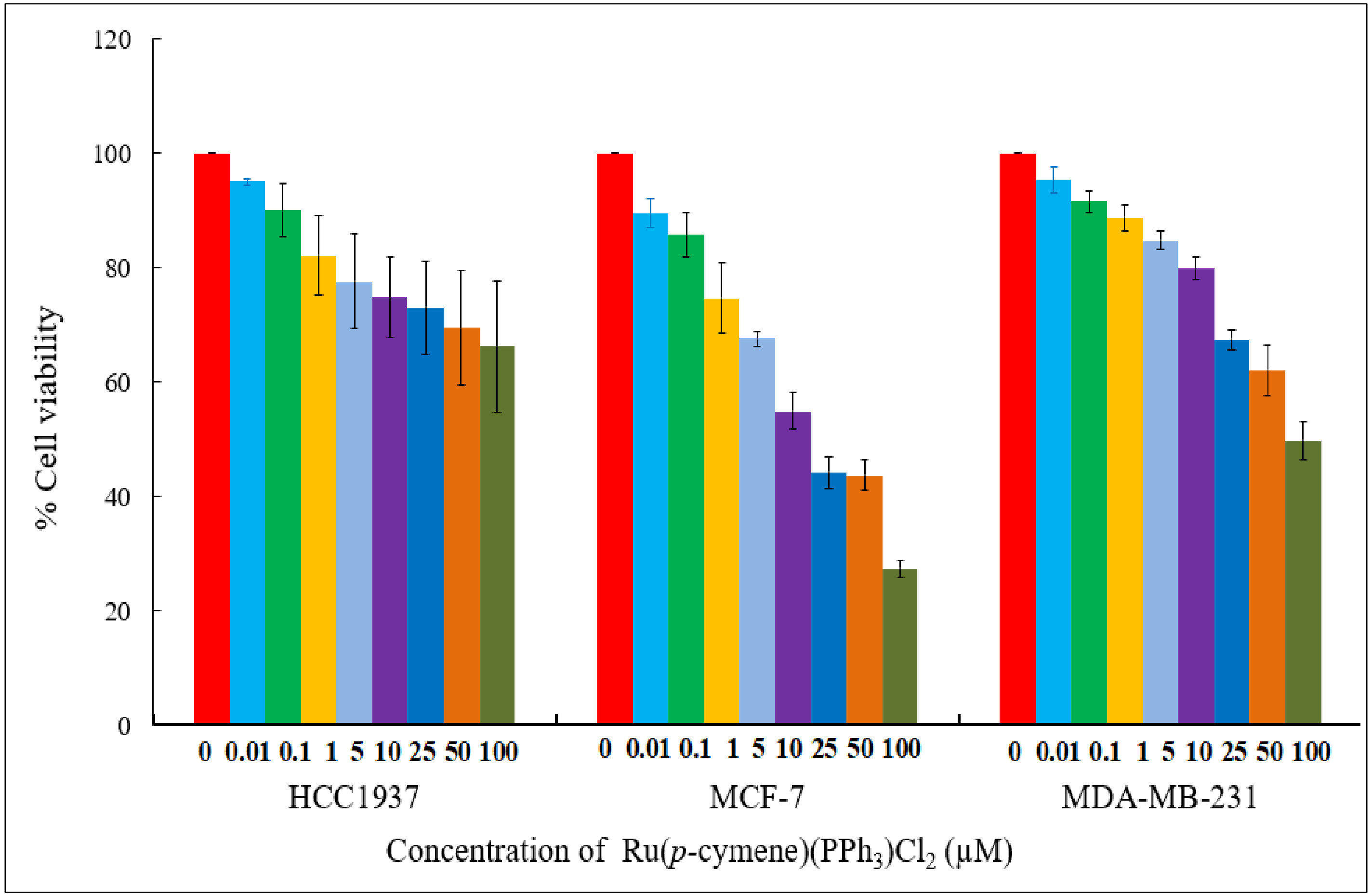

Figure 59. The chart shows the cytotoxic effect of Ru(*p*-cymene)(PPh_3)Cl_2 at concentrations of 0, 0.01, 0.1, 1, 5, 10, 25, 50, and 100 μM on the cell viability of HCC1937, MCF-7 and MDA-MB-231 cells after 48 h.

CHAPTER 4

CONCLUSION

Single crystal X-ray diffraction, elemental analysis, and spectroscopic methods were used to analyze [Ru(*p*-cymene)(tmp)Cl]·CH_2Cl_2 (**1**), [Ir(ppy)$_2$(tmp)]·CH_2Cl_2 (**2**), and Ru(*p*-cymene)(PPh_3)Cl_2 (**3**) complexes. The complexes were synthesized in order to explore their biological properties on antimicrobial and anti-breast cancer activity. Moreover, a metal ion sensing capacity of photoactive complex **2** was found. The complex **2** can detect Fe(III) in dimethylformamide (DMF) solvent with good 1:1 stoichiometric binding affinity and good quantum yield (Φ). Moreover, the electronic transition charge of complex **3** was investigated using the density functional theory (DTF). Additionally, this study revealed that the complexes **1** and **3** geometry were pseudo-tetrahedral or distorted tetrahedral. Complex **2** adopted pseudo-octahedral geometry. The complex **3** exhibited its cytotoxicity specifically against human breast cancer cells of MCF-7 as a consequence of this experiment, with better activity and a lower IC_{50} value than that of cisplatin. Additionally, complex **2** showed moderate to high antibacterial efficacy of growth inhibition against yeast, filamentous fungus, SA, and MRSA Gram-positive bacteria. Complex **2** in this study was more lipophilic and penetrated to the microbial cells more extensively than complex **1**.

REFERENCES

Agonigi, G., Riedel, T., Zacchini, S., Paunescu, E., Pampaloni, G., Bartalucci, N., Dyson, P. J., Marchetti, F. (2015). Synthesis and antiproliferative activity of new ruthenium complexes with ethacrynic-acid-modified pyridine and triphenylphosphine ligands. *Inorganic Chemistry*, *54*(13), 6504–6512.

Ahmad-Mansour, N., Loubet, P., Pouget, C., Dunyach-Remy, C., Sotto, A., Lavigne, J.-P., Molle, V. (2021). Staphylococcus aureus Toxins: An Update on Their Pathogenic Properties and Potential Treatments. *Toxins*, *13*(10), 677.

Aird, R. E., Cummings, J., Ritchie, A. A., Muir, M., Morris, R. E., Chen, H., Sadler, P. J., Jodrell, D. I. (2002). *In vitro* and *in vivo* activity and cross resistance profiles of novel ruthenium (II) organometallic arene complexes in human ovarian cancer. *British Journal of Cancer*, *86*(10), 1652–1657.

Ajibade, P. A., and Andrew, F. P. (2021). Synthesis, characterization, and in vitro anticancer studies of chlorido(triphenylphosphine)ruthenium(II) dithiocarbamate complexes. *Phosphorus, Sulfur and Silicon and the Related Elements*, *196*(9), 832–838.

Alessio, E., and Messori, L. (2019). Anticancer drug candidates face-to-face: a case story in medicinal inorganic chemistry. *Molecules*, *24*, 1–20.

Allardyce, C. S., and Dyson, P. J. (2001). Ruthenium in medicine: Current clinical uses and future prospects. *Platinum Metals Review*, *45*(2), 62–69.

Allardyce, Claire S, Dyson, P. J., Ellis, D. J., Salter, P. A., Scopelliti, R. (2003). Synthesis and characterisation of some water soluble ruthenium(II)-arene complexes and an investigation of their antibiotic and antiviral properties. *Journal of Organometallic Chemistry*, *668*(1–2), 35–42.

Almodares, Z., Lucas, S. J., Crossley, B. D., Basri, A. M., Pask, C. M., Hebden, A. J., Phillips, R. M., McGowan, P. C. (2014). Rhodium, iridium, and ruthenium half-sandwich picolinamide complexes as anticancer agents. *Inorganic Chemistry*, *53*(2), 727–736.

Baker, R. P., Chrissian, C., Stark, R. E., Casadevall, A. (2022). Cryptococcus neoformans melanization incorporates multiple catecholamines to produce polytypic melanin. *Journal of Biological Chemistry*, *298*(1), 101519.

Banerjee, S., and Sadler, P. J. (2021). Transfer hydrogenation catalysis in cells. *RSC*

Chemical Biology, *2*(1), 12–29.

Bedford, R. B., Chaloner, P. A., and Hitchcock, P. B. (1994). An iridium complex of tris (4-methoxyphenyl) phosphine. *Acta Crystallographica Section C: Crystal Structure Communications*, *50*(3), 354-356.

Berndsen, R. H., Weiss, A., Abdul, U. K., Wong, T. J., Meraldi, P., Griffioen, A. W., Dyson, P. J., Nowak-Sliwinska, P. (2017). Combination of ruthenium(II)-arene complex [Ru(η^6-*p*-cymene)Cl_2(pta)] (RAPTA-C) and the epidermal growth factor receptor inhibitor erlotinib results in efficient angiostatic and antitumor activity. *Scientific Reports*, *7*(July 2016), 1–16.

Böttcher, H. C., Graf, M., Krüger, H., Wagner, C. (2005). Synthesis and X-ray crystal structure of a heteroleptic tris-cyclometalated iridium(III) complex. *Inorganic Chemistry Communications*, *8*(3), 278–280.

Bray, F., Ferlay, J., Soerjomataram, I., Siegel, R. L., Torre, L. A., and Jemal, A. (2018). Global cancer statistics 2018: GLOBOCAN estimates of incidence and mortality worldwide for 36 cancers in 185 countries. *CA: A Cancer Journal for Clinicians*, *68*(6), 394–424.

Bott, R. C., Healy, P. C., and Smith, G. (2007). Structural studies of two-coordinate complexes of tris (2-methoxylphenyl) phosphine and tris (4-methoxyphenyl) phosphine with gold (I) halides. *Polyhedron*, *26*(12), 2803-2809.

Chastain, D. B., Henao-Martínez, A. F., and Franco-Paredes, C. (2017). Opportunistic Invasive Mycoses in AIDS: Cryptococcosis, Histoplasmosis, Coccidiodomycosis, and Talaromycosis. *Current Infectious Disease Reports*, *19*(10).

Chen, B. B., Pan, N. L., Liao, J. X., Huang, M. Y., Jiang, D. C., Wang, J. J., and Sun, J. (2021). Cyclometalated iridium(III) complexes as mitochondria-targeted anticancer and antibacterial agents to induce both autophagy and apoptosis. *Journal of Inorganic Biochemistry*, *219*, 111450.

Chuklin, P., Chalermpanaphan, V., Nhukeaw, T., Saithong, S., Chainok, K., Phongpaichit, S., Ratanaphan, A., Leesakul, N. (2017). Synthesis, X-ray structure of organometallic ruthenium(II) *p*-cymene complexes based on P- and N- donor ligands and their *in vitro* antibacterial and anticancer studies. *Journal of Organometallic Chemistry*, *846*(Ii), 242–250.

Conesa, J. J., Carrasco, A. C., Rodríguez-Fanjul, V., Yang, Y., Carrascosa, J. L., Cloetens, P., Pereiro, E., Pizarro, A. M. (2020). Unambiguous Intracellular Localization and Quantification of a Potent Iridium Anticancer Compound by Correlative 3D Cryo X-Ray Imaging. *Angewandte Chemie - International Edition, 59*(3), 1270–1278.

Crispini, A., Harrison, K. N., Orpen, A. G., Pringle, P. G., Wheatcroft, J. R. (1996). *Tris(2-methoxyphenyl) phosphite complexes of platinum(n): the. 1*, 1069–1076.

da Silva, J. P., Silva, I. C., Pavan, F. R., Back, D. F., de Araujo, M. P. (2017). Bis (diphenylphosphino) amines-containing ruthenium cymene complexes as potential anti-Mycobacterium tuberculosis agents. *Journal of Inorganic Biochemistry*, *173*, 134–140.

Das, S., Sinha, S., Britto, R., Somasundaram, K., Samuelson, A. G. (2010). Cytotoxicity of half sandwich ruthenium(II) complexes with strong hydrogen bond acceptor ligands and their mechanism of action. *Journal of Inorganic Biochemistry*, *104*(2), 93–104.

Du, Q., Guo, L., Tian, M., Ge, X., Yang, Y., Jian, X., ... and Liu, Z. (2018). Potent half-sandwich iridium(III) and ruthenium(II) anticancer complexes containing a P^ O-chelated ligand. *Organometallics*, *37*(17), 2880-2889.

Du, Q., Yang, Y., Guo, L., Tian, M., Ge, X., Tian, Z., Zhao, L., Xu, Z., Li, J., Liu, Z. (2019). Fluorescent half-sandwich phosphine-sulfonate iridium(III) and ruthenium(II) complexes as potential lysosome-targeted anticancer agents. *Dyes and Pigments*, *162*(Iii), 821–830.

Elsayed, S. A., Harrypersad, S., Sahyon, H. A., El-Magd, M. A., Walsby, C. J. (2020). Ruthenium(II)/(III) DMSO-based complexes of 2-aminophenyl benzimidazole with in vitro and *in vivo* anticancer activity. *Molecules*, *25*(18), 4284.

Elsegood, M. R. J., Smith, M. B., Sanchez-Ballester, N. M. (2006). Dichloro(η^6-*p*-cymene)(triphenylphosphine)-ruthenium(II). *Acta Crystallographica Section E: Structure Reports Online, 62*(11), 2838–2840.

Engelbrecht, Z., Roberts, K. E., Hussan, A., Amenuvor, G., Cronjé, M. J., Darkwa, J., Makhubela, B. C. E., Sitole, L. (2020). Synthesis and anti-cancer activity of bis-amino-phosphine ligand and its ruthenium(II) complexes. *Bioorganic and Medicinal Chemistry Letters, 30*(20), 127492.

Filkins, L. M., Graber, J. A., Olson, D. G., Dolben, E. L., Lynd, L. R., Bhuju, S., O'Toole, G. A. (2015). Coculture of Staphylococcus aureus with Pseudomonas aeruginosa drives S. aureus towards fermentative metabolism and reduced viability in a cystic fibrosis model. *Journal of Bacteriology*, *197*(14), 2252–2264.

Gajera, S. B., Mehta, J. V., Thakor, P., Thakkar, V. R., Chudasama, P. C., Patel, J. S., and Patel, M. N. (2016). Half-sandwich iridium(III) complexes with pyrazole-substituted heterocyclic frameworks and their biological applications. *New Journal of Chemistry*, *40*(12), 9968-9980.

Gichumbi, J. M., Friedrich, H. B., Omondi, B. (2016). Synthesis and characterization of piano-stool ruthenium complexes with N,N′-pyridine imine bidentate ligands and their application in styrene oxidation. *Journal of Organometallic Chemistry*, *808*, 87–96.

Golfeto, C. C., Poelhsitz, G. Von, Selistre-de-Araújo, H. S., de Araujo, M. P., Ellena, J., Castellano, E. E., Lopes, L. G. L., Moreira, I. S., Batista, A. A. (2010). Synthesis, characterization and cytotoxic activities of the $[RuCl_2(NO)(dppp)(L)]PF_6$ complexes. *Journal of Inorganic Biochemistry*, *104*(5), 489–495.

Gopalakrishnan, D., Sumithaa, C., Kumar, A. M., Bhuvanesh, N. S. P., Ghorai, S., Das, P., Ganeshpandian, M. (2020). Encapsulation of a Ru(η^6-*p*-cymene) complex of the antibacterial drug trimethoprim into a polydiacetylene-phospholipid assembly to enhance its *in vitro* anticancer and antibacterial activities. *New Journal of Chemistry*, *44*(46), 20047–20059.

Govindaswamy, P., Mozharivskyj, Y. A., Kollipara, M. R. (2004). New neutral and cationic η^6-arene ruthenium complexes with phosphine and amine ligands: Syntheses and molecular structures of $[(\eta^6\text{-}p\text{-cymene})Ru(NH_2CH_2C_6H_5)Cl_2]$, $[(\eta^6\text{-}C_6Me_6)Ru(PPh_2Py)Cl_2]$ and $[(\eta^6\text{-}C_6Me_6)Ru(PPh_2Py)Cl]^+$. *Polyhedron*, *23*(18), 3115–3123.

Guerriero, A., Oberhauser, W., Riedel, T., Peruzzini, M., Dyson, P. J., Gonsalvi, L. (2017). New class of half-sandwich ruthenium (II) arene complexes bearing the water-soluble CAP ligand as an in vitro anticancer agent. *Inorganic Chemistry*, *56*(10), 5514–5518.

Gürses, C., Aktaş, A., Balcıoğlu, S., Fadhilah, A., Gök, Y., Ateş, B. (2022). Synthesis, characterization, DNA binding and anticancer activities of the imidazolidine-functionalized (NHC)Ru(II) complexes. *Journal of Molecular*

Structure, 1247.

Gurusamy, K. S., Koti, R., Toon, C. D., Wilson, P., and Davidson, B. R. (2013). Antibiotic therapy for the treatment of methicillin-resistant Staphylococcus aureus (MRSA) in non surgical wounds. *Cochrane Database of Systematic Reviews*, *2013*(11).

Hammadi, S. Y., Ali, A. (n.d.). *Role of some microbes and fungal species to treat different infections caused by other microorganisms*.

Hao, L., Li, Z. W., Zhang, D. Y., He, L., Liu, W., Yang, J., Tan, C. P., Ji, L. N., Mao, Z. W. (2019). Monitoring mitochondrial viscosity with anticancer phosphorescent Ir(III) complexes: Via two-photon lifetime imaging. *Chemical Science*, *10*(5), 1285–1293.

He, J., Gao, F., Li, Y. L., Liu, X. F., Wu, H., Jiang, Z. Q., Wu, H. K. (2019). Synthesis, characterization and electrochemistry of diiron 1,2-dithiolate complexes with a trans-cinnamate ester. *Journal of Coordination Chemistry*, *72*(3), 452–467.

Helbok, R., Broessner, G., Pfausler, B., Schmutzhard, E. (2009). Chronic meningitis. *Journal of Neurology*, *256*(2), 168–175.

Hildebrand, J. H., Benesi, H. A. (1949). Interaction of iodine with aromatic hydrocarbons [15]. *Nature*, *164*(4179), 963.

Hongthong, K., Nhukeaw, T., Temboot, P., Dyson, P. J., and Ratanaphan, A. (2021). Anticancer activity of RAPTA-EA1 in triple-negative BRCA1 proficient breast cancer cells: single and combined treatment with the PARP inhibitor olaparib. *Heliyon*, *7*(8), e07749.

Honorato, J., Oliveira, K. M., Leite, C. M., Colina-Vegas, L., Nóbrega, J. A., Castellano, E. E., Ellena, J., Correa, R. S., and Batista, A. A. (2020). "Half-Sandwich"/RuII Anticancer Complexes Containing Triphenylphosphine and p-Substituted Benzoic Acids. *Journal of the Brazilian Chemical Society*, *31*, 2237–2249.

Huber, W., Bröhler, P., Wätjen, W., Frank, W., Spingler, B., and Kunz, P. C. (2012). Cytotoxicity of ruthenium(II) piano-stool complexes with imidazole-based PN ligands. *Journal of Organometallic Chemistry*, *717*, 187–194.

Hummer, A. A., Heffeter, P., Berger, W., Filipits, M., Batchelor, D., Büchel, G. E., Jakupec, M. A., Keppler, B. K., Rompel, A. (2013). X-ray absorption near edge structure spectroscopy to resolve the in vivo chemistry of the redox-active indazolium trans-[tetrachlorobis(1H-indazole) ruthenate(III)] (KP1019). *Journal of Medicinal Chemistry*, *56*(3), 1182–1196.

Hunt, L. B. (1987). History of Iridium. *Platinum Metals Review*, *31*(1), 32–41.

Hyde, K. D., Al-Hatmi, A. M. S., Andersen, B., Boekhout, T., Buzina, W., Dawson, T. L., Eastwood, D. C., Jones, E. B. G., de Hoog, S., Kang, Y., and others. (2018). The world's ten most feared fungi. *Fungal Diversity*, *93*(1), 161–194.

Jaouen, G., Beck, W., and McGlinchey, M. J. (2006). A novel field of research: bioorganometallic chemistry, origins, and founding principles. *Bioorganometallics: Biomolecules, Labeling, Medicine*.

Jiménez Riobóo, R. J., Philipp, M., Ramos, M. A., and Krüger, J. K. (2009). Concentration and temperature dependence of the refractive index of ethanol-water mixtures: Influence of intermolecular interactions. *European Physical Journal E*, *30*(1), 19–26.

Kang, P. S., Ko, S. B., Ko, J. M., and Park, J. H. (2009). Tris (2-methoxyphenyl) phosphine as a Highly Active Ligand for the Synthesis of Biaryls by Suzuki Coupling Reaction. *Bulletin of the Korean Chemical Society*, *30*(11), 2697-2700.

Klaimanee, E., Nhukeaw, T., Saithong, S., Ratanaphan, A., Phongpaichit, S., Tantirungrotechai, Y., and Leesakul, N. (2021). Half-sandwich ruthenium(II) *p*-cymene complexes based on organophosphorus ligands: Structure determination, computational investigation, *in vitro* antiproliferative effect in breast cancer cells and antimicrobial activity. *Polyhedron*, *204*, 115244.

Köhler, J. R., Hube, B., Puccia, R., Casadevall, A., and Perfect, J. R. (2017). Fungi that infect humans. *Microbiology Spectrum*, *5*(3), 3–5.

Kotelevskiy, S. I. (1998). The true refractive index correction to the fluorescence intensity in the commercial fluorescence spectrophotometer. *Journal of Luminescence*, *79*(3), 211–214.

Lapasam, A., Banothu, V., Addepally, U., Kollipara, M. R. (2020). Half-sandwich arene ruthenium, rhodium and iridium thiosemicarbazone complexes: synthesis, characterization and biological evaluation. *Journal of Chemical Sciences*, *132*(1), 1–10.

Lapasam, A., and Kollipara, M. R. (2020). A survey of crystal structures and biological activities of platinum group metal complexes containing N-acylthiourea ligands.

Phosphorus, Sulfur and Silicon and the Related Elements, *195*(10), 779–804.

Lee, R. F. S., Escrig, S., Maclachlan, C., Knott, G. W., Meibom, A., Sava, G., Dyson, P. J. (2017). The differential distribution of RAPTA-T in non-invasive and invasive breast cancer cells correlates with its anti-invasive and anti-metastatic effects. *International Journal of Molecular Sciences*, *18*(9).

Lee, S. Y., Kim, C. Y., and Nam, T. G. (2020). Ruthenium complexes as anticancer agents: A brief history and perspectives. *Drug Design, Development and Therapy*, *14*, 5375–5392.

Leesakul, N., Kullawanichaiyanan, K., Mutić, S., Guzsvány, V., Nhukeaw, T., Ratanaphan, A., Saithong, S., Konno, T., Sirimahachai, U., and Promarak, V. (2021). A photoactive iridium(III) complex with 3-methyl-2-phenyl pyridine and 1,1-bis(diphenylphosphino)methane: Synthesis, structural characterization and cytotoxicity in breast cancer cells. *Journal of Coordination Chemistry*, *74*(14), 2380–2394.

Leesakul, N., Neang, R., Chuklin, P., Saithong, S., and Vittaya, L. (2019). The Synthesis, characterization and antimicrobial activity of organometallic Ru(II) complex containing phenylthiourea ligand. *วารสาร วิจัย ม ทร. กรุงเทพ*, *13*(2), 170–186.

Li, J. J., Tian, Z., Xu, Z., Zhang, S., Feng, Y., Zhang, L., and Liu, Z. (2018). Highly potent half-sandwich iridium and ruthenium complexes as lysosome-targeted imaging and anticancer agents. *Dalton Transactions*, *47*(44), 15772–15782.

Li, J., Tian, M., Tian, Z., Zhang, S., Yan, C., Shao, C., and Liu, Z. (2018). Half-sandwich iridium(III) and ruthenium(II) complexes containing P^P-chelating ligands: A new class of potent anticancer agents with unusual redox features. *Inorganic Chemistry*, *57*(4), 1705–1716.

Liu, Jian, Yuan, P. Sen, Liang, A. H., and Ma, D. G. (2018). Synthesis of a novel iridium complex and its exhaustive investigations of photophysics, electrochemistry, luminescent mechanism and electroluminescent performances. *Journal of Luminescence*, *203*(April), 83–89.

Liu, Jie, Chan, A. K. W., Ng, M., Hong, E. Y. H., Wu, N. M. W., Wu, L., and Yam, V. W. W. (2019). Synthesis, Characterization, and Photochromic Studies of Cyclometalated Iridium(III) Complexes Containing a Spironaphthoxazine Moiety. *Organometallics*, *38*(19), 3542–3552.

Liu, X.-F. (2016). Synthesis and structures of diiron dithiolate complexes with 1, 2-bis(diphenylphosphino)acetylene or tris(2-methoxyphenyl)phosphine. *Polyhedron*, *117*, 672–678.

Liu, Z., Li, J. J., Ge, X. X., Zhang, S., Xu, Z., and Gao, W. (2019). Design, synthesis, and evaluation of phosphorescent Ir(III)complexes with anticancer activity. *Journal of Inorganic Biochemistry*, *197*(May), 110703.

Ludwig, G., Kalu\djerović, G. N., Bette, M., Block, M., Paschke, R., and Steinborn, D. (2012). Highly active neutral ruthenium(II) arene complexes: Synthesis, characterization, and investigation of their anticancer properties. *Journal of Inorganic Biochemistry*, *113*, 77–82.

Ma, W., Zhang, S., Tian, Z., Xu, Z., Zhang, Y., Xia, X., Chen, X., and Liu, Z. (2019). Potential anticancer agent for selective damage to mitochondria or lysosomes: Naphthalimide-modified fluorescent biomarker half-sandwich iridium(III) and ruthenium(II) complexes. *European Journal of Medicinal Chemistry*, *181*, 111599.

Mandal, P., Kundu, B. K., Vyas, K., Sabu, V., Helen, A., Dhankhar, S. S., Nagaraja, C. M., Bhattacherjee, D., Bhabak, K. P., and Mukhopadhyay, S. (2018). Ruthenium(II) arene NSAID complexes: Inhibition of cyclooxygenase and antiproliferative activity against cancer cell lines. *Dalton Transactions*, *47*(2), 517–527.

Masalha, M., Borovok, I., Schreiber, R., Aharonowitz, Y., and Cohen, G. (2001). Analysis of transcription of the Staphylococcus aureus aerobic class Ib and anaerobic class III ribonucleotide reductase genes in response to oxygen. *Journal of Bacteriology*, *183*(24), 7260–7272.

Masternak, J., Gilewska, A., Kowalik, M., Kazimierczuk, K., Sitkowski, J., Okła, K., Wietrzyk, J., and Barszcz, B. (2022). Synthesis, crystal structure and spectroscopic characterization of new anionic iridium(III) complexes and their interaction with biological targets. *Polyhedron*, *221*(April).

Mba, I. E., Nweze, E. I., Eze, E. A., and Anyaegbunam, Z. K. G. (2022). Genome plasticity in Candida albicans: A cutting-edge strategy for evolution, adaptation, and survival. *Infection, Genetics and Evolution*, *99*(February), 105256.

Mennucci, B., Cancès, E., and Tomasi, J. (1997). Evaluation of solvent effects in isotropic and anisotropic dielectrics and in ionic solutions with a unified integral equation method: Theoretical bases, computational implementation, and numerical applications. *Journal of Physical Chemistry B*, *101*(49), 10506–10517.

Motswainyana, W. M., and Ajibade, P. A. (2015). Anticancer activities of mononuclear ruthenium(II) coordination complexes. *Advances in Chemistry*, *2015*, 1–21.

Neethu, K. S., Eswaran, J., Theetharappan, M., Nattamai S.P, B., Neelakantan, M. A., and Velusamy, K. M. (2019). Organoruthenium(II) complexes featuring pyrazole-linked Schiff base ligands: Crystal structure, DNA/BSA interactions, cytotoxicity and molecular docking. *Applied Organometallic Chemistry*, *33*(3), 1–16.

Niu, S.-J., Yu, X.-Y., Liu, X.-F., and Li, Y.-L. (2017). Tris(2-methoxyphenyl) phosphine substituted diiron ethanedithiolate complexes containing hydroxymethyl, methyl or ethyl groups. *Polyhedron*, *137*, 127–133.

Odachowski, M., Marschner, C., and Blom, B. (2020). A review on 1, 1-bis (diphenylphosphino)methane bridged homo-and heterobimetallic complexes for anticancer applications: Synthesis, structure, and cytotoxicity. *European Journal of Medicinal Chemistry*, 112613.

Odularu, A. T., Ajibade, P. A., Mbese, J. Z., and Oyedeji, O. O. (2019). Developments in Platinum-Group Metals as Dual Antibacterial and Anticancer Agents. *Journal of Chemistry*, *2019*.

Patil, S. A., Hoagland, A. P., Patil, S. A., and Bugarin, A. (2020). N-heterocyclic carbene-metal complexes as bio-organometallic antimicrobial and anticancer drugs, an update (2015-2020). *Future Medicinal Chemistry*, *12*(24), 2239–2275.

Pradhan, K. C., Barik, S., Singh, B. C., Mohapatra, P., Kisan, H. K., and Pal, S. (2020). Synthesis, characterisation and theoretical studies of a series of Iridium(III) heteroleptic complexes with Schiff base ligands. *Journal of Molecular Structure*, *1211*, 128058.

Pruchnik, F. P., Starosta, R., Ciunik, Z., Opolski, A., Wietrzyk, J., Wojdat, E., and Dus, D. (2001). Tetraacetatodirhodium(II) complexes with tris(methoxyphenyl) phosphines, their reactivity, structure, and antitumor activity. *Canadian Journal of Chemistry*, *79*(5-6), 868-877.

Qin, Q.-P., Wang, Z.-F., Huang, X.-L., Tan, M.-X., Shi, B.-B., and Liang, H. (2019). High *in vitro* and *in vivo* tumor-selective novel ruthenium(II) complexes with 3-(2′-Benzimidazolyl)-7-fluoro-coumarin. *ACS Medicinal Chemistry Letters*, *10*(6), 936–

940.

Rane, H. S., Bernardo, S. M., Raines, S. M., Binder, J. L., Parra, K. J., and Lee, S. A. (2013). Candida albicans VMA3 is necessary for V-ATPase assembly and function and contributes to secretion and filamentation. *Eukaryotic Cell*, *12*(10), 1369–1382.

Renfrew, A. K., Egger, A. E., Scopelliti, R., Hartinger, C. G., and Dyson, P. J. (2010). Synthesis and characterisation of the water soluble bis-phosphine complex [Ru(η^6-cymene)(PPh_2(o-C_6H_4O)-κ^2-*P,O*)(pta)]$^+$ and an investigation of its cytotoxic effects. *Comptes Rendus Chimie*, *13*(8–9), 1144–1150.

Rojas, S., Carmona, F. J., Barea, E., and Maldonado, C. R. (2017). Inorganic mesoporous silicas as vehicles of two novel anthracene-based ruthenium metalloarenes. *Journal of Inorganic Biochemistry*, *166*, 87–93.

Roy, L. E., Hay, P. J., and Martin, R. L. (2008). Revised basis sets for the LANL effective core potentials. *Journal of Chemical Theory and Computation*, *4*(7), 1029–1031.

Sahu, A. K., Dash, D. K., Mishra, K., Mishra, S. P., Yadav, R., and Kashyap, P. (2018). Properties and Applications of Ruthenium. *Noble and Precious Metals - Properties, Nanoscale Effects and Applications*, *17*(Mc).

Sarwar, A., Saharin, S. M., Bahron, H., and Alias, Y. (2021). Dual emissive dinuclear Iridium(III) azomethine complexes: Synthesis, luminescence, thermal stability and antibacterial studies. *Journal of Luminescence*, *233*(October 2020), 117861.

Sengupta, P., Ghosh, S., and Mak, T. C. W. (2001). A new route for the synthesis of bis(pyridine dicarboxylato) bis(triphenylphosphine) complexes of ruthenium(II) and X-ray structural characterisation of the biologically active *trans*-[Ru(PPh_3)$_2$(L^1H)$_2$](L^1H_2 = pyridine 2, 3-dicarboxylic acid). *Polyhedron*, *20*(9–10), 975–980.

Smith, G. S., and Therrien, B. (2011). Targeted and multifunctional arene ruthenium chemotherapeutics. *Dalton Transactions*, *40*(41), 10793–10800.

Souza, B. da S., Sartori, D. S., Andrade, C. de, Weisheimer, E., and Kiszewski, A. E. (2016). Dermatophytosis caused by Microsporum gypseum in infants: report of four cases and review of the literature. *Anais Brasileiros de Dermatologia*, *91*, 823–825.

Souza, B. da S., Sartori, D. S., de Andrade, C., Weisheimer, E., and Kiszewski, A. E. (2016). Dermatophytosis caused by microsporum gypseum in infants: Report of four cases and review of the literature. *Anais Brasileiros de Dermatologia*, *91*(6), 823–825.

Sung, H., Ferlay, J., Siegel, R. L., Laversanne, M., Soerjomataram, I., Jemal, A., and Bray, F. (2021). Global cancer statistics 2020: GLOBOCAN estimates of incidence and mortality worldwide for 36 cancers in 185 countries. *CA: A Cancer Journal for Clinicians*, *71*(3), 209–249.

Tabares, J. P. G., Santos, R. L. S. R., Cassiano, J. L., Zaim, M. H., Honorato, J., Batista, A. A., Teixeira, S. F., Ferreira, A. K., Viana, R. B., Martínez, S. Q., Stábile, A. C., and de Oliveira Silva, D. (2019). A Ru(II)-*p*-cymene compound bearing naproxen-pyridineamide. Synthesis, spectroscopic studies, computational analysis and *in vitro* anticancer activity against lung cells compared to Ru(II)-*p*-cymene-naproxen and the corresponding drug ligands. *Inorganica Chimica Acta*, *489*(December 2018), 27–38.

Tabrizi, L., and Chiniforoshan, H. (2017). Designing new iridium(III) arene complexes of naphthoquinone derivatives as anticancer agents: a structure-activity relationship study. In *Dalton Transactions* (Vol. 46, Issue 7).

Tomaz, A. I., Jakusch, T., Morais, T. S., Marques, F., de Almeida, R. F. M., Mendes, F., Enyedy, É. A., Santos, I., Pessoa, J. C., Kiss, T., and others. (2012). $[Ru^{II}(\eta^5\text{-}C_5H_5)(bipy)(PPh_3)]^+$, a promising large spectrum antitumor agent: Cytotoxic activity and interaction with human serum albumin. *Journal of Inorganic Biochemistry*, *117*, 261–269.

Vijayan, P., Viswanathamurthi, P., Sugumar, P., Ponnuswamy, M. N., Balakumaran, M. D., Kalaichelvan, P. T., Velmurugan, K., Nandhakumar, R., and Butcher, R. J. (2015). Unprecedented formation of organo-ruthenium(II) complexes containing 2-hydroxy-1-naphthaldehyde S-benzyldithiocarbazate: Synthesis, X-ray crystal structure, DFT study and their biological activities *in vitro*. *Inorganic Chemistry Frontiers*, *2*(7), 620–639.

Wang, C., Liu, J., Tian, Z., Tian, M., Tian, L., Zhao, W., and Liu, Z. (2017). Half-sandwich iridium N-heterocyclic carbene anticancer complexes. *Dalton Transactions*, *46*(21), 6870–6883.

Wang, D. D., Zhu, Q. M., Song, L., Guo, J. Y., Shen, H. Y., Wang, X. R., and Chai, W. X. (2020). A new series of three-coordinate cuprous complexes formed by steric hindrance of a phosphine ligand: Synthesis, structure characterization, properties and TD-DFT calculations. *Polyhedron*, *175*, 114178.

Wang, Y., Teng, F., Tang, A., and Xu, X. (2005). Chlorobis [2-(2-pyridyl) phenyl-$\kappa^2 N$, C1](triphenylphosphine-κP) iridium(III) dichloromethane sesquisolvate. *Acta Crystallographica Section E: Structure Reports Online*, *61*(4), m778-m780.

Wu, W., Jin, Y., Bai, F., and Jin, S. (2015). Pseudomonas aeruginosa. In *Molecular medical microbiology* (pp. 753–767). Elsevier.

Yan, L., Hu, M. Y., Mu, C., Li, A., Liu, X. F., Zhao, P. H., Li, Y. L., Jiang, Z. Q., and Wu, H. K. (2019). Synthesis, characterization, and electrochemistry of five diiron propane-1,3-dithiolate complexes with substituted phosphine ligands. *Journal of Coordination Chemistry*, *72*(15), 2499–2516.

Yoopensuk, S., Tongying, P., Hansongnern, K., Pakawatchai, C., Saithong, S., Tantirungrotechai, Y., and Leesakul, N. (2012). Photoactive azoimine dyes: 4-(2-Pyridylazo)-N,N-diethylaniline and 4-(2-pyridylazo)-N,N-dimethylaniline: Computational and experimental investigation. *Spectrochimica Acta - Part A: Molecular and Biomolecular Spectroscopy*, *86*(2), 538–546.

Zeng, L., Gupta, P., Chen, Y., Wang, E., Ji, L., Chao, H., and Chen, Z. S. (2017). The development of anticancer ruthenium(II) complexes: From single molecule compounds to nanomaterials. *Chemical Society Reviews*, *46*(19), 5771–5804.

APPENDIX

1. Crystallization and recrystallization techniques

The complex **1** was entirely dissolved in 10 mL of dichloromethane and 5 mL of acetonitrile. Another bottle was filled with around 20 mL of diethyl ether solvent and this complex solution was then placed into the store. For around 5-7 days, the compound was kept at room temperature. The crystal was obtained, and the process is described here.

The complex **2** was completely dissolved in 10 mL of dichloromethane. This complex solution was then put into another bottle and supplied with a 20 mL solution of diethyl ether solvent. The compound was maintained at room temperature for around 5-7 days. Here is a description of how the crystal was obtained.

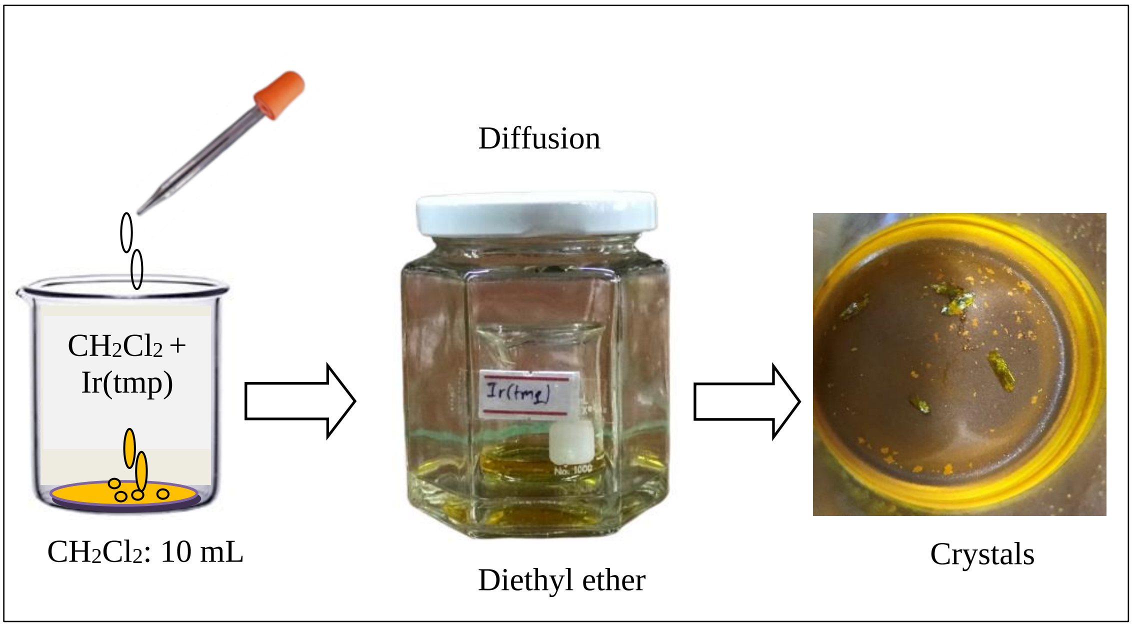

The complex **3** was filtrated and crystallized by mixing dichloromethane and acetonitrile 2:1 ratio and diffused by diethyl ether vapor for 10 mL and left at room temperature for a few days to receive the single crystal. The obtained brown single crystals were filtered and washed with diethyl ether. The complex was recrystallized again in the same solvent mixture.

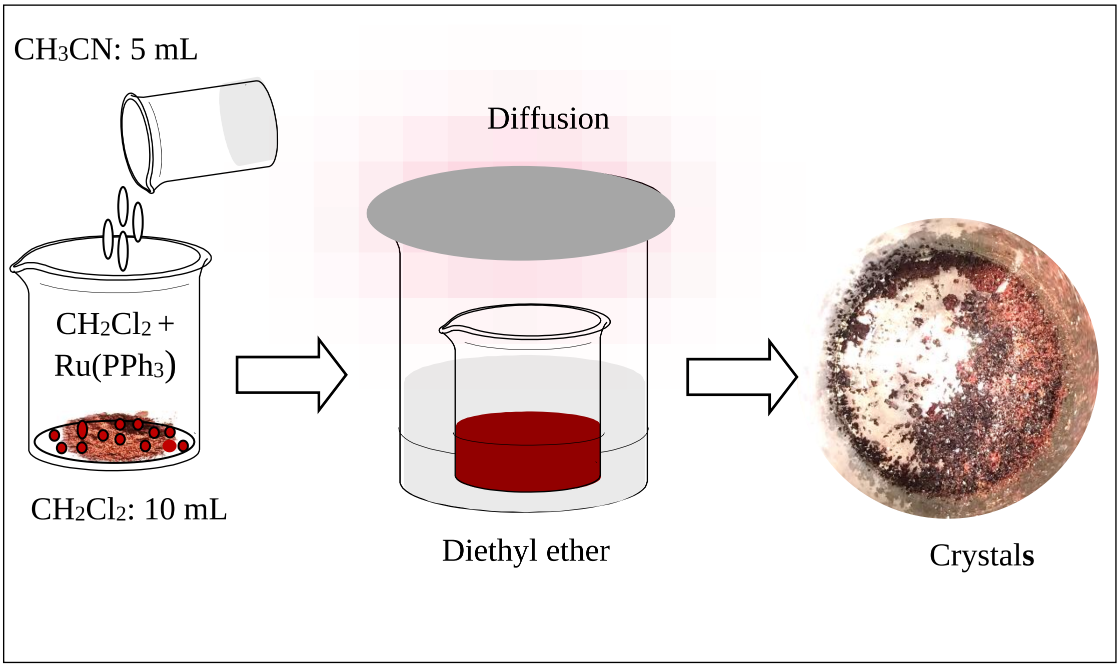

Table 1. Crystal data and structure refinement for complex **1.**

Identification code	Complex 1
Empirical formula	$C_{30}H_{32}ClO_3PRu$, CH_2Cl_2
Formula weight	692.97
Temperature	296(2) K
Wavelength	1.54178 Å
Crystal system	Triclinic
Space group	$P\bar{1}$
Unit cell dimensions	a = 10.0522(2) Å α = 83.5800(10)° b = 10.8482(2) Å β = 75.5990(10)° c = 16.1698(3) Å γ = 65.0900(10)°
Volume	1548.95(5) $Å^3$
Z	2
Density (calculated)	1.486 Mg/m^3
Absorption coefficient	7.208 mm^{-1}
F(000)	708
Crystal size	0.238 × 0.146 × 0.061 mm^3
Theta range for data collection	2.821 to 68.486°
Index ranges	-12<=h<=12, -13<=k<=13, -18<=l<=19
Reflections collected	47929
Independent reflections	10521 [R(int) = 0.0404]
Completeness to theta = 67.679°	99.2 %
Absorption correction	Semi-empirical from equivalents
Max. and min. transmission	0.7531 and 0.4158
Refinement method	Full-matrix least-squares on F^2
Data / restraints / parameters	10521 / 3 / 714
Goodness-of-fit on F^2	1.026
Final R indices [I>2σ(I)]	$R1$ = 0.0267, $wR2$ = 0.0695
R indices (all data)	$R1$ = 0.0269, $wR2$ = 0.0698
Absolute structure parameter	0.104(8)
Extinction coefficient	n/a
Largest diff. peak and hole	0.442 and -0.413 e.$Å^{-3}$

Table 2. Atomic coordinates ($\times 10^4$) and equivalent isotropic displacement parameters (Å^2 $\times 10^3$) complex 1. U(eq) is defined as one-third of the trace of the orthogonalized U^{ij} tensor.

	x	y	z	U(eq)
Ru(1)	6488(1)	9033(1)	2454(1)	38(1)
Ru(2)	5610(1)	1076(1)	7467(1)	36(1)
Cl(1)	6074(2)	9562(2)	1021(1)	57(1)
Cl(2)	5717(2)	575(2)	6026(1)	55(1)
P(1)	3974(1)	9340(1)	2895(1)	36(1)
P(2)	3395(1)	739(1)	7891(1)	34(1)
O(1)	6726(3)	7100(3)	2211(2)	47(1)
O(2)	598(4)	10216(4)	3427(3)	57(1)
O(3)	3149(5)	11243(4)	4269(2)	57(1)
O(4)	4086(4)	3001(3)	7205(2)	46(1)
O(5)	4273(4)	-1200(4)	9279(2)	56(1)
O(6)	873(4)	-223(4)	8403(3)	58(1)
C(1)	4069(5)	7900(4)	2382(3)	38(1)
C(2)	2856(6)	7657(5)	2293(3)	47(1)
C(3)	3104(6)	6461(5)	1931(4)	55(1)
C(4)	4552(6)	5496(5)	1678(4)	57(1)
C(5)	5766(6)	5698(5)	1778(4)	54(1)
C(6)	5558(5)	6921(4)	2127(3)	41(1)
C(7)	2477(5)	10936(4)	2655(3)	42(1)
C(8)	2862(6)	11944(5)	2196(3)	53(1)
C(9)	1780(7)	13240(5)	2095(4)	67(2)
C(10)	277(8)	13531(6)	2479(5)	75(2)
C(11)	-114(6)	12557(6)	2940(4)	63(1)
C(12)	950(6)	11253(5)	3021(3)	48(1)
C(13)	-586(7)	10514(8)	4178(4)	69(2)
C(14)	3312(5)	9095(5)	4036(3)	42(1)
C(15)	3139(6)	7906(5)	4343(3)	53(1)
C(16)	2600(7)	7742(7)	5203(4)	67(1)

C(17)	2254(7)	8752(8)	5764(4)	70(2)
C(18)	2423(7)	9937(7)	5472(4)	64(2)
C(19)	2945(5)	10111(5)	4613(3)	47(1)
C(20)	2532(9)	12406(7)	4789(5)	82(2)
C(21)	7352(6)	10616(6)	2358(4)	57(1)
C(22)	8619(7)	9351(7)	2084(4)	55(2)
C(23)	8838(5)	8225(6)	2603(4)	56(1)
C(24)	7879(6)	8245(5)	3418(3)	49(1)
C(25)	6678(6)	9494(6)	3703(4)	47(1)
C(26)	6413(6)	10672(5)	3166(4)	53(1)
C(27)	7055(9)	11847(7)	1767(6)	85(2)
C(28)	8195(7)	6958(6)	3956(4)	65(1)
C(29)	6969(10)	7098(9)	4766(6)	100(3)
C(30)	9696(11)	6540(11)	4195(7)	119(4)
C(31)	2171(5)	2179(4)	7368(3)	36(1)
C(32)	754(5)	2402(5)	7275(3)	45(1)
C(33)	-94(5)	3597(5)	6889(3)	52(1)
C(34)	494(6)	4558(5)	6618(3)	52(1)
C(35)	1871(6)	4372(4)	6716(3)	48(1)
C(36)	2762(5)	3164(4)	7106(3)	38(1)
C(37)	2485(5)	961(4)	9025(3)	39(1)
C(38)	1240(6)	2134(5)	9327(3)	50(1)
C(39)	536(6)	2287(6)	10180(4)	63(1)
C(40)	1086(7)	1259(7)	10754(4)	66(1)
C(41)	2319(7)	92(7)	10470(4)	59(1)
C(42)	3033(5)	-63(5)	9615(3)	45(1)
C(43)	4678(9)	-2377(7)	9796(5)	80(2)
C(44)	3397(5)	-875(4)	7653(3)	42(1)
C(45)	4725(6)	-1848(5)	7205(3)	52(1)
C(46)	4873(8)	-3184(6)	7138(4)	66(2)
C(47)	3677(8)	-3519(6)	7523(4)	68(2)
C(48)	2354(8)	-2554(6)	7961(4)	61(1)
C(49)	2195(6)	-1234(5)	8014(3)	47(1)
C(50)	-46(8)	-548(8)	9134(5)	72(2)
C(51)	7875(5)	-551(5)	7430(4)	54(1)
C(52)	6948(5)	-532(5)	8234(4)	51(1)

C(53)	6153(6)	674(6)	8733(4)	45(1)
C(54)	6284(5)	1899(5)	8411(3)	47(1)
C(55)	7268(6)	1849(5)	7593(3)	52(1)
C(56)	8036(7)	697(7)	7120(4)	53(1)
C(57)	8679(7)	-1801(7)	6887(6)	82(2)
C(58)	5497(7)	3204(6)	8895(4)	64(1)
C(59)	6614(9)	3423(9)	9283(7)	102(3)
C(60)	4151(11)	3289(12)	9583(9)	147(6)
C(61)	8953(13)	6425(12)	284(8)	127(4)
Cl(3)	10604(3)	6338(3)	509(2)	124(1)
Cl(4)	9177(3)	5984(2)	-745(2)	118(1)
C(62)	5663(11)	3922(11)	5344(6)	109(3)
Cl(5)	7432(3)	3562(2)	5491(2)	101(1)
Cl(6)	5557(3)	4096(3)	4261(2)	108(1)

Table 3: Bond lengths [Å] and angles [°] for [Ru(*p*-cymene)(tmp)Cl]·CH_2Cl_2.

Ru(1)-O(1)	2.079(3)
Ru(1)-C(26)	2.189(5)
Ru(1)-C(21)	2.204(5)
Ru(1)-C(25)	2.206(5)
Ru(1)-C(24)	2.212(4)
Ru(1)-C(23)	2.213(5)
Ru(1)-C(22)	2.237(6)
Ru(1)-P(1)	2.3345(13)
Ru(1)-Cl(1)	2.4207(13)
Ru(2)-O(4)	2.079(3)
Ru(2)-C(52)	2.181(5)
Ru(2)-C(53)	2.198(5)
Ru(2)-C(51)	2.207(4)
Ru(2)-C(55)	2.215(5)
Ru(2)-C(54)	2.216(5)
Ru(2)-C(56)	2.227(6)
Ru(2)-P(2)	2.3301(12)
Ru(2)-Cl(2)	2.4182(13)

P(1)-C(1)	1.807(4)
P(1)-C(14)	1.829(5)
P(1)-C(7)	1.832(5)
P(2)-C(31)	1.808(4)
P(2)-C(37)	1.827(5)
P(2)-C(44)	1.833(4)
O(1)-C(6)	1.308(6)
O(2)-C(12)	1.370(7)
O(2)-C(13)	1.429(7)
O(3)-C(19)	1.365(6)
O(3)-C(20)	1.416(7)
O(4)-C(36)	1.315(6)
O(5)-C(42)	1.374(6)
O(5)-C(43)	1.410(7)
O(6)-C(49)	1.369(7)
O(6)-C(50)	1.419(7)
C(1)-C(2)	1.394(7)
C(1)-C(6)	1.411(6)
C(2)-C(3)	1.383(7)
C(2)-H(2)	0.9300
C(3)-C(4)	1.378(8)
C(3)-H(3)	0.9300
C(4)-C(5)	1.377(8)
C(4)-H(4)	0.9300
C(5)-C(6)	1.414(7)
C(5)-H(5)	0.9300
C(7)-C(8)	1.390(7)
C(7)-C(12)	1.404(7)
C(8)-C(9)	1.391(8)
C(8)-H(8)	0.9300
C(9)-C(10)	1.394(10)
C(9)-H(9)	0.9300
C(10)-C(11)	1.362(10)
C(10)-H(10)	0.9300
C(11)-C(12)	1.384(7)
C(11)-H(11)	0.9300

C(13)-H(13A)	0.9600
C(13)-H(13B)	0.9600
C(13)-H(13C)	0.9600
C(14)-C(19)	1.391(7)
C(14)-C(15)	1.395(7)
C(15)-C(16)	1.382(8)
C(15)-H(15)	0.9300
C(16)-C(17)	1.375(10)
C(16)-H(16)	0.9300
C(17)-C(18)	1.383(10)
C(17)-H(17)	0.9300
C(18)-C(19)	1.379(8)
C(18)-H(18)	0.9300
C(20)-H(20A)	0.9600
C(20)-H(20B)	0.9600
C(20)-H(20C)	0.9600
C(21)-C(26)	1.399(8)
C(21)-C(22)	1.444(9)
C(21)-C(27)	1.519(7)
C(22)-C(23)	1.371(9)
C(22)-H(22)	0.9800
C(23)-C(24)	1.423(8)
C(23)-H(23)	0.9800
C(24)-C(25)	1.411(8)
C(24)-C(28)	1.516(7)
C(25)-C(26)	1.428(8)
C(25)-H(25)	0.9800
C(26)-H(26)	0.9800
C(27)-H(27A)	0.9600
C(27)-H(27B)	0.9600
C(27)-H(27C)	0.9600
C(28)-C(30)	1.519(10)
C(28)-C(29)	1.531(11)
C(28)-H(28)	0.9800
C(29)-H(29A)	0.9600
C(29)-H(29B)	0.9600

C(29)-H(29C)	0.9600
C(30)-H(30A)	0.9600
C(30)-H(30B)	0.9600
C(30)-H(30C)	0.9600
C(31)-C(32)	1.386(6)
C(31)-C(36)	1.407(6)
C(32)-C(33)	1.396(7)
C(32)-H(32)	0.9300
C(33)-C(34)	1.385(7)
C(33)-H(33)	0.9300
C(34)-C(35)	1.360(7)
C(34)-H(34)	0.9300
C(35)-C(36)	1.423(6)
C(35)-H(35)	0.9300
C(37)-C(38)	1.385(7)
C(37)-C(42)	1.399(6)
C(38)-C(39)	1.378(8)
C(38)-H(38)	0.9300
C(39)-C(40)	1.384(9)
C(39)-H(39)	0.9300
C(40)-C(41)	1.369(10)
C(40)-H(40)	0.9300
C(41)-C(42)	1.383(8)
C(41)-H(41)	0.9300
C(43)-H(43A)	0.9600
C(43)-H(43B)	0.9600
C(43)-H(43C)	0.9600
C(44)-C(45)	1.388(7)
C(44)-C(49)	1.395(7)
C(45)-C(46)	1.407(7)
C(45)-H(45)	0.9300
C(46)-C(47)	1.382(10)
C(46)-H(46)	0.9300
C(47)-C(48)	1.375(10)
C(47)-H(47)	0.9300
C(48)-C(49)	1.383(7)

C(48)-H(48)	0.9300
C(50)-H(50A)	0.9600
C(50)-H(50B)	0.9600
C(50)-H(50C)	0.9600
C(51)-C(52)	1.395(8)
C(51)-C(56)	1.450(9)
C(51)-C(57)	1.501(8)
C(52)-C(53)	1.427(8)
C(52)-H(52)	0.9800
C(53)-C(54)	1.418(8)
C(53)-H(53)	0.9800
C(54)-C(55)	1.432(8)
C(54)-C(58)	1.497(7)
C(55)-C(56)	1.360(9)
C(55)-H(55)	0.9800
C(56)-H(56)	0.9800
C(57)-H(57A)	0.9600
C(57)-H(57B)	0.9600
C(57)-H(57C)	0.9600
C(58)-C(60)	1.498(12)
C(58)-C(59)	1.523(9)
C(58)-H(58)	0.9800
C(59)-H(59A)	0.9600
C(59)-H(59B)	0.9600
C(59)-H(59C)	0.9600
C(60)-H(60A)	0.9600
C(60)-H(60B)	0.9600
C(60)-H(60C)	0.9600
C(61)-Cl(4)	1.718(13)
C(61)-Cl(3)	1.748(14)
C(61)-H(61A)	0.9700
C(61)-H(61B)	0.9700
C(62)-Cl(5)	1.725(11)
C(62)-Cl(6)	1.765(11)
C(62)-H(62A)	0.9700
C(62)-H(62B)	0.9700

O(1)-Ru(1)-C(26)	158.18(17)
O(1)-Ru(1)-C(21)	152.35(18)
C(26)-Ru(1)-C(21)	37.1(2)
O(1)-Ru(1)-C(25)	120.27(18)
C(26)-Ru(1)-C(25)	37.9(2)
C(21)-Ru(1)-C(25)	67.7(2)
O(1)-Ru(1)-C(24)	92.24(15)
C(26)-Ru(1)-C(24)	68.03(18)
C(21)-Ru(1)-C(24)	80.57(19)
C(25)-Ru(1)-C(24)	37.2(2)
O(1)-Ru(1)-C(23)	91.25(17)
C(26)-Ru(1)-C(23)	78.8(2)
C(21)-Ru(1)-C(23)	66.8(2)
C(25)-Ru(1)-C(23)	66.6(2)
C(24)-Ru(1)-C(23)	37.5(2)
O(1)-Ru(1)-C(22)	114.8(2)
C(26)-Ru(1)-C(22)	67.1(2)
C(21)-Ru(1)-C(22)	37.9(2)
C(25)-Ru(1)-C(22)	78.9(2)
C(24)-Ru(1)-C(22)	66.9(2)
C(23)-Ru(1)-C(22)	35.9(2)
O(1)-Ru(1)-P(1)	80.65(9)
C(26)-Ru(1)-P(1)	99.59(14)
C(21)-Ru(1)-P(1)	126.42(16)
C(25)-Ru(1)-P(1)	95.61(15)
C(24)-Ru(1)-P(1)	116.97(14)
C(23)-Ru(1)-P(1)	153.37(16)
C(22)-Ru(1)-P(1)	164.34(18)
O(1)-Ru(1)-Cl(1)	84.79(10)
C(26)-Ru(1)-Cl(1)	117.03(15)
C(21)-Ru(1)-Cl(1)	90.50(16)
C(25)-Ru(1)-Cl(1)	154.93(15)
C(24)-Ru(1)-Cl(1)	154.78(15)
C(23)-Ru(1)-Cl(1)	117.36(16)
C(22)-Ru(1)-Cl(1)	91.60(18)
P(1)-Ru(1)-Cl(1)	87.32(5)

O(4)-Ru(2)-C(52)	156.70(17)
O(4)-Ru(2)-C(53)	118.67(18)
C(52)-Ru(2)-C(53)	38.0(2)
O(4)-Ru(2)-C(51)	154.87(18)
C(52)-Ru(2)-C(51)	37.1(2)
C(53)-Ru(2)-C(51)	68.0(2)
O(4)-Ru(2)-C(55)	92.58(16)
C(52)-Ru(2)-C(55)	78.78(19)
C(53)-Ru(2)-C(55)	67.0(2)
C(51)-Ru(2)-C(55)	67.0(2)
O(4)-Ru(2)-C(54)	91.72(15)
C(52)-Ru(2)-C(54)	68.17(18)
C(53)-Ru(2)-C(54)	37.5(2)
C(51)-Ru(2)-C(54)	80.89(19)
C(55)-Ru(2)-C(54)	37.7(2)
O(4)-Ru(2)-C(56)	117.0(2)
C(52)-Ru(2)-C(56)	67.1(2)
C(53)-Ru(2)-C(56)	79.2(2)
C(51)-Ru(2)-C(56)	38.2(2)
C(55)-Ru(2)-C(56)	35.7(2)
C(54)-Ru(2)-C(56)	66.9(2)
O(4)-Ru(2)-P(2)	80.67(9)
C(52)-Ru(2)-P(2)	98.18(14)
C(53)-Ru(2)-P(2)	95.50(14)
C(51)-Ru(2)-P(2)	123.97(16)
C(55)-Ru(2)-P(2)	155.43(15)
C(54)-Ru(2)-P(2)	118.40(14)
C(56)-Ru(2)-P(2)	162.07(18)
O(4)-Ru(2)-Cl(2)	84.37(10)
C(52)-Ru(2)-Cl(2)	118.92(15)
C(53)-Ru(2)-Cl(2)	156.96(15)
C(51)-Ru(2)-Cl(2)	91.23(15)
C(55)-Ru(2)-Cl(2)	115.23(15)
C(54)-Ru(2)-Cl(2)	152.61(14)
C(56)-Ru(2)-Cl(2)	90.73(17)
P(2)-Ru(2)-Cl(2)	87.77(5)

C(1)-P(1)-C(14)	105.2(2)
C(1)-P(1)-C(7)	112.3(2)
C(14)-P(1)-C(7)	102.9(2)
C(1)-P(1)-Ru(1)	99.64(15)
C(14)-P(1)-Ru(1)	115.93(15)
C(7)-P(1)-Ru(1)	120.20(17)
C(31)-P(2)-C(37)	104.8(2)
C(31)-P(2)-C(44)	112.91(19)
C(37)-P(2)-C(44)	102.6(2)
C(31)-P(2)-Ru(2)	99.92(14)
C(37)-P(2)-Ru(2)	116.36(14)
C(44)-P(2)-Ru(2)	119.59(17)
C(6)-O(1)-Ru(1)	119.6(3)
C(12)-O(2)-C(13)	118.7(4)
C(19)-O(3)-C(20)	118.0(5)
C(36)-O(4)-Ru(2)	119.5(2)
C(42)-O(5)-C(43)	118.1(5)
C(49)-O(6)-C(50)	118.9(5)
C(2)-C(1)-C(6)	120.8(4)
C(2)-C(1)-P(1)	126.7(3)
C(6)-C(1)-P(1)	112.3(3)
C(3)-C(2)-C(1)	120.1(4)
C(3)-C(2)-H(2)	119.9
C(1)-C(2)-H(2)	119.9
C(4)-C(3)-C(2)	119.8(5)
C(4)-C(3)-H(3)	120.1
C(2)-C(3)-H(3)	120.1
C(5)-C(4)-C(3)	121.2(5)
C(5)-C(4)-H(4)	119.4
C(3)-C(4)-H(4)	119.4
C(4)-C(5)-C(6)	120.6(5)
C(4)-C(5)-H(5)	119.7
C(6)-C(5)-H(5)	119.7
O(1)-C(6)-C(1)	122.8(4)
O(1)-C(6)-C(5)	119.8(4)
C(1)-C(6)-C(5)	117.5(4)

C(8)-C(7)-C(12)	118.2(4)
C(8)-C(7)-P(1)	119.1(4)
C(12)-C(7)-P(1)	122.1(4)
C(7)-C(8)-C(9)	121.6(5)
C(7)-C(8)-H(8)	119.2
C(9)-C(8)-H(8)	119.2
C(8)-C(9)-C(10)	118.7(6)
C(8)-C(9)-H(9)	120.6
C(10)-C(9)-H(9)	120.6
C(11)-C(10)-C(9)	120.2(5)
C(11)-C(10)-H(10)	119.9
C(9)-C(10)-H(10)	119.9
C(10)-C(11)-C(12)	121.4(6)
C(10)-C(11)-H(11)	119.3
C(12)-C(11)-H(11)	119.3
O(2)-C(12)-C(11)	123.5(5)
O(2)-C(12)-C(7)	116.8(4)
C(11)-C(12)-C(7)	119.7(5)
O(2)-C(13)-H(13A)	109.5
O(2)-C(13)-H(13B)	109.5
H(13A)-C(13)-H(13B)	109.5
O(2)-C(13)-H(13C)	109.5
H(13A)-C(13)-H(13C)	109.5
H(13B)-C(13)-H(13C)	109.5
C(19)-C(14)-C(15)	118.8(4)
C(19)-C(14)-P(1)	120.3(4)
C(15)-C(14)-P(1)	120.9(4)
C(16)-C(15)-C(14)	120.7(5)
C(16)-C(15)-H(15)	119.7
C(14)-C(15)-H(15)	119.7
C(17)-C(16)-C(15)	119.7(6)
C(17)-C(16)-H(16)	120.1
C(15)-C(16)-H(16)	120.1
C(16)-C(17)-C(18)	120.4(6)
C(16)-C(17)-H(17)	119.8
C(18)-C(17)-H(17)	119.8

C(19)-C(18)-C(17)	120.0(6)
C(19)-C(18)-H(18)	120.0
C(17)-C(18)-H(18)	120.0
O(3)-C(19)-C(18)	124.0(5)
O(3)-C(19)-C(14)	115.6(4)
C(18)-C(19)-C(14)	120.4(5)
O(3)-C(20)-H(20A)	109.5
O(3)-C(20)-H(20B)	109.5
H(20A)-C(20)-H(20B)	109.5
O(3)-C(20)-H(20C)	109.5
H(20A)-C(20)-H(20C)	109.5
H(20B)-C(20)-H(20C)	109.5
C(26)-C(21)-C(22)	118.7(5)
C(26)-C(21)-C(27)	121.5(6)
C(22)-C(21)-C(27)	119.8(6)
C(26)-C(21)-Ru(1)	70.8(3)
C(22)-C(21)-Ru(1)	72.2(3)
C(27)-C(21)-Ru(1)	127.8(4)
C(23)-C(22)-C(21)	119.6(6)
C(23)-C(22)-Ru(1)	71.1(3)
C(21)-C(22)-Ru(1)	69.8(3)
C(23)-C(22)-H(22)	119.5
C(21)-C(22)-H(22)	119.5
Ru(1)-C(22)-H(22)	119.5
C(22)-C(23)-C(24)	122.8(5)
C(22)-C(23)-Ru(1)	73.0(3)
C(24)-C(23)-Ru(1)	71.2(3)
C(22)-C(23)-H(23)	117.9
C(24)-C(23)-H(23)	117.9
Ru(1)-C(23)-H(23)	117.9
C(25)-C(24)-C(23)	117.7(5)
C(25)-C(24)-C(28)	122.5(5)
C(23)-C(24)-C(28)	119.8(5)
C(25)-C(24)-Ru(1)	71.1(3)
C(23)-C(24)-Ru(1)	71.2(3)
C(28)-C(24)-Ru(1)	130.0(4)

C(24)-C(25)-C(26)	120.3(5)
C(24)-C(25)-Ru(1)	71.6(3)
C(26)-C(25)-Ru(1)	70.4(3)
C(24)-C(25)-H(25)	119.2
C(26)-C(25)-H(25)	119.2
Ru(1)-C(25)-H(25)	119.2
C(21)-C(26)-C(25)	120.8(5)
C(21)-C(26)-Ru(1)	72.0(3)
C(25)-C(26)-Ru(1)	71.7(3)
C(21)-C(26)-H(26)	119.1
C(25)-C(26)-H(26)	119.1
Ru(1)-C(26)-H(26)	119.1
C(21)-C(27)-H(27A)	109.5
C(21)-C(27)-H(27B)	109.5
H(27A)-C(27)-H(27B)	109.5
C(21)-C(27)-H(27C)	109.5
H(27A)-C(27)-H(27C)	109.5
H(27B)-C(27)-H(27C)	109.5
C(24)-C(28)-C(30)	109.1(6)
C(24)-C(28)-C(29)	113.5(5)
C(30)-C(28)-C(29)	109.5(7)
C(24)-C(28)-H(28)	108.2
C(30)-C(28)-H(28)	108.2
C(29)-C(28)-H(28)	108.2
C(28)-C(29)-H(29A)	109.5
C(28)-C(29)-H(29B)	109.5
H(29A)-C(29)-H(29B)	109.5
C(28)-C(29)-H(29C)	109.5
H(29A)-C(29)-H(29C)	109.5
H(29B)-C(29)-H(29C)	109.5
C(28)-C(30)-H(30A)	109.5
C(28)-C(30)-H(30B)	109.5
H(30A)-C(30)-H(30B)	109.5
C(28)-C(30)-H(30C)	109.5
H(30A)-C(30)-H(30C)	109.5
H(30B)-C(30)-H(30C)	109.5

C(32)-C(31)-C(36)	121.0(4)
C(32)-C(31)-P(2)	126.5(3)
C(36)-C(31)-P(2)	112.3(3)
C(31)-C(32)-C(33)	120.2(4)
C(31)-C(32)-H(32)	119.9
C(33)-C(32)-H(32)	119.9
C(34)-C(33)-C(32)	118.9(4)
C(34)-C(33)-H(33)	120.6
C(32)-C(33)-H(33)	120.6
C(35)-C(34)-C(33)	121.9(4)
C(35)-C(34)-H(34)	119.0
C(33)-C(34)-H(34)	119.0
C(34)-C(35)-C(36)	120.4(4)
C(34)-C(35)-H(35)	119.8
C(36)-C(35)-H(35)	119.8
O(4)-C(36)-C(31)	122.7(4)
O(4)-C(36)-C(35)	119.8(4)
C(31)-C(36)-C(35)	117.5(4)
C(38)-C(37)-C(42)	118.1(4)
C(38)-C(37)-P(2)	121.5(3)
C(42)-C(37)-P(2)	120.5(4)
C(39)-C(38)-C(37)	121.4(5)
C(39)-C(38)-H(38)	119.3
C(37)-C(38)-H(38)	119.3
C(38)-C(39)-C(40)	119.8(5)
C(38)-C(39)-H(39)	120.1
C(40)-C(39)-H(39)	120.1
C(41)-C(40)-C(39)	119.9(5)
C(41)-C(40)-H(40)	120.1
C(39)-C(40)-H(40)	120.1
C(40)-C(41)-C(42)	120.6(5)
C(40)-C(41)-H(41)	119.7
C(42)-C(41)-H(41)	119.7
O(5)-C(42)-C(41)	124.2(4)
O(5)-C(42)-C(37)	115.5(4)
C(41)-C(42)-C(37)	120.3(5)

O(5)-C(43)-H(43A)	109.5
O(5)-C(43)-H(43B)	109.5
H(43A)-C(43)-H(43B)	109.5
O(5)-C(43)-H(43C)	109.5
H(43A)-C(43)-H(43C)	109.5
H(43B)-C(43)-H(43C)	109.5
C(45)-C(44)-C(49)	118.8(4)
C(45)-C(44)-P(2)	118.3(4)
C(49)-C(44)-P(2)	122.2(4)
C(44)-C(45)-C(46)	120.6(5)
C(44)-C(45)-H(45)	119.7
C(46)-C(45)-H(45)	119.7
C(47)-C(46)-C(45)	119.3(6)
C(47)-C(46)-H(46)	120.4
C(45)-C(46)-H(46)	120.4
C(48)-C(47)-C(46)	120.3(5)
C(48)-C(47)-H(47)	119.8
C(46)-C(47)-H(47)	119.8
C(47)-C(48)-C(49)	120.6(6)
C(47)-C(48)-H(48)	119.7
C(49)-C(48)-H(48)	119.7
O(6)-C(49)-C(48)	122.6(5)
O(6)-C(49)-C(44)	117.0(4)
C(48)-C(49)-C(44)	120.4(5)
O(6)-C(50)-H(50A)	109.5
O(6)-C(50)-H(50B)	109.5
H(50A)-C(50)-H(50B)	109.5
O(6)-C(50)-H(50C)	109.5
H(50A)-C(50)-H(50C)	109.5
H(50B)-C(50)-H(50C)	109.5
C(52)-C(51)-C(56)	117.7(5)
C(52)-C(51)-C(57)	122.2(6)
C(56)-C(51)-C(57)	120.0(6)
C(52)-C(51)-Ru(2)	70.4(3)
C(56)-C(51)-Ru(2)	71.7(3)
C(57)-C(51)-Ru(2)	128.4(4)

C(51)-C(52)-C(53)	121.7(5)
C(51)-C(52)-Ru(2)	72.5(3)
C(53)-C(52)-Ru(2)	71.6(3)
C(51)-C(52)-H(52)	118.6
C(53)-C(52)-H(52)	118.6
Ru(2)-C(52)-H(52)	118.6
C(54)-C(53)-C(52)	120.0(5)
C(54)-C(53)-Ru(2)	71.9(3)
C(52)-C(53)-Ru(2)	70.3(3)
C(54)-C(53)-H(53)	119.4
C(52)-C(53)-H(53)	119.4
Ru(2)-C(53)-H(53)	119.4
C(53)-C(54)-C(55)	117.3(5)
C(53)-C(54)-C(58)	123.3(5)
C(55)-C(54)-C(58)	119.3(5)
C(53)-C(54)-Ru(2)	70.6(3)
C(55)-C(54)-Ru(2)	71.1(3)
C(58)-C(54)-Ru(2)	131.1(3)
C(56)-C(55)-C(54)	122.7(5)
C(56)-C(55)-Ru(2)	72.7(3)
C(54)-C(55)-Ru(2)	71.2(3)
C(56)-C(55)-H(55)	117.9
C(54)-C(55)-H(55)	117.9
Ru(2)-C(55)-H(55)	117.9
C(55)-C(56)-C(51)	120.5(5)
C(55)-C(56)-Ru(2)	71.7(3)
C(51)-C(56)-Ru(2)	70.2(3)
C(55)-C(56)-H(56)	119.0
C(51)-C(56)-H(56)	119.0
Ru(2)-C(56)-H(56)	119.0
C(51)-C(57)-H(57A)	109.5
C(51)-C(57)-H(57B)	109.5
H(57A)-C(57)-H(57B)	109.5
C(51)-C(57)-H(57C)	109.5
H(57A)-C(57)-H(57C)	109.5
H(57B)-C(57)-H(57C)	109.5

C(54)-C(58)-C(60)	114.7(6)
C(54)-C(58)-C(59)	109.1(5)
C(60)-C(58)-C(59)	109.4(7)
C(54)-C(58)-H(58)	107.8
C(60)-C(58)-H(58)	107.8
C(59)-C(58)-H(58)	107.8
C(58)-C(59)-H(59A)	109.5
C(58)-C(59)-H(59B)	109.5
H(59A)-C(59)-H(59B)	109.5
C(58)-C(59)-H(59C)	109.5
H(59A)-C(59)-H(59C)	109.5
H(59B)-C(59)-H(59C)	109.5
C(58)-C(60)-H(60A)	109.5
C(58)-C(60)-H(60B)	109.5
H(60A)-C(60)-H(60B)	109.5
C(58)-C(60)-H(60C)	109.5
H(60A)-C(60)-H(60C)	109.5
H(60B)-C(60)-H(60C)	109.5
Cl(4)-C(61)-Cl(3)	113.5(5)
Cl(4)-C(61)-H(61A)	108.9
Cl(3)-C(61)-H(61A)	108.9
Cl(4)-C(61)-H(61B)	108.9
Cl(3)-C(61)-H(61B)	108.9
H(61A)-C(61)-H(61B)	107.7
Cl(5)-C(62)-Cl(6)	113.6(5)
Cl(5)-C(62)-H(62A)	108.8
Cl(6)-C(62)-H(62A)	108.8
Cl(5)-C(62)-H(62B)	108.8
Cl(6)-C(62)-H(62B)	108.8
H(62A)-C(62)-H(62B)	107.7

Symmetry transformations were used to generate equivalent atoms.

Table 4. Anisotropic displacement parameters ($Å^2 \times 10^3$) for Ru(tmp). The anisotropic displacement factor exponent takes the form: $-2\pi^2[\, h^2 a^{*2} U^{11} + \cdots + 2\, h\, k\, a^*\, b^* U^{12}]$.

	U^{11}	U^{22}	U^{33}	U^{23}	U^{13}	U^{12}
Ru(1)	36(1)	36(1)	40(1)	1(1)	-10(1)	-13(1)
Ru(2)	35(1)	34(1)	39(1)	-1(1)	-9(1)	-14(1)
Cl(1)	64(1)	61(1)	42(1)	3(1)	-15(1)	-20(1)
Cl(2)	66(1)	59(1)	41(1)	-3(1)	-12(1)	-26(1)
P(1)	38(1)	33(1)	34(1)	-2(1)	-9(1)	-12(1)
P(2)	36(1)	32(1)	35(1)	3(1)	-11(1)	-14(1)
O(1)	43(2)	35(2)	59(2)	-6(1)	-13(1)	-10(1)
O(2)	42(2)	56(2)	63(2)	-8(2)	-2(2)	-15(2)
O(3)	69(2)	52(2)	49(2)	-15(2)	-7(2)	-24(2)
O(4)	46(2)	34(2)	62(2)	7(1)	-18(1)	-20(1)
O(5)	61(2)	50(2)	49(2)	13(2)	-19(2)	-15(2)
O(6)	55(2)	58(2)	69(2)	14(2)	-17(2)	-34(2)
C(1)	45(2)	32(2)	35(2)	-3(2)	-8(2)	-13(2)
C(2)	47(2)	43(2)	52(3)	-7(2)	-8(2)	-19(2)
C(3)	53(3)	54(3)	66(3)	-8(2)	-14(2)	-25(2)
C(4)	68(3)	36(2)	71(3)	-8(2)	-18(3)	-22(2)
C(5)	55(3)	35(2)	65(3)	-7(2)	-12(2)	-10(2)
C(6)	44(2)	36(2)	42(2)	0(2)	-11(2)	-14(2)
C(7)	46(2)	39(2)	40(2)	-5(2)	-14(2)	-12(2)
C(8)	61(3)	42(2)	56(3)	4(2)	-18(2)	-18(2)
C(9)	76(4)	39(3)	82(4)	4(2)	-26(3)	-16(3)
C(10)	84(4)	38(3)	81(4)	-4(3)	-32(3)	3(3)
C(11)	50(3)	59(3)	61(3)	-19(3)	-16(2)	2(2)
C(12)	46(2)	43(2)	46(3)	-9(2)	-11(2)	-9(2)
C(13)	52(3)	88(4)	66(4)	-15(3)	0(3)	-32(3)
C(14)	40(2)	49(2)	33(2)	0(2)	-9(2)	-15(2)
C(15)	61(3)	52(3)	45(3)	5(2)	-15(2)	-23(2)
C(16)	70(3)	78(4)	54(3)	19(3)	-18(3)	-36(3)
C(17)	69(4)	102(5)	39(3)	8(3)	-12(2)	-38(3)

C(18)	63(3)	82(4)	44(3)	-11(3)	-12(2)	-24(3)
C(19)	41(2)	57(3)	39(2)	-5(2)	-9(2)	-16(2)
C(20)	96(5)	59(3)	82(5)	-29(3)	-10(4)	-24(3)
C(21)	55(3)	55(3)	74(4)	14(2)	-26(3)	-33(2)
C(22)	42(3)	66(4)	60(4)	1(3)	-12(3)	-26(3)
C(23)	33(2)	64(3)	69(3)	-8(2)	-17(2)	-14(2)
C(24)	50(2)	46(2)	57(3)	1(2)	-27(2)	-18(2)
C(25)	47(3)	52(3)	49(3)	-7(2)	-18(2)	-20(2)
C(26)	49(3)	41(2)	74(3)	-4(2)	-25(2)	-18(2)
C(27)	93(5)	64(4)	119(6)	42(4)	-47(4)	-50(4)
C(28)	80(4)	52(3)	67(4)	10(2)	-37(3)	-22(3)
C(29)	104(6)	89(5)	93(6)	42(4)	-22(5)	-37(5)
C(30)	91(5)	124(7)	124(8)	66(6)	-58(6)	-24(5)
C(31)	41(2)	33(2)	32(2)	3(1)	-10(2)	-14(2)
C(32)	43(2)	44(2)	52(3)	9(2)	-16(2)	-20(2)
C(33)	44(2)	52(3)	58(3)	5(2)	-21(2)	-14(2)
C(34)	54(3)	37(2)	57(3)	6(2)	-22(2)	-8(2)
C(35)	53(3)	31(2)	58(3)	5(2)	-16(2)	-15(2)
C(36)	45(2)	30(2)	39(2)	2(2)	-13(2)	-13(2)
C(37)	43(2)	44(2)	34(2)	3(2)	-11(2)	-21(2)
C(38)	50(3)	49(2)	46(3)	-2(2)	-11(2)	-15(2)
C(39)	56(3)	72(3)	50(3)	-12(2)	-4(2)	-18(3)
C(40)	67(3)	91(4)	39(3)	-5(3)	-7(2)	-35(3)
C(41)	67(3)	73(4)	42(3)	13(2)	-21(2)	-33(3)
C(42)	49(2)	55(3)	38(2)	4(2)	-17(2)	-25(2)
C(43)	86(4)	57(3)	80(5)	23(3)	-25(4)	-15(3)
C(44)	55(3)	36(2)	40(2)	5(2)	-21(2)	-21(2)
C(45)	62(3)	40(2)	55(3)	-1(2)	-17(2)	-18(2)
C(46)	88(4)	39(2)	69(4)	-8(2)	-22(3)	-19(3)
C(47)	105(5)	43(3)	75(4)	7(2)	-43(4)	-38(3)
C(48)	91(4)	60(3)	60(3)	19(3)	-38(3)	-50(3)
C(49)	59(3)	47(2)	46(3)	12(2)	-23(2)	-29(2)
C(50)	62(4)	91(5)	73(4)	24(3)	-20(3)	-43(4)
C(51)	31(2)	53(3)	69(3)	-12(2)	-15(2)	-5(2)
C(52)	43(2)	42(2)	68(3)	5(2)	-24(2)	-14(2)
C(53)	42(2)	50(3)	49(3)	4(2)	-21(2)	-19(2)

C(54)	45(2)	46(2)	55(3)	-2(2)	-22(2)	-16(2)
C(55)	52(3)	57(3)	61(3)	6(2)	-22(2)	-32(2)
C(56)	40(3)	70(4)	53(3)	-2(3)	-9(2)	-26(3)
C(57)	51(3)	65(4)	111(6)	-34(4)	-13(3)	0(3)
C(58)	72(3)	48(3)	71(4)	-12(2)	-28(3)	-15(2)
C(59)	92(5)	95(5)	131(8)	-54(5)	-25(5)	-38(4)
C(60)	85(6)	143(9)	202(13)	-127(9)	36(7)	-43(6)
C(61)	114(8)	116(8)	122(9)	-23(6)	34(6)	-46(6)
Cl(3)	109(2)	119(2)	99(2)	9(1)	-25(1)	-6(1)
Cl(4)	123(2)	84(1)	135(2)	2(1)	-32(2)	-30(1)
C(62)	103(6)	104(6)	98(7)	12(5)	3(5)	-39(5)
Cl(5)	124(2)	79(1)	101(1)	3(1)	-35(1)	-38(1)
Cl(6)	103(2)	99(1)	113(2)	-10(1)	-30(1)	-25(1)

Table 5. Hydrogen coordinates ($\times 10^4$) and isotropic displacement parameters ($Å^2 \times 10^3$) for Ru(tmp) or [Ru(*p*-cymene)(tmp)]·CH_2Cl_2 complex.

	x	y	z	U(eq)
H(2)	1878	8300	2477	57
H(3)	2296	6308	1859	66
H(4)	4712	4693	1435	69
H(5)	6732	5023	1615	65
H(8)	3869	11748	1949	64
H(9)	2054	13900	1778	80
H(10)	-461	14393	2421	90
H(11)	-1117	12772	3206	75
H(13A)	-1534	11042	4026	103
H(13B)	-428	11021	4566	103
H(13C)	-592	9681	4447	103
H(15)	3388	7216	3965	63
H(16)	2472	6952	5401	80
H(17)	1904	8638	6344	83
H(18)	2184	10618	5855	77

H(20A)	2602	13167	4446	122
H(20B)	3081	12236	5228	122
H(20C)	1495	12604	5047	122
H(22)	9171	9246	1486	66
H(23)	9540	7338	2352	67
H(25)	5904	9506	4213	57
H(26)	5463	11474	3319	63
H(27A)	7659	12308	1823	127
H(27B)	6010	12453	1915	127
H(27C)	7308	11557	1187	127
H(28)	8273	6235	3608	78
H(29A)	6027	7331	4614	150
H(29B)	6878	7800	5117	150
H(29C)	7233	6253	5076	150
H(30A)	10430	6592	3699	178
H(30B)	10020	5624	4411	178
H(30C)	9587	7139	4625	178
H(32)	367	1753	7469	55
H(33)	-1039	3744	6815	62
H(34)	-70	5355	6361	62
H(35)	2233	5038	6527	57
H(38)	871	2834	8946	60
H(39)	-306	3078	10370	75
H(40)	619	1360	11331	79
H(41)	2679	-602	10856	71
H(43A)	5450	-3129	9458	120
H(43B)	3813	-2576	10030	120
H(43C)	5047	-2228	10252	120
H(45)	5525	-1616	6947	63
H(46)	5766	-3835	6838	80
H(47)	3767	-4401	7485	82
H(48)	1560	-2792	8224	73
H(50A)	-818	275	9401	109
H(50B)	559	-1067	9530	109
H(50C)	-501	-1072	8966	109
H(52)	6684	-1310	8409	61

H(53)	5366	702	9239	54
H(55)	7208	2712	7311	62
H(56)	8513	763	6519	64
H(57A)	8559	-1563	6312	123
H(57B)	8263	-2452	7111	123
H(57C)	9730	-2187	6892	123
H(58)	5158	3945	8487	76
H(59A)	7500	3322	8848	152
H(59B)	6883	2765	9728	152
H(59C)	6164	4322	9515	152
H(60A)	3761	4121	9891	221
H(60B)	4438	2531	9968	221
H(60C)	3390	3270	9330	221
H(61A)	8597	5826	675	153
H(61B)	8187	7344	385	153
H(62A)	4954	4759	5638	131
H(62B)	5363	3201	5602	131

Table 6. Torsion angles [º] for Ru(tmp) or [Ru(*p*-cymene)(tmp)].CH_2Cl_2 complex.

C(14)-P(1)-C(1)-C(2)	71.0(4)
C(7)-P(1)-C(1)-C(2)	-40.2(5)
Ru(1)-P(1)-C(1)-C(2)	-168.6(4)
C(14)-P(1)-C(1)-C(6)	-103.6(3)
C(7)-P(1)-C(1)-C(6)	145.2(3)
Ru(1)-P(1)-C(1)-C(6)	16.9(3)
C(6)-C(1)-C(2)-C(3)	-1.6(7)
P(1)-C(1)-C(2)-C(3)	-175.8(4)
C(1)-C(2)-C(3)-C(4)	1.6(8)
C(2)-C(3)-C(4)-C(5)	0.0(9)
C(3)-C(4)-C(5)-C(6)	-1.5(9)
Ru(1)-O(1)-C(6)-C(1)	-14.9(6)
Ru(1)-O(1)-C(6)-C(5)	166.0(4)
C(2)-C(1)-C(6)-O(1)	-178.9(4)

P(1)-C(1)-C(6)-O(1)	-4.0(6)
C(2)-C(1)-C(6)-C(5)	0.2(7)
P(1)-C(1)-C(6)-C(5)	175.1(4)
C(4)-C(5)-C(6)-O(1)	-179.5(5)
C(4)-C(5)-C(6)-C(1)	1.4(8)
C(1)-P(1)-C(7)-C(8)	-115.5(4)
C(14)-P(1)-C(7)-C(8)	131.9(4)
Ru(1)-P(1)-C(7)-C(8)	1.2(4)
C(1)-P(1)-C(7)-C(12)	73.8(4)
C(14)-P(1)-C(7)-C(12)	-38.9(4)
Ru(1)-P(1)-C(7)-C(12)	-169.6(3)
C(12)-C(7)-C(8)-C(9)	0.1(8)
P(1)-C(7)-C(8)-C(9)	-171.0(4)
C(7)-C(8)-C(9)-C(10)	1.0(9)
C(8)-C(9)-C(10)-C(11)	-0.2(10)
C(9)-C(10)-C(11)-C(12)	-1.8(10)
C(13)-O(2)-C(12)-C(11)	-37.7(7)
C(13)-O(2)-C(12)-C(7)	143.9(5)
C(10)-C(11)-C(12)-O(2)	-175.3(5)
C(10)-C(11)-C(12)-C(7)	3.0(8)
C(8)-C(7)-C(12)-O(2)	176.3(4)
P(1)-C(7)-C(12)-O(2)	-12.9(6)
C(8)-C(7)-C(12)-C(11)	-2.2(7)
P(1)-C(7)-C(12)-C(11)	168.7(4)
C(1)-P(1)-C(14)-C(19)	-172.5(4)
C(7)-P(1)-C(14)-C(19)	-54.8(4)
Ru(1)-P(1)-C(14)-C(19)	78.5(4)
C(1)-P(1)-C(14)-C(15)	6.3(4)
C(7)-P(1)-C(14)-C(15)	124.0(4)
Ru(1)-P(1)-C(14)-C(15)	-102.7(4)
C(19)-C(14)-C(15)-C(16)	0.5(8)
P(1)-C(14)-C(15)-C(16)	-178.3(4)
C(14)-C(15)-C(16)-C(17)	-1.0(9)
C(15)-C(16)-C(17)-C(18)	0.8(10)
C(16)-C(17)-C(18)-C(19)	-0.2(10)
C(20)-O(3)-C(19)-C(18)	-12.3(8)

C(20)-O(3)-C(19)-C(14)	168.2(5)
C(17)-C(18)-C(19)-O(3)	-179.9(5)
C(17)-C(18)-C(19)-C(14)	-0.4(8)
C(15)-C(14)-C(19)-O(3)	179.7(4)
P(1)-C(14)-C(19)-O(3)	-1.5(6)
C(15)-C(14)-C(19)-C(18)	0.2(7)
P(1)-C(14)-C(19)-C(18)	179.0(4)
C(26)-C(21)-C(22)-C(23)	2.7(8)
C(27)-C(21)-C(22)-C(23)	-176.7(6)
Ru(1)-C(21)-C(22)-C(23)	-52.7(5)
C(26)-C(21)-C(22)-Ru(1)	55.4(4)
C(27)-C(21)-C(22)-Ru(1)	-124.0(5)
C(21)-C(22)-C(23)-C(24)	-1.2(9)
Ru(1)-C(22)-C(23)-C(24)	-53.3(5)
C(21)-C(22)-C(23)-Ru(1)	52.1(5)
C(22)-C(23)-C(24)-C(25)	-1.5(8)
Ru(1)-C(23)-C(24)-C(25)	-55.7(4)
C(22)-C(23)-C(24)-C(28)	-179.9(5)
Ru(1)-C(23)-C(24)-C(28)	126.0(4)
C(22)-C(23)-C(24)-Ru(1)	54.1(5)
C(23)-C(24)-C(25)-C(26)	2.8(7)
C(28)-C(24)-C(25)-C(26)	-178.9(5)
Ru(1)-C(24)-C(25)-C(26)	-52.9(4)
C(23)-C(24)-C(25)-Ru(1)	55.7(4)
C(28)-C(24)-C(25)-Ru(1)	-125.9(5)
C(22)-C(21)-C(26)-C(25)	-1.4(8)
C(27)-C(21)-C(26)-C(25)	177.9(5)
Ru(1)-C(21)-C(26)-C(25)	54.7(4)
C(22)-C(21)-C(26)-Ru(1)	-56.1(5)
C(27)-C(21)-C(26)-Ru(1)	123.3(5)
C(24)-C(25)-C(26)-C(21)	-1.4(7)
Ru(1)-C(25)-C(26)-C(21)	-54.8(4)
C(24)-C(25)-C(26)-Ru(1)	53.5(4)
C(25)-C(24)-C(28)-C(30)	-114.1(7)
C(23)-C(24)-C(28)-C(30)	64.2(8)
Ru(1)-C(24)-C(28)-C(30)	154.0(6)

C(25)-C(24)-C(28)-C(29)	8.3(8)
C(23)-C(24)-C(28)-C(29)	-173.4(6)
Ru(1)-C(24)-C(28)-C(29)	-83.6(7)
C(37)-P(2)-C(31)-C(32)	-70.4(4)
C(44)-P(2)-C(31)-C(32)	40.6(5)
Ru(2)-P(2)-C(31)-C(32)	168.8(4)
C(37)-P(2)-C(31)-C(36)	104.9(3)
C(44)-P(2)-C(31)-C(36)	-144.1(3)
Ru(2)-P(2)-C(31)-C(36)	-15.9(3)
C(36)-C(31)-C(32)-C(33)	2.2(7)
P(2)-C(31)-C(32)-C(33)	177.1(4)
C(31)-C(32)-C(33)-C(34)	-1.1(8)
C(32)-C(33)-C(34)-C(35)	0.0(8)
C(33)-C(34)-C(35)-C(36)	0.0(8)
Ru(2)-O(4)-C(36)-C(31)	15.9(6)
Ru(2)-O(4)-C(36)-C(35)	-163.8(3)
C(32)-C(31)-C(36)-O(4)	178.2(4)
P(2)-C(31)-C(36)-O(4)	2.7(5)
C(32)-C(31)-C(36)-C(35)	-2.1(6)
P(2)-C(31)-C(36)-C(35)	-177.6(3)
C(34)-C(35)-C(36)-O(4)	-179.3(4)
C(34)-C(35)-C(36)-C(31)	0.9(7)
C(31)-P(2)-C(37)-C(38)	-7.6(4)
C(44)-P(2)-C(37)-C(38)	-125.8(4)
Ru(2)-P(2)-C(37)-C(38)	101.7(4)
C(31)-P(2)-C(37)-C(42)	172.3(4)
C(44)-P(2)-C(37)-C(42)	54.1(4)
Ru(2)-P(2)-C(37)-C(42)	-78.5(4)
C(42)-C(37)-C(38)-C(39)	-1.3(7)
P(2)-C(37)-C(38)-C(39)	178.6(4)
C(37)-C(38)-C(39)-C(40)	0.7(9)
C(38)-C(39)-C(40)-C(41)	-0.5(9)
C(39)-C(40)-C(41)-C(42)	0.8(9)
C(43)-O(5)-C(42)-C(41)	12.4(8)
C(43)-O(5)-C(42)-C(37)	-166.2(5)
C(40)-C(41)-C(42)-O(5)	-179.9(5)

C(40)-C(41)-C(42)-C(37)	-1.4(8)
C(38)-C(37)-C(42)-O(5)	-179.8(4)
P(2)-C(37)-C(42)-O(5)	0.4(6)
C(38)-C(37)-C(42)-C(41)	1.6(7)
P(2)-C(37)-C(42)-C(41)	-178.3(4)
C(31)-P(2)-C(44)-C(45)	115.6(4)
C(37)-P(2)-C(44)-C(45)	-132.1(4)
Ru(2)-P(2)-C(44)-C(45)	-1.5(4)
C(31)-P(2)-C(44)-C(49)	-74.4(4)
C(37)-P(2)-C(44)-C(49)	37.9(4)
Ru(2)-P(2)-C(44)-C(49)	168.5(3)
C(49)-C(44)-C(45)-C(46)	-1.9(7)
P(2)-C(44)-C(45)-C(46)	168.5(4)
C(44)-C(45)-C(46)-C(47)	0.1(9)
C(45)-C(46)-C(47)-C(48)	0.4(9)
C(46)-C(47)-C(48)-C(49)	0.8(9)
C(50)-O(6)-C(49)-C(48)	35.3(7)
C(50)-O(6)-C(49)-C(44)	-145.7(5)
C(47)-C(48)-C(49)-O(6)	176.3(5)
C(47)-C(48)-C(49)-C(44)	-2.7(8)
C(45)-C(44)-C(49)-O(6)	-175.8(4)
P(2)-C(44)-C(49)-O(6)	14.2(6)
C(45)-C(44)-C(49)-C(48)	3.1(7)
P(2)-C(44)-C(49)-C(48)	-166.8(4)
C(56)-C(51)-C(52)-C(53)	1.3(7)
C(57)-C(51)-C(52)-C(53)	-178.1(5)
Ru(2)-C(51)-C(52)-C(53)	-54.3(4)
C(56)-C(51)-C(52)-Ru(2)	55.7(4)
C(57)-C(51)-C(52)-Ru(2)	-123.7(5)
C(51)-C(52)-C(53)-C(54)	0.6(7)
Ru(2)-C(52)-C(53)-C(54)	-54.1(4)
C(51)-C(52)-C(53)-Ru(2)	54.7(4)
C(52)-C(53)-C(54)-C(55)	-2.0(7)
Ru(2)-C(53)-C(54)-C(55)	-55.3(4)
C(52)-C(53)-C(54)-C(58)	-179.6(5)
Ru(2)-C(53)-C(54)-C(58)	127.1(5)

C(52)-C(53)-C(54)-Ru(2)	53.3(4)
C(53)-C(54)-C(55)-C(56)	1.4(7)
C(58)-C(54)-C(55)-C(56)	179.1(5)
Ru(2)-C(54)-C(55)-C(56)	-53.6(5)
C(53)-C(54)-C(55)-Ru(2)	55.1(4)
C(58)-C(54)-C(55)-Ru(2)	-127.3(4)
C(54)-C(55)-C(56)-C(51)	0.5(8)
Ru(2)-C(55)-C(56)-C(51)	-52.4(5)
C(54)-C(55)-C(56)-Ru(2)	53.0(4)
C(52)-C(51)-C(56)-C(55)	-1.9(8)
C(57)-C(51)-C(56)-C(55)	177.5(5)
Ru(2)-C(51)-C(56)-C(55)	53.1(5)
C(52)-C(51)-C(56)-Ru(2)	-55.1(4)
C(57)-C(51)-C(56)-Ru(2)	124.4(5)
C(53)-C(54)-C(58)-C(60)	-21.4(10)
C(55)-C(54)-C(58)-C(60)	161.0(8)
Ru(2)-C(54)-C(58)-C(60)	71.2(9)
C(53)-C(54)-C(58)-C(59)	101.7(7)
C(55)-C(54)-C(58)-C(59)	-75.9(7)
Ru(2)-C(54)-C(58)-C(59)	-165.7(6)

Symmetry transformations were used to generate equivalent atoms.

Table 7. Hydrogen bonds for Ru(tmp) or [Ru(*p*-cymene)(tmp)]·CH_2Cl_2 [Å and °].

D-H···A	d(D-H)	d(H···A)	d(D···A)	<(DHA)
C(2)-H(2)···O(2)	0.93	2.41	3.159(6)	137.5
C(8)-H(8)···Cl(1)	0.93	2.74	3.425(6)	131.3
C(32)-H(32)···O(6)	0.93	2.42	3.180(6)	138.4
C(45)-H(45)···Cl(2)	0.93	2.71	3.418(6)	133.3
C(61)-H(61B)···Cl(1)	0.97	2.55	3.503(11)	166.2
C(62)-H(62B)···O(4)	0.97	2.62	3.295(10)	126.9
C(62)-H(62B)···Cl(2)	0.97	2.75	3.657(10)	156.6

Symmetry transformations were used to generate equivalent atoms: #1 x-1,y+1,z.

Table 8. Crystal data and structure refinement for $[Ir(ppy)_2(tmp)]\cdot CH_2Cl_2$ complex.

Identification code	$[Ir(ppy)_2(tmp)]\cdot CH_2Cl_2$	
Empirical formula	$C_{42}\ H_{34}\ Ir\ N_2\ O_3\ P,\ C\ H_2\ Cl_2$	
Formula weight	922.83	
Temperature	296(2) K	
Wavelength	1.54178 Å	
Crystal system	Monoclinic	
Space group	$P2_1/c$	
Unit cell dimensions	a = 12.6715(4) Å	α = 90°
	b = 12.5690(4) Å	β = 94.8360(10)°
	c = 24.3914(8) Å	γ = 90°.
Volume	3870.9(2) $Å^3$	
Z	4	
Density (calculated)	1.583 Mg/m^3	
Absorption coefficient	8.670 mm^{-1}	
F(000)	1832	
Crystal size	0.393 × 0.110 × 0.066 mm^3	
Theta range for data collection	5.062 to 70.063°	
Index ranges	-14<=h<=15, -15<=k<=15, -29<=l<=29	
Reflections collected	79532	
Independent reflections	7312 [*R*(int) = 0.0456]	
Completeness to theta = 67.679°	99.1 %	
Absorption correction	Semi-empirical from equivalents	
Max. and min. transmission	0.7536 and 0.3235	
Refinement method	Full-matrix least-squares on F^2	
Data / restraints / parameters	7312/0/471	
Goodness-of-fit on F^2	1.053	
Final *R* indices [$I > 2\sigma(I)$]	$R1$ = 0.0292, $wR2$ = 0.0778	
R indices (all data)	$R1$ = 0.0296, $wR2$ = 0.0783	
Extinction coefficient	n/a	
Largest diff. peak and hole	1.377 and -1.003 e.$Å^{-3}$	

Table 9. Atomic coordinates ($\times 10^4$) and equivalent isotropic displacement parameters ($Å^2 \times 10^3$) for Ir(tmp). U(eq) was defined as one third of the trace of the orthogonalized U^{ij} tensor.

	x	y	z	U(eq)
Ir(1)	2778(1)	5634(1)	7455(1)	33(1)
P(1)	1769(1)	5944(1)	6604(1)	34(1)
Cl(1)	5739(5)	7555(3)	5668(1)	251(2)
N(1)	1728(2)	6264(2)	7971(1)	38(1)
N(2)	3959(2)	4961(2)	7058(1)	37(1)
O(1)	3220(2)	7250(2)	7289(1)	47(1)
O(2)	2211(2)	3844(2)	6158(1)	52(1)
O(3)	373(2)	6188(3)	5537(1)	60(1)
C(1)	717(3)	6549(3)	7833(1)	43(1)
C(2)	45(3)	6931(3)	8200(2)	54(1)
C(3)	424(4)	7037(4)	8740(2)	70(1)
C(4)	1461(4)	6782(4)	8890(2)	68(1)
C(5)	2122(3)	6408(3)	8506(1)	46(1)
C(6)	3238(3)	6131(3)	8619(1)	50(1)
C(7)	3813(4)	6284(4)	9132(2)	68(1)
C(8)	4859(4)	5995(5)	9210(2)	80(1)
C(9)	5329(4)	5516(4)	8784(2)	71(1)
C(10)	4783(3)	5370(3)	8273(2)	54(1)
C(11)	3719(3)	5689(2)	8175(2)	42(1)
C(12)	4652(3)	5527(3)	6785(2)	44(1)
C(13)	5478(3)	5045(4)	6553(2)	57(1)
C(14)	5607(3)	3959(4)	6604(2)	64(1)
C(15)	4907(3)	3385(3)	6890(2)	55(1)
C(16)	4073(2)	3888(3)	7113(1)	40(1)
C(17)	3262(2)	3390(3)	7420(1)	39(1)
C(18)	3224(3)	2296(3)	7516(2)	52(1)
C(19)	2430(3)	1873(3)	7802(2)	58(1)
C(20)	1685(3)	2543(3)	7996(2)	55(1)
C(21)	1719(3)	3630(3)	7906(1)	45(1)

C(22)	2507(3)	4091(3)	7614(1)	37(1)
C(23)	1703(3)	7380(3)	6635(1)	42(1)
C(24)	954(3)	8045(3)	6355(2)	56(1)
C(25)	1008(4)	9137(4)	6413(2)	71(1)
C(26)	1833(4)	9580(3)	6746(2)	69(1)
C(27)	2572(3)	8951(3)	7031(2)	55(1)
C(28)	2526(3)	7832(3)	6994(1)	42(1)
C(29)	2481(3)	5652(3)	5994(1)	43(1)
C(30)	2899(3)	6463(4)	5694(2)	60(1)
C(31)	3469(4)	6202(5)	5239(2)	75(1)
C(32)	3623(3)	5180(5)	5105(2)	72(1)
C(33)	3224(3)	4350(4)	5402(2)	61(1)
C(34)	2648(3)	4597(3)	5849(1)	46(1)
C(35)	2456(4)	2760(3)	6061(2)	64(1)
C(36)	428(3)	5442(3)	6420(1)	38(1)
C(37)	-48(3)	4826(3)	6807(1)	43(1)
C(38)	-1075(3)	4454(3)	6699(2)	57(1)
C(39)	-1617(3)	4673(4)	6204(2)	64(1)
C(40)	-1168(3)	5252(4)	5809(2)	58(1)
C(41)	-139(3)	5632(3)	5912(2)	45(1)
C(42)	-222(4)	6571(5)	5060(2)	81(2)
Cl(2)	7509(4)	8692(4)	5395(2)	266(2)
C(43)	6616(9)	8418(8)	5870(4)	158(4)

Table 10. Bond lengths [Å] and angles [º] for Ir(tmp) or [Ir(ppy)$_2$(tmp)]·CH_2Cl_2.

Ir(1)-C(22)	2.014(3)
Ir(1)-N(2)	2.034(3)
Ir(1)-C(11)	2.039(3)
Ir(1)-N(1)	2.065(3)
Ir(1)-O(1)	2.154(2)
Ir(1)-P(1)	2.3766(8)
P(1)-C(23)	1.809(3)
P(1)-C(36)	1.833(3)
P(1)-C(29)	1.840(4)
Cl(1)-C(43)	1.600(10)
N(1)-C(1)	1.345(4)
N(1)-C(5)	1.368(4)
N(2)-C(12)	1.349(4)
N(2)-C(16)	1.362(5)
O(1)-C(28)	1.311(4)
O(2)-C(34)	1.358(5)
O(2)-C(35)	1.421(5)
O(3)-C(41)	1.359(5)
O(3)-C(42)	1.419(5)
C(1)-C(2)	1.374(5)
C(1)-H(1)	0.9300
C(2)-C(3)	1.369(6)
C(2)-H(2)	0.9300
C(3)-C(4)	1.372(7)
C(3)-H(3)	0.9300
C(4)-C(5)	1.390(6)
C(4)-H(4)	0.9300
C(5)-C(6)	1.461(5)
C(6)-C(11)	1.402(5)
C(6)-C(7)	1.406(5)
C(7)-C(8)	1.372(7)
C(7)-H(7)	0.9300
C(8)-C(9)	1.378(8)
C(8)-H(8)	0.9300

C(9)-C(10)	1.387(6)
C(9)-H(9)	0.9300
C(10)-C(11)	1.408(5)
C(10)-H(10)	0.9300
C(12)-C(13)	1.372(5)
C(12)-H(12)	0.9300
C(13)-C(14)	1.380(7)
C(13)-H(13)	0.9300
C(14)-C(15)	1.378(6)
C(14)-H(14)	0.9300
C(15)-C(16)	1.383(5)
C(15)-H(15)	0.9300
C(16)-C(17)	1.462(5)
C(17)-C(18)	1.397(5)
C(17)-C(22)	1.412(5)
C(18)-C(19)	1.377(6)
C(18)-H(18)	0.9300
C(19)-C(20)	1.379(6)
C(19)-H(19)	0.9300
C(20)-C(21)	1.384(5)
C(20)-H(20)	0.9300
C(21)-C(22)	1.400(5)
C(21)-H(21)	0.9300
C(23)-C(24)	1.399(5)
C(23)-C(28)	1.424(5)
C(24)-C(25)	1.381(6)
C(24)-H(24)	0.9300
C(25)-C(26)	1.386(7)
C(25)-H(25)	0.9300
C(26)-C(27)	1.369(6)
C(26)-H(26)	0.9300
C(27)-C(28)	1.410(5)
C(27)-H(27)	0.9300
C(29)-C(30)	1.386(5)
C(29)-C(34)	1.393(5)
C(30)-C(31)	1.412(6)

C(30)-H(30)	0.9300
C(31)-C(32)	1.345(8)
C(31)-H(31)	0.9300
C(32)-C(33)	1.389(7)
C(32)-H(32)	0.9300
C(33)-C(34)	1.397(5)
C(33)-H(33)	0.9300
C(35)-H(35A)	0.9600
C(35)-H(35B)	0.9600
C(35)-H(35C)	0.9600
C(36)-C(37)	1.398(5)
C(36)-C(41)	1.399(5)
C(37)-C(38)	1.387(5)
C(37)-H(37)	0.9300
C(38)-C(39)	1.365(7)
C(38)-H(38)	0.9300
C(39)-C(40)	1.370(7)
C(39)-H(39)	0.9300
C(40)-C(41)	1.391(5)
C(40)-H(40)	0.9300
C(42)-H(42A)	0.9600
C(42)-H(42B)	0.9600
C(42)-H(42C)	0.9600
Cl(2)-C(43)	1.720(13)
C(43)-H(43A)	0.9700
C(43)-H(43B)	0.9700
C(22)-Ir(1)-N(2)	80.52(12)
C(22)-Ir(1)-C(11)	87.92(12)
N(2)-Ir(1)-C(11)	91.35(13)
C(22)-Ir(1)-N(1)	97.06(12)
N(2)-Ir(1)-N(1)	170.91(10)
C(11)-Ir(1)-N(1)	79.77(13)
C(22)-Ir(1)-O(1)	174.76(11)
N(2)-Ir(1)-O(1)	95.12(10)
C(11)-Ir(1)-O(1)	89.31(11)
N(1)-Ir(1)-O(1)	86.81(10)

C(22)-Ir(1)-P(1)	103.74(9)
N(2)-Ir(1)-P(1)	90.87(7)
C(11)-Ir(1)-P(1)	168.33(9)
N(1)-Ir(1)-P(1)	98.22(8)
O(1)-Ir(1)-P(1)	79.09(7)
C(23)-P(1)-C(36)	107.95(15)
C(23)-P(1)-C(29)	105.07(16)
C(36)-P(1)-C(29)	103.91(15)
C(23)-P(1)-Ir(1)	98.67(11)
C(36)-P(1)-Ir(1)	125.27(11)
C(29)-P(1)-Ir(1)	114.17(11)
C(1)-N(1)-C(5)	117.9(3)
C(1)-N(1)-Ir(1)	126.7(2)
C(5)-N(1)-Ir(1)	115.4(2)
C(12)-N(2)-C(16)	120.2(3)
C(12)-N(2)-Ir(1)	123.5(2)
C(16)-N(2)-Ir(1)	116.2(2)
C(28)-O(1)-Ir(1)	117.1(2)
C(34)-O(2)-C(35)	118.1(3)
C(41)-O(3)-C(42)	118.4(3)
N(1)-C(1)-C(2)	123.9(3)
N(1)-C(1)-H(1)	118.0
C(2)-C(1)-H(1)	118.0
C(3)-C(2)-C(1)	118.4(4)
C(3)-C(2)-H(2)	120.8
C(1)-C(2)-H(2)	120.8
C(2)-C(3)-C(4)	119.0(4)
C(2)-C(3)-H(3)	120.5
C(4)-C(3)-H(3)	120.5
C(3)-C(4)-C(5)	121.1(4)
C(3)-C(4)-H(4)	119.4
C(5)-C(4)-H(4)	119.4
N(1)-C(5)-C(4)	119.7(3)
N(1)-C(5)-C(6)	114.8(3)
C(4)-C(5)-C(6)	125.6(3)
C(11)-C(6)-C(7)	121.0(4)

C(11)-C(6)-C(5)	115.2(3)
C(7)-C(6)-C(5)	123.8(4)
C(8)-C(7)-C(6)	120.6(4)
C(8)-C(7)-H(7)	119.7
C(6)-C(7)-H(7)	119.7
C(7)-C(8)-C(9)	119.1(4)
C(7)-C(8)-H(8)	120.5
C(9)-C(8)-H(8)	120.5
C(8)-C(9)-C(10)	121.4(5)
C(8)-C(9)-H(9)	119.3
C(10)-C(9)-H(9)	119.3
C(9)-C(10)-C(11)	120.8(4)
C(9)-C(10)-H(10)	119.6
C(11)-C(10)-H(10)	119.6
C(6)-C(11)-C(10)	117.1(3)
C(6)-C(11)-Ir(1)	114.7(3)
C(10)-C(11)-Ir(1)	128.2(3)
N(2)-C(12)-C(13)	121.5(3)
N(2)-C(12)-H(12)	119.2
C(13)-C(12)-H(12)	119.2
C(12)-C(13)-C(14)	119.2(4)
C(12)-C(13)-H(13)	120.4
C(14)-C(13)-H(13)	120.4
C(15)-C(14)-C(13)	119.2(4)
C(15)-C(14)-H(14)	120.4
C(13)-C(14)-H(14)	120.4
C(14)-C(15)-C(16)	120.4(4)
C(14)-C(15)-H(15)	119.8
C(16)-C(15)-H(15)	119.8
N(2)-C(16)-C(15)	119.5(3)
N(2)-C(16)-C(17)	113.6(3)
C(15)-C(16)-C(17)	126.8(3)
C(18)-C(17)-C(22)	121.6(3)
C(18)-C(17)-C(16)	122.9(3)
C(22)-C(17)-C(16)	115.5(3)
C(19)-C(18)-C(17)	120.1(4)

C(19)-C(18)-H(18)	119.9
C(17)-C(18)-H(18)	119.9
C(18)-C(19)-C(20)	119.3(3)
C(18)-C(19)-H(19)	120.4
C(20)-C(19)-H(19)	120.4
C(19)-C(20)-C(21)	121.1(4)
C(19)-C(20)-H(20)	119.5
C(21)-C(20)-H(20)	119.5
C(20)-C(21)-C(22)	121.5(4)
C(20)-C(21)-H(21)	119.2
C(22)-C(21)-H(21)	119.2
C(21)-C(22)-C(17)	116.4(3)
C(21)-C(22)-Ir(1)	129.6(3)
C(17)-C(22)-Ir(1)	113.9(2)
C(24)-C(23)-C(28)	119.6(3)
C(24)-C(23)-P(1)	127.5(3)
C(28)-C(23)-P(1)	112.9(2)
C(25)-C(24)-C(23)	121.3(4)
C(25)-C(24)-H(24)	119.4
C(23)-C(24)-H(24)	119.4
C(24)-C(25)-C(26)	119.2(4)
C(24)-C(25)-H(25)	120.4
C(26)-C(25)-H(25)	120.4
C(27)-C(26)-C(25)	121.1(4)
C(27)-C(26)-H(26)	119.5
C(25)-C(26)-H(26)	119.5
C(26)-C(27)-C(28)	121.3(4)
C(26)-C(27)-H(27)	119.3
C(28)-C(27)-H(27)	119.3
O(1)-C(28)-C(27)	119.9(3)
O(1)-C(28)-C(23)	122.5(3)
C(27)-C(28)-C(23)	117.5(3)
C(30)-C(29)-C(34)	119.4(3)
C(30)-C(29)-P(1)	121.1(3)
C(34)-C(29)-P(1)	119.4(3)
C(29)-C(30)-C(31)	119.3(4)

C(29)-C(30)-H(30)	120.4
C(31)-C(30)-H(30)	120.4
C(32)-C(31)-C(30)	120.5(4)
C(32)-C(31)-H(31)	119.7
C(30)-C(31)-H(31)	119.7
C(31)-C(32)-C(33)	121.6(4)
C(31)-C(32)-H(32)	119.2
C(33)-C(32)-H(32)	119.2
C(32)-C(33)-C(34)	118.5(4)
C(32)-C(33)-H(33)	120.8
C(34)-C(33)-H(33)	120.8
O(2)-C(34)-C(29)	116.4(3)
O(2)-C(34)-C(33)	122.9(4)
C(29)-C(34)-C(33)	120.8(4)
O(2)-C(35)-H(35A)	109.5
O(2)-C(35)-H(35B)	109.5
H(35A)-C(35)-H(35B)	109.5
O(2)-C(35)-H(35C)	109.5
H(35A)-C(35)-H(35C)	109.5
H(35B)-C(35)-H(35C)	109.5
C(37)-C(36)-C(41)	118.3(3)
C(37)-C(36)-P(1)	118.0(3)
C(41)-C(36)-P(1)	123.7(3)
C(38)-C(37)-C(36)	120.6(3)
C(38)-C(37)-H(37)	119.7
C(36)-C(37)-H(37)	119.7
C(39)-C(38)-C(37)	119.6(4)
C(39)-C(38)-H(38)	120.2
C(37)-C(38)-H(38)	120.2
C(38)-C(39)-C(40)	121.4(4)
C(38)-C(39)-H(39)	119.3
C(40)-C(39)-H(39)	119.3
C(39)-C(40)-C(41)	119.6(4)
C(39)-C(40)-H(40)	120.2
C(41)-C(40)-H(40)	120.2
O(3)-C(41)-C(40)	123.3(3)

O(3)-C(41)-C(36)	116.4(3)
C(40)-C(41)-C(36)	120.3(4)
O(3)-C(42)-H(42A)	109.5
O(3)-C(42)-H(42B)	109.5
H(42A)-C(42)-H(42B)	109.5
O(3)-C(42)-H(42C)	109.5
H(42A)-C(42)-H(42C)	109.5
H(42B)-C(42)-H(42C)	109.5
Cl(1)-C(43)-Cl(2)	114.1(6)
Cl(1)-C(43)-H(43A)	108.7
Cl(2)-C(43)-H(43A)	108.7
Cl(1)-C(43)-H(43B)	108.7
Cl(2)-C(43)-H(43B)	108.7
H(43A)-C(43)-H(43B)	107.6

Symmetry transformations were used to generate equivalent atoms.

Table 11. Anisotropic displacement parameters (Å^{2}x10^3) for Ir(tmp). The anisotropic displacement factor exponent takes the form: $-2\pi^2[h^2 a^{*2} U^{11} + \cdots + 2 h k a^* b^* U^{12}]$.

	U^{11}	U^{22}	U^{33}	U^{23}	U^{13}	U^{12}
Ir(1)	32(1)	32(1)	33(1)	1(1)	-2(1)	-2(1)
P(1)	32(1)	36(1)	34(1)	2(1)	-1(1)	1(1)
Cl(1)	422(7)	158(3)	162(3)	-15(2)	-34(3)	-70(4)
N(1)	45(1)	32(1)	37(1)	-3(1)	1(1)	-2(1)
N(2)	31(1)	42(1)	37(1)	2(1)	-4(1)	-1(1)
O(1)	44(1)	36(1)	59(1)	5(1)	-9(1)	-6(1)
O(2)	51(1)	51(1)	55(1)	-8(1)	9(1)	3(1)
O(3)	50(1)	89(2)	38(1)	14(1)	-5(1)	0(1)
C(1)	45(2)	40(2)	44(2)	-8(1)	2(1)	-1(1)
C(2)	53(2)	53(2)	57(2)	-11(2)	8(2)	3(2)
C(3)	72(3)	85(3)	52(2)	-21(2)	11(2)	14(2)
C(4)	84(3)	79(3)	40(2)	-18(2)	1(2)	12(2)
C(5)	57(2)	40(2)	41(2)	-6(1)	-1(1)	0(2)

C(6)	56(2)	48(2)	42(2)	-1(2)	-10(2)	-4(2)
C(7)	75(3)	79(3)	46(2)	-14(2)	-14(2)	1(2)
C(8)	75(3)	102(4)	57(3)	-11(3)	-28(2)	0(3)
C(9)	53(2)	88(3)	68(3)	7(2)	-23(2)	-3(2)
C(10)	44(2)	61(2)	54(2)	4(2)	-11(2)	-4(2)
C(11)	45(2)	39(2)	41(2)	5(1)	-8(1)	-7(1)
C(12)	35(2)	49(2)	47(2)	5(1)	2(1)	-6(1)
C(13)	41(2)	66(2)	65(2)	4(2)	11(2)	-6(2)
C(14)	40(2)	64(3)	90(3)	-5(2)	18(2)	6(2)
C(15)	40(2)	47(2)	79(3)	-3(2)	2(2)	6(2)
C(16)	34(2)	39(2)	46(2)	3(1)	-7(1)	2(1)
C(17)	37(2)	37(2)	43(2)	3(1)	-4(1)	-2(1)
C(18)	55(2)	39(2)	61(2)	3(2)	-2(2)	3(2)
C(19)	66(2)	38(2)	69(2)	11(2)	-5(2)	-9(2)
C(20)	55(2)	55(2)	54(2)	12(2)	-1(2)	-17(2)
C(21)	44(2)	49(2)	41(2)	7(1)	2(1)	-6(2)
C(22)	36(2)	39(2)	35(2)	2(1)	-7(1)	-4(1)
C(23)	43(2)	35(2)	46(2)	5(1)	1(1)	1(1)
C(24)	55(2)	49(2)	63(2)	7(2)	-8(2)	7(2)
C(25)	75(3)	45(2)	91(3)	12(2)	-9(3)	14(2)
C(26)	77(3)	35(2)	93(3)	5(2)	3(3)	5(2)
C(27)	57(2)	38(2)	70(2)	1(2)	3(2)	-3(2)
C(28)	43(2)	36(2)	49(2)	4(1)	6(1)	-3(1)
C(29)	32(2)	60(2)	35(2)	6(1)	1(1)	2(1)
C(30)	49(2)	74(3)	57(2)	19(2)	9(2)	0(2)
C(31)	58(2)	114(4)	55(2)	28(3)	14(2)	-4(3)
C(32)	48(2)	121(4)	49(2)	-4(3)	11(2)	12(3)
C(33)	42(2)	93(3)	47(2)	-12(2)	4(2)	8(2)
C(34)	34(2)	66(2)	36(2)	-6(2)	-3(1)	6(2)
C(35)	66(2)	55(2)	71(3)	-16(2)	0(2)	5(2)
C(36)	33(2)	40(2)	39(2)	-4(1)	0(1)	3(1)
C(37)	44(2)	39(2)	47(2)	-4(1)	5(1)	-1(1)
C(38)	51(2)	53(2)	70(3)	-6(2)	17(2)	-9(2)
C(39)	34(2)	73(3)	86(3)	-14(2)	3(2)	-5(2)
C(40)	37(2)	77(3)	58(2)	-10(2)	-10(2)	4(2)
C(41)	37(2)	55(2)	41(2)	-5(1)	-2(1)	4(1)

C(42)	82(3)	110(4)	48(2)	19(2)	-14(2)	15(3)
Cl(2)	224(4)	296(5)	288(5)	-105(4)	78(4)	42(4)
C(43)	169(9)	152(8)	143(7)	-47(6)	-54(7)	21(7)

Table 12. Hydrogen coordinates ($\times 10^4$) and isotropic displacement parameters ($Å^2 \times 10^3$) for Ir(tmp) complex.

	x	y	z	U(eq)
H(1)	458	6484	7466	52
H(2)	-650	7113	8086	65
H(3)	-14	7278	9001	83
H(4)	1726	6860	9255	82
H(7)	3481	6584	9421	81
H(8)	5245	6121	9545	96
H(9)	6028	5287	8841	85
H(10)	5124	5057	7991	65
H(12)	4568	6260	6752	52
H(13)	5945	5447	6363	68
H(14)	6161	3618	6447	77
H(15)	4996	2654	6932	66
H(18)	3735	1852	7387	63
H(19)	2397	1144	7863	70
H(20)	1151	2261	8191	66
H(21)	1207	4063	8043	54
H(24)	410	7747	6125	67
H(25)	497	9570	6230	85
H(26)	1884	10315	6778	82
H(27)	3116	9269	7253	66
H(30)	2806	7170	5791	71
H(31)	3740	6742	5031	90
H(32)	4006	5024	4806	86
H(33)	3339	3646	5306	73
H(35A)	2186	2323	6340	97
H(35B)	3210	2676	6070	97

H(35C)	2137	2550	5706	97
H(37)	327	4664	7141	52
H(38)	-1393	4058	6962	69
H(39)	-2307	4424	6134	77
H(40)	-1548	5391	5474	70
H(42A)	232	6969	4840	122
H(42B)	-781	7024	5166	122
H(42C)	-522	5982	4850	122
H(43A)	7001	8163	6205	190
H(43B)	6262	9073	5958	190

Table 13. Torsion angles [º] for Ir(tmp) or [Ir(ppy)$_2$(tmp)]·CH_2Cl_2.

C(5)-N(1)-C(1)-C(2)	-3.0(5)
Ir(1)-N(1)-C(1)-C(2)	177.6(3)
N(1)-C(1)-C(2)-C(3)	0.5(6)
C(1)-C(2)-C(3)-C(4)	1.4(7)
C(2)-C(3)-C(4)-C(5)	-0.8(8)
C(1)-N(1)-C(5)-C(4)	3.6(5)
Ir(1)-N(1)-C(5)-C(4)	-177.0(3)
C(1)-N(1)-C(5)-C(6)	-177.1(3)
Ir(1)-N(1)-C(5)-C(6)	2.3(4)
C(3)-C(4)-C(5)-N(1)	-1.8(7)
C(3)-C(4)-C(5)-C(6)	179.0(4)
N(1)-C(5)-C(6)-C(11)	-4.3(5)
C(4)-C(5)-C(6)-C(11)	175.0(4)
N(1)-C(5)-C(6)-C(7)	175.7(4)
C(4)-C(5)-C(6)-C(7)	-5.0(7)
C(11)-C(6)-C(7)-C(8)	-0.5(7)
C(5)-C(6)-C(7)-C(8)	179.4(5)
C(6)-C(7)-C(8)-C(9)	-2.4(9)
C(7)-C(8)-C(9)-C(10)	3.3(9)
C(8)-C(9)-C(10)-C(11)	-1.3(7)
C(7)-C(6)-C(11)-C(10)	2.5(6)
C(5)-C(6)-C(11)-C(10)	-177.5(3)

C(7)-C(6)-C(11)-Ir(1)	-175.8(3)
C(5)-C(6)-C(11)-Ir(1)	4.2(4)
C(9)-C(10)-C(11)-C(6)	-1.6(6)
C(9)-C(10)-C(11)-Ir(1)	176.4(3)
C(16)-N(2)-C(12)-C(13)	0.5(5)
Ir(1)-N(2)-C(12)-C(13)	175.7(3)
N(2)-C(12)-C(13)-C(14)	-0.5(6)
C(12)-C(13)-C(14)-C(15)	-0.4(6)
C(13)-C(14)-C(15)-C(16)	1.2(7)
C(12)-N(2)-C(16)-C(15)	0.4(5)
Ir(1)-N(2)-C(16)-C(15)	-175.2(3)
C(12)-N(2)-C(16)-C(17)	180.0(3)
Ir(1)-N(2)-C(16)-C(17)	4.4(3)
C(14)-C(15)-C(16)-N(2)	-1.2(6)
C(14)-C(15)-C(16)-C(17)	179.2(4)
N(2)-C(16)-C(17)-C(18)	179.0(3)
C(15)-C(16)-C(17)-C(18)	-1.4(6)
N(2)-C(16)-C(17)-C(22)	-0.8(4)
C(15)-C(16)-C(17)-C(22)	178.8(3)
C(22)-C(17)-C(18)-C(19)	0.7(5)
C(16)-C(17)-C(18)-C(19)	-179.1(3)
C(17)-C(18)-C(19)-C(20)	-0.8(6)
C(18)-C(19)-C(20)-C(21)	0.4(6)
C(19)-C(20)-C(21)-C(22)	0.1(6)
C(20)-C(21)-C(22)-C(17)	-0.3(5)
C(20)-C(21)-C(22)-Ir(1)	-176.9(3)
C(18)-C(17)-C(22)-C(21)	-0.1(5)
C(16)-C(17)-C(22)-C(21)	179.7(3)
C(18)-C(17)-C(22)-Ir(1)	177.0(3)
C(16)-C(17)-C(22)-Ir(1)	-3.2(4)
C(36)-P(1)-C(23)-C(24)	-26.1(4)
C(29)-P(1)-C(23)-C(24)	84.3(4)
Ir(1)-P(1)-C(23)-C(24)	-157.6(3)
C(36)-P(1)-C(23)-C(28)	153.6(2)
C(29)-P(1)-C(23)-C(28)	-96.0(3)
Ir(1)-P(1)-C(23)-C(28)	22.1(3)

C(28)-C(23)-C(24)-C(25)	1.1(6)
P(1)-C(23)-C(24)-C(25)	-179.2(4)
C(23)-C(24)-C(25)-C(26)	1.3(8)
C(24)-C(25)-C(26)-C(27)	-2.0(8)
C(25)-C(26)-C(27)-C(28)	0.2(8)
Ir(1)-O(1)-C(28)-C(27)	157.2(3)
Ir(1)-O(1)-C(28)-C(23)	-22.2(4)
C(26)-C(27)-C(28)-O(1)	-177.2(4)
C(26)-C(27)-C(28)-C(23)	2.2(6)
C(24)-C(23)-C(28)-O(1)	176.6(3)
P(1)-C(23)-C(28)-O(1)	-3.2(4)
C(24)-C(23)-C(28)-C(27)	-2.8(5)
P(1)-C(23)-C(28)-C(27)	177.5(3)
C(23)-P(1)-C(29)-C(30)	4.5(3)
C(36)-P(1)-C(29)-C(30)	117.8(3)
Ir(1)-P(1)-C(29)-C(30)	-102.5(3)
C(23)-P(1)-C(29)-C(34)	-178.8(3)
C(36)-P(1)-C(29)-C(34)	-65.5(3)
Ir(1)-P(1)-C(29)-C(34)	74.2(3)
C(34)-C(29)-C(30)-C(31)	1.2(6)
P(1)-C(29)-C(30)-C(31)	178.0(3)
C(29)-C(30)-C(31)-C(32)	-1.3(6)
C(30)-C(31)-C(32)-C(33)	0.5(7)
C(31)-C(32)-C(33)-C(34)	0.3(6)
C(35)-O(2)-C(34)-C(29)	-173.4(3)
C(35)-O(2)-C(34)-C(33)	7.4(5)
C(30)-C(29)-C(34)-O(2)	-179.6(3)
P(1)-C(29)-C(34)-O(2)	3.6(4)
C(30)-C(29)-C(34)-C(33)	-0.5(5)
P(1)-C(29)-C(34)-C(33)	-177.3(3)
C(32)-C(33)-C(34)-O(2)	178.8(3)
C(32)-C(33)-C(34)-C(29)	-0.3(6)
C(23)-P(1)-C(36)-C(37)	-115.1(3)
C(29)-P(1)-C(36)-C(37)	133.7(3)
Ir(1)-P(1)-C(36)-C(37)	0.0(3)
C(23)-P(1)-C(36)-C(41)	65.6(3)

C(29)-P(1)-C(36)-C(41)	-45.6(3)
Ir(1)-P(1)-C(36)-C(41)	-179.4(2)
C(41)-C(36)-C(37)-C(38)	-2.8(5)
P(1)-C(36)-C(37)-C(38)	177.8(3)
C(36)-C(37)-C(38)-C(39)	1.4(6)
C(37)-C(38)-C(39)-C(40)	0.2(6)
C(38)-C(39)-C(40)-C(41)	-0.3(7)
C(42)-O(3)-C(41)-C(40)	12.1(6)
C(42)-O(3)-C(41)-C(36)	-168.4(4)
C(39)-C(40)-C(41)-O(3)	178.3(4)
C(39)-C(40)-C(41)-C(36)	-1.2(6)
C(37)-C(36)-C(41)-O(3)	-176.8(3)
P(1)-C(36)-C(41)-O(3)	2.6(5)
C(37)-C(36)-C(41)-C(40)	2.7(5)
P(1)-C(36)-C(41)-C(40)	-177.9(3)

Symmetry transformations were used to generate equivalent atoms.

Table 14. Hydrogen bonds for Ir(tmp) or [Ir(ppy)$_2$(tmp)]·CH_2Cl_2 [Å and °].

D-H···A	d(D-H)	d(H···A)	d(D···A)	<(DHA)
C(12)-H(12)···O(1)	0.93	2.56	3.143(4)	121.0
C(24)-H(24)···O(3)	0.93	2.43	3.118(5)	131.2

Symmetry transformations were used to generate equivalent atoms.

Table 15. Crystal data and structure refinement for Ru(*p*-cymene)(PPh_3)Cl_2 complex.

Empirical formula	$C_{28}H_{29}Cl_2PRu$
Formula weight	568.45
Wavelength	1.54178 Å
Crystal system	Monoclinic
Space group	$P2_1/n$
Unit cell dimensions	a = 15.5596(3) Å α = 90°
	b = 9.2708(2) Å β = 96.2930(10)°
	c = 35.2545(6) Å γ = 90°
Temperature	296(2) K
Z	8
Density (calculated)	1.494 Mg/m^3
Absorption coefficient	7.659 mm^{-1}
F(000)	2320
Crystal size	0.429 x 0.080 x 0.055 mm^3
Theta range for data collection	2.994 to 68.539°
Index ranges	-18<=h<=18, -9<=k<=11, -42<=l<=42
Reflections collected	142578
Independent reflections	9273 [R(int) = 0.0542]
Completeness to theta = 67.679°	99.8 %
Absorption correction	Semi-empirical from equivalents
Max. and min. transmission	0.7531 and 0.4727
Refinement method	Full-matrix least-squares on F^2
Data/restraints/parameters	9273/0/583
Goodness-of-fit on F^2	1.092
Final R indices [I>2σ(I)]	$R1$ = 0.0267, $wR2$ = 0.0680
R indices (all data)	$R1$ = 0.0267, $wR2$ = 0.0680
Extinction coefficient	n/a
Largest diff. peak and hole	0.467 and -0.438 e.Å^{-3}

Table 16. Atomic coordinates ($x10^4$) and equivalent isotropic displacement parameters ($Å^2 x 10^3$) for Ru(PPh_3). U(eq) was defined as one third of the trace of the orthogonalized U^{ij} tensor.

	x	y	z	U(eq)
Ru(1)	9564(1)	2884(1)	6761(1)	33(1)
Ru(2)	4518(1)	10673(1)	6755(1)	35(1)
Cl(1)	11044(1)	2113(1)	6906(1)	53(1)
Cl(2)	10083(1)	5324(1)	6711(1)	47(1)
Cl(3)	6000(1)	11405(1)	6921(1)	55(1)
Cl(4)	5014(1)	8229(1)	6692(1)	51(1)
P(1)	9686(1)	2655(1)	6105(1)	31(1)
P(2)	4685(1)	10993(1)	6106(1)	34(1)
C(1)	9051(2)	891(3)	7004(1)	56(1)
C(2)	8459(2)	1431(3)	6707(1)	53(1)
C(3)	8134(2)	2848(3)	6709(1)	51(1)
C(4)	8409(2)	3798(3)	7009(1)	46(1)
C(5)	9007(2)	3269(3)	7313(1)	45(1)
C(6)	9316(2)	1870(3)	7309(1)	51(1)
C(7)	9379(3)	-629(3)	7010(1)	82(1)
C(8)	8068(2)	5311(4)	7037(1)	59(1)
C(9)	7774(3)	6032(5)	6658(1)	96(1)
C(10)	7335(2)	5249(5)	7295(1)	96(1)
C(11)	9755(2)	822(2)	5920(1)	39(1)
C(12)	10207(2)	-208(3)	6149(1)	50(1)
C(13)	10341(2)	-1586(3)	6010(1)	63(1)
C(14)	10035(2)	-1937(3)	5639(1)	62(1)
C(15)	9587(2)	-940(3)	5411(1)	63(1)
C(16)	9444(2)	429(3)	5548(1)	54(1)
C(17)	10556(1)	3518(2)	5872(1)	36(1)
C(18)	11317(2)	3991(3)	6075(1)	45(1)
C(19)	11969(2)	4564(3)	5880(1)	57(1)
C(20)	11864(2)	4661(3)	5487(1)	58(1)
C(21)	11107(2)	4207(3)	5286(1)	54(1)

C(22)	10459(2)	3641(3)	5477(1)	46(1)
C(23)	8730(1)	3462(3)	5842(1)	37(1)
C(24)	8741(2)	4950(3)	5794(1)	46(1)
C(25)	8023(2)	5667(4)	5626(1)	63(1)
C(26)	7282(2)	4928(5)	5509(1)	75(1)
C(27)	7252(2)	3464(5)	5560(1)	77(1)
C(28)	7974(2)	2715(3)	5727(1)	56(1)
C(29)	4005(2)	12634(3)	7009(1)	56(1)
C(30)	4247(2)	11623(3)	7307(1)	54(1)
C(31)	3934(2)	10225(3)	7297(1)	48(1)
C(32)	3346(2)	9739(3)	6982(1)	48(1)
C(33)	3089(2)	10734(3)	6689(1)	51(1)
C(34)	3423(2)	12146(3)	6703(1)	55(1)
C(35)	4343(3)	14151(3)	7026(1)	82(1)
C(36)	3009(2)	8217(4)	6988(1)	64(1)
C(37)	2710(3)	7588(5)	6598(1)	106(2)
C(38)	2286(3)	8201(5)	7250(1)	104(2)
C(39)	4764(2)	12860(3)	5942(1)	43(1)
C(40)	5248(2)	13827(3)	6179(1)	55(1)
C(41)	5401(2)	15219(3)	6056(1)	73(1)
C(42)	5074(2)	15648(4)	5693(1)	77(1)
C(43)	4581(2)	14718(4)	5461(1)	76(1)
C(44)	4425(2)	13331(3)	5581(1)	62(1)
C(45)	5594(1)	10191(3)	5886(1)	37(1)
C(46)	5591(2)	10271(3)	5492(1)	50(1)
C(47)	6277(2)	9755(3)	5314(1)	55(1)
C(48)	6974(2)	9145(3)	5527(1)	52(1)
C(49)	6985(2)	9051(3)	5916(1)	53(1)
C(50)	6299(2)	9577(3)	6098(1)	44(1)
C(51)	3745(1)	10240(3)	5817(1)	39(1)
C(52)	3759(2)	8801(3)	5721(1)	52(1)
C(53)	3037(2)	8143(4)	5529(1)	73(1)
C(54)	2290(2)	8909(5)	5440(1)	79(1)
C(55)	2258(2)	10322(5)	5544(1)	75(1)
C(56)	2983(2)	11005(4)	5728(1)	55(1)

Table 17. Bond lengths [Å] and angles [º] for Ru(PPh_3) complex.

Ru(1)-C(2)	2.176(2)
Ru(1)-C(3)	2.211(2)
Ru(1)-C(6)	2.221(2)
Ru(1)-C(1)	2.221(3)
Ru(1)-C(5)	2.245(2)
Ru(1)-C(4)	2.248(2)
Ru(1)-P(1)	2.3489(5)
Ru(1)-Cl(1)	2.4134(6)
Ru(1)-Cl(2)	2.4145(6)
Ru(2)-C(34)	2.175(2)
Ru(2)-C(33)	2.210(2)
Ru(2)-C(29)	2.215(3)
Ru(2)-C(30)	2.218(2)
Ru(2)-C(32)	2.244(2)
Ru(2)-C(31)	2.245(2)
Ru(2)-P(2)	2.3486(5)
Ru(2)-Cl(4)	2.4119(6)
Ru(2)-Cl(3)	2.4135(6)
P(1)-C(23)	1.826(2)
P(1)-C(11)	1.828(2)
P(1)-C(17)	1.842(2)
P(2)-C(51)	1.826(2)
P(2)-C(39)	1.834(3)
P(2)-C(45)	1.844(2)
C(1)-C(2)	1.409(4)
C(1)-C(6)	1.433(4)
C(1)-C(7)	1.498(4)
C(2)-C(3)	1.408(4)
C(2)-H(2)	0.9800
C(3)-C(4)	1.406(4)
C(3)-H(3)	0.9800
C(4)-C(5)	1.427(4)
C(4)-C(8)	1.507(4)
C(5)-C(6)	1.384(4)

C(5)-H(5)	0.9800
C(6)-H(6)	0.9800
C(7)-H(7A)	0.9600
C(7)-H(7B)	0.9600
C(7)-H(7C)	0.9600
C(8)-C(9)	1.522(5)
C(8)-C(10)	1.535(4)
C(8)-H(8)	0.9800
C(9)-H(9A)	0.9600
C(9)-H(9B)	0.9600
C(9)-H(9C)	0.9600
C(10)-H(10A)	0.9600
C(10)-H(10B)	0.9600
C(10)-H(10C)	0.9600
C(11)-C(12)	1.391(4)
C(11)-C(16)	1.396(3)
C(12)-C(13)	1.392(4)
C(12)-H(12)	0.9300
C(13)-C(14)	1.380(4)
C(13)-H(13)	0.9300
C(14)-C(15)	1.366(5)
C(14)-H(14)	0.9300
C(15)-C(16)	1.384(4)
C(15)-H(15)	0.9300
C(16)-H(16)	0.9300
C(17)-C(18)	1.384(3)
C(17)-C(22)	1.391(3)
C(18)-C(19)	1.392(3)
C(18)-H(18)	0.9300
C(19)-C(20)	1.381(4)
C(19)-H(19)	0.9300
C(20)-C(21)	1.371(4)
C(20)-H(20)	0.9300
C(21)-C(22)	1.377(3)
C(21)-H(21)	0.9300
C(22)-H(22)	0.9300

C(23)-C(28)	1.386(3)
C(23)-C(24)	1.390(3)
C(24)-C(25)	1.377(4)
C(24)-H(24)	0.9300
C(25)-C(26)	1.366(5)
C(25)-H(25)	0.9300
C(26)-C(27)	1.371(6)
C(26)-H(26)	0.9300
C(27)-C(28)	1.396(4)
C(27)-H(27)	0.9300
C(28)-H(28)	0.9300
C(29)-C(34)	1.406(4)
C(29)-C(30)	1.426(4)
C(29)-C(35)	1.500(5)
C(30)-C(31)	1.384(4)
C(30)-H(30)	0.9800
C(31)-C(32)	1.432(4)
C(31)-H(31)	0.9800
C(32)-C(33)	1.410(4)
C(32)-C(36)	1.506(4)
C(33)-C(34)	1.407(4)
C(33)-H(33)	0.9800
C(34)-H(34)	0.9800
C(35)-H(35A)	0.9600
C(35)-H(35B)	0.9600
C(35)-H(35C)	0.9600
C(36)-C(37)	1.518(5)
C(36)-C(38)	1.531(4)
C(36)-H(36)	0.9800
C(37)-H(37A)	0.9600
C(37)-H(37B)	0.9600
C(37)-H(37C)	0.9600
C(38)-H(38A)	0.9600
C(38)-H(38B)	0.9600
C(38)-H(38C)	0.9600
C(39)-C(40)	1.389(4)

C(39)-C(44)	1.394(4)
C(40)-C(41)	1.390(4)
C(40)-H(40)	0.9300
C(41)-C(42)	1.383(5)
C(41)-H(41)	0.9300
C(42)-C(43)	1.365(5)
C(42)-H(42)	0.9300
C(43)-C(44)	1.383(4)
C(43)-H(43)	0.9300
C(44)-H(44)	0.9300
C(45)-C(50)	1.381(3)
C(45)-C(46)	1.390(3)
C(46)-C(47)	1.381(3)
C(46)-H(46)	0.9300
C(47)-C(48)	1.370(4)
C(47)-H(47)	0.9300
C(48)-C(49)	1.373(4)
C(48)-H(48)	0.9300
C(49)-C(50)	1.393(3)
C(49)-H(49)	0.9300
C(50)-H(50)	0.9300
C(51)-C(52)	1.377(4)
C(51)-C(56)	1.387(3)
C(52)-C(53)	1.387(4)
C(52)-H(52)	0.9300
C(53)-C(54)	1.370(5)
C(53)-H(53)	0.9300
C(54)-C(55)	1.362(6)
C(54)-H(54)	0.9300
C(55)-C(56)	1.390(4)
C(55)-H(55)	0.9300
C(56)-H(56)	0.9300
C(2)-Ru(1)-C(3)	37.42(11)
C(2)-Ru(1)-C(6)	66.61(10)
C(3)-Ru(1)-C(6)	78.27(10)
C(2)-Ru(1)-C(1)	37.35(11)

C(3)-Ru(1)-C(1)	67.61(12)
C(6)-Ru(1)-C(1)	37.65(10)
C(2)-Ru(1)-C(5)	78.32(9)
C(3)-Ru(1)-C(5)	66.02(9)
C(6)-Ru(1)-C(5)	36.11(10)
C(1)-Ru(1)-C(5)	66.96(10)
C(2)-Ru(1)-C(4)	67.04(10)
C(3)-Ru(1)-C(4)	36.73(9)
C(6)-Ru(1)-C(4)	66.35(10)
C(1)-Ru(1)-C(4)	80.08(11)
C(5)-Ru(1)-C(4)	37.05(9)
C(2)-Ru(1)-P(1)	90.39(7)
C(3)-Ru(1)-P(1)	96.15(6)
C(6)-Ru(1)-P(1)	149.14(8)
C(1)-Ru(1)-P(1)	112.05(7)
C(5)-Ru(1)-P(1)	161.51(7)
C(4)-Ru(1)-P(1)	124.84(6)
C(2)-Ru(1)-Cl(1)	124.19(9)
C(3)-Ru(1)-Cl(1)	160.23(8)
C(6)-Ru(1)-Cl(1)	86.68(8)
C(1)-Ru(1)-Cl(1)	92.65(8)
C(5)-Ru(1)-Cl(1)	108.23(7)
C(4)-Ru(1)-Cl(1)	144.48(6)
P(1)-Ru(1)-Cl(1)	90.21(2)
C(2)-Ru(1)-Cl(2)	147.28(9)
C(3)-Ru(1)-Cl(2)	110.49(8)
C(6)-Ru(1)-Cl(2)	123.43(8)
C(1)-Ru(1)-Cl(2)	160.79(7)
C(5)-Ru(1)-Cl(2)	94.48(7)
C(4)-Ru(1)-Cl(2)	87.91(7)
P(1)-Ru(1)-Cl(2)	87.112(19)
Cl(1)-Ru(1)-Cl(2)	88.46(2)
C(34)-Ru(2)-C(33)	37.42(11)
C(34)-Ru(2)-C(29)	37.34(11)
C(33)-Ru(2)-C(29)	67.58(12)
C(34)-Ru(2)-C(30)	66.55(10)

C(33)-Ru(2)-C(30)	78.27(10)
C(29)-Ru(2)-C(30)	37.54(10)
C(34)-Ru(2)-C(32)	67.20(11)
C(33)-Ru(2)-C(32)	36.90(10)
C(29)-Ru(2)-C(32)	80.15(11)
C(30)-Ru(2)-C(32)	66.42(11)
C(34)-Ru(2)-C(31)	78.52(10)
C(33)-Ru(2)-C(31)	66.29(9)
C(29)-Ru(2)-C(31)	66.98(10)
C(30)-Ru(2)-C(31)	36.12(11)
C(32)-Ru(2)-C(31)	37.21(9)
C(34)-Ru(2)-P(2)	90.47(7)
C(33)-Ru(2)-P(2)	96.40(7)
C(29)-Ru(2)-P(2)	111.97(7)
C(30)-Ru(2)-P(2)	148.89(8)
C(32)-Ru(2)-P(2)	125.25(7)
C(31)-Ru(2)-P(2)	162.07(7)
C(34)-Ru(2)-Cl(4)	146.89(9)
C(33)-Ru(2)-Cl(4)	110.04(8)
C(29)-Ru(2)-Cl(4)	160.34(8)
C(30)-Ru(2)-Cl(4)	123.16(8)
C(32)-Ru(2)-Cl(4)	87.20(7)
C(31)-Ru(2)-Cl(4)	93.90(7)
P(2)-Ru(2)-Cl(4)	87.62(2)
C(34)-Ru(2)-Cl(3)	124.25(9)
C(33)-Ru(2)-Cl(3)	160.31(8)
C(29)-Ru(2)-Cl(3)	92.76(9)
C(30)-Ru(2)-Cl(3)	86.76(8)
C(32)-Ru(2)-Cl(3)	144.45(7)
C(31)-Ru(2)-Cl(3)	108.07(7)
P(2)-Ru(2)-Cl(3)	89.81(2)
Cl(4)-Ru(2)-Cl(3)	88.81(2)
C(23)-P(1)-C(11)	105.95(11)
C(23)-P(1)-C(17)	101.08(10)
C(11)-P(1)-C(17)	99.75(10)
C(23)-P(1)-Ru(1)	108.33(7)

C(11)-P(1)-Ru(1)	116.80(7)
C(17)-P(1)-Ru(1)	122.84(7)
C(51)-P(2)-C(39)	105.25(11)
C(51)-P(2)-C(45)	102.49(10)
C(39)-P(2)-C(45)	99.60(11)
C(51)-P(2)-Ru(2)	109.09(7)
C(39)-P(2)-Ru(2)	116.39(8)
C(45)-P(2)-Ru(2)	122.06(7)
C(2)-C(1)-C(6)	116.3(3)
C(2)-C(1)-C(7)	122.6(3)
C(6)-C(1)-C(7)	121.1(3)
C(2)-C(1)-Ru(1)	69.59(14)
C(6)-C(1)-Ru(1)	71.15(14)
C(7)-C(1)-Ru(1)	130.6(2)
C(3)-C(2)-C(1)	122.2(2)
C(3)-C(2)-Ru(1)	72.64(14)
C(1)-C(2)-Ru(1)	73.06(15)
C(3)-C(2)-H(2)	118.5
C(1)-C(2)-H(2)	118.5
Ru(1)-C(2)-H(2)	118.5
C(4)-C(3)-C(2)	120.6(3)
C(4)-C(3)-Ru(1)	73.05(14)
C(2)-C(3)-Ru(1)	69.94(14)
C(4)-C(3)-H(3)	119.1
C(2)-C(3)-H(3)	119.1
Ru(1)-C(3)-H(3)	119.1
C(3)-C(4)-C(5)	118.0(3)
C(3)-C(4)-C(8)	123.6(2)
C(5)-C(4)-C(8)	118.3(2)
C(3)-C(4)-Ru(1)	70.22(14)
C(5)-C(4)-Ru(1)	71.35(13)
C(8)-C(4)-Ru(1)	132.75(18)
C(6)-C(5)-C(4)	120.9(2)
C(6)-C(5)-Ru(1)	70.99(13)
C(4)-C(5)-Ru(1)	71.60(12)
C(6)-C(5)-H(5)	118.9

C(4)-C(5)-H(5)	118.9
Ru(1)-C(5)-H(5)	118.9
C(5)-C(6)-C(1)	122.0(3)
C(5)-C(6)-Ru(1)	72.90(14)
C(1)-C(6)-Ru(1)	71.21(14)
C(5)-C(6)-H(6)	118.4
C(1)-C(6)-H(6)	118.4
Ru(1)-C(6)-H(6)	118.4
C(1)-C(7)-H(7A)	109.5
C(1)-C(7)-H(7B)	109.5
H(7A)-C(7)-H(7B)	109.5
C(1)-C(7)-H(7C)	109.5
H(7A)-C(7)-H(7C)	109.5
H(7B)-C(7)-H(7C)	109.5
C(4)-C(8)-C(9)	115.1(2)
C(4)-C(8)-C(10)	107.1(3)
C(9)-C(8)-C(10)	111.5(3)
C(4)-C(8)-H(8)	107.6
C(9)-C(8)-H(8)	107.6
C(10)-C(8)-H(8)	107.6
C(8)-C(9)-H(9A)	109.5
C(8)-C(9)-H(9B)	109.5
H(9A)-C(9)-H(9B)	109.5
C(8)-C(9)-H(9C)	109.5
H(9A)-C(9)-H(9C)	109.5
H(9B)-C(9)-H(9C)	109.5
C(8)-C(10)-H(10A)	109.5
C(8)-C(10)-H(10B)	109.5
H(10A)-C(10)-H(10B)	109.5
C(8)-C(10)-H(10C)	109.5
H(10A)-C(10)-H(10C)	109.5
H(10B)-C(10)-H(10C)	109.5
C(12)-C(11)-C(16)	117.9(2)
C(12)-C(11)-P(1)	118.40(18)
C(16)-C(11)-P(1)	123.45(19)
C(11)-C(12)-C(13)	120.7(3)

C(11)-C(12)-H(12)	119.6
C(13)-C(12)-H(12)	119.6
C(14)-C(13)-C(12)	120.0(3)
C(14)-C(13)-H(13)	120.0
C(12)-C(13)-H(13)	120.0
C(15)-C(14)-C(13)	120.0(3)
C(15)-C(14)-H(14)	120.0
C(13)-C(14)-H(14)	120.0
C(14)-C(15)-C(16)	120.4(3)
C(14)-C(15)-H(15)	119.8
C(16)-C(15)-H(15)	119.8
C(15)-C(16)-C(11)	120.9(3)
C(15)-C(16)-H(16)	119.5
C(11)-C(16)-H(16)	119.5
C(18)-C(17)-C(22)	119.0(2)
C(18)-C(17)-P(1)	122.46(17)
C(22)-C(17)-P(1)	118.53(18)
C(17)-C(18)-C(19)	119.7(2)
C(17)-C(18)-H(18)	120.2
C(19)-C(18)-H(18)	120.2
C(20)-C(19)-C(18)	120.5(3)
C(20)-C(19)-H(19)	119.7
C(18)-C(19)-H(19)	119.7
C(21)-C(20)-C(19)	119.9(2)
C(21)-C(20)-H(20)	120.1
C(19)-C(20)-H(20)	120.1
C(20)-C(21)-C(22)	119.9(2)
C(20)-C(21)-H(21)	120.1
C(22)-C(21)-H(21)	120.1
C(21)-C(22)-C(17)	121.0(2)
C(21)-C(22)-H(22)	119.5
C(17)-C(22)-H(22)	119.5
C(28)-C(23)-C(24)	118.8(2)
C(28)-C(23)-P(1)	124.2(2)
C(24)-C(23)-P(1)	116.63(18)
C(25)-C(24)-C(23)	120.8(3)

C(25)-C(24)-H(24)	119.6
C(23)-C(24)-H(24)	119.6
C(26)-C(25)-C(24)	120.4(3)
C(26)-C(25)-H(25)	119.8
C(24)-C(25)-H(25)	119.8
C(25)-C(26)-C(27)	119.7(3)
C(25)-C(26)-H(26)	120.1
C(27)-C(26)-H(26)	120.1
C(26)-C(27)-C(28)	120.7(3)
C(26)-C(27)-H(27)	119.6
C(28)-C(27)-H(27)	119.6
C(23)-C(28)-C(27)	119.5(3)
C(23)-C(28)-H(28)	120.2
C(27)-C(28)-H(28)	120.2
C(34)-C(29)-C(30)	116.7(3)
C(34)-C(29)-C(35)	121.7(3)
C(30)-C(29)-C(35)	121.6(3)
C(34)-C(29)-Ru(2)	69.81(15)
C(30)-C(29)-Ru(2)	71.34(15)
C(35)-C(29)-Ru(2)	130.1(2)
C(31)-C(30)-C(29)	122.3(3)
C(31)-C(30)-Ru(2)	73.01(14)
C(29)-C(30)-Ru(2)	71.12(14)
C(31)-C(30)-H(30)	118.2
C(29)-C(30)-H(30)	118.2
Ru(2)-C(30)-H(30)	118.2
C(30)-C(31)-C(32)	120.4(2)
C(30)-C(31)-Ru(2)	70.88(14)
C(32)-C(31)-Ru(2)	71.38(13)
C(30)-C(31)-H(31)	119.1
C(32)-C(31)-H(31)	119.1
Ru(2)-C(31)-H(31)	119.1
C(33)-C(32)-C(31)	118.0(3)
C(33)-C(32)-C(36)	123.4(3)
C(31)-C(32)-C(36)	118.6(2)
C(33)-C(32)-Ru(2)	70.23(14)

C(31)-C(32)-Ru(2)	71.41(14)
C(36)-C(32)-Ru(2)	131.60(19)
C(34)-C(33)-C(32)	120.6(3)
C(34)-C(33)-Ru(2)	69.96(14)
C(32)-C(33)-Ru(2)	72.88(14)
C(34)-C(33)-H(33)	119.1
C(32)-C(33)-H(33)	119.1
Ru(2)-C(33)-H(33)	119.1
C(29)-C(34)-C(33)	122.1(2)
C(29)-C(34)-Ru(2)	72.85(15)
C(33)-C(34)-Ru(2)	72.63(15)
C(29)-C(34)-H(34)	118.6
C(33)-C(34)-H(34)	118.6
Ru(2)-C(34)-H(34)	118.6
C(29)-C(35)-H(35A)	109.5
C(29)-C(35)-H(35B)	109.5
H(35A)-C(35)-H(35B)	109.5
C(29)-C(35)-H(35C)	109.5
H(35A)-C(35)-H(35C)	109.5
H(35B)-C(35)-H(35C)	109.5
C(32)-C(36)-C(37)	114.9(3)
C(32)-C(36)-C(38)	107.3(3)
C(37)-C(36)-C(38)	111.7(3)
C(32)-C(36)-H(36)	107.5
C(37)-C(36)-H(36)	107.5
C(38)-C(36)-H(36)	107.5
C(36)-C(37)-H(37A)	109.5
C(36)-C(37)-H(37B)	109.5
H(37A)-C(37)-H(37B)	109.5
C(36)-C(37)-H(37C)	109.5
H(37A)-C(37)-H(37C)	109.5
H(37B)-C(37)-H(37C)	109.5
C(36)-C(38)-H(38A)	109.5
C(36)-C(38)-H(38B)	109.5
H(38A)-C(38)-H(38B)	109.5
C(36)-C(38)-H(38C)	109.5

H(38A)-C(38)-H(38C)	109.5
H(38B)-C(38)-H(38C)	109.5
C(40)-C(39)-C(44)	118.2(3)
C(40)-C(39)-P(2)	118.09(19)
C(44)-C(39)-P(2)	123.5(2)
C(39)-C(40)-C(41)	120.8(3)
C(39)-C(40)-H(40)	119.6
C(41)-C(40)-H(40)	119.6
C(42)-C(41)-C(40)	119.8(3)
C(42)-C(41)-H(41)	120.1
C(40)-C(41)-H(41)	120.1
C(43)-C(42)-C(41)	119.9(3)
C(43)-C(42)-H(42)	120.1
C(41)-C(42)-H(42)	120.1
C(42)-C(43)-C(44)	120.7(3)
C(42)-C(43)-H(43)	119.7
C(44)-C(43)-H(43)	119.7
C(43)-C(44)-C(39)	120.6(3)
C(43)-C(44)-H(44)	119.7
C(39)-C(44)-H(44)	119.7
C(50)-C(45)-C(46)	118.6(2)
C(50)-C(45)-P(2)	122.61(17)
C(46)-C(45)-P(2)	118.71(17)
C(47)-C(46)-C(45)	121.1(2)
C(47)-C(46)-H(46)	119.4
C(45)-C(46)-H(46)	119.4
C(48)-C(47)-C(46)	119.9(2)
C(48)-C(47)-H(47)	120.0
C(46)-C(47)-H(47)	120.0
C(47)-C(48)-C(49)	119.7(2)
C(47)-C(48)-H(48)	120.1
C(49)-C(48)-H(48)	120.1
C(48)-C(49)-C(50)	120.7(2)
C(48)-C(49)-H(49)	119.6
C(50)-C(49)-H(49)	119.6
C(45)-C(50)-C(49)	119.9(2)

C(45)-C(50)-H(50)	120.1
C(49)-C(50)-H(50)	120.1
C(52)-C(51)-C(56)	118.4(2)
C(52)-C(51)-P(2)	118.32(19)
C(56)-C(51)-P(2)	122.9(2)
C(51)-C(52)-C(53)	120.8(3)
C(51)-C(52)-H(52)	119.6
C(53)-C(52)-H(52)	119.6
C(54)-C(53)-C(52)	120.3(3)
C(54)-C(53)-H(53)	119.8
C(52)-C(53)-H(53)	119.8
C(55)-C(54)-C(53)	119.5(3)
C(55)-C(54)-H(54)	120.3
C(53)-C(54)-H(54)	120.3
C(54)-C(55)-C(56)	120.8(3)
C(54)-C(55)-H(55)	119.6
C(56)-C(55)-H(55)	119.6
C(51)-C(56)-C(55)	120.2(3)
C(51)-C(56)-H(56)	119.9
C(55)-C(56)-H(56)	119.9

Symmetry transformations were used to generate equivalent atoms.

Table 18. Anisotropic displacement parameters ($Å^2x10^3$) for $Ru(PPh_3)$. The anisotropic displacement factor exponent takes the form: $-2\pi^2[h^2a^{*2}U^{11} + ... + 2 h k a^* b^* U^{12}]$.

	U^{11}	U^{22}	U^{33}	U^{23}	U^{13}	U^{12}
Ru(1)	35(1)	40(1)	25(1)	0(1)	6(1)	-4(1)
Ru(2)	35(1)	44(1)	24(1)	-2(1)	6(1)	5(1)
Cl(1)	42(1)	67(1)	49(1)	5(1)	-1(1)	7(1)
Cl(2)	61(1)	41(1)	42(1)	-4(1)	14(1)	-9(1)
Cl(3)	44(1)	73(1)	47(1)	-6(1)	-3(1)	-6(1)
Cl(4)	64(1)	45(1)	47(1)	1(1)	18(1)	9(1)
P(1)	35(1)	34(1)	25(1)	0(1)	6(1)	-2(1)
P(2)	35(1)	42(1)	25(1)	-1(1)	5(1)	4(1)
C(1)	69(2)	53(2)	48(2)	5(1)	25(1)	-16(1)
C(2)	52(1)	65(2)	46(1)	-15(1)	20(1)	-26(1)
C(3)	34(1)	83(2)	37(1)	-10(1)	11(1)	-10(1)
C(4)	39(1)	67(2)	34(1)	-7(1)	15(1)	-4(1)
C(5)	48(1)	61(2)	28(1)	-3(1)	15(1)	-11(1)
C(6)	60(2)	63(2)	33(1)	10(1)	14(1)	-9(1)
C(7)	129(3)	50(2)	73(2)	15(2)	39(2)	-11(2)
C(8)	51(2)	78(2)	50(2)	-11(1)	15(1)	14(1)
C(9)	106(3)	110(3)	71(2)	0(2)	7(2)	55(3)
C(10)	72(2)	129(4)	94(3)	-27(3)	45(2)	15(2)
C(11)	46(1)	38(1)	36(1)	-1(1)	13(1)	-5(1)
C(12)	60(2)	43(1)	49(1)	1(1)	8(1)	0(1)
C(13)	74(2)	38(1)	78(2)	4(1)	16(2)	5(1)
C(14)	72(2)	40(1)	78(2)	-15(1)	28(2)	-11(1)
C(15)	86(2)	51(2)	55(2)	-18(1)	17(2)	-13(2)
C(16)	77(2)	46(1)	39(1)	-6(1)	6(1)	-3(1)
C(17)	40(1)	36(1)	33(1)	0(1)	12(1)	0(1)
C(18)	46(1)	52(1)	40(1)	-1(1)	11(1)	-7(1)
C(19)	49(2)	61(2)	62(2)	-7(1)	14(1)	-18(1)
C(20)	65(2)	52(2)	62(2)	0(1)	34(1)	-16(1)
C(21)	68(2)	59(2)	38(1)	2(1)	22(1)	-5(1)

C(22)	51(1)	54(2)	35(1)	-1(1)	12(1)	-5(1)
C(23)	40(1)	46(1)	27(1)	2(1)	7(1)	2(1)
C(24)	50(1)	48(1)	41(1)	2(1)	10(1)	8(1)
C(25)	67(2)	68(2)	54(2)	8(1)	15(1)	26(2)
C(26)	60(2)	109(3)	56(2)	15(2)	6(1)	34(2)
C(27)	41(2)	122(3)	65(2)	-1(2)	-5(1)	-6(2)
C(28)	48(2)	66(2)	53(2)	1(1)	-1(1)	-11(1)
C(29)	70(2)	56(2)	46(1)	-7(1)	24(1)	19(1)
C(30)	60(2)	70(2)	34(1)	-10(1)	15(1)	12(1)
C(31)	50(1)	67(2)	28(1)	4(1)	14(1)	13(1)
C(32)	39(1)	71(2)	36(1)	6(1)	17(1)	4(1)
C(33)	34(1)	86(2)	36(1)	5(1)	10(1)	8(1)
C(34)	54(2)	67(2)	45(1)	11(1)	19(1)	25(1)
C(35)	130(3)	53(2)	71(2)	-15(2)	39(2)	11(2)
C(36)	56(2)	79(2)	58(2)	9(2)	17(1)	-16(2)
C(37)	115(3)	125(4)	78(3)	-10(2)	11(2)	-66(3)
C(38)	78(2)	135(4)	108(3)	23(3)	49(2)	-22(2)
C(39)	47(1)	46(1)	38(1)	2(1)	15(1)	7(1)
C(40)	63(2)	49(2)	55(2)	-3(1)	15(1)	1(1)
C(41)	79(2)	46(2)	97(3)	-12(2)	29(2)	-3(2)
C(42)	85(2)	51(2)	103(3)	22(2)	45(2)	18(2)
C(43)	89(2)	67(2)	74(2)	30(2)	22(2)	18(2)
C(44)	74(2)	62(2)	50(2)	11(1)	11(1)	7(2)
C(45)	36(1)	44(1)	31(1)	-2(1)	7(1)	1(1)
C(46)	44(1)	72(2)	34(1)	0(1)	6(1)	12(1)
C(47)	56(2)	75(2)	37(1)	-2(1)	15(1)	11(1)
C(48)	50(1)	55(2)	53(2)	-2(1)	22(1)	10(1)
C(49)	44(1)	60(2)	55(2)	7(1)	9(1)	17(1)
C(50)	46(1)	52(1)	36(1)	4(1)	9(1)	8(1)
C(51)	37(1)	52(1)	27(1)	0(1)	6(1)	2(1)
C(52)	50(1)	51(2)	55(2)	-1(1)	4(1)	-3(1)
C(53)	72(2)	71(2)	73(2)	-11(2)	1(2)	-25(2)
C(54)	57(2)	119(3)	58(2)	-9(2)	-2(1)	-32(2)
C(55)	39(2)	128(3)	55(2)	2(2)	-5(1)	10(2)
C(56)	45(1)	76(2)	44(1)	-3(1)	-2(1)	13(1)

Table 19. Hydrogen coordinates (x10^4) and isotropic displacement parameters (Å^{2}x 10^3) for Ru(PPh_3) complex.

	x	y	z	U(eq)
H(2)	8344	859	6473	64
H(3)	7809	3231	6477	61
H(5)	9294	3958	7496	54
H(6)	9813	1608	7491	62
H(7A)	9220	-1069	6765	123
H(7B)	9131	-1165	7203	123
H(7C)	9998	-627	7063	123
H(8)	8534	5901	7167	71
H(9A)	8251	6088	6507	144
H(9B)	7568	6987	6702	144
H(9C)	7317	5476	6523	144
H(10A)	6870	4673	7175	144
H(10B)	7130	6207	7335	144
H(10C)	7547	4827	7536	144
H(12)	10421	26	6398	61
H(13)	10638	-2269	6167	75
H(14)	10134	-2852	5545	74
H(15)	9377	-1182	5162	76
H(16)	9136	1097	5389	65
H(18)	11391	3927	6339	55
H(19)	12480	4884	6015	68
H(20)	12306	5032	5358	69
H(21)	11032	4282	5021	64
H(22)	9947	3336	5339	56
H(24)	9238	5468	5877	55
H(25)	8044	6661	5591	75
H(26)	6799	5416	5394	90
H(27)	6744	2965	5483	92
H(28)	7949	1722	5761	67
H(30)	4738	11860	7494	65
H(31)	4209	9514	7477	57

H(33)	2773	10384	6451	62
H(34)	3324	12749	6474	65
H(35A)	4227	14591	6779	124
H(35B)	4956	14139	7099	124
H(35C)	4063	14693	7209	124
H(36)	3478	7607	7105	76
H(37A)	2248	8164	6475	159
H(37B)	2511	6618	6627	159
H(37C)	3184	7583	6445	159
H(38A)	1815	8791	7141	156
H(38B)	2503	8571	7496	156
H(38C)	2087	7229	7276	156
H(40)	5473	13540	6422	66
H(41)	5721	15860	6218	87
H(42)	5191	16569	5607	92
H(43)	4347	15020	5220	91
H(44)	4090	12708	5419	74
H(46)	5120	10679	5346	60
H(47)	6266	9821	5051	66
H(48)	7436	8795	5408	62
H(49)	7457	8632	6060	63
H(50)	6315	9514	6362	53
H(52)	4258	8264	5785	63
H(53)	3062	7176	5460	87
H(54)	1807	8469	5310	94
H(55)	1746	10836	5491	90
H(56)	2957	11977	5791	66

Table 20. Torsion angles [º] for Ru(PPh_3) complex.

C(6)-C(1)-C(2)-C(3)	-0.6(4)
C(7)-C(1)-C(2)-C(3)	178.2(3)
Ru(1)-C(1)-C(2)-C(3)	-55.9(2)
C(6)-C(1)-C(2)-Ru(1)	55.3(2)
C(7)-C(1)-C(2)-Ru(1)	-125.9(3)
C(1)-C(2)-C(3)-C(4)	1.3(4)
Ru(1)-C(2)-C(3)-C(4)	-54.8(2)
C(1)-C(2)-C(3)-Ru(1)	56.1(2)
C(2)-C(3)-C(4)-C(5)	-1.5(3)
Ru(1)-C(3)-C(4)-C(5)	-54.85(19)
C(2)-C(3)-C(4)-C(8)	-177.8(2)
Ru(1)-C(3)-C(4)-C(8)	128.8(2)
C(2)-C(3)-C(4)-Ru(1)	53.3(2)
C(3)-C(4)-C(5)-C(6)	1.1(3)
C(8)-C(4)-C(5)-C(6)	177.6(2)
Ru(1)-C(4)-C(5)-C(6)	-53.2(2)
C(3)-C(4)-C(5)-Ru(1)	54.29(19)
C(8)-C(4)-C(5)-Ru(1)	-129.2(2)
C(4)-C(5)-C(6)-C(1)	-0.4(4)
Ru(1)-C(5)-C(6)-C(1)	-53.9(2)
C(4)-C(5)-C(6)-Ru(1)	53.5(2)
C(2)-C(1)-C(6)-C(5)	0.1(4)
C(7)-C(1)-C(6)-C(5)	-178.6(3)
Ru(1)-C(1)-C(6)-C(5)	54.7(2)
C(2)-C(1)-C(6)-Ru(1)	-54.5(2)
C(7)-C(1)-C(6)-Ru(1)	126.7(3)
C(3)-C(4)-C(8)-C(9)	-29.2(4)
C(5)-C(4)-C(8)-C(9)	154.5(3)
Ru(1)-C(4)-C(8)-C(9)	64.3(4)
C(3)-C(4)-C(8)-C(10)	95.3(3)
C(5)-C(4)-C(8)-C(10)	-81.0(3)
Ru(1)-C(4)-C(8)-C(10)	-171.2(2)
C(23)-P(1)-C(11)-C(12)	-156.93(19)
C(17)-P(1)-C(11)-C(12)	98.5(2)

Ru(1)-P(1)-C(11)-C(12)	-36.2(2)
C(23)-P(1)-C(11)-C(16)	28.9(2)
C(17)-P(1)-C(11)-C(16)	-75.7(2)
Ru(1)-P(1)-C(11)-C(16)	149.6(2)
C(16)-C(11)-C(12)-C(13)	-0.1(4)
P(1)-C(11)-C(12)-C(13)	-174.6(2)
C(11)-C(12)-C(13)-C(14)	0.9(4)
C(12)-C(13)-C(14)-C(15)	-1.1(5)
C(13)-C(14)-C(15)-C(16)	0.6(5)
C(14)-C(15)-C(16)-C(11)	0.2(5)
C(12)-C(11)-C(16)-C(15)	-0.5(4)
P(1)-C(11)-C(16)-C(15)	173.7(2)
C(23)-P(1)-C(17)-C(18)	139.8(2)
C(11)-P(1)-C(17)-C(18)	-111.7(2)
Ru(1)-P(1)-C(17)-C(18)	19.2(2)
C(23)-P(1)-C(17)-C(22)	-43.1(2)
C(11)-P(1)-C(17)-C(22)	65.5(2)
Ru(1)-P(1)-C(17)-C(22)	-163.59(16)
C(22)-C(17)-C(18)-C(19)	-0.7(4)
P(1)-C(17)-C(18)-C(19)	176.5(2)
C(17)-C(18)-C(19)-C(20)	-0.1(4)
C(18)-C(19)-C(20)-C(21)	0.9(5)
C(19)-C(20)-C(21)-C(22)	-0.8(4)
C(20)-C(21)-C(22)-C(17)	0.0(4)
C(18)-C(17)-C(22)-C(21)	0.8(4)
P(1)-C(17)-C(22)-C(21)	-176.5(2)
C(11)-P(1)-C(23)-C(28)	36.3(2)
C(17)-P(1)-C(23)-C(28)	139.9(2)
Ru(1)-P(1)-C(23)-C(28)	-89.8(2)
C(11)-P(1)-C(23)-C(24)	-151.35(17)
C(17)-P(1)-C(23)-C(24)	-47.73(19)
Ru(1)-P(1)-C(23)-C(24)	82.59(18)
C(28)-C(23)-C(24)-C(25)	-2.0(4)
P(1)-C(23)-C(24)-C(25)	-174.9(2)
C(23)-C(24)-C(25)-C(26)	1.2(4)
C(24)-C(25)-C(26)-C(27)	0.2(5)

C(25)-C(26)-C(27)-C(28)	-0.8(5)
C(24)-C(23)-C(28)-C(27)	1.4(4)
P(1)-C(23)-C(28)-C(27)	173.7(2)
C(26)-C(27)-C(28)-C(23)	0.0(5)
C(34)-C(29)-C(30)-C(31)	0.3(4)
C(35)-C(29)-C(30)-C(31)	179.3(3)
Ru(2)-C(29)-C(30)-C(31)	-54.4(2)
C(34)-C(29)-C(30)-Ru(2)	54.7(2)
C(35)-C(29)-C(30)-Ru(2)	-126.2(3)
C(29)-C(30)-C(31)-C(32)	0.2(4)
Ru(2)-C(30)-C(31)-C(32)	-53.5(2)
C(29)-C(30)-C(31)-Ru(2)	53.6(2)
C(30)-C(31)-C(32)-C(33)	-1.1(3)
Ru(2)-C(31)-C(32)-C(33)	-54.37(19)
C(30)-C(31)-C(32)-C(36)	-178.9(2)
Ru(2)-C(31)-C(32)-C(36)	127.9(2)
C(30)-C(31)-C(32)-Ru(2)	53.2(2)
C(31)-C(32)-C(33)-C(34)	1.7(3)
C(36)-C(32)-C(33)-C(34)	179.3(2)
Ru(2)-C(32)-C(33)-C(34)	-53.2(2)
C(31)-C(32)-C(33)-Ru(2)	54.94(19)
C(36)-C(32)-C(33)-Ru(2)	-127.5(2)
C(30)-C(29)-C(34)-C(33)	0.3(4)
C(35)-C(29)-C(34)-C(33)	-178.8(3)
Ru(2)-C(29)-C(34)-C(33)	55.8(2)
C(30)-C(29)-C(34)-Ru(2)	-55.5(2)
C(35)-C(29)-C(34)-Ru(2)	125.4(3)
C(32)-C(33)-C(34)-C(29)	-1.3(4)
Ru(2)-C(33)-C(34)-C(29)	-55.9(2)
C(32)-C(33)-C(34)-Ru(2)	54.6(2)
C(33)-C(32)-C(36)-C(37)	26.4(4)
C(31)-C(32)-C(36)-C(37)	-156.0(3)
Ru(2)-C(32)-C(36)-C(37)	-66.1(4)
C(33)-C(32)-C(36)-C(38)	-98.5(3)
C(31)-C(32)-C(36)-C(38)	79.1(3)
Ru(2)-C(32)-C(36)-C(38)	169.0(2)

C(51)-P(2)-C(39)-C(40)	161.24(19)
C(45)-P(2)-C(39)-C(40)	-92.9(2)
Ru(2)-P(2)-C(39)-C(40)	40.3(2)
C(51)-P(2)-C(39)-C(44)	-24.1(2)
C(45)-P(2)-C(39)-C(44)	81.7(2)
Ru(2)-P(2)-C(39)-C(44)	-145.1(2)
C(44)-C(39)-C(40)-C(41)	-1.0(4)
P(2)-C(39)-C(40)-C(41)	173.9(2)
C(39)-C(40)-C(41)-C(42)	-0.5(5)
C(40)-C(41)-C(42)-C(43)	2.1(5)
C(41)-C(42)-C(43)-C(44)	-2.0(5)
C(42)-C(43)-C(44)-C(39)	0.4(5)
C(40)-C(39)-C(44)-C(43)	1.1(4)
P(2)-C(39)-C(44)-C(43)	-173.5(2)
C(51)-P(2)-C(45)-C(50)	-133.6(2)
C(39)-P(2)-C(45)-C(50)	118.3(2)
Ru(2)-P(2)-C(45)-C(50)	-11.4(2)
C(51)-P(2)-C(45)-C(46)	49.6(2)
C(39)-P(2)-C(45)-C(46)	-58.5(2)
Ru(2)-P(2)-C(45)-C(46)	171.90(18)
C(50)-C(45)-C(46)-C(47)	-0.2(4)
P(2)-C(45)-C(46)-C(47)	176.6(2)
C(45)-C(46)-C(47)-C(48)	0.3(5)
C(46)-C(47)-C(48)-C(49)	0.0(5)
C(47)-C(48)-C(49)-C(50)	-0.3(4)
C(46)-C(45)-C(50)-C(49)	-0.1(4)
P(2)-C(45)-C(50)-C(49)	-176.9(2)
C(48)-C(49)-C(50)-C(45)	0.4(4)
C(39)-P(2)-C(51)-C(52)	146.50(19)
C(45)-P(2)-C(51)-C(52)	42.8(2)
Ru(2)-P(2)-C(51)-C(52)	-87.92(19)
C(39)-P(2)-C(51)-C(56)	-40.9(2)
C(45)-P(2)-C(51)-C(56)	-144.7(2)
Ru(2)-P(2)-C(51)-C(56)	84.6(2)
C(56)-C(51)-C(52)-C(53)	1.8(4)
P(2)-C(51)-C(52)-C(53)	174.7(2)

C(51)-C(52)-C(53)-C(54)	-1.6(5)
C(52)-C(53)-C(54)-C(55)	-0.4(5)
C(53)-C(54)-C(55)-C(56)	2.1(5)
C(52)-C(51)-C(56)-C(55)	-0.2(4)
P(2)-C(51)-C(56)-C(55)	-172.8(2)
C(54)-C(55)-C(56)-C(51)	-1.7(5)

Symmetry transformations were used to generate equivalent atoms.

Table 21. Hydrogen bonds for Ru(PPh_3) [Å and º] complex.

D-H···A	d(D-H)	d(H···A)	d(D···A)	<(DHA)
C(12)-H(12)···Cl(1)	0.93	2.74	3.564(3)	147.9
C(18)-H(18)···Cl(1)	0.93	2.71	3.476(3)	140.1
C(18)-H(18)···Cl(2)	0.93	2.85	3.345(2)	114.6
C(40)-H(40)···Cl(3)	0.93	2.71	3.548(3)	149.7
C(50)-H(50)···Cl(3)	0.93	2.72	3.435(2)	134.2
C(50)-H(50)···Cl(4)	0.93	2.72	3.295(2)	121.1

Symmetry transformations were used to generate equivalent atoms.

VITAE

Name **Mr. Vannara Soem**

Student ID 6410220028

Educational Attainment

Degree	Name of Institution	Year of Graduation
Bachelor of Science (Biochemistry)	Cambodia University for Specialties (Phnom Penh)	2014
High School Teacher	National Institute of Education (Phnom Penh)	2015

Scholarship Awards during Enrolment

1. Her Royal Highness Princess Maha Chakri Sirindhorn Education Project.
2. Graduate School, Prince of Songkla University.

Work – Position and Address (If Possible)

1. Sok Arn Sobin High School (Takeo Province 2010-2012).
2. Sok Arn Tramcar High School (Takeo Province 2012-Present).

List of Publication and Proceeding (If Possible)

1. Synthesis, Characterization, Theoretical Calculation-Based Density Functional Theory, and *In vitro* Cytotoxicity Against Breast Cancer Cells of Ru(*p*-cymene)(PPh_3)Cl_2 Complex.
2. Synthesis, Characterization, and Biological Activity of Ruthenium(II) and Iridium(III) Complexes Containing Tris(2-methoxyphenyl)phosphine Ligand.